Water Resources in the Anthropocene

Assessing the impact of climate change on freshwater supply and the scope for adaptation in the livestock sector

DISSERTATION

zur Erlangung des akademischen Grades
doctor rerum naturalium
(Dr. rer. nat.)
im Fach Geographie

eingereicht and der
Mathematisch-Naturwissenschaftlichen Fakultät der Humboldt-Universität zu Berlin

von
Dipl.-Hydrol. Jens Heinke

Präsidentin der Humboldt-Universität zu Berlin
Prof. Dr.-Ing. Dr. Sabine Kunst

Dekan der Mathematisch-Naturwissenschaftlichen Fakultät
Prof. Dr. Elmar Kulke

Gutachter:
Prof. Dr. Dieter Gerten
Prof. Dr. Stefan Siebert
PD Dr. Stefan Hagemann

Tag der mündlichen Prüfung: 27. Oktober 2020

For JCC

Abstract

Water is essential for human wellbeing—for drinking, washing, sanitation, food production, industrial processes, and many other activities. The hydrological cycle provides humanity with water resources by replenishing the water in lakes, rivers, aquifers and soils.

Humanity's impact on the Earth System has reached the scale of Earth's natural geological forces. Anthropogenic alterations of biogeochemical cycles, the land surface, and Earth's energy balance are so profound that a new human-dominated geological epoch has been proposed: the Anthropocene. These alterations also affect the functioning of the hydrological cycle and may impair its capacity to provide humanity with water resources.

One major pathway of human interference with the global hydrological cycle is through anthropogenic climate change. The aim of this thesis is to advance the understanding of climate-related changes in the hydrological cycle, how they will affect the availability of water resources in the future, and what opportunities exist to reduce anthropogenic water use to lower the pressure on water resources. Specifically, the thesis assesses the impact of climate change on river discharge and the consequences for freshwater supply. All climate-related impacts are analysed as a function of global mean temperature increase, which is tailored to inform the public debate and negotiations about climate change mitigation that are centred around temperature goals. On the demand side, the focus is on water use in livestock production and the opportunities and constraints for improving livestock water productivity.

The results corroborate earlier findings that climate change will likely lead to an increases in average river discharge in the high northern latitudes and eastern Africa, and to a decreases in the Mediterranean, the Middle East, and parts of North and South America. In most other regions, however, projected hydrological change is subject to large uncertainties. Despite the large uncertainties in climate projections, their translation into hydrological change, and the implications of hydrological change for human water resources, this thesis demonstrates that climate change is a large threat to freshwater supply of future populations. Severe climate-related impacts on river discharge and human water resources can be largely mitigated by constraining global mean temperature increase to 2 K above pre-industrial levels. However, some regions such as the Mediterranean will 'more likely than not' be affected by severe hydrological change at 2 K or even 1.5 K warming above pre-industrial levels. Because of the large uncertainties in the results, severe change in hydrological conditions in many other parts of world cannot be excluded even for such low levels of global mean temperature increase.

The assessment of water use in global livestock production shows that about 4666 km^3/yr of water—about 44 % of total water use for human-appropriated agricultural biomass—can be attributed to feed production. Large improvements in livestock water productivity can

be achieved for pigs and poultry by improving management in feed production and livestock management alike. For ruminants, the largest potential lies in improving livestock management. However, improvements in feed use efficiency of ruminants achieved or accompanied by increased supplementation with feed crops come at the cost of higher water requirements to produce the feed, which reduces the overall improvement in livestock water productivity. This inverse effect of feed composition on feed water productivity and feed use efficiency is an important constraint for the achievable livestock water productivity in ruminant production.

Zusammenfassung

Wasser ist für das menschliche Wohlergehen unerlässlich—zum Trinken und Waschen, zur sanitären Grundversorgung, zur Nahrungsmittelproduktion, für industrielle Prozesse und viele andere Aktivitäten. Der hydrologische Kreislauf stellt die Versorgung der Menschheit mit Wasserressourcen sicher, indem er das Wasser in Seen, Flüssen, Grundwasserleitern und Böden stetig auffüllt.

Der Einfluss der Menschheit auf das Erdsystem hat das Ausmaß der natürlichen geologischen Kräfte der Erde erreicht. Die anthropogenen Veränderungen der biogeochemischen Kreisläufe, der Landoberfläche und der Energiebilanz der Erde sind so tiefgreifend, dass eine neue geologische Epoche vorgeschlagen wurde: das Anthropozän. Diese Veränderungen wirken sich auch auf das Funktionieren des Wasserkreislaufs aus und können seine Fähigkeit beeinträchtigen, die Menschheit mit Wasserressourcen zu versorgen.

Ein wesentlicher Faktor menschlicher Eingriffe in den globalen Wasserkreislauf ist der anthropogene Klimawandel. Ziel dieser Arbeit ist es, das Verständnis über klimabedingte Veränderungen des hydrologischen Kreislaufs zu verbessern, wie diese die Verfügbarkeit von Wasserressourcen in der Zukunft beeinflussen werden und welche Möglichkeiten bestehen, den anthropogenen Wasserverbrauch zu reduzieren, um den Druck auf die verfügbaren Wasserressourcen zu verringern. Konkret werden die Auswirkungen des Klimawandels auf den Abfluss von Flüssen und die Folgen für die Wasserversorgung untersucht. Alle klimabedingten Auswirkungen werden in Relation zum globalen mittleren Temperaturanstieg analysiert, um eine Beitrag zur öffentliche Debatte und den Verhandlungen über die Eindämmung des Klimawandels zu leisten, bei denen Temperaturziele im Mittelpunkt stehen. Beider Untersuchung der Nachfrageseite liegt der Schwerpunkt auf der Wassernutzung in der Tierproduktion und den Möglichkeiten und Beschränkungen zur Verbesserung der Wasserproduktivität in der Viehwirtschaft.

Die Ergebnisse untermauern frühere Erkenntnisse, dass der Klimawandel in den hohen nördlichen Breitengraden und in Ostafrika wahrscheinlich zu einem Anstieg des durchschnittlichen Abflussvolumens der Flüsse und im Mittelmeerraum, im Nahen Osten und in Teilen Nord- und Südamerikas zu einem Rückgang führen wird. In den meisten anderen Regionen sind die prognostizierten hydrologischen Veränderungen jedoch mit großen Unsicherheiten behaftet. Trotz der großen Unsicherheiten bei den Klimaprojektionen, ihrer Übersetzung in hydrologische Veränderungen und der Auswirkungen des hydrologischen Wandels auf die menschlichen Wasserressourcen zeigt diese Dissertation, dass der Klimawandel eine große Bedrohung für die Wasserversorgung der zukünftigen Bevölkerung darstellt. Die schwerwiegenden klimabedingten Auswirkungen auf den Abfluss von Flüssen und die menschlichen Wasserressourcen können jedoch weitgehend vermieden werden, indem der Anstieg der globalen Mitteltemperatur über das vorindustrielle Niveau auf 2 K

begrenzt wird. Allerdings werden auch bei einer Begrenzung des globalen Temperaturanstiegs auf 2 K oder sogar 1.5 K über dem vorindustriellen Niveau einige Regionen wie der Mittelmeerraum „eher wahrscheinlich“ von schwerwiegenden hydrologischen Veränderungen betroffen sein. Aufgrund der großen Unsicherheiten bei den Ergebnissen können aber selbst bei einem geringen Anstieg der globalen Mitteltemperatur gravierende Veränderungen der hydrologischen Bedingungen in vielen anderen Teilen der Welt nicht ausgeschlossen werden.

Die Abschätzung des Wasserverbrauchs in der globalen Viehwirtschaft zeigt, dass jährlich etwa 4666 km^3 Wasser für die Produktion von Tierfutter verbraucht werden. Dies entspricht etwa 44 % des gesamten Wasserverbrauchs für die vom Menschen genutzte landwirtschaftliche Biomasse. Durch ein verbessertes Management sowohl in der Futtermittelproduktion als auch in der Tierhaltung können bei Schweinen und Geflügel große Verbesserungen der Wasserproduktivität erzielt werden. Bei Wiederkäuern liegt das größte Potenzial in der Verbesserung der Tierhaltung. Verbesserungen in der Effizienz der Futterverwertung bei Wiederkäuern, die durch eine erhöhte Beigabe von Kraftfutter erreicht werden, gehen jedoch auf Kosten eines höheren Wasserbedarfs für die Futtermittelproduktion, was die Steigerung der Wasserproduktivität verringert. Dieser umgekehrte Effekt der Futterzusammensetzung auf die Wasserproduktivität der Futterproduktion einerseits und die Effizienz der Futterverwertung andererseits beschränkt die erreichbare Wasserproduktivität bei Wiederkäuern erheblich.

Contents

List of Figures

List of Tables

Chapter 1

Introduction

1.1 Setting the scene

1.1.1 Humanity in the Anthropocene

Throughout the Holocene, the current geological epoch that began after the last glacial period about 12 000 years ago, Earth's climate has been remarkably stable (Dansgaard et al. 1993). Under these favourable conditions, humanity has evolved to become a global geophysical force that now surpasses Earth's natural geological forces. Human alterations of biogeochemical cycles, land surface, and the Earth's energy balance are so profound that it warrants the definition of a new human-dominated geological epoch: the Anthropocene (Steffen et al. 2007). Although the exact beginning of the Anthropocene is still debated (Lewis and Maslin 2015), the 'Great Acceleration' in a range of socio-economic and Earth System indicators over the last 50 years provides convincing evidence that humanity has altered the state and functioning of the Earth System beyond the range of variability in the Holocene (Steffen et al. 2015a). Such departure from the Holocene state poses a significant risk to humanity, with detrimental consequences for human wellbeing and development prospects in many parts of the world (Rockström et al. 2009). Humanity has started to take action against its impact on the Earth System, with the Paris climate agreement (UNFCCC 2015) being the most prominent example.

Water plays a pivotal role in the functioning of the Earth System from cellular processes to atmospheric circulation. The global hydrological cycle sustains all terrestrial life and provides humanity with freshwater to fulfil basic human needs (drinking, hygiene, sanitation, food preparation), to produce energy and industrial goods, and to produce various forms of biomass (food, feed, fibre, fuel, wood) (Rockström et al. 2014). Insufficient access to water resources can have adverse effects on human wellbeing, food security, and economic prosperity.

Humanity directly alters the dynamics of the global hydrological cycle through reservoir

operation and withdrawals for industrial, domestic, and agricultural purposes. However, the dominant driver of change in global river discharge over the 20$^{\text{th}}$ century has been climate change (Gerten et al. 2008). With global mean temperature continuing to rise, climate change will remain a major force of change in the hydrological cycle in the 21$^{\text{st}}$ century. How strong these impacts will be and where they occur, crucially depends on the effectiveness of climate mitigation efforts and the response of the climate system and the hydrological cycle to the residual warming.

1.1.2 The global hydrological cycle

An estimated 1386 million km^3 of water on, above and underneath the Earth's surface in solid, liquid, and gaseous form and constitute the hydrosphere (Shiklomanov and Rodda 2003). About 1338 million km^3 of water (96.5 % of the total water in the hydrosphere) is salt water in the world's oceans, which cover 71 % of the Earth's surface. Most of the remaining 48 million km^3 are stored in about equal parts in aquifers (23.4 million km^3) and glaciers (24.1 million km^3). Another 300 000 km^3 are ground ice in permafrost soils, 16 500 km^3 are soil moisture, 12.900 km^3 are water in the atmosphere, and 1120 km^3 are water in living organisms. Last but not least, 190 000 km^3 (0.014 % of all the water in the hydrosphere) are stored in rivers, lakes and wetlands and constitute the water that we commonly perceive as an element of landscapes.

The water in the different compartments of the hydrosphere is connected through the hydrological cycle—the process of constant movement of water within and between these compartments. The hydrological cycle is driven by an imbalance between the radiative budgets of the Earth's surface and the atmosphere. While the Earth's surface has a positive annual mean radiation balance of 106 W/m^2, the atmosphere has a negative radiation balance of the same size (L'Ecuyer et al. 2015). This imbalance drives and is balanced by turbulent fluxes of sensible and latent heat from the surface to the atmosphere. About one quarter (25 W/m^2) is exchanged by the sensible heat flux—the warming and uprise of warm air from the surface. The remaining three quarters of the energy at the Earth's surface (81 W/m^2) are used up in the evaporation of water, which rises to the atmosphere where it condensates and releases the energy. The excess water forms clouds and falls back to the Earth's surface as precipitation.

The amount of water that is transported from the Earth's surface to the atmosphere via the latent heat flux is 2.79 mm/d, which amounts to an annual total water flux into the atmosphere of 520 000 km^3/yr (Rodell et al. 2015)—40 times more than the amount of water stored in the atmosphere. About 449 400 km^3/yr (86.4 %) of this water evaporates from the world's oceans and 70 600 km^3/yr evaporates from the global land surface. The flux of water into the atmosphere is balanced by precipitation, of which 403 500 km^3/yr (77.6 %) fall over oceans and 116 500 km^3/yr over land, implying a net transport of water

from the oceans to the land surface of 45 800 km^3/yr. Ignoring storage change in the terrestrial compartments of the hydrosphere, the same amount of water flows back from the land surface into the oceans. Most of it returns as river discharge, but about 1 % (∼490 km^3/yr; Zhou et al. 2019) enters the oceans as submarine groundwater discharge and about 6 % as ice discharge from Greenland and Antarctica (∼2730 km^3/yr; Mankoff et al. 2019, Rignot et al. 2019).

Before returning to the ocean or the atmosphere, the precipitation over the land surface passes through and sustains the various compartments of the terrestrial hydrosphere. About 10 % of precipitation is intercepted by vegetation and evaporates quickly (typically within the same day), making up about 16 % of the total terrestrial vapour flux to the atmosphere (Dirmeyer et al. 2006). About half of total precipitation is stored in the soil as soil moisture from where it is either taken up by plants and transpires through the stomata of leaves or evaporates directly from the soil surface. Plant transpiration and soil evaporation constitute about 48 % and 36 % of the total terrestrial vapour flux to the atmosphere, respectively. The remaining 42 % of total precipitation run off and enter the river system—either directly from the soil surface or after passing through soils and aquifers.

Additional water—between one quarter and four times of the quantity stored in the hydrosphere—is stored in Earth's mantle (Hirschmann 2006). Exchange between this water and the hydrosphere is only relevant on geological time scales but is has been hypothesised that the hydrosphere has been formed from it by degasification (Sorokhtin et al. 2011).

1.1.3 The role of water in the Earth System

The already mentioned energy exchange between the surface and the atmosphere through latent heat transfer is one of the main linkages between the hydrological cycle and the climate system. Without this process, the Earth's surface would have to have a much higher temperature to emit this energy through increased longwave irradiation and enhanced sensible heat exchange with the atmosphere. This compensating effect of the water cycle does not only act vertically between surface and atmosphere but also horizontally because water vapour can travel large distances in the atmosphere before it releases its heat through condensation and precipitates as liquid water back to the surface.

In addition, clouds and water vapour in the atmosphere also have a direct impact on the radiative balance of the atmosphere, the surface, and the Earth as a whole. Clouds enhance the reflectance of incoming shortwave radiation and are responsible for about 48 % of total reflected solar radiation (Stephens et al. 2012). Clouds also absorb about 7 % of the longwave radiation emitted by the Earth's surface (net effect accounting for irradiation from cloud tops). Together, this amounts to a net cooling effect of 21 W/m^2 (6 % of incoming solar radiation) through clouds. Water vapour in the atmosphere shows very weak interaction with shortwave radiation (Pope and Fry 1997) but is a powerful

greenhouse gas and absorbs about 20 % of the longwave radiation emitted by the Earth's surface (net effect accounting for remittance to the space; Schmidt et al. 2010). As a result, clouds and water vapour in the atmosphere lead to a net gain of 58 W/m^2, which is about twice as much as the gain of 30 W/m^2 from absorption by CO_2 in the atmosphere. However, because the saturation vapour pressure of water increases with temperature (Clausius-Clapeyron relation), the current level of water vapour contained in the atmosphere and the corresponding gain in the radiative balance is sustained by the greenhouse effect of CO_2 and other temperature independent factors.

The water cycle is also tightly linked to the biosphere. Although the water contained in living organisms is one of the smallest compartments of the hydrosphere, life as we know it would not be possible without this water due to the importance of water as a transport medium in cells and organisms and as a solvent in which chemical processes at cellular level take place. Living organisms—by definition—exchange energy and substances with their environment and the uptake and release of water by plants is one of the major fluxes in the hydrological cycle. Terrestrial plants take up CO_2 from the atmosphere through their stomata but at the same time loose water from their leaves' interior to the atmosphere. The loss of water is replenished by water uptake from the soil and generates a water flow to the atmosphere that makes up almost half of total terrestrial evapotranspiration.

The hydrological cycle is also intertwined with geological processes within the Earth system. Precipitation, surface runoff, and river discharge are the main drivers of the withering of rocks and the transport of sediments across landscapes and to the ocean. Annually, about 19 Pg of sediment are transported through rivers to the ocean and with it 197 Tg of organic carbon, 30 Tg of nitrogen, and 9 Tg of phosphorus (Beusen et al. 2005). This continuous transport of material driven by the hydrological cycle is a major force shaping the surface of the Earth and providing nutrient input to coastal ecosystems. Even more important, the hydrological cycle is a key driver in the geochemical carbon cycle. CO_2 dissolved in rain water reacts with silicate rocks and forms calcium and hydrogencarbonate ions, which are transported with runoff and river discharge to the ocean. Marine calcifying organisms use these ions to build carbonate structures (shells and outer skeletons), which sink to the ocean floor and are eventually incorporated into the Earth's mantel by subduction of oceanic crust. Only about 0.12 Gt of CO_2 per year ($\sim$1 % of anthropogenic CO_2 emissions, 0.004 % of atmospheric CO_2) are removed from the atmosphere by this process but it operates persistently over very long time scales and is the main process to balance the release of CO_2 from the Earth's mantle to the atmosphere by volcanism (Ruddiman 2007). Because the chemical weathering of silicate rock is enhanced in warmer climate (due to higher temperature and increased rainfall), the enhanced removal of CO_2 results in lower atmospheric CO_2 content and a reduction of the greenhouse effect. Conversely, CO_2 removal is reduced in colder climate leading to higher atmospheric CO_2 content and

enhanced greenhouse effect. This negative feedback between global mean temperature and geochemical CO_2 removal stabilises Earth's climate on time scales of millions of years.

1.1.4 Human dependence on water resources

Importance of water for the human body

The survival of the human body—like all living organisms—crucially depends on water. About 60 % of the human body weight is water, making it the main constituent of the body (Institute of Medicine 2006). Besides being an important building material, water fulfils many roles in maintaining the proper function of the human body. It is a universal solvent that acts as a reaction medium and a reactant in cellular processes as well as transport medium that supplies nutrients and removes waste (Jéquier and Constant 2010). Also, water plays an important role for regulating body temperature, acts as lubricant in joints and intestines, and provides protection against mechanical shocks for the brain and the foetus.

Water is lost from the body through the respiratory tract, skin, kidneys, and the digestive system. Water evaporates within the lungs and is exhaled at an average rate of 200 ml/d to 600 ml/d, depending on activity and environmental conditions (Institute of Medicine 2006). Water is lost through the skin at a relatively constant rate of 450 ml/d, whereas the rate of sweating varies greatly depending on the need for cooling and can reach as much as 2 l/h (Sawka et al. 2005). Average urine production of a healthy adult is about 1 l/d to 2 l/d but can be much higher or lower depending on body hydration status (Institute of Medicine 2006). Water loss with faeces is about 100 ml/d to 200 ml/d. In total, average daily water loss of an adult amounts to about 2 l to 3 l, which need to be replenished to maintain a healthy hydration status. About 600 ml/d to 750 ml/d are taken up as dietary water with foods and another 300 ml/d are generated by metabolic processes. The remaining 1 l/d to 2 l/d must be met by beverages. This amount increases sharply with increased activity and in warmer environments and can reach up to 12 l/d (Sawka et al. 2005).

Water for human wellbeing, food, and economic prosperity

Drinking water is essential for human survival but many other aspects of human wellbeing are dependent on water as well. Sanitation, bathing, and food preparation are among basic human needs and important to sustain health. Gleick (1996) estimated that every person should have at least 50 l/d available to fulfil the water requirements for drinking and these basic needs.

Large quantities of water are required to produce the food for human consumption. A daily diet of 3000 kcal with 20 % of energy from animal products requires in average 3600 l/d

(Rockström et al. 2007). The vast majority of this water is transpiration by crops and evaporation from agricultural soils and not actually contained in the final foods. Depending on diet composition, climatic conditions, management intensity in the agricultural sector, agricultural water management, and the amount of food losses, the amount of water needed to supply a given amount of calories can vary tremendously (Molden 2007). However, the given average shows the scale of food water requirements compared to water requirements for other human uses.

Water is also an important resource for electricity generation and economic activity. Thermoelectric power plants require water for cooling and many industrial process require water for cooling, cleaning, or as a raw material. Global water withdrawals in 2010 for the manufacturing sector and electricity generation are estimated to $335\,\mathrm{km}^3/\mathrm{yr}$ and $619\,\mathrm{km}^3/\mathrm{yr}$, respectively (Flörke et al. 2013), which amounts to a combined average per capita water use of $376\,\mathrm{l/d}$. However, these are actual uses and it is inherently difficult to estimate normative water needs for electricity and economic prosperity because the required water quantities strongly depend on the type of power generation, the industrial sector, and the technologies in place to use water in the most efficient way.

Green and blue water resources

The water resources used to fulfil water requirements for the various human needs can be distinguished by two fundamental types: blue water and green water (Falkenmark and Rockström 2006).

Blue water is the liquid water in lakes, rivers, and aquifer. It is appropriated by withdrawal directly from these compartments of the hydrosphere with impacts for downstream users and aquatic ecosystems. Blue water can be used to fulfil all types of human water requirements and can be stored and transported to overcome temporal and spatial mismatches between resource availability and water requirements. During use, some of the blue water is incorporated into a product or evaporates and is lost to the atmosphere as vapour (consumptive water use; CWU). With most uses, however, the larger part of the water returns to rivers and aquifers and becomes available again to downstream users. Thus, blue water resources are only depleted by the amount of CWU although water quality might be impaired by pollutants in return flows. The average fraction of CWU in total water withdrawals varies widely among uses from less than 3 % of cooling of thermoelectric power plants (Flörke et al. 2013) to more than half for irrigation of crops (Jägermeyr et al. 2016).

Green water, on the other hand, is soil moisture that originates from rainfall. It is appropriated from natural vegetation by land use change at the cost of reducing the extent of natural ecosystems. Replacing forests with agricultural crops also tends to decrease evapotranspiration and reduces infiltration into the soil, thereby reducing vapour flow to

the atmosphere and increasing runoff (Rockström et al. 2014). Green water can only be used to grow crops, grasses, or other biomass (biofuels, fibre) and the potential to do so is determined by the biophysical factors at a given site. Transport of green water to use at sites that are more favourable is not possible and storage to bridge temporal mismatches only to a limited degree (Jägermeyr et al. 2016). Green water is depleted by plant transpiration and evaporation from the soil surface and therefore is always a consumptive use of water.

Traditionally, water management has focused on freshwater resources in lakes, rivers, and aquifers. But despite its importance for fulfilling many human water needs, the CWU from these sources makes up only 16 % of total CWU when evapotranspiration of rainfed soil moisture on global croplands is taken into account (Rockström et al. 2014). To highlight the importance of rainfed soil moisture in the context of agriculture, the concept of 'green water' was introduced by Prof. Malin Falkenmark in 1995 (Sood et al. 2014).

1.1.5 Human alteration of the hydrological cycle

Humanity—the major force of Earth system change in the Anthropocene—alters the hydrological cycle in many ways. By construction dams and canals, withdrawing water from surface and groundwater bodies, and transporting it over sometimes great distances, humanity intentionally shapes the water cycle to fulfil its freshwater requirements. Global freshwater withdrawals around the year 2010 amount to about 3850 km^3/yr of which about 1430 km^3/yr (37 %) evaporate to the atmosphere and do not return to rivers, lakes, or aquifers (Flörke et al. 2013, Jägermeyr et al. 2016). These quantities appear small compared to 45 800 km^3/yr total global runoff from continents and 70 600 km^3/yr evaporation from the land surface to the atmosphere, but water withdrawals are unevenly distributed over the globe and can have severe local impacts. Many rivers around the world—particularly in China, South Asia, southern Europe, and the Middle East—are at high risk of overuse at least in some parts of the year (Steffen et al. 2015b), and enhanced evaporation from large-scale irrigation projects have been shown to alter local weather systems (Alter et al. 2015). Beyond these changes in total fluxes, the regulation of rivers for freshwater supply, hydropower, and flood protection alters the timing and variability of river flow with severe impacts on riparian ecosystems and sediment transport (Nilsson and Berggren 2006). Construction of dams also leads to enhanced evaporation from enlarged open water surfaces (Destouni et al. 2012) and to fragmentation of many of the world's rivers (Grill et al. 2019).

Not only the management and appropriation of blue water resources but also the appropriation of green water has an impact on the hydrological cycle. Unlike blue water, green water is not appropriated by redirecting water flows but by utilising an existing green water flow (evapotranspiration from natural vegetation) for growing crops, pastures or other

plants. Because cropland and grazing lands tend to have less leaf area, less available energy (higher albedo), and a lower surface roughness than the replaced natural vegetation, evapotranspiration is substantially reduced (Sterling et al. 2013). For example, conversion of forest to (non-irrigated) cropland or grazing land reduces ET in average by 36 % and 32 %, respectively. In total, historic land cover change through cropland and pasture extension has led to a decrease of global terrestrial evapotranspiration by 6.3 % or about 4400 km^3/yr (Sterling et al. 2013), excluding ET enhancement through irrigation. A reduction of moisture input to the atmosphere can lead to a decrease in rainfall in downwind areas with a large contribution of terrestrial evaporation to precipitation (Zemp et al. 2014). On the other hand, the corresponding increase in runoff in principal increases blue water availability but not necessarily in regions with high water demand and may lead to potential unwanted side effects such as increased flood hazard (Rogger et al. 2017).

Apart from the effects of water resource appropriation, a third major pathway for alterations of the hydrological cycle by human activity is the emission of CO_2 (and other greenhouse gases) to the atmosphere. CO_2 and other greenhouse gases (e.g., CH_4 and N_2O) increase the absorption of upwelling longwave radiation by the atmosphere, which leads to a temperature increase in the Earth system.

Driven by anthropogenic emission of greenhouse gases, global mean temperature has increased by 0.72 K to 0.85 K since the beginning of the industrialisation (2003–2012 compared to 1850–1900; Hartmann et al. (2013). This warming was accompanied by changes in many aspects of the climate system connected to the hydrological cycle, which are, however, often difficult to detect in observations due to high temporal variability and lack of data from the early part of the 20^{th} century and before. Changes that can be established with high or very high confidence from available data records include: general increases in near surface air temperature and temperature extremes, increases in near surface air specific humidity and tropospheric water vapour, increases in average and heavy precipitation in parts of the northern hemisphere, increasing droughts in the Mediterranean and West Africa, and decreasing droughts in North America and north-western Australia (Hartmann et al. 2013). General increases in land precipitation, land evaporation, and a decrease in snowfall can be inferred from observations with low or medium confidence, only. In addition, due to feedbacks in the climate system, some trends are not constant over time. For example, the increase in evapotranspiration over land has slowed down after 1998 due to lack of soil moisture availability in the southern hemisphere (Jung et al. 2010).

Apart from the effect on climate, the increase in atmospheric CO_2 concentrations has a direct effect on the biosphere by increasing plant water use efficiency—i.e., the ratio of CO_2 uptake to water lost by transpiration through the stomata (Ciais et al. 2013). Depending on whether the rate of photosynthesis is constrained by water or other environmental factors (e.g., radiation, temperature, or nutrients), the increased water use efficiency is caused

by an increase in the rate of photosynthesis and/or a decrease in plant transpiration, respectively.

Detecting the effect of climate change and increased atmospheric CO_2 concentration on river discharge in observations is not only hampered by temporal variability and availability of long historic records, but also by the presence of other important drivers of hydrological change such as water withdrawals and land cover changes. Modelling studies attempting to attribute changes in river discharge over the 20^{th} century to the different drivers of change indicate that climate change has led to a moderate increase in total continental runoff but is the dominating factor explaining the spatial pattern of runoff change (Piao et al. 2007, Gerten et al. 2008, Alkama et al. 2010). However, the results are subject to large uncertainties in the climate datasets used (Gerten et al. 2008). The effect of increased ambient CO_2 concentrations on 20^{th} century runoff changes is small compared to other effects but further increasing levels of atmospheric CO_2 concentrations throughout the 21^{st} century may lead to a stronger control of transpiration with a corresponding increase in runoff (Piao et al. 2007, Gerten et al. 2008, Alkama et al. 2010).

1.1.6 The challenge ahead

Already to today, appropriation of blue water resources for human needs infers with water requirements for the environment in many river basins (Steffen et al. 2015b) and in some cases available resource are insufficient to meet water requirements during all parts of the year (Falkenmark and Molden 2008). Likewise, green water use already exceeds the sustainably available green water flow in many regions of the world with adverse effects on terrestrial ecosystems (Schyns et al. 2019).

Without the adoption of water saving technologies, blue water withdrawals are projected to increase by 30 % to 72 % until 2100 depending on assumptions about total population, urbanisation, per-capita GDP, and other socio-economic drivers (Graham et al. 2018). Green water consumption is projected to increase by around 50 % until 2050 in the middle-of-the-road scenario SSP2 (Weindl et al. 2017). Adoption of water saving technologies and changes in dietary patterns can drastically reduce the projected increases in blue and green water requirements but strong increases remain in most scenarios (Graham et al. 2018, Weindl et al. 2017). Estimates of future water requirements are subject to large uncertainties in projected socio-economic drivers and other scenario and modelling assumptions (Wada et al. 2016). However, most studies of future water requirements indicate a general increase in global water demand and even in scenarios where global water demand is projected to decline, increases still occur in many locations (Wada et al. 2016, Bijl et al. 2016, Graham et al. 2018). To meet growing demands, investments in water management infrastructure (e.g., reservoirs, canals, purification) are needed. However, in situations where a lack of water resources restricts a further increase in supply, demand side

measures become unavoidable. Such measures range from technical solutions to improve water use efficiency to prioritisation of water allocation between competing uses and may carry high economic and social costs (Ohlsson and Turton 1999).

In addition to increasing water demand, human alterations of the hydrological cycle pose great challenges for future water management. In particular, climate change has the potential to aggravate the challenge of fulfilling future water demands by reducing available water resources, increasing hydrological variability, and increasing agricultural water demand through enhanced evapotranspiration, (Jiménez Cisneros et al. 2014). Renewable freshwater resources are projected to decline under climate change in many already dry mid-latitude and subtropical regions such as the Mediterranean, parts of southern Africa, and parts of South and East Asia. Increases are projected for high-latitude regions such as the temperate and boreal zone and the humid tropics but even there, changes in seasonality and higher variability of streamflow can lead to more frequent and pronounced temporary shortages. Basic physical principles dictate that potential evapotranspiration increases with higher temperatures, but changes in actual evapotranspiration also depend on other uncertain factors such as changes in soil moisture and the response of plants to elevated atmospheric CO_2 concentrations and different climate conditions.

Hydrological change is particularly challenging for the design of freshwater supply infrastructure such as reservoirs and canals (Milly et al. 2008, Hallegatte 2009). Because of their long lifetimes, such infrastructure has to be designed to operate equally well under both present and future hydrological condition. This is aggravated by the large uncertainties in projections of climate-related hydrological change, which makes planning more difficult and increases construction costs. Hydrological change affecting green water availability can be addressed by a broad range of strategies like rainwater harvesting (Jägermeyr et al. 2016), change in on-field residue management and tillage practices (Lutz et al. 2019), or by managing risks through insurance schemes (Vermeulen et al. 2012). Such changes in agricultural management practices and risk management can be implemented incrementally in response to changing conditions (Vermeulen et al. 2013) and are easily reversible, which makes them well suited to deal with projection uncertainties. However, such measure are insufficient to adapt to higher levels of climate change and large-scale transformative changes like a shift from rainfed to irrigated agriculture or from crop production to livestock rearing may be needed, entailing large social and economic costs (Vermeulen et al. 2013).

1.2 Research questions

Increasing water demand driven by socio-economic change and climate change impacts on human water resources pose the biggest challenges for the water sector in the Anthropocene. Understanding and quantifying the hydrological change caused by climate change, its uncertainties, and its consequences for water resource availability are important for informing negations about climate mitigation efforts and the development of adaptation strategies in the water sector alike. Exploiting opportunities to reduce anthropogenic water demand can make an important contribution to adaptation to reduced water availability but also lower the environment impacts of water resource use. Thus, the overarching research question of this thesis is:

How will climate-related changes in the hydrological cycle affect the availability of water resources, and what opportunities exist to reduce anthropogenic water use to lower the pressure on water resources?

Chapters 2 to 6 constitute the main part of this thesis and address the following three different aspects of the overarching research question.

What is the impact of different levels of global warming on river discharge?

A large body of literature is concerned with this topic, but most studies assess climate-related hydrological change by comparing scenarios of greenhouse-gas emissions or radiative forcing. This is inapt to inform the ongoing political debate and negotiations about climate change mitigation, which have become centred around temperature targets. Chapters 2, 3 and 5 of this thesis aim to fill this gap by assessing climate change impacts on river discharge for different levels of global mean temperature increase. Chapter 4 provides the description of a new climate dataset specifically designed for such temperature-stratified analyses of climate change impacts, which is used in chapter 5. To quantify the uncertainty in projection of river discharge, chapters 2 and 3 analyse results from an ensemble of hydrological models forced with climate projections from several different general circulation models (GCMs). Chapter 5 is based on a single hydrological model but uses the full ensemble of 23 different GCM patterns provided by the forcing data set described in chapter 4 to account for climate projection uncertainty. All three studies analyse climate-related changes in mean annual discharge but chapter 3 also analyses the effects of anthropogenic water withdrawals and chapter 5 also analyses changes in other properties of streamflow, namely hydrological droughts and flood hazards.

How do climate-related changes in river discharge affect human water resources?

Building on the analysis of changes in river discharge, chapters 2, 3 and 5 assess how these changes affect human water resources. Chapter 2 focusses on number of people affected by severe decreases in mean annual discharge and changes in number of people affected by water scarcity. Looking beyond changes in mean water availability, chapter 5 assesses the number of people affected by a severe decrease in mean annual discharge, a severe increase in the number of drought month, or a severe increase in the magnitude of flood hazards. The population pressure on water resources without climate change is used to determine where adaptation to these changes will be particularly challenging. Chapter 3 analyses changes in anthropogenic water withdrawals driven by climate change impacts on river discharge and changes in irrigation water demand.

How much water is used by the global livestock sector, and what are the opportunities and constraints for improving water productivity?

The agricultural sector is by far the biggest anthropogenic water user (Hoekstra and Mekonnen 2012) with large a contribution originating from feed production for livestock. Driven by increasing demand for animal sourced foods, water use for livestock feed is projected to increase further in the coming decades (Weindl et al. 2017). While assessments of the potential to reduce livestock water use focus on dietary choices, the possibilities to increase livestock water productivity by appropriate management interventions have received little attention. Based on a new and highly detailed global dataset of feed use and livestock production (Herrero et al. 2013), chapter 6 provides a comprehensive assessment of livestock water use and livestock water productivity in the global livestock sector. By analysing the variations in water productivity of feed production and feed use efficiencies of livestock systems, potential opportunities but also the constraints to improving livestock water productivity are assessed.

1.3 Methodology

1.3.1 Temperature-stratified analysis of climate change impacts

The majority of scientific literature concerned with the analysis of climate change impacts relies on climate projections generated by GCMs within the Coupled Model Intercomparison Project (CMIP). Within the different iterations of the project, GCMs from various working groups were forced with four scenarios of greenhouse-gas emissions (CMIP3; Meehl et al. 2007b) or four scenarios of radiative forcing (CMIP5; Taylor et al. 2012). This resulted in model ensembles of climate projections driven by a very small selection of possible

forcing scenarios. In the past, impact studies have mostly followed the design of the CMIP experiments and have focussed on comparing the outcomes of the different forcing scenarios. While this approach generates useful information to assess the sensitivity of different regions and different domains (water cycle, biosphere, agriculture, etc.) to climate change (IPCC 2007b, 2014)), it falls short on providing the detail required to evaluate the efficacy of mitigation measures. In addition, the political debate on climate mitigation has become increasingly centred around temperature targets (levels of global mean temperature increase), which requires climate change impact assessments that analyse impacts at different levels of global mean temperature increase in a systematic manner.

All assessments of climate change impacts on the water cycle and human water resources within this thesis (chapters 2, 3 and 5) employ a temperature-stratification approach to analyse the consequences of global warming as a function of global mean temperature increase. The analyses in chapters 2 and 3 are based on model simulations using CMIP3 and CMIP5 climate projections. The temperature stratification is achieved by determining the time periods in theses projections (31 and 30 years long, respectively) during which the levels of global mean temperature increase of interest are reached. Climate impacts are evaluated by calculating changes in these time periods relative to a reference period that represents present-day conditions. While relying on available climate projections and being easy to implement, this method comes with the major caveat that the same level of global mean temperature increase is reached in different years in different GCM projections and lower levels are generally reached earlier than higher levels. When climate-driven changes from these time periods are combined with corresponding atmospheric CO_2 concentrations and socio-economic data from these time periods (e.g., population data to assess exposure to changes in water availability as in chapter 2), the result is affected by the differences in these variables at different points in time and the effect of climate change alone is difficult to isolate. Another major disadvantage is that the range of global mean temperature increase that can be analysed is constrained by the maximum level reached by the 'coldest' GCM in the ensemble, as otherwise the GCM sample would differ at different temperature levels. A third problem that is not unique to this specific approach, however, is the existence of inter-annual variability in climate projections, which hampers the estimation of differential impacts for small increments of global mean temperature increase (James et al. 2017).

To address these shortcomings, a new dataset of climate scenarios was developed, which is described in detail in chapter 4 and applied in the analysis in chapter 5. The dataset is based on a pattern-scaling approach (Mitchell 2003, Osborn et al. 2016) using monthly normalised climate change patterns (regional changes for each month of the year per 1 K of global mean temperature increase) of 19 different GCMs from the CMIP3 multi-model dataset for near-surface air temperature, cloud cover, monthly precipitation sum, and rain-month frequency. The patterns were used to compute monthly time series of regional

climate anomalies for the global land area at 0.5 degree resolution for 8 different pathways of global mean temperature increase, reaching 1.5 K to 5 K above the pre-industrial level in steps of 0.5 K around the year 2100 (2086–2115 average; see Figure 4.2). To obtain actual time series of regional climate projections that can be used as input to impact models, the anomalies were applied to monthly time series of reference climate representing present-day climatic average and variability. Reference time series for temperature and cloud cover were derived from the CRU TS3.1 dataset (Harris et al. 2014) and for precipitation from the GPCC full reanalysis dataset version 5 (Rudolf et al. 2010). Because identical reference time series were used for all 8 scenarios, differences between scenarios are only caused by climate anomalies allowing robust detection of impacts even for small changes in global mean temperature increase. The central assumption of pattern scaling is that of a linear relationship between local climate change and global mean temperature increase, which is shown to hold very well for near-surface air temperature and cloud cover, and reasonably well for precipitation (Table 4.2). This is in line with other studies, demonstrating that pattern scaling can be used to emulate regional climate change in both high and low warming scenarios without introducing large errors (Tebaldi and Knutti 2018, Osborn et al. 2018), However, pattern scaling performs less reliable in scenarios in which global mean temperature stabilises or declines after a peak (Tebaldi and Arblaster 2014). The dataset described in chapter 4 proved valuable for the scientific community and has been used, apart from the analysis in chapter 5, in more than ten other studies (e.g., Schaphoff et al. 2013, Boysen et al. 2017, Heck et al. 2018, Stenzel et al. 2019).

1.3.2 Addressing uncertainty by using multi-model ensembles

The assessments of future hydrological conditions relies on the use of numerical models. General Circulation Models (GCMs) are required to obtain climate projections under assumed future developments of radiative forcing caused by the increase in atmospheric greenhouse-gas concentrations. Along with projections of various climatic variables (e.g., temperature, precipitation, radiation), GCMs also provide projections of hydrological variables (e.g., runoff, soil moisture, evapotranspiration), which can be used to assess future hydrological conditions (Milly et al. 2005). However, most studies on climate-driven hydrologic change and corresponding impacts on water resources are based on simulations with standalone (global) hydrological models forced with climate projections from GCMs. This is because GCMs lack many of the processes that are important from a hydrological or water resource perspective (e.g., flow in river channels, water withdrawal for human use, reservoir operation), but are not needed to account for the role of the hydrological cycle in the climate system (e.g., controlling heat and mass change between surface and atmosphere). Despite their greater detail in hydrological processes, global hydrological models are computationally relatively inexpensive, which allows for the incorporation of

additional and more detailed information, and facilitates experiments requiring multiple simulations.

However, both GCMs and hydrological models are only approximate descriptions of real-world systems, and their estimates of past, present, and future conditions are associated with large uncertainties. A large body of literature is concerned with the uncertainty of GCMs (e.g., Gleckler et al. 2008, Knutti and Sedláček 2013, Eyring et al. 2016b) and the different phases of the Coupled Model Intercomparison Project (CMIP) have been designed to synthesise the knowledge from different GCMs, systematically analyse their uncertainties, and to provide the scientific community with multi-model ensembles of climate projections (Meehl 1995, Meehl et al. 2000, 2007b, Taylor et al. 2012). In many cases, the use of a multi-model ensemble has been shown to provide better predictions than using a single model (Palmer et al. 2005, Gleckler et al. 2008, Weigel et al. 2008) and can provide valuable information on the robustness and uncertainties of model projections (Knutti and Sedláček 2013). However, the usefulness of the inter-model spread as a measure for projection uncertainty has been challenged (Stainforth et al. 2007), and interpreting and synthesising the range of different outcomes in a multi-model ensemble remains challenging (Knutti et al. 2010, Flato et al. 2013). A systematic assessment of the uncertainties in global hydrological models was not conducted until the Water Model Intercomparison Project (WaterMIP) was initiated in 2009 as part of the European Union Water and Global Change (EU WATCH) project (Haddeland et al. 2011, Harding et al. 2011). After the end of the project in 2011, this work was continued under the framework of the Inter-Sectoral Impact Model Intercomparison Project (ISIMIP; Warszawski et al. 2014). I have actively been involved in both the WaterMIP and ISIMIP projects, contributing to the development of modelling protocols, performing simulations, and analysing results.

Chapter 2 in this thesis is a direct outcome of the ISIMIP project, analysing climate change impacts on mean annual discharge and human water resources from 11 global hydrological models and 5 GCMs. Chapter 3 synthesises results from both the WaterMIP and ISIMIP projects to obtain a larger ensemble (7 hydrological models and 8 GCMs), analysing impacts of direct human intervention (water withdrawals and reservoir operation) and climate change. Both studies follow IPCC guidelines on treatment of uncertainties (Mastrandrea et al. 2011) in that they do not only provide a best-guess from the ensemble (median or mean) but also analyse the spread of different outcomes. Chapter 5 is based on a single hydrological model but uses the climate dataset described in chapter 4, which provides climate projections consistent with 19 different GCMs from the CMIP3 multi-model dataset. The analysis focusses on determining the level of global mean temperature increase at which severe hydrological change is projected by the majority of the 19 GCMs—a threshold that corresponds to the 'more likely than not' likelihood category defined in the IPCC guidelines (Mastrandrea et al. 2011).

Although chapter 6 is concerned with assessing a present-day situation and projection uncertainty is irrelevant, an ensemble approach using alternative models and datasets would also be useful to assess the uncertainties associated with the obtained estimates. However, many of the datasets used in the analysis are unique and the model simulations are very specific so that large efforts would be needed to run other models in a similar way.

1.3.3 Livestock water use and livestock water productivity

Identifying opportunities to reduce water demand requires information about the water quantities appropriated for different societal and economic activities (water use) and the respective benefits derived per unit of water (water productivity; Batchelor et al. 2017). For the quantification of water use, it is critical to distinguish between consumptive water use, which is evaporated or incorporated in a product, and non-consumptive water use, which is returned to rivers and aquifers (Batchelor et al. 2017). Non-consumptive use of water can impair the quality and timing of river flow for downstream users but does not reduce the amount of available water resources, whereas consumptive water use depletes local water resources. All uses of water (except some in-stream uses) entail at least a fraction of consumptive water use—either because evaporation of water is a direct consequence of its use, water gets incorporated into a product, or because evaporative losses occur during use, storage, or transport. From a water supply perspective, the combined amount of consumptive and non-consumptive use is relevant because it is the quantity, which has to be provided. However, the sum of consumptive and non-consumptive water use over a large domains such as a river basin is difficult to interpret (e.g., it can exceed the total amount of available water resources) because water that is not consumed can be used multiple times. Only the sum of consumptive water use provides an unambiguous measure of water resource depletion. Therefore, water productivity should always be measured against consumptive water use to avoid misinterpretation (van Halsema and Vincent 2012, Batchelor et al. 2017). Unlike blue water use, which can be consumptive and non-consumptive, green water use is always entirely consumptive (Falkenmark and Rockström 2006).

Chapter 6 provides a comprehensive and detailed quantification of consumptive water use and water productivity in global livestock production. Livestock consumptive water use is determined by estimating the part of agricultural ET associated with the production of feed. Agricultural ET thereby does not only comprise soil evaporation, evaporation from interception, and plant transpiration during the growing period (crop ET), but also includes soil evaporation during fallow periods. Previous assessment of livestock water use have only accounted for crop ET (de Fraiture et al. 2007, Mekonnen and Hoekstra 2012, Weindl et al. 2017), but for a meaningful comparison of water use for different feed components (e.g., seasonal crops versus perennial grasses), it is important to relate production to the total agricultural ET associated with it. For blue water, this also includes

evaporative conveyance losses from open canals and leakage from pipelines (Rost et al. 2008). Livestock production also requires blue water for drinking, servicing, and processing but the quantities are very small compared to water use for feed production (<2 % of total livestock water use; Mekonnen and Hoekstra 2012) and are not accounted for in the analysis in chapter 6.

Livestock water productivity in chapter 6 is expressed in kg protein per m^3 of consumptive water use for the production of animal feed. The use of protein as a metric for measuring the output of livestock production is motivated by the role of animal sourced foods as a source of protein rather than energy in the human diet (Smith et al. 2013), and allows to aggregate different products (e.g., milk and meat from dairy system) and to compare different livestock types (e.g., meat producing pigs versus egg producing layer hens). However, the focus on animal sourced foods as the only output from livestock systems ignores important non-food benefits such as traction power, hide production, and insurance against crop failure, which are important for smallholder farmers in developing countries (van Breugel et al. 2010). Accounting for non-food benefits in livestock water productivity can be achieved by expressing output in terms of total economic value (Haileslassie et al. 2009), but the economic value of some benefits like insurance is difficult to define and for those for which it is possible, the required information about prices is often difficult to obtain. In addition, prices can exhibit high variation in space and time, which hampers the comparability of estimates of economic water productivity across different regions and point in time.

Chapter 2

Multimodel assessment of water scarcity under climate change

An edited version of this chapter has been published as: J. Schewe, J. Heinke, D. Gerten, I. Haddeland, N. W. Arnell, D. B. Clark, R. Dankers, S. Eisner, B. M. Fekete, F. J. Colón-González, S. N. Gosling, H. Kim, X. Liu, Y. Masaki, F. T. Portmann, Y. Satoh, T. Stacke, Q. Tang, Y. Wada, D. Wisser, T. Albrecht, K. Frieler, F. Piontek, L. Warszawski, and P. Kabat. Multimodel assessment of water scarcity under climate change. *Proceedings of the National Academy of Sciences of the United States of America*, 111(9):3245–50, 2014. doi: 10.1073/pnas.1222460110

Abstract

Water scarcity severely impairs food security and economic prosperity in many countries today. Expected future population changes will, in many countries as well as globally, increase the pressure on available water resources. On the supply side, renewable water resources will be affected by projected changes in precipitation patterns, temperature, and other climate variables. Here we use a large ensemble of global hydrological models (GHMs) forced by five global climate models and the latest greenhouse-gas concentration scenarios (Representative Concentration Pathways) to synthesize the current knowledge about climate change impacts on water resources. We show that climate change is likely to exacerbate regional and global water scarcity considerably. In particular, the ensemble average projects that a global warming of 2 °C above present (approximately 2.7 °C above preindustrial) will confront an additional approximate 15 % of the global population with a severe decrease in water resources and will increase the number of people living under absolute water scarcity (<500 m^3 per capita per year) by another 40 % (according to some models, more than 100 %) compared with the effect of population growth alone. For some indicators of moderate impacts, the steepest increase is seen between the present day and 2 °C, whereas indicators of very severe impacts increase unabated beyond 2 °C. At the same time, the study highlights large uncertainties associated with these estimates, with both global climate models and GHMs contributing to the spread. GHM uncertainty is particularly dominant in many regions affected by declining water resources, suggesting a high potential for improved water resource projections through hydrological model development.

2.1 Introduction

Freshwater is one of the most vital natural resources of the planet. The quantities that humans need for drinking and sanitation are relatively small, and the fact that these basic needs are not satisfied for many people today is primarily a matter of access to, and quality of, available water resources (Ohlsson and Turton 1999). Much larger quantities of water are required for many other purposes, most importantly irrigated agriculture, but also for industrial use, in particular for hydropower and the cooling of thermoelectric power plants (Wallace 2000, Kummu et al. 2010). These activities critically depend on a sufficient amount of freshwater that can be withdrawn from rivers, lakes, and groundwater aquifers. Whereas scarcity of freshwater resources already constrains development and societal well-being in many countries (Oki et al. 2001, Rijsberman 2006), the expected growth of global population over the coming decades, together with growing economic prosperity, will increase water demand and thus aggravate these problems (Vörösmarty 2000, Arnell 2004, Alcamo et al. 2007).

Climate change poses an additional threat to water security because changes in precipitation and other climatic variables may lead to significant changes in water supply in many regions (Vörösmarty 2000, Arnell 2004, Alcamo et al. 2007, Milly et al. 2005, Fung et al. 2011, Hagemann et al. 2012). The effect of climate change on water resources is, however, uncertain for a number of reasons. Climate model projections, although rather consistent in terms of global average changes, disagree on the magnitude, and in many cases even the sign, of change at a regional scale, in particular when it comes to precipitation patterns (Meehl et al. 2007a). In addition, the way in which precipitation changes translate into changes in hydrological variables such as surface or subsurface runoff and river discharge (i.e., runoff accumulated along the river network), and thus in renewable water resources, depends on many biophysical characteristics of the affected region (e.g., orography, vegetation, and soil properties) and is the subject of hydrological models, which represent a second level of uncertainty (Hagemann et al. 2012, Haddeland et al. 2011).

In the framework of the Inter-Sectoral Impact Model Intercomparison Project (ISI-MIP; Warszawski et al. (2013) in this issue of PNAS) a set of nine global hydrological models, one global land-surface model, and one dynamic global vegetation model (here summarized as global hydrological models (GHMs); Materials and Methods) has been applied using bias-corrected forcing from five different global climate models (GCMs) under the newly developed Representative Concentration Pathways (RCPs). The purpose is to explore the associated uncertainties and to synthesize the current state of knowledge about the impact of climate change on renewable water resources at the global scale. In this paper we investigate the multimodel ensemble projections and the associated spread for changes in annual discharge—taken here as a first-order measure of the water resources available

to humans. We then reconcile these hydrological changes with global population patterns to estimate how many people will be living in areas affected by a given change in water resources. Finally, we apply a commonly used measure of water scarcity to estimate the percentage of the world's population living in water-scarce countries and to quantify the contributions of both climate change and population change to the change in water scarcity. Results are presented as a function of global mean warming above the present day to account for the relative independence of regional temperature, precipitation, and runoff changes of the rate of warming (Frieler et al. 2012, Tang and Lettenmaier 2012) and to allow for systematic comparison of climate change impacts across scenarios and sectors.

2.2 Results

2.2.1 Discharge Trends and Uncertainties

We first consider the spatial pattern of relative change in annual mean discharge at 2 °C global warming compared with present day (the term "present day" in this study refers to the 1980—2010 average, which is ∼0.7 °C warmer globally than preindustrial), under RCP8.5 (Figure 2.1). The multimodel mean across all GHMs and GCMs (Figure 2.1, Upper) exhibits a number of robust large-scale features. In particular, discharge is projected to increase at high northern latitudes, in eastern Africa and on the Indian peninsula, and to decrease in a number of regions including the Mediterranean and large parts of North and South America. In these regions, a relatively high level of agreement across the multimodel ensemble on the sign of change indicates high confidence. Most of these patterns are consistent with previous studies (Alcamo et al. 2007, Hagemann et al. 2012, Arnell et al. 2011, Gosling et al. 2010), but there are also some differences. For example, ensemble projections using the previous generation of GCMs and climate scenarios found a robust runoff increase in southeastern South America (Bates et al. 2008, Füssel et al. 2012), where we find no clear trend, or partly even a drying trend. Whereas those latter studies used larger GCM ensembles, we apply an unprecedented number of GHMs as well as the new RCP climate forcing. At 3 °C of global mean warming, the pattern of change is similar to that at 2 °C, although the changes are enhanced in many regions, and new robust trends emerge in some regions (most notably a strong negative trend in Mesoamerica; Appendix A, Figure A.1).

In other parts of the globe, however, the projections are subject to a large spread across the ensemble. In many regions, forcing by different GCMs yields discharge changes (averaged across GHMs) that are large but of opposite sign (Appendix A, Figure A.2 shows individual maps of precipitation and discharge changes). Accordingly, the spread owing to differences between GCMs dominates the total ensemble spread in these regions (Figure 2.1, *Lower*). By contrast, GHM spread is dominant in many regions that are subject to discharge reductions (e.g., northern and southern Africa). In most other regions showing a

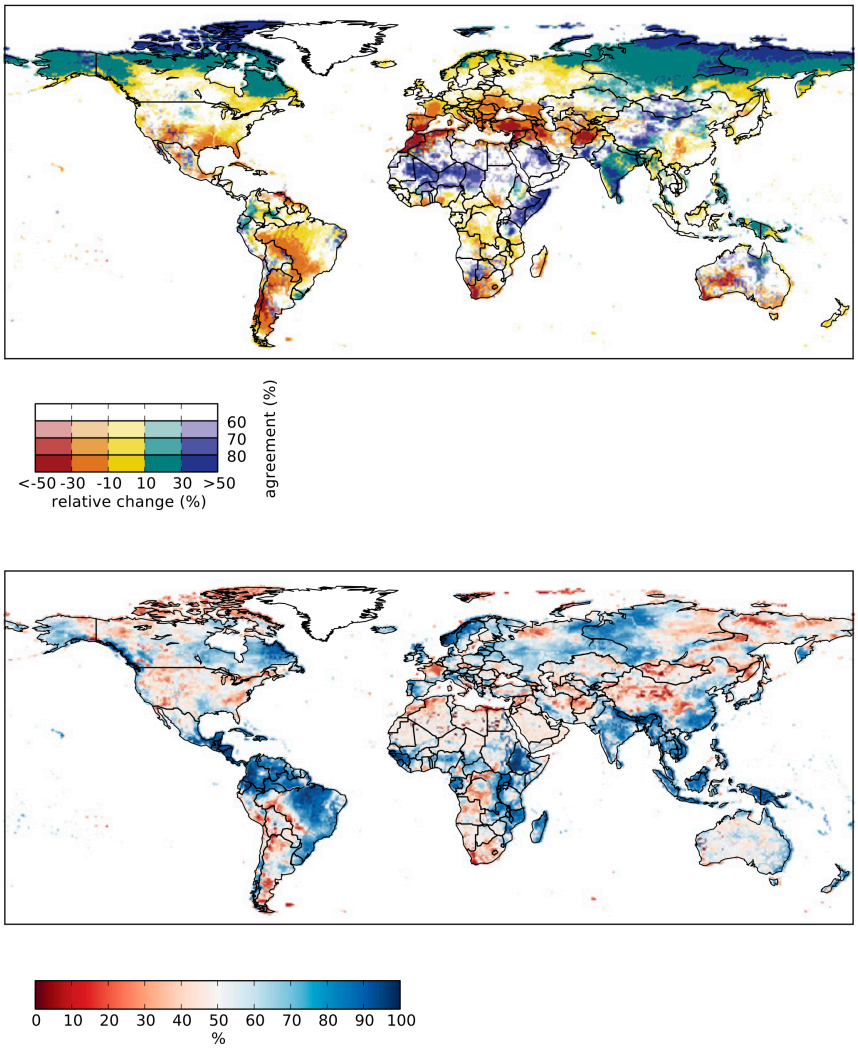

Figure 2.1: Relative change in annual discharge at 2 °C compared with present day, under RCP8.5. (*Upper*) Color hues show the multimodel mean change, and saturation shows the agreement on the sign of change across all GHM–GCM combinations (percentage of model runs agreeing on the sign; color scheme following Kaye et al. (2012)). (*Lower*) Ratio of GCM variance to total variance; in red (blue) areas, GHM (GCM) variance predominates. GHM variance was computed across all GHMs for each GCM individually, and then averaged over all GCMs; vice versa for GCM variance. Greenland has been masked.

large total spread, GHMs and GCMs contribute about equally. Note that the bias correction applied to the GCM data (Materials and Methods) substantially reduces the spread among the GCMs' present-day climatologies, but not among their future temperature and precipitation trends (Hempel et al. 2013).

2.2.2 Population Affected by Severe Changes in Water Resources

To put these discharge changes into a societal perspective, we reconcile them with the spatial distribution of population, using population projections from the newly developed Shared Socioeconomic Pathways (SSPs) (O'Neill et al. 2012). In the following, we will focus on the middle-of-the-road population scenario according to SSP2, which projects global population to increase up to a peak at around 10 billion by the year 2090 and includes substantial changes in relative population densities among countries; constant present-day population will be considered additionally as a reference case.

We first consider two criteria for a severe decrease in average annual discharge, as an indicator of renewable water resources: a reduction by more than 20 % and a reduction by more than 1 SD (σ) of 1980—2010 annual discharge. Both criteria can be seen as first-order indicators of when available water resources consistently fall short of what a given population has adapted to and thus serious adaptation challenges are likely to arise. In many cases, a given discharge decrease may be detected using either criterion. In regions where interannual variability is high but baseline discharge is low, the first criterion is particularly important because even discharge reductions smaller than 1σ can aggravate water stress significantly in these regions. Conversely, in regions with low interannual variability, the second criterion detects low-amplitude changes that may nonetheless require substantial adaptation action as they transgress the range of past variability (e.g., in central and western Africa; Piontek et al. (2014) in this issue of PNAS). Based on grid-cell discharge averaged over 31-y periods that correspond to a given level of global warming, and on gridded population projections (Materials and Methods and Appendix A, Table A.1), we compute the percentage of global population living in countries with a discharge reduction according to either or both of the criteria (Figure 2.2). With global mean warming on the horizontal axis, the differences between the different RCPs in this population-weighted metric, as well as in globally averaged runoff, are small and in the range of interdecadal variability (Appendix A, Figure A.3), meaning that these global, long-term indicators do not depend strongly on the rate of global warming. We therefore concentrate on RCP8.5 (the only RCP compatible with >3 °C warming by 2100) to span a large range of temperature levels, while noting that on smaller spatial and temporal scales larger dependencies on the warming rate as well as on climate model internal variability might be observed (Heinke et al. 2012).

The multimodel median (MMM) suggests that even a relatively modest global warming

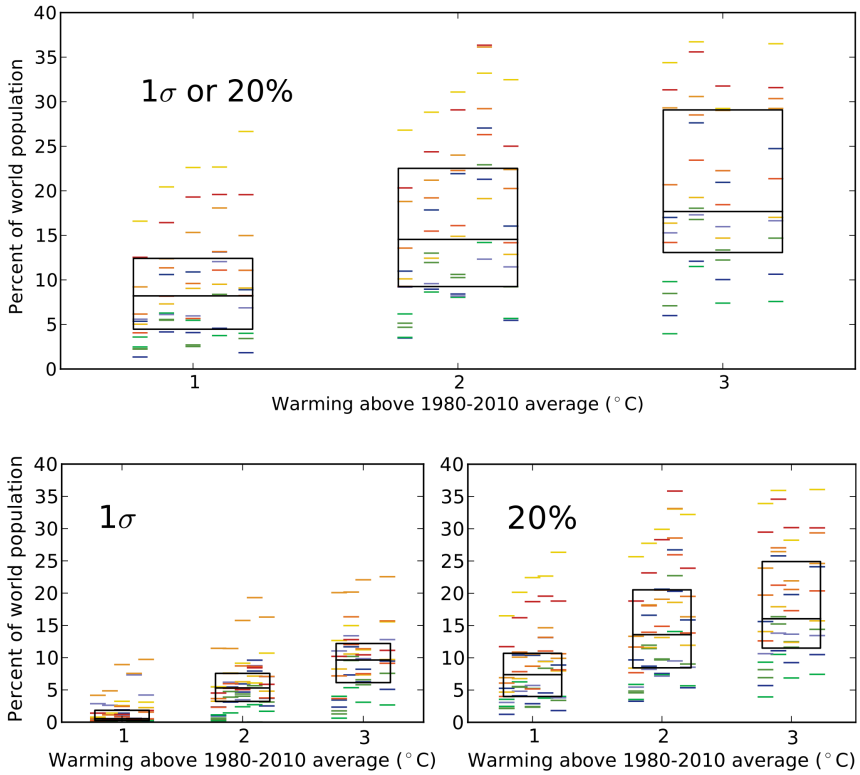

Figure 2.2: Adverse impact of climate change on renewable water resources at different levels of global warming. Markers show the percentage of the world population living in $0.5^\circ \times 0.5^\circ$ grid cells where the 31-y average of annual discharge falls short of the 1980—2010 average by more than 1σ (SD of annual discharge during 1980—2010), or by more than 20 %, under the RCP8.5 climate scenario and SSP2 population scenario. The five GCMs are displayed in separate vertical columns (in the order in which they are listed in Materials and Methods; note that only four GCMs have sufficient coverage of the 3 °C warming level), and the 11 GHMs are displayed in unique colors. The black boxes give the interquartile range, and the horizontal black lines the median, across all GCMs and GHMs.

of 1 °C above present day will lead to a severe reduction in water resources, by at least one of the two criteria, for about 8 % of the global population. This figure rises to about 14 % for 2 °C and 17 % for 3 °C. When only one criterion is applied, the numbers are somewhat smaller (Figure 2.2, *Lower*): At 2 °C, about 13 % (6 %) of the global population is projected to experience a discharge reduction >20 % (>1σ). When a stricter criterion of a discharge reduction >40 % or >2σ is used, about 5 % of the global population is affected at 2 °C, according to the MMM (Appendix A, Figure A.4).

Importantly, however, the spread across the multimodel ensemble is large. For a few GHM–GCM combinations, the figure for the 20 % or 1σ criterion never exceeds 10 %, whereas others project that more than 30 % of the global population will already be affected at 2 °C. Note that in many of the regions that experience the strongest relative reduction in discharge, GHM variance is larger than GCM variance (Figure 2.1, *Lower*). Accordingly, the spread across GHMs in Figure 2.2 is comparable to or even larger than the spread across GCMs. Moreover, the two models included in the study that simulate vegetation distribution and dynamics (green markers in Figure 2.2) yield generally smaller reductions in water resources than most stand-alone hydrological models, suggesting systematic differences between the two types of models (Davie et al. 2013). Sensitivity experiments confirm that the effect of additional CO_2 fertilization of vegetation on the hydrology is comparatively small (Piao et al. 2007) (Appendix A, Figure A.5). Dynamic vegetation changes or details of the parameterizations of evapotranspiration may contribute to the divergence as well, but this requires a more systematic investigation.

The metric discussed here (percentage of population experiencing a given discharge change) depends on the population scenario only through the geographical distribution of population, not through the global totals. Holding the total and the geographical distribution of population constant at the year-2000 level suggests slightly lower impacts, indicating that under SSP2 the population increase is, on average, somewhat stronger in regions affected by discharge reductions than in other regions (Appendix A, Figure A.4). This, however, has only a relatively small effect at the global scale.

As seen in the previous section, the projected changes in discharge are regionally very heterogeneous, with water resources decreasing in many regions but increasing in others. Grouping the world population into categories of percentage discharge change (e.g., 10 % to 30 % increase/decrease, measured by the multimodel mean; Appendix A, Figure A.6), the number of people falling into a given increase category is often very similar to the number of people falling into the corresponding decrease category. Combined with up to ∼15 % of the global population who are projected to experience increases exceeding 10 % of today's discharge, overall more people will be affected by discharge increases than will be by decreases. Whereas such increases may enhance actual water availability in many cases, they can also entail adverse impacts such as increasing flood risk, deteriorating water

quality, and malfunctioning of water-related infrastructure (Kundzewicz et al. 2008).

2.2.3 Water Scarcity

The impact metric considered in the previous section measures, at the grid-cell level, significant departures from present levels of resource availability, irrespective of what those levels are. It is thus an indicator of adaptation challenges that may arise, but not necessarily of resource scarcity in an absolute sense. Moreover, because most water is used for irrigated agriculture, which does not necessarily take place in the same location where people live, water scarcity can be assessed more appropriately on a larger spatial scale than on the grid-cell level. A widely used, simple indicator of water scarcity, the water crowding index (Falkenmark et al. 1989, 2007), relates water resources to population at the country scale. Defined originally as the number of people depending on a given resource unit, we use the inverse (i.e., annual mean water resources per capita). Considering only supply-side changes, this indicator is suitable for assessing the impact of climate change on physical water scarcity, whereas the actual water stress experienced by people will also depend on changes in per-capita water requirements and uses (Ashton 2002). We base our water scarcity assessment on the "blue" water (BW) resource (Gerten et al. 2011), defined here as runoff redistributed across the river basin according to the distribution of discharge (Materials and Methods). Compared with using discharge itself, this avoids counting a given water unit more than once, while retaining the spatial distribution of discharge across the basin. The latter is important, for example, in countries like Egypt, where most of the available water resource is generated by runoff outside the country (in this case, in the Nile River headwaters).

We consider the percentage of global population in either of two water scarcity classes: annual BW availability below $500\,\mathrm{m}^3$ per capita (also termed absolute water scarcity) and below $1000\,\mathrm{m}^3$ per capita (chronic water scarcity). The MMM suggests that at present $\sim$1.5 % and $\sim$3 % of the global population fall into these two scarcity classes, respectively (the first class being a subset of the second; Figure 2.3 *A* and *B*). This is similar to previous estimates at the country level (Arnell 2004) but much lower than estimates done at the grid-cell level (Oki et al. 2001, Arnell et al. 2011) or river basin level (Arnell 2004) because larger countries may not be classified as water-scarce even though significant parts of their population live in water-scarce grid cells. Whereas the country level might in some cases be too coarse for a realistic assessment of water scarcity and generally underestimate the global figure, the grid-cell level likely overestimates it because water transfers between grid cells (and also virtual water imports related to trade of water-intensive goods (Hanasaki et al. 2010)) are large in reality.

Our present-day estimate is already subject to a significant spread across the multimodel ensemble (ranging from 0 % to 4 % for the $<500\,\mathrm{m}^3$ class and 1 % to 8 % for the $<1000\,\mathrm{m}^3$

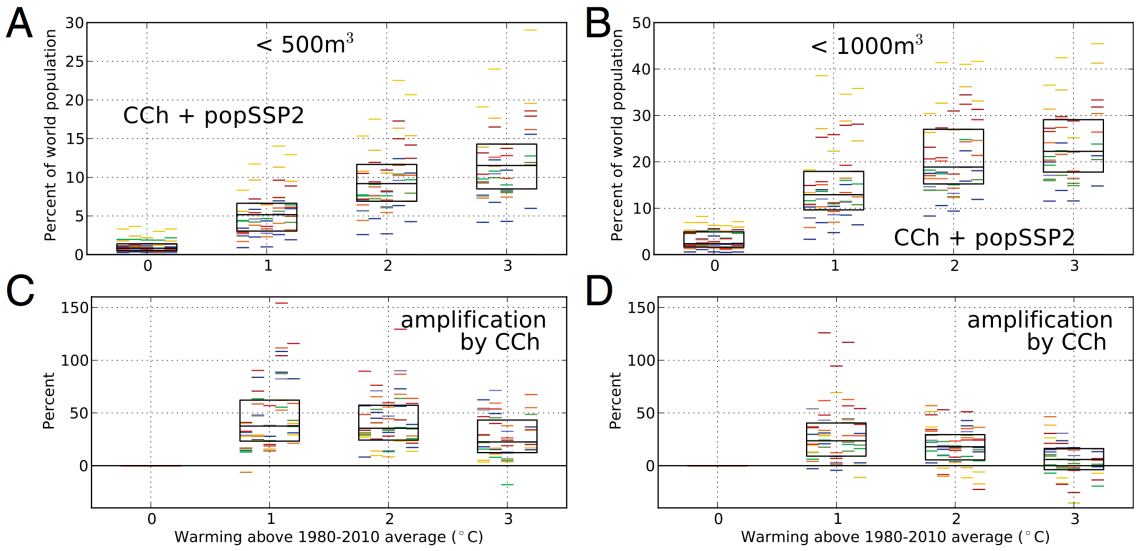

Figure 2.3: Percentage of world population living in countries with annual mean BW availability (Materials and Methods) below 500 m^3 per capita (*Left*) and below 1000 m^3 per capita (*Right*). Symbols as in Figure 2.2. (*A* and *B*) RCP8.5 climate scenario, population change according to SSP2. (*C* and *D*) Amplification by climate change of the level of water scarcity that is expected from population change alone; computed as the difference between a constant-climate scenario (Appendix A, Figure A.7) and the full scenario shown above, divided by the constant-climate scenario, and expressed as percentage (so that the population-only case equals 100 %). For example, in *C*, the MMM indicates that at 2 °C global warming, climate change amplifies the level of absolute water scarcity (number of people below 500 m^3 per capita) expected from population change alone by about 36 %.

class), owing mainly to differences in present-day discharge simulated by the different GHMs ((Haddeland et al. 2011)). The present-day discharge estimates also depend to a certain extent on the observation-based dataset that was used for bias-correcting the climate input data (Materials and Methods). Under the SSP2 population scenario (and again using 31-y averages associated with the different warming levels), the percentage of people living in countries below 500 m^3 per capita (1000 m^3 per capita) is projected to rise to 6 % (13 %) at 1 °C, 9 % (6 %) at 2 °C, and 12 % (24 %) at 3 °C of global warming, according to the MMM (Figure 2.3 *A* and *B*). The high rates of rise between present-day and 1 °C could be partly related to the fact that the present-day estimate is very low, and different spatial scales of analysis may lead to different relative changes.

Population growth plays a major role in this increase in water scarcity because it reduces per-capita availability even with unchanged resources. To separate the population signal from the climate signal, we use each model combination's average 1980-–2010 discharge pattern to compute the percentage of people that would fall into a scarcity class if climate were to remain constant and population changed according to SSP2 (Appendix A, Figure A.7).

As found in previous studies (Vörösmarty 2000, Gerten et al. 2011, Hanasaki et al. 2010), population change explains the larger part of the overall change in water scarcity. Subtracting the constant-climate scenario from the full scenario and dividing by the constant-climate scenario indicates by how much the level of water scarcity expected owing to population change alone is amplified by climate change (Figure 2.3 *C* and *D*). According to the MMM, this amplification is nearly 40 % for the <500 m^3 class at 1 °C and 2 °C global warming. The factor is somewhat lower (approximately 25 %) at 3 °C, indicating that at this level of warming the effect of additional climate change on this global metric becomes smaller compared with the effect of population changes. Note that this is partly related to the relative timing of warming and population change: In an even faster-warming scenario than RCP8.5, a warming from 2 °C to 3 °C might still have a relatively larger impact because it would be associated with generally lower population numbers. This observation illustrates how climate change and population change combine to aggravate global water scarcity: A country can move toward the water scarcity threshold both through population growth and through declining water resources, and depending on the relative rates of change, it may be one or the other factor that eventually causes the threshold to be crossed.

Along similar lines, for the ≤1000 m^3 class, the MMM amplification due to climate change is nearly 30 % at 1 °C, drops to about 20 % at 2 °C, and is close to zero at 3 °C. A number of model combinations yield negative values in Figure 2.3 *C* and *D*; in these cases, climate change is projected to alleviate the global increase in water-scarce population that is expected owing to population change. The GHMs projecting a positive effect of

climate change on chronic water scarcity (i.e., yielding negative values in Figure 2.3 *D*) are primarily models that show a large number of people in this scarcity class in the first place (yellow and red markers in Figure 2.3 *B*). This suggests that in these models many countries in regions that get drier are already in this class at present, such that the potential for additional countries to move into the class is smaller compared with the potential for countries to move out of the class in regions that get wetter.

2.3 Discussion

Our multimodel assessment adds to extensive previous work, in particular in the framework of the European Union Integrated Project Water and Global Change (EU-WATCH) and Water Model Intercomparison Project (WaterMIP) (Haddeland et al. 2011), which demonstrated that hydrological models are a significant source of uncertainty in projections of runoff and evapotranspiration (Hagemann et al. 2012). The present study, using a larger ensemble ensemble of GHMs and GCMs and the state-of-the-art RCP climate forcing available from Coupled Model Intercomparison Project Phase 5 (CMIP-5), explores the range of uncertainty not only in hydrological change but also in its effect on people. Results are mapped against global mean temperature increase to allow direct comparison of the impacts at different levels of global warming.

It is important to note that our globally aggregated water scarcity estimates can obscure potentially much more severe changes at the scale of individual countries or locations. For example, if a number of countries were to move into a given water scarcity class, but at the same time other countries with a similar share of global population were to move out of this class, the resulting change on the global scale would be close to zero. Likewise, if the amplification of the global water scarcity signal by climate change becomes small at higher levels of warming, as seen in Figure 2.3 *C* and *D*, this could mean that climate change continues to force additional countries into the scarcity class, but at the same time other countries move out of the class (e.g., because of more pronounced regional precipitation increases at this temperature level). The results in Figure 2.3 must thus be interpreted with care, and the numbers in Figure 2.3 *C* and *D* in particular are more likely to represent a lower bound to the climate change contribution in regions that are affected by a discharge decrease. Moreover, changes within a given water scarcity class are not detected here but can be very important. Countries that are already extremely water-scarce will be all the more vulnerable to even small decreases in resource availability.

Although the water crowding index is an appropriate measure for supply-side effects on global water scarcity, it is not a measure of the actual problems that countries and people face in satisfying their water needs because it does not take the demand side into account. Future water stress (as measured, for instance, by the ratio of water use to

availability) will depend on changes in demand, for example, related to economic growth, lifestyle changes, or technological developments, as well as on water management practices and infrastructure. Alternative sources of water for agriculture, such as "green" water contained in the soil (Gerten et al. 2011, Rockström et al. 2009, Rost et al. 2008), and nonrenewable water resources (Taylor et al. 2013, Wada et al. 2010), also affect actual BW requirements.

We have only considered long-term averages, neglecting potential changes in the interannual and seasonal availability of water resources and their variability (Fung et al. 2011, Gosling et al. 2011). Changes in seasonality can have severe impacts even if the annual average is stable e.g., if irrigation water availability in the growing season changes, or if flood hazard is affected by changes in snow-melt runoff (Dankers et al. (2014) in this issue of PNAS). Again, infrastructure such as dams and reservoirs can substantially alter the timing of water resource availability (Biemans et al. 2011). Moreover, hydrological changes can have consequences going far beyond the availability of water resources for human uses, for instance, by altering the occurrence of damaging extreme events like floods and droughts (Prudhomme et al. (2013) in this issue of PNAS), affecting aquatic and terrestrial ecosystems (Gerten et al. 2007), and potentially interacting with, and amplifying, climate change impacts in other sectors (Parry et al. 2001).

2.4 Conclusions

We have synthesized results from 11 GHMs with forcing from five GCMs to provide an overview of the state of the art of modeling the impact of climate change on global water resources. In all metrics considered, we find a considerable spread across the simulation ensemble. GHMs and GCMs contribute to similar extents to the spread in relative discharge changes globally. When changes in water scarcity are considered, GHM spread is in fact larger than GCM spread. This finding suggests that, although climate model uncertainty remains an important concern, further impact model development promises major improvements in water scarcity projections.

The multimodel mean projected changes in annual discharge are spatially heterogenous. As the planet gets warmer, a rising share of the world population will be affected by severe reductions in water resources, measured as deviation from present-day discharge in terms of either SD or percentage. However, a similar fraction of the population will experience increases in average discharge, which could potentially improve water availability, but also entail adverse effects.

Our estimate of water scarcity at the country scale indicates that climate change may substantially aggravate the water scarcity problem. Depending on the rates of both population change and global warming, the level of water scarcity expected owing to population

change alone is amplified by up to 40 % owing to climate change, according to the multimodel mean; some models suggest an amplification by more than 100 %. This adds up to between 5 % and 20 % of global population likely exposed to absolute water scarcity at 2 °C of global warming. For chronic water scarcity, most adverse climate change impacts already occur between present day and 2 °C, whereas beyond this temperature positive and negative additional impacts of climate change are of a similar magnitude (although they affect different groups of people and therefore cannot be offset against each other). However, absolute water scarcity continues to be substantially amplified by climate change on the global scale even beyond 2 °C. We conclude that the combination of unmitigated climate change and further population growth will expose a significant fraction of the world population to chronic or absolute water scarcity. This dwindling per-capita water availability is likely to pose major challenges for societies to adapt their water use and management.

2.5 Materials and Methods

2.5.1 Models and Data

The GHMs used in this study are the DBH (Tang et al. 2007), H08 (Hanasaki et al. 2008a), Mac-PDM.09 (Gosling and Arnell 2011), MATSIRO (Takata et al. 2003), MPI-HM (Stacke and Hagemann 2012a), PCR-GLOBWB (Wada et al. 2010), VIC (Liang et al. 1994), WaterGAP (Döll et al. 2003), and WBMplus (Wisser et al. 2010) hydrological models, the JULES (Best et al. 2011) land-surface model, and the LPJmL (Bondeau et al. 2007) dynamic global vegetation model; the latter two also represent vegetation dynamics in addition to hydrological processes. Appendix A, Table A.2 gives further model details. Forcing data were derived from climate projections with the HadGEM2-ES, IPSL-CM5A-LR, MIROC-ESM-CHEM, GFDL-ESM2M, and NorESM1-M GCMs under the RCPs (Moss et al. 2010), which were prepared for the CMIP-5 (Taylor et al. 2012). All required climate variables have been bias-corrected (Ehret et al. 2012) toward an observation-based dataset (Weedon et al. 2011) using a newly developed method (Hempel et al. 2013) that builds on earlier approaches (Hagemann et al. 2011) but was specifically designed to preserve the long-term trends in temperature and precipitation projections to facilitate climate change studies. GHMs were run without direct coupling to GCMs, so that potential feedbacks (e.g., from GHM-simulated evapotranspiration on precipitation) were not represented. Further details about the GHM simulations can be found in the ISI-MIP simulation protocol available at `http://www.isi-mip.org/`. Country-level United Nations World Population Prospects (historical) and SSP (projections) population data at a 5-y time step were obtained from the SSP Database at `https://secure.iiasa.ac.at/web-apps/ene/SspDb` and linearly interpolated to obtain annual values. A gridded population dataset was also used in which the National Aeronautics and Space Administration GPWv3 y-2010 gridded population

dataset (`http://sedac.ciesin.columbia.edu/data/collection/gpw-v3`) was scaled up to match the SSP country totals (neglecting changes in population distribution within countries).

2.5.2 Temperature Axis

Global mean temperature is calculated from the GCM data (including ocean cells) and presented as the difference from the 1980-–2010 average. For each GCM and RCP, 31-y periods are selected whose average temperature corresponds to the different levels of global warming (Appendix A, Table A.1; note that GFDL-ESM2M does not reach the 3 °C warming level). Population affected by discharge changes (Figure 2.2) was calculated using the population distribution corresponding to the middle year of each individual 31-y period (except for the baseline period 1980—2010, which was assumed to correspond to year-2000 population). Water scarcity (Figure 2.3) was calculated annually, using annual population values, and then averaged over the 31-y periods; results for the 0 °C baseline were obtained from the "constant-climate" run, that is, using 1980—2010 average BW resources and annual population values (discussed in the following section).

2.5.3 Water Scarcity

For assessing country-scale water scarcity, we calculate the annual mean BW resource availability following Gerten et al. (2011): The sum of annual mean runoff R in each river basin b is redistributed across the basin according to the relative distribution of discharge Q, yielding the BW resource in each grid cell i:

$$BW_i = R_b Q_i \Big/ \sum Q_i \tag{2.1}$$

where Σ is the sum over all grid cells in basin b. BW is then summed up over all grid cells within a country and divided by the country's population to yield the water crowding index. Finally, for each year, the total number of people living in countries that are below a given threshold of this index (500 m^3 or 1000 m^3 per capita) is calculated and divided by global population to yield the corresponding percentage of world population. Results are again averaged over the 31-y periods that correspond to the different levels of global warming shown in Figure 2.3 *A* and *B*. For the climate change contribution shown in Figure 2.3 *C* and *D*, the subtraction of, and division by, the results from the constant-climate run is done year by year, and the resulting percentage is averaged over the 31-y periods.

2.5.4 Ensemble Statistics

Statistics across the multimodel ensemble were computed after the calculation of the respective metric. For instance, in Figure 2.1 the relative change in discharge was calculated for each model combination individually before computing the multimodel mean, agreement, and variances.

Supplementary material related to this chapter is available in Appendix A.

Acknowledgments

The authors acknowledge the World Climate Research Programme's Working Group on Coupled Modelling, which is responsible for the Coupled Model Intercomparison Project, and thank the climate modeling groups for producing and making available their model output. J.S. wishes to thank A. Levermann for helpful discussions. This work has been conducted under the framework of the Inter-Sectoral Impact Model Intercomparison Project (ISI-MIP). The ISI-MIP Fast Track project underlying this paper was funded by the German Federal Ministry of Education and Research with project funding reference number 01LS1201A. R.D. was supported by the joint Department of Energy and Climate Change/Defra Met Office Hadley Centre Climate Programme (GA01101). F.J.C.-G. was jointly funded by the European Union Seventh Framework Programme Quantifying Weather and Climate Impacts on health in developing countries and HEALTHY FUTURES projects. S.N.G. was supported by a Science, Technology and Society Priority Group grant from University of Nottingham. Y.M. was supported by the Environment Research and Technology Development Fund (S-10) of the Ministry of the Environment, Japan. F.T.P. received funding from the European Union's Seventh Framework Programme (FP7/2007-2013) under Grant 266992. K.F. was supported by the Federal Ministry for the Environment, Nature Conservation and Nuclear Safety, Germany (11_II_093_Global_A_SIDS and LDCs). H.K. and Y.S. were jointly supported by Japan Society for the Promotion of Science KAKENHI (23226012) and Ministry of Education, Culture, Sports, Science and Technology SOUSEI Program.

Chapter 3

Global water resources affected by human interventions and climate change

An edited version of this chapter has been published as: I. Haddeland, J. Heinke, H. Biemans, S. Eisner, M. Flörke, N. Hanasaki, M. Konzmann, F. Ludwig, Y. Masaki, J. Schewe, T. Stacke, Z. D. Tessler, Y. Wada, and D. Wisser. Global water resources affected by human interventions and climate change. *Proceedings of the National Academy of Sciences of the United States of America*, 111(9):3251–6, 2014. doi: 10.1073/pnas.1222475110

Significance

Humans alter the water cycle by constructing dams and through water withdrawals. Climate change is expected to additionally affect water supply and demand. Here, model analyses of climate change and direct human impacts on the terrestrial water cycle are presented. The results indicate that the impact of man-made reservoirs and water withdrawals on the long-term global terrestrial water balance is small. However, in some river basins, impacts of human interventions are significant. In parts of Asia and the United States, the effects of human interventions exceed the impacts expected for moderate levels of global warming. This study also identifies areas where irrigation water is currently scarce, and where increases in irrigation water scarcity are projected.

Abstract

Humans directly change the dynamics of the water cycle through dams constructed for water storage, and through water withdrawals for industrial, agricultural, or domestic purposes. Climate change is expected to additionally affect water supply and demand. Here, analyses of climate change and direct human impacts on the terrestrial water cycle are presented and compared using a multimodel approach. Seven global hydrological models have been forced with multiple climate projections, and with and without taking into account impacts of human interventions such as dams and water withdrawals on the hydrological cycle. Model results are analyzed for different levels of global warming, allowing for analyses in line with temperature targets for climate change mitigation. The results indicate that direct human impacts on the water cycle in some regions, e.g., parts of Asia and in the western United States, are of the same order of magnitude, or even exceed impacts to be expected for moderate levels of global warming (+2 K). Despite some spread in model projections, irrigation water consumption is generally projected to increase with higher global mean temperatures. Irrigation water scarcity is particularly large in parts of southern and eastern Asia, and is expected to become even larger in the future.

3.1 Introduction

Terrestrial water fluxes are affected by both climate and direct human interventions, e.g., dam operations and water withdrawals. Climate change is expected to alter the water cycle and will subsequently impact water availability and demand. Several hydrologic modeling studies have focused on climate change impacts on discharge in large river basins or global terrestrial areas under naturalized conditions using a single hydrologic model forced with multiple climate projections (Nijssen et al. 2001, Arnell 2003). Recently, hydrological projections from eight global hydrological models (GHMs) were compared (Hagemann et al. 2013). In many areas, there was a large spread in projected runoff changes within the climate–hydrology modeling chain. However, at high latitudes there was a clear increase in runoff, whereas some midlatitude regions showed a robust signal of reduced runoff. The study also concluded that the choice of GHM adds to the uncertainty for hydrological change caused by the choice of atmosphere–ocean general circulation models (hereafter called GCMs) (Hagemann et al. 2013). Expected runoff increases in the north and decreases in parts of the middle latitudes have been found also when analyzing runoff from 23 GCMs (Tang and Lettenmaier 2012).

These studies focused on the naturalized hydrological cycle, i.e., the effects of direct human interventions were not taken into account. However, in many river basins humans substantially alter the hydrological cycle by constructing dams and through water withdrawals. Reservoir operations alter the timing of discharge, although mean annual discharge does not necessarily change much. A study with the water balance model (WBM) showed that the impact of human disturbances, i.e., dams and water consumption, in some river basins is equal to or greater than the impact of expected climate changes on annual runoff over the next 40 y (Fekete et al. 2010). Also, rising water demands are found to outweigh global warming in defining the state of global water systems in the near future (Vörösmarty 2000). Water for irrigation is the largest water use sector, currently accounting for about 70 % of global water withdrawals and nearly 90 % of consumptive water use (Shiklomanov and Rodda 2003). A recent synthesis of simulations from seven GHMs found that irrigation water consumption currently amounts to $1250\,\mathrm{km^3 \cdot y^{-1}}$ ($\pm 25\,\%$) and that considerable differences among models appear in the spatiotemporal patterns of water consumption (Hoff et al. 2010).

Direct comparisons of the climate impact and human intervention modeling studies can be difficult given that the setups are not identical, i.e., the input forcing data and climate models vary. Also, because of the uncertainty of model-specific results, a multimodel approach is preferable in impact modeling studies (Hagemann et al. 2013, Haddeland et al. 2011). This approach is similar to assessments performed within the climate community. Here, multimodel results on current and future water availability and consumption at

the global scale from the Water Model Intercomparison Project (WaterMIP) within the European Union Water and Global Change (EU WATCH) project (Haddeland et al. 2011, Harding et al. 2011), and Inter-Sectoral Impact Model Intercomparison Project (ISI-MIP) (Warszawski et al. 2014) are presented. (Information on how to get access to WaterMIP and ISI-MIP simulation results can be found at `www.eu-watch.org` and `www.isi-mip.org`, respectively.) Results from these two projects are synthesized to obtain a large ensemble of impact model results. The integration of results from the different projects is achieved by extracting impacts for time periods of global mean temperature (GMT) increases of 2 and 3 K from the simulations, largely following the method of Tang and Lettenmaier (2012). The advantage of this approach is that it allows presenting results in a way that is in line with temperature targets used in climate mitigation discussions.

Other studies have focused on future water scarcity using results from WaterMIP and ISI-MIP, but have analyzed changes of naturalized runoff only (Hagemann et al. 2013, Schewe et al. 2014). We here aim to fill this knowledge gap by comparing the different impacts from climate change and direct human impacts and analyzing their interplay. The models included take into account water withdrawals and consumption in different sectors; for more information, see Models and Data and Appendix B, SI Models and Data. The objectives of this study are to (*i*) assess the relative contribution of anthropogenic impacts and climate change to river basin scale water fluxes, and (*ii*) identify areas where climate change can be expected to cause substantial changes in water consumption and water scarcity, focusing on water for irrigation. The effects of future changes in irrigated areas or irrigation practices are not taken into account, and only dams that currently exist are included in the analyses. In this paper, simulations considering man-made reservoirs, water withdrawals, and water consumption are referred to as human impact simulations, whereas the simulations without these disturbances are referred to as naturalized simulations. The results are mainly presented in a way intended to give an overview of impacts at larger spatial scales (river basin and country levels). However, some finer-scale results are included to reveal effects that can be concealed at coarse spatial scales.

3.2 Results

3.2.1 Human Impacts Versus Climate Change

Anthropogenic water consumption results in mean annual runoff decreases of 5 % or more in many river basins during the control period (1971—2000) (Figure 3.1*A* and Appendix B, River Basin Information and Results). The effect is especially noticeable in heavily irrigated regions at middle latitudes across Asia, and in the western part of the United States. In some river basins in the Middle East, central Asia, and the Indian subcontinent, the median ensemble runoff decrease is more than 15 % as a result of water consumption

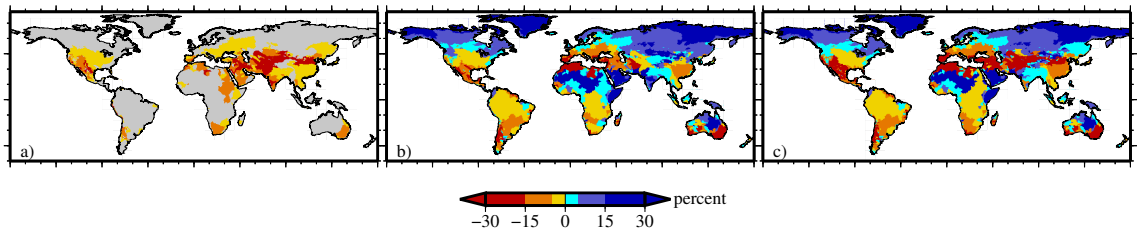

Figure 3.1: Comparison of human impact and climate change effects on runoff at the river basin level. Basin averaged runoff values are calculated based on simulated discharge at the outlet of the river basins, and the median ensemble results are shown. (*A*) Control period (1971—2000) human impact simulations compared with control period naturalized simulations. (*B*) Basin averaged naturalized runoff for 2 K GMT increase, compared with control period naturalized simulations. (*C*) Basin averaged human impact runoff for 2 K GMT, compared with control period naturalized simulations.

within the river basin. In several other Asian river basins, and in the Colorado, Nile, Orange, Murray–Darling River basins, the ensemble median decrease in runoff resulting from anthropogenic water consumption is between 5 % and 15 %.

Water consumption always results in runoff decreases, whereas the climate change signal can be in both directions. Climate change affects naturalized runoff in river basins in all parts of the world. Projected runoff decreases are especially noticeable in the Mediterranean area and in the Middle East, but also in Central and South America and parts of Australia (Figure 3.1*B*). Runoff is projected to increase at northern latitudes, corresponding to areas with large projected increases in precipitation (Meehl et al. 2007a). Runoff increases are also projected in parts of the Arabian Peninsula, the Horn of Africa, and the Indian subcontinent (Figure 3.1*B*).

The pattern of the total impacts, i.e., runoff changes caused by both 2 K GMT increase and human impacts (Figure 3.1*C*), is dominated by the impacts of climate change alone (Figure 3.1*B*). However, noticeable differences exist in southwestern United States and central Asia. To highlight the relationship between the human impacts and climate change effects, differences between the absolute values of the individual impacts are presented (Figure 3.2). This comparison shows that, in several river basins, current water consumption affects annual averaged runoff more than climate change (2 K) is expected to impact naturalized runoff. Figure 3.2*A* shows the river basins in which the climate signal mitigates the human impact signal to some extent or even exceeds it, e.g., in the Nile River basin. Figure 3.2*B* shows the river basins in which the impact of climate change adds to the human impact signal. The combined effect is hence enhancement, e.g., in the Colorado and the Indus River basin.

Despite the locally significant decreases in runoff, anthropogenic water consumption amounts to only 1.3 % of median global terrestrial runoff (Figure 3.3*A*). Among the world's

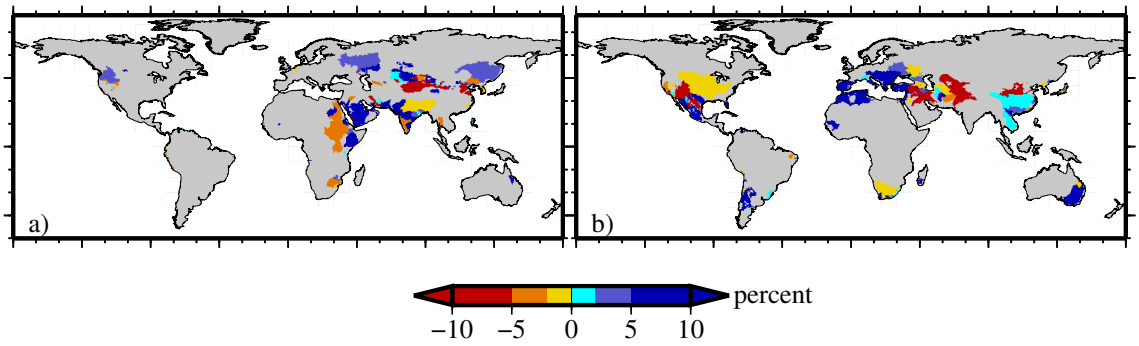

Figure 3.2: (*A*) The difference between the absolute values in Figure 3.1 *A* and *B* in basins where the human impact and climate signals are opposite, i.e., naturalized runoff increases. (*B*) The differences between the absolute values in Figure 3.1 *A* and *B* in basins where both the climate signal and human impact signal are negative, i.e., runoff decreases. The red and yellow colors indicate that the control period human impacts are larger than future climate effects on naturalized runoff.

large river basins, and according to the model ensemble included in this study, the Indus River basin is the most affected by human impacts at the annual level. According to the median ensemble result, as much as 47 % of current runoff is consumed within the Indus River basin (Figure 3.3*F*). Figure 3.3 also shows that the results across the model ensemble for the human impact simulations are significantly different at the river basin level. The interquartile range for the Indus River basin is from 29 % to 62 %, and the individual model results vary between 18 % and 79 %. Large intermodel variations are also found in the Huang He River basin (Figure 3.3*G*), where the simulated anthropogenic water consumption varies between 7 % and 51 % of current naturalized runoff. Moreover, for most of the river basins presented, the impact of a 3 K GMT increase is more pronounced than a 2 K GMT increase, both when looking at the total effect of climate change and human impacts and when looking at the decomposed effects separately (Figure 3.3). In the Colorado and Mississippi River basins, and in several river basins in Asia, the human impact effect is larger than the climate effect (Figures 3.2 and 3.3). In the Mediterranean area, both the climate and human impact signals are negative, but the climate signal dominates (Figure 3.2*B*).

3.2.2 Irrigation Water Consumption and Scarcity

The number of water use sectors included in the results presented so far varies between the different GHMs (Models and Data). However, all GHMs include the agriculture sector, i.e., water used for irrigation, which is the largest water consumer globally (Shiklomanov and Rodda 2003). Here, an index called the cumulative abstraction-to-demand (CAD) ratio (Hanasaki et al. 2008b) is used as a measure of irrigation water scarcity. The higher this

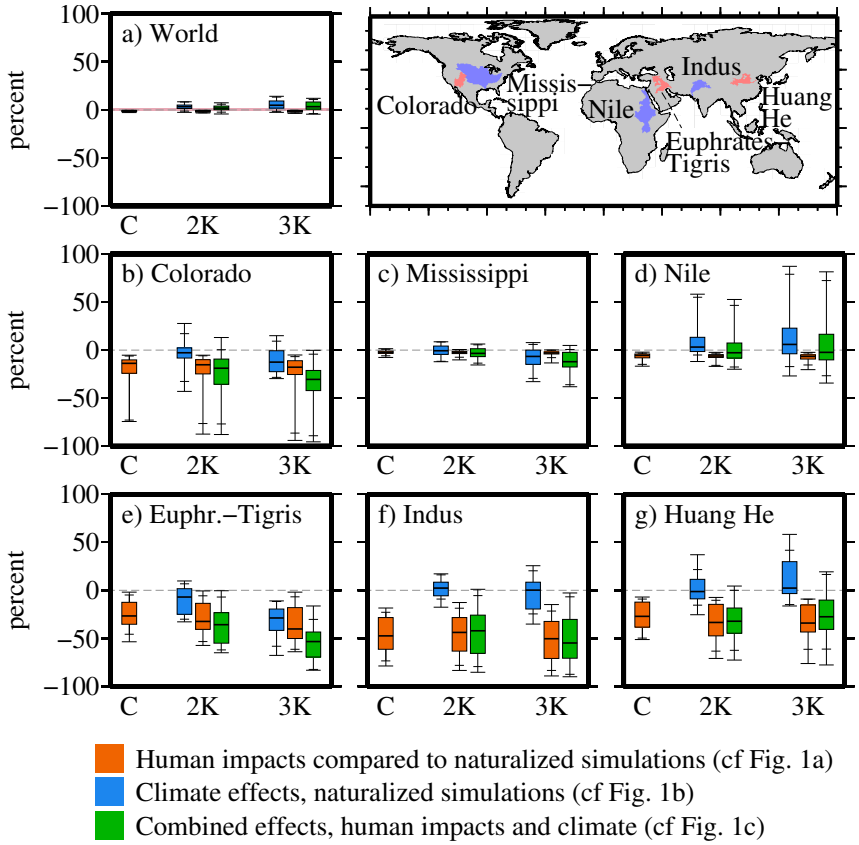

Figure 3.3: Box plots of relative changes in runoff for (A) the world, (B) Colorado, (C) Mississippi, (D) Nile, (E) Euphrates-Tigris, (F) Indus, and (G) Huang He for the control period (C) (1971–2000), 2 and 3 K GMT increases. The boxes illustrate the 25th, 50th, and 75th percentiles of the ensemble (47 members). The whiskers represent the total sample spread, and in addition the 5th and 95th percentiles are marked. The human impact results (orange bars) are compared with the naturalized simulations during the same time period, e.g., 2 K human impacts are compared with 2 K naturalized simulations. All climate and combined effects (blue and green bars) are compared with the control period naturalized simulations.

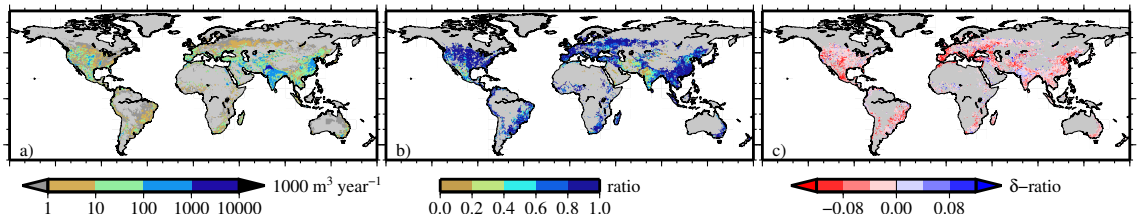

Figure 3.4: Irrigation water consumption and cumulative abstraction-to-demand (CAD) ratio at the grid cell level. (*A*) Ensemble median potential irrigation water consumption, control period (1971–2000). Light gray color represents areas where there is no, or very little, irrigation. (*B*) Ensemble median CAD, control period. (*C*) Differences in CAD between the control period and the 2 K GMT increase period. Negative numbers mean the CAD ratio decreases.

number is, the closer the crops are to having their water requirements fulfilled. Thus, a decrease in CAD represents an increase in water scarcity. The highest potential irrigation water consumption numbers (water consumed given water is freely available) during the control period (1971—2000) are found in the Indian subcontinent (Figure 3.4*A*). Although the CAD ratio is low in the Indian subcontinent (Figure 3.4*B*), actual water consumption (water consumed taking water availability into account) in the area is still considerable, which is reflected in the human impact results for the Indus River basin (Figures 3.1*A* and 3.3).

The CAD ratio is projected to decrease with increasing GMT in most areas where irrigation exists today (Figure 3.4*C*), meaning an increase in irrigation water scarcity. The CAD ratio is projected to increase in only a few scattered areas, e.g., western India. This increase in the CAD ratio can be linked to increased water availability in this area (Figure 3.1*C*). Figure 3.4 reveals some areas impacted by direct human interventions that are not revealed in Figure 3.1, because subbasin variations can be concealed when presenting basin averaged results. For example, in parts of the Mississippi River basin, water consumption is considerable, whereas the effect at the basin total level is small (Figures 3.1–3.3). A decrease in the CAD ratio is projected in the United States, southwestern Europe, Pakistan, India, and China (Figure 3.4*C*). Some statistics on the impact of 2 and 3 K of global warming on irrigation water in these areas, in addition to the global total numbers, are presented in Figure 3.5. The global median potential irrigation water consumption for the entire ensemble (47 members) is 1171 $km^3 \cdot y^{-1}$ in the control period (Figure 3.5*A*). The interquartile range for the same time period ranges from 940 $km^3 \cdot y^{-1}$ to 1284 $km^3 \cdot y^{-1}$. The corresponding number for the subensemble, i.e., for those models simulating both potential and actual water consumption (29 of the 47 members; Models and Data), is 1174 $km^3 \cdot y^{-1}$ (942 $km^3 \cdot y^{-1}$ to 1292 $km^3 \cdot y^{-1}$). These numbers are close to the 1250 $km^3 \cdot y^{-1}$ (±25 %) reported previously (Hoff et al. 2010), and represent about 1 %

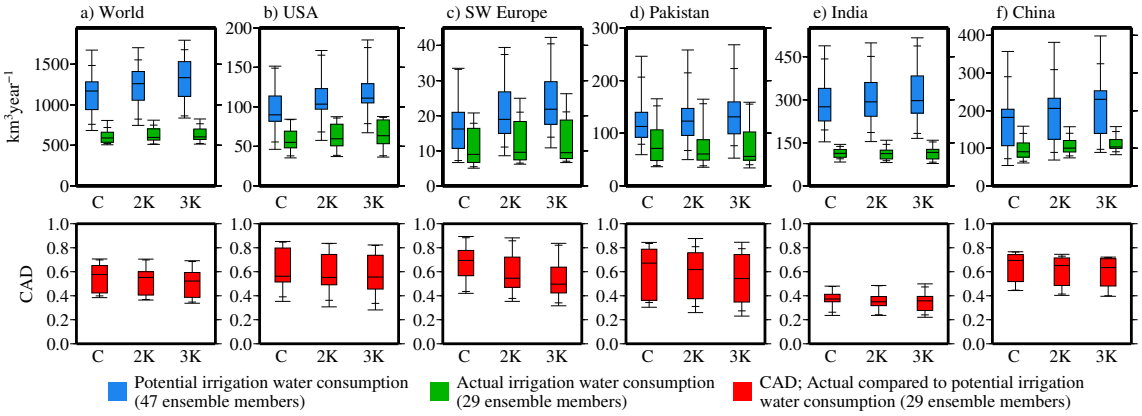

Figure 3.5: Ensemble statistics on irrigation water consumption for the control period (C) (1971–2000), 2 and 3 K GMT increases for (*A*) the world, (*B*) United States, (*C*) southwest Europe (here comprising Portugal, Spain, and France, (*D*) Pakistan, (*E*) India, and (*F*) China. The upper panels show annual potential and actual irrigation water consumption. The lower panels show CAD, i.e., the relationship between the actual and potential irrigation water consumption. The boxes illustrate the 25th, 50th, and 75th percentiles of the ensemble. The whiskers represent the total sample spread, and in addition the 5th and 95th percentiles are marked.

of mean annual terrestrial precipitation in the forcing datasets used here, and between 1 % and 2 % of simulated annual terrestrial runoff.

Substantial differences exist in the ensemble estimates of the amount of potential irrigation water consumed, i.e., when water demands are always met (Figure 3.5). However, potential irrigation water consumption will increase with increasing GMT, both globally and regionally (Figure 3.5). Irrigation water consumed when water availability is taken into account is more similar across the ensemble, despite the differences in human impact parameterizations (Models and Data). Global actual irrigation water consumption increases slightly with increasing GMT (Figure 3.5*A*). The projected changes in actual irrigation water consumption are less apparent than the projected changes in potential irrigation water consumption (Figure 3.5). The spread in irrigation water consumption numbers for a given time period reflects the spread in human impacts seen for the river basins presented in Figure 3.3. More importantly, there is a general agreement that the CAD ratio will decrease in the areas in question, and more so the more GMT increases. The global CAD ratio varies from 0.4 to 0.7 across the simulations, decreasing to 0.35–0.68 at 3 K GMT increase. The corresponding median number decreases from 0.58 to 0.52. The smallest change in the CAD ratio is found in India. Here, increased water availability (Figure 3.1) results in almost constant water scarcity, despite a slight increase in potential irrigation water consumption (Figure 3.4). Among the areas presented in Figure 3.5, the relative decrease in the CAD ratio is most pronounced in southwestern Europe. Here, the

control period median CAD ratio is simulated at 0.69, whereas the median result at 3 K GMT is 0.5. Actual irrigation water consumption does not change much with increasing GMT, indicating that the decrease in the CAD ratio for the areas considered is mainly caused by an increase in water demands.

3.3 Discussion

The climate effects on naturalized runoff presented here are broadly consistent with results presented elsewhere (Hagemann et al. 2013, Tang and Lettenmaier 2012, Schewe et al. 2014). In large parts of the world, the additional impact on runoff caused by anthropogenic water consumption does not contribute much to the total changes. However, this study emphasizes the importance of taking anthropogenic water consumption into account in areas where direct human interventions are large, and highlights areas where water consumption leads to substantial changes in land surface water fluxes. It has previously been indicated that it is unlikely that irrigation has a significant global-scale impact on the Earth's climate (Pitman et al. 2012), but regional predictions within global climate models can be improved by taking into account local-scale processes (Pitman et al. 2012).

Surface water evaporation from man-made reservoirs and reservoir operations causing seasonal regime shifts across multiyears can cause slight changes in annual runoff numbers. However, reservoirs influence the shape of the hydrograph profoundly in many areas of the world and seasonally impact discharge much more than the reduction caused by water consumption (Hanasaki et al. 2006, Biemans et al. 2011).Seasonal changes in discharge caused by storing and releasing of water in reservoirs are not presented in this study, which focuses on annual runoff numbers. Also, because only annual results are presented, it is not revealed whether water scarcity is constant over the time period considered, or whether interannual or intraannual variations exist. The reservoir storage capacity within a river basin indirectly impacts annual runoff numbers through its ability to accommodate seasonal variations in flow volume and hence to satisfy irrigation water requirements. This effect has not been specifically studied here, but it has previously been indicated that nearly one-half of the irrigation water extracted globally originates from reservoirs built for irrigation purposes (Hanasaki et al. 2006).

The model ensemble indicates that irrigation water scarcity is expected to increase with increasing GMT. About 40 % of total agricultural production relies on irrigation (Molden 2007). In light of this, the increase in water scarcity and potential decline in food production could affect people worldwide through food price changes on the global market (Timmer 2012). In areas with a projected increase in irrigation water scarcity, and hence possible decreases in food productivity, adaptation measures need to be addressed. To increase food production, better water management and improved irrigation practices

(reduced losses) have been suggested (Hoff et al. 2010). Irrigation area expansion in regions with sufficient freshwater is also projected to increase food production (Elliott et al. 2014). These issues must all be discussed in light of other water demands, including environmental flow requirements (Hoff et al. 2010).

The areas for which irrigation water consumption and water scarcity are presented in Figures 3.4 and 3.5 do not overlap directly with the river basins presented in Figures 3.1–3.3. However, Figures 3.4 and 3.5 still indicate that, if more water was available for use, the anthropogenic impacts on river basin runoff seen in Figures 3.1–3.3 would have been even larger. The range in estimates in Figure 3.3 is a result of both differences in the baseline runoff (naturalized simulations) and amount of water consumed. Parameterization differences among GHMs that influence naturalized simulation results (Haddeland et al. 2011) will subsequently influence the human impact simulations. Reservoir operations and water withdrawal parameterizations further influence the results and contribute to the rather large differences (Figures 3.3 and 3.5). The largest relative runoff decreases for the human impact simulations in the Colorado River basin, for example, originate from the hydrologic model simulating the lowest naturalized runoff and among the highest water consumption numbers within the river basin. In other areas, e.g., in the Indus and Huang He River basins, the differences are also influenced by whether or not multicropping is taken into account in the hydrologic model.

It should be noted that none of the models considers water transportation between river basins, e.g., water transported from the Colorado River basin to California, and groundwater extractions are poorly represented in most models. Hence, the actual irrigation water consumption numbers might be somewhat underestimated. However, three of the GHMs assume that anthropogenic water demands are always met (Models and Data). Furthermore, not all models take into account water consumption in sectors other than agriculture, although the impact may be small because those sectors currently account for only a small fraction of the total. In addition, irrigation water withdrawals and consumption depend on the irrigation map used (Wisser et al. 2008). These differences in human impact parameterization clearly contribute to the spread in runoff changes and water consumption numbers, in addition to naturalized simulation differences. In addition, both GCMs and GHMs contribute substantially to the spread in future projections (Hagemann et al. 2013, Schewe et al. 2014).

Only climate change effects on water demands and consumption are accounted for in this study, whereas other variables, such as irrigated area and irrigation efficiencies are kept constant at the year 2000 level. Also, the indirect effect of rising CO_2 concentrations on runoff and irrigation water consumption through its direct effect on evaporative demand is not considered. Increasing CO_2 can lead to lower irrigation water demands (Elliott et al. 2014, Konzmann et al. 2013). However, nutrient limitations may influence crop

growth. The combined effect on crop growth, irrigation water demands, and resulting food production is still somewhat uncertain (Konzmann et al. 2013). The positive trend in potential irrigation water consumption presented here is more profound than for specialized crop models (Elliott et al. 2014). Possible reasons for this lie in the different representation of agricultural land and agrohydrological processes in the models (Elliott et al. 2014). These and other impacts on the hydrological cycle should be addressed in future hydrological model developments and multimodel studies. Note also that bias correction has been applied to the GCM data (Hagemann et al. 2011, Hempel et al. 2013). The assumptions and implications of bias correction on forcing data used in hydrological simulations are thoroughly discussed in the study by Ehret et al. (2012). Bias correction can impact present-day simulated runoff numbers strongly, but the impact on projected relative water flux changes, which is the focus in this paper, are much smaller (Hagemann et al. 2011, Haddeland et al. 2012).

3.4 Conclusions

Based on a large ensemble of simulations using eight GCMs and seven GHMs, this study provides a comprehensive assessment of the effects of climate change and direct anthropogenic disturbances on the terrestrial water cycle. Despite considerable spread in the individual results, a number of robust conclusions can be drawn at the regional and global scale. The results indicate that the impacts of man-made reservoirs, water withdrawals, and water consumption on the long-term global terrestrial water balance are small. However, impacts of anthropogenic interventions are significant in several large river basins. In particular, in irrigation-rich areas in Asia and in the western United States, the effect of current anthropogenic interventions on mean annual runoff is stronger than the projected changes for a 2 or 3 K increase in GMT. Climate change tends to increase potential irrigation water consumption on currently irrigated lands with further detrimental effects in regions with significant irrigation. The climate change signal on runoff can be positive or negative, and hence has the potential to alleviate or aggravate irrigation water scarcity. Globally, the relationship between actual and potential irrigation water consumption is expected to decrease, indicating an increase in irrigation water scarcity.

3.5 Models and Data

Seven GHMs are included in this study. The nature and magnitude of human disturbances at which direct anthropogenic impacts like dams, water withdrawals, and water consumption are included in the models vary (Table 3.1 and Appendix B, SI Models and Data). All models were forced with climate data from a total of eight GCMs included in the Coupled

Table 3.1: Hydrologic models

Model name	Human impact parameterizations
H08 (Hanasaki et al. 2008a)	Two-purpose reservoir scheme (irrigation and nonirrigation). Potential and actual irrigation water withdrawals and consumption. Irrigation water extracted from nearby river. Actual industrial and domestic water withdrawals and use. Water withdrawals and consumption for industrial and domestic sectors (Hanasaki et al. 2006, 2008a).
LPJmL (Bondeau et al. 2007)	Multipurpose reservoir scheme. Potential and actual irrigation water withdrawals and consumption. Irrigation water extracted locally and from reservoirs. Actual water withdrawals and consumption in other sectors taken from WaterGAP estimates (Rost et al. 2008, Biemans et al. 2011).
MPI-HM (Stacke and Hagemann 2012b)	Potential irrigation water consumption. Irrigation water extracted from nearby river and from a hypothetical aquifer if needed. No reservoirs. No published references.
PCR-GLOBWB (Wada et al. 2011)	Two-purpose reservoir scheme (water supply and nonwater supply). Potential and actual irrigation water withdrawals and consumption. Irrigation water extracted locally from surface water and groundwater, and from reservoirs. Potential water withdrawals and consumption for domestic and industrial sectors (Wada et al. 2011, 2012).
VIC (Liang et al. 1994)	Multipurpose reservoir scheme. Potential and actual irrigation water withdrawals and consumption. Irrigation water extracted from nearby river and from reservoirs (Haddeland et al. 2006).
WaterGAP (Döll et al. 2003)	Two-purpose reservoir scheme (irrigation and nonirrigation) (Hanasaki et al. 2006). Potential irrigation water withdrawals and consumption (Döll and Siebert 2002). Potential water withdrawals and consumption for domestic and industrial sectors (Flörke et al. 2013).
WBMplus (Wisser et al. 2008)	Reservoir operation is a function of current inflow compared with long-term inflow. Potential irrigation water withdrawals and consumption. Irrigation water extracted locally (small local reservoirs, groundwater and nearby river) (Wisser et al. 2008).

LPJmL, Lund-Potsdam-Jena managed land dynamic global vegetation and water balance model; MPI-HM, Max Planck Institute – hydrology model; PCR-GLOBWB, PCRaster global water balance model; VIC, variable infiltration capacity macroscale hydrologic model; WaterGAP, water – a global assessment and prognosis model; WBMplus, water balance/transport model.

Model Intercomparison Project 3 (CMIP3) and CMIP5 archives (Table 3.2). CMIP3 data were prepared for the hydrological model simulations within the WATCH project (Hagemann et al. 2013, 2011), and the CMIP5 data were prepared for ISI-MIP (Hempel et al. 2013). Included in the analyses presented here are results when using forcing data from the A2 emission scenario (CMIP3 models) and RCP8.5 (CMIP5 models). Thirty-year periods of GMTs at 2 and 3 K above preindustrial level are extracted from the GCMs (Table 3.2). The control period (1971—2000) is assumed to be 0.4 K above preindustrial level for all GCMs.

All hydrological models are run at a daily time step at a spatial resolution of 0.5° latitude by longitude, and runoff is routed through the DDM30 river network (Döll and Lehner 2002). Simulation results are submitted for the period 1971–2099. Not all GHMs are run

Table 3.2: First year of 30-y periods for each GCM and mean GMT increases above preindustrial level

Mean GMT increase	CMIP3–A2			CMIP5–RCP8.5				
	CNRM-CM3	ECHAM5/MPI-OM	IPSL-LMDZ-4	GFDL-ESM2M	HadGEM2-ES	IPSL-CM5A-LR	MIROC-ESM-CHEM	NorESM1-M
+2 K	2037	2041	2032	2039	2016	2019	2018	2032
+3 K	2058	2059	2055	2068	2036	2039	2037	2058
GHM simulations	*H08*, *LPJmL*, *VIC*, WaterGAP			*H08*, *LPJmL*, MPI-HM, *PCR-GLOBWB*, *VIC*, WBMplus, WaterGAP				

The table includes information on which GCM–GHM combinations that have been simulated (ensemble size is 47). GHM names in italics denote those that have performed both the actual and potential human impact simulations (ensemble size is 29). CMIP3-A2, Coupled Model Intercomparison Project 3, A2 emission scenario; CMIP5-RCP8.5, Coupled Model Intercomparison Project 5, Representative Concentration Pathway 8.5; CNRM-CM3, Centre National de Recherches Météorologiques Coupled global climate Model, version 3; ECHAM5/MPI-OM, European Centre for medium range weather forecasts, HAMburg, version 5, Max Planck Institute for meteorologi, Ocean Model; IPSL-LMDZ-4, Institut Pierre Simon Laplace, Laboratoire de Meteorologie Dynamique, Zoom capability, 4th assessment report; GFDL-ESM2M, Geophysical Fluid Dynamics Laboratory, Earth System Model version 2, Modular ocean model; HadGEM2-ES, Hadley centre Global Environment Model version 2, Earth System model; IPSL-CM5A-LR, Institut Pierre Simon Laplace, CMip5 version A, Low Resolution; MIROC-ESM-CHEM, Model for Interdisciplinary Research on Climate, Earth System Model, Chemistry; NorESM1-M, Norwegian Earth System Model version 1, interMediate resolution.

using input data from all GCMs (Table 3.2). Simulated discharge at the basin outlets are used when calculating basin averaged, or world total, runoff numbers. In this paper, potential water consumption represents water consumed given water is freely available. All models included in the study simulate this quantity. Four of the models—H08, the Lund-Potsdam-Jena managed land dynamic global vegetation (LPJmL), the PCRaster global water balance model (PCR-GLOBWB), and the variable infiltration capacity macroscale hydrologic model (VIC)—also simulate actual water consumption, which is defined as water consumed when water availability is taken into account. The CAD ratio (Hanasaki et al. 2008b) is used as a measure of irrigation water scarcity (Appendix B, Glossary). Both actual and potential irrigation water consumption are calculated at a daily temporal resolution, and hence subannual variations are imbedded in the final CAD numbers.

Annual runoff and water consumption numbers are calculated for each GCM–GHM combination independently, creating an ensemble of up to 47 annual time series for the period 1971—2099. Differences between simulations are thereafter calculated for each time period of interest (Table 3.2) for each ensemble member. Finally, median numbers and other statistic measures are calculated. All results are treated equally, and no attempt to give weights to GCMs or GHMs based on performance has been made.

Supplementary material related to this chapter is available in Appendix B.

Acknowledgments

We acknowledge the World Climate Research Programme's Working Group on Coupled Modeling, which is responsible for CMIP, and we thank the climate modeling groups (Table 3.2) for making available their model output. We appreciate the reviewers' constructive and valuable comments. This study was conducted in the framework of the ISI-MIP project and the EU WATCH Integrated Project (Contract 036946), in collaboration with the Global Water System Project. The ISI-MIP Fast Track project was funded by the German Federal Ministry of Education and Research (Bundesministerium für Bildung und Forschung) with project funding reference number OlLS1201A. Y.M. and N.H. were supported by the Environment Research and Technology Development Fund (S-10) of the Ministry of the Environment, Japan.

Chapter 4

A new climate dataset for systematic assessments of climate change impacts as a function of global warming

An edited version of this chapter has been published as: J. Heinke, S. Ostberg, S. Schaphoff, K. Frieler, C. Müller, D. Gerten, M. Meinshausen, and W. Lucht. A new climate dataset for systematic assessments of climate change impacts as a function of global warming. *Geoscientific Model Development*, 6(5):1689–1703, 2013a. doi: 10.5194/gmd-6-1689-2013

Abstract

In the ongoing political debate on climate change, global mean temperature change (ΔT_{glob}) has become the yardstick by which mitigation costs, impacts from unavoided climate change, and adaptation requirements are discussed. For a scientifically informed discourse along these lines, systematic assessments of climate change impacts as a function of ΔT_{glob} are required. The current availability of climate change scenarios constrains this type of assessment to a narrow range of temperature change and/or a reduced ensemble of climate models. Here, a newly composed dataset of climate change scenarios is presented that addresses the specific requirements for global assessments of climate change impacts as a function of ΔT_{glob}. A pattern-scaling approach is applied to extract generalised patterns of spatially explicit change in temperature, precipitation and cloudiness from 19 Atmosphere-Ocean General Circulation Models (AOGCMs). The patterns are combined with scenarios of global mean temperature increase obtained from the reduced-complexity climate model MAGICC6 to create climate scenarios covering warming levels from 1.5 to 5 degrees above pre-industrial levels around the year 2100. The patterns are shown to sufficiently maintain the original AOGCMs' climate change properties, even though they, necessarily, utilise a simplified relationships between ΔT_{glob} and changes in local climate properties. The dataset (made available online upon final publication of this paper) facilitates systematic analyses of climate change impacts as it covers a wider and finer-spaced range of climate change scenarios than the original AOGCM simulations.

4.1 Introduction

Impacts of anticipated future climate change on ecosystems and human societies are reason for major concern. Projections of such impacts are, however, characterised by uncertainties in greenhouse gas (GHG) emissions scenarios, their implementation in climate models (involving *inter alia* structural uncertainties of climate models) and their subsequent use in impact models. Despite intense research summarised, for example, by the Intergovernmental Panel on Climate Change's Working Group II report (IPCC 2007b), assessments commonly lack systematic quantification of impacts as a function of global warming, as only a small and often opportunistic selection of available climate change scenarios is employed. This hampers direct comparisons between studies (e.g. Müller et al. 2011) and also our understanding of how impacts and their likelihood change over time or as a function of global mean temperature (T_{glob}). The magnitude of impacts to be expected given specific degrees of T_{glob} rise has gained increasing attention in recent years due to the United Nations Framework Convention on Climate Change's stipulation to prevent "dangerous climate change" and the ensuing discussion on whether this would be met by a 2-degree mitigation target (rather than, for example, a 1.5 or 3 degree target). Besides requiring an understanding of how impacts individually and collectively accumulate with increasing T_{glob}, an understanding of the consequences of missing a given target is important for this discussion (e.g. Mann 2009). Compilations of individual impact studies have helped to illustrate the underlying "reasons for concern" (Smith et al. 2009) but do not provide the consistent quantitative information needed.

In view of the importance of mitigation targets for the debate on climate change mitigation and the substantial investments required to meet them, the number of studies that scrutinise systematically and consistently the worldwide impacts to be expected as a function of ΔT_{glob}, let alone their uncertainties, is surprisingly small. Examples for global assessments of impacts ordered along ΔT_{glob} and derived with single impact modelling frameworks are those by Arnell et al. (2011); Gosling et al. (2010), and Murray et al. (2012) for freshwater availability, and those by Gerber et al. (2004); Scholze et al. (2006); Sitch et al. (2008), and Heyder et al. (2011) for ecosystems and the carbon cycle. Other assessments have focused on diverse impacts given a ΔT_{glob} of 4 degrees (see New et al. 2011).

While much of the uncertainty in T_{glob} is attributable to the fact that the exact development of future GHG emissions cannot be known—requiring a scenario approach (Hawkins and Sutton 2009)—the parameterisation of Atmosphere-Ocean General Circulation Models (AOGCMs) additionally contributes to uncertainty in regional temperature and precipitation changes associated with a given ΔT_{glob} (Hawkins and Sutton 2011). Most of above-mentioned studies could account only partly for the latter, as they either relied on a

small selection of AOGCMs or grouped larger ensembles according to the ΔT_{glob} reached by the individual AOGCMs by the end of their simulation period (e.g. Scholze et al. 2006). More rigorous assessments of impacts as a function of global warming are generally limited by the availability of AOGCM simulations in the CMIP3 archive. The range of warming levels covered by the different AOGCMs differs widely and the increase in T_{glob} over the twenty-first century for the highest emission scenario A2 is only 3.4 in the multi-model mean (Meehl et al. 2007b).

Overall, systematic assessments of climate change impacts as a function of global warming require that a large ΔT_{glob} range be covered (from, for example, 1.5 to 5 degrees), and that the respective ΔT_{glob} levels are reached at around the same time. Furthermore, for every ΔT_{glob} level, information on local changes in key climate variables (such as temperature, precipitation, radiation or cloudiness) should consider an AOGCM multi-model ensemble as large as possible, in order to account for the substantial climate model-structural uncertainty. Such consistent information is not directly available in the existing CMIP3 and CMIP5 climate databases—it requires fusion of comprehensive datasets on climate change patterns from different AOGCMs with different ΔT_{glob} trajectories (and underlying emissions trajectories), information on observed climate (without AOGCM biases), and reduced-complexity models able to overcome the high computation requirements of AOGCMs.

To address some of these features, a number of studies (e.g. Gosling et al. 2010, Murray et al. 2012) have used emulated rather than original AOGCM output, calculated with the so-called "pattern-scaling" technique (Mitchell 2003) that makes use of the correlation between local long-term mean changes of climate variables and ΔT_{glob}. Scaling coefficients were found to differ spatially and seasonally, but particularly for temperature they are nearly independent of the GHG emission scenarios considered and sufficiently accurate over a wide range of ΔT_{glob} (Solomon et al. 2009, Mitchell 2003, Huntingford and Cox 2000). Hence, pattern-scaling is an efficient method to generate climate scenarios for systematic analyses of climate impacts as a function of ΔT_{glob}.

Using a comprehensive pattern-scaling approach covering monthly mean surface temperature, cloudiness and precipitation, we here present a newly collated global dataset of climate change scenarios that overcomes most of the above problems and is suited for systematic, macro-scale impact assessments with empirical or process-based impact models. It is based on GCM-specific scaling patterns that are combined with time series of ΔT_{glob} generated by a reduced-complexity climate model, MAGICC6 (Meinshausen et al. 2011a). The emissions scenarios are designed such that each of eight ΔT_{glob} levels (1.5 to 5 degrees above pre-industrial levels in 0.5 degree steps) is reached by 2100. Monthly climate anomaly patterns are derived for each of 19 AOGCMs available from the World Climate Research Programme's (WCRP's) Coupled Model Intercomparison Project phase

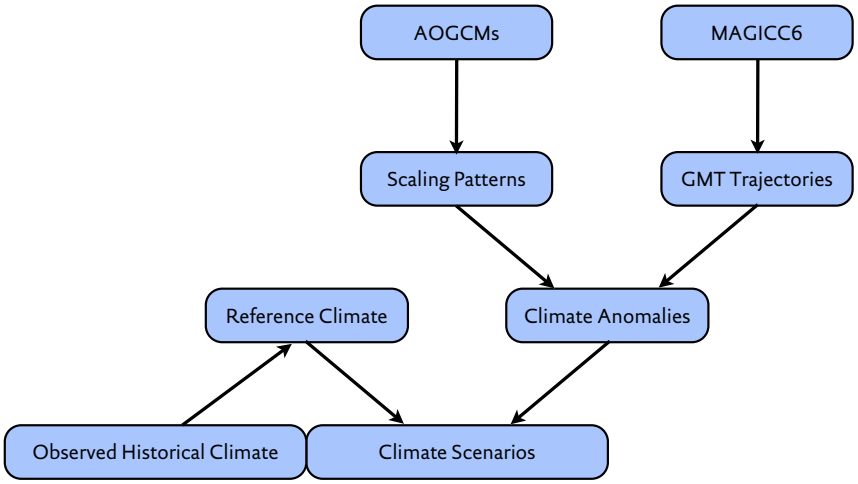

Figure 4.1: Flow chart of data processing for the generation of climate scenarios.

3 (CMIP3) multi-model dataset. Scaling the derived generic change patterns per degree of global mean warming with the ΔT_{glob} trajectories generates transient time series of climate anomalies up to 2100. This dataset enables consistent analyses of impacts as a function of ΔT_{glob} at the end of the century, and improved comparability of climate patterns and resulting impacts for given T_{glob} levels. The dataset is referred to as "PanClim" (PAtterN scaling CLIMate dataset) to indicate its methodological background and its wide-spanning coverage of the scenario space (pan, Greek for "all", "involving all members"). The complete PanClim dataset is available for download from `http://www.panclim.org`.

4.2 Methods

Figure 4.1 sketches the steps of data processing and combination involved in the creation of the climate scenarios, described in detail in the following sections. Section 4.2.1 describes the extraction of scaling patterns—i.e. the spatial fields of local (monthly) climate change per one degree of ΔT_{glob} — from AOGCM simulations. Section 4.2.2 covers the generation of T_{glob} trajectories by the MAGICC6 model, and their combination with the derived scaling patterns to generate time series of mean local climate anomalies for the given warming scenarios. Section 4.2.3 focuses on the combination of these local anomalies with data on observed variability and climatological means to generate climate scenarios harmonised with historical observations, covering the entire global land area.

4.2.1 Derivation of scaling patterns from AOGCM simulations

The basic concept behind the methodology described in this paper is that any simulated or observed monthly time series $V(x, m, y)$ of a climate variable V (e.g. air temperature)

in location x, month m, and year y can be decomposed as follows:

$$V(x,m,y) = \overline{V}(x,m) + \Delta\overline{V}(x,m,y) + e(x,m,y) \tag{4.1}$$

where $\overline{V}(x,m)$ denotes the long-term mean and $\Delta\overline{V}(x,m,y)$ the long-term mean change of variable V; the term $e(x,m,y)$ describes the natural interannual variability around the long-term mean.

The general idea of the pattern scaling approach is to relate the local anomalies in the long-term mean $\Delta\overline{V}(x,m,y)$ in Equation 4.1 to a global scaler for which scenario trajectories can be easily obtained (Mitchell 2003). In agreement with previous studies (e.g. Huntingford and Cox 2000, Mitchell 2003), we here use global mean temperature ΔT_{glob} as scaler and assume a linear relationship between local monthly climate anomalies $\Delta\overline{V}(x,m,y)$ and $\Delta T_{\text{glob}}(y)$:

$$\Delta\overline{V}(x,m,y) = V^*(x,m) \cdot \Delta T_{\text{glob}}(y) \tag{4.2}$$

where $V^*(x,m)$ is the *scaling coefficient*, i.e. the change in $\overline{V}(x,m)$ per degree of ΔT_{glob} for each location and month but independent of time (y). The entirety of all scaling coefficients $V^*(x,m)$ for a particular variable and AOGCM is referred to as *scaling pattern*.

Substitution of Equation 4.2 in Equation 4.1 and subtraction of $\overline{V}(x,m)$ from both sides of the equation gives:

$$V(x,m,y) - \overline{V}(x,m) = V^*(x,m) \cdot \Delta T_{\text{glob}}(y) + e(x,m,y) \tag{4.3}$$

Equation 4.3 describes all deviations of V from the long-term mean $\overline{V}(x,m)$ as sum of changes in the long-term mean (expressed by the linear relationship to $\Delta T_{\text{glob}}(y)$) and interannual variation around the long term mean. This equation has the form of a simple linear regression model that provides the basis for estimating scaling coefficients from AOGCM simulations. For the estimation of $V^*(x,m)$ from AOGCM simulations, the monthly data were linearly interpolated from their original spatial resolution to the target resolution used here, a regular 0.5×0.5 arc-degree grid. Estimates of $\overline{V}(x,m)$ are obtained from the pre-industrial control run (equilibrium simulation without any anthropogenic forcing) available for all AOGCMs with lengths between 100 and 990 simulation years. Subtraction of $\overline{V}(x,m)$ from simulations with climate forcing yields deviations from the long-term climatological mean that are taken as a dependent variable in the estimation of $V^*(x,m)$ by linear regression. The corresponding independent variable $\Delta T_{\text{glob}}(y)$ is obtained from estimates of $T_{\text{glob}}(y)$ that are calculated as annual area-weighted global averages (including oceans) of $T(x,m,y)$. Since the extraction of patterns of $V^*(x,m)$ is based on linear regression, the residual errors $e(x,m,y)$ in Equation 4.3 are in fact a mix-

ture of interannual variability and the imperfection of the regression model. The quality of the fit obtained can thus be evaluated by comparison of residual errors and respective interannual variability estimated from the control simulation (see section 4.4). We applied the above methodology to estimate scaling patterns for near-surface air temperature, cloudiness and precipitation. Additionally, we studied logarithmic precipitation to reflect an alternate assumption of exponential rather than linear precipitation change. In the logarithmic precipitation regression model, exclusion of dry months alters the estimated trend of precipitation amounts under climate change. This problem is not purely of numerical nature but highlights that the change in frequency of rain months and the change in the rainfall amounts for rain months represent qualitatively different information that should be addressed separately. Hence, we removed dry months ($<$1 mm per month) from the linear fit (Equation 4.3) of both precipitation and logarithmic precipitation so that both regression models capture the change in rainfall amounts for rain months only.

Building on the basic principle of the pattern-scaling approach, the change in frequency of rain months (p) was considered separately by applying a logistic regression model, in which probabilities are logit-transformed and related to a linear predictor term, which gives a generalised linear regression model:

$$\begin{aligned} \text{logit}\left(p(x,m,y)\right) &= \ln\left(\frac{p(x,m,y)}{1-p(x,m,y)}\right) \\ &= \beta_0(x,m) + \beta^*(x,m)\cdot\Delta T_{\text{glob}}(y) \end{aligned} \tag{4.4}$$

where $\beta_0(x,m)$ and $\beta^*(x,m)$ denote the pre-industrial value and the scaling coefficient, respectively, for logit-transformed probability of rain month occurrence in location x and month m. For the estimation of both model coefficients from time series of dry/rain month occurrence we used the glm() function (Generalised Linear Model) from the core package "stats" of the statistical software R (R Development Core Team 2011).

4.2.2 Construction of climate scenarios from derived patterns

Construction of scenarios of global mean temperature increase

The derived scaling patterns $V^*(x,m)$ for the different climate variables are the basis for constructing time series of local anomalies of climate variables consistent with prescribed T_{glob} trajectories. We ran the MAGICC6 model to obtain physically and systemically plausible ΔT_{glob} trajectories and corresponding trajectories of atmospheric CO_2 concentration ($[CO_2]$) (required for some impact models). MAGICC6 is a highly efficient reduced-complexity carbon cycle climate model (Meinshausen et al. 2011a) that has been shown to closely emulate mean results of complex AOGCMs from the CMIP3 data base (Meinshausen et al. 2011b). Here, MAGICC6 was used to calculate ΔT_{glob} and $[CO_2]$ for a large

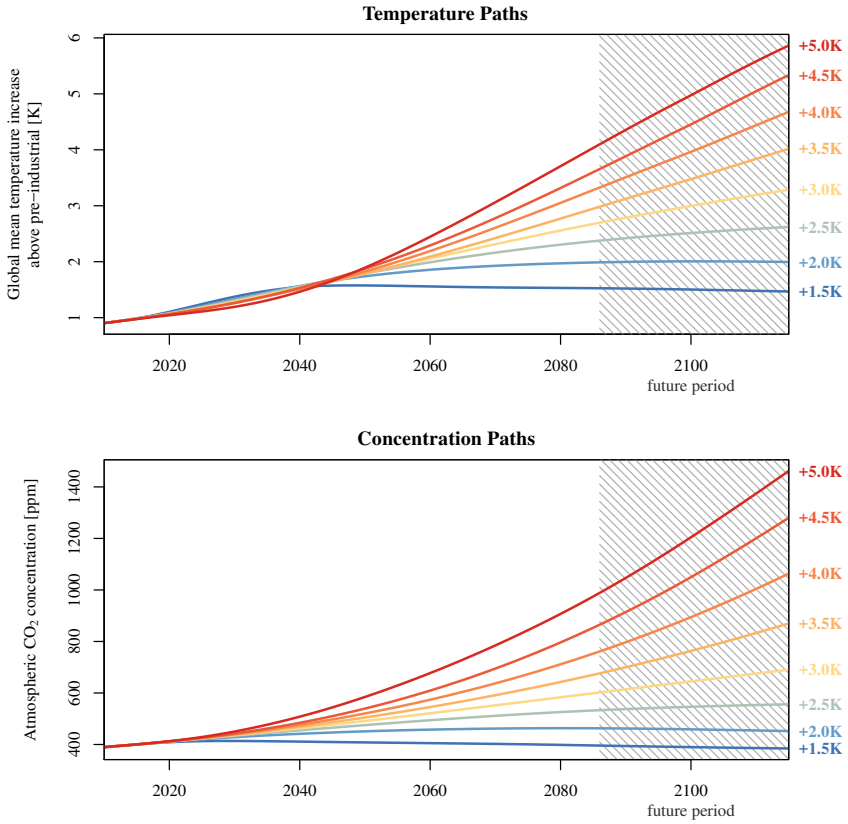

Figure 4.2: Trajectories of global mean temperature increase used in this study and corresponding atmospheric CO_2 concentrations from the MAGICC6 model. The shaded area indicates the time period for which the temperature targets are calculated.

number of artificial emissions pathways, constructed as described by Meinshausen et al. (2009). For that purpose MAGICC's carbon cycle parameters were adjusted to reproduce the Bern carbon cycle model and the climate model parameters were chosen to reproduce the median responses of the CMIP3 AOGCM ensemble. Climate sensitivity, for example, was set to 3.0 K.

From the generated large ensemble of pathways we selected those pairs of ΔT_{glob} and $[CO_2]$ trajectories where average ΔT_{glob} in the period 2086–2115 reached 1.5, 2.0, 2.5, 3.0, 3.5, 4.0, 4.5, and 5.0 degrees above the pre-industrial level (see Figure 4.2). The definition of the temperature target for a period rather than for a single year (e.g. 2100) was chosen because the analysis of time periods is common practice in impact assessments to avoid spurious effects from interannual variability. 30 yr is a typical length used in impact studies in hydrology, agriculture, and ecosystems, for which our new data set is designed.

An outstanding feature in Figure 4.2 that illustrates the above-mentioned physical and systemic plausibility is the initially stronger increase in T_{glob} in the lower than in the

high temperature scenarios. Stronger mitigation scenarios tend to show a much faster decrease in aerosol emissions than in CO_2 emissions, as a rapid decrease of CO_2 emissions is accompanied by a switch to "cleaner" sources of energy. This correlation between CO_2 and aerosol emissions results from our use of the Equal Quantile Walk method (Meinshausen et al. 2006) to create the different emission profiles that led to the various warming levels. The drop in aerosol emissions in combination with the much shorter residence time of aerosols in the atmosphere results in a rapid reduction of the aerosol cooling effect (see Ramanathan and Feng 2008). As a consequence, the committed warming from current $[CO_2]$ can unfold before a further reduction of CO_2 emissions eventually results in an overall decrease in radiative forcing and temperature. Conversely, the CO_2 emissions in the high temperature scenarios are accompanied by high aerosol emissions that maintain the cooling effect. Besides the possibility to produce T_{glob} scenarios together with consistent $[CO_2]$ trajectories, the consideration of such effects is the major advantage of applying MAGICC6 in this study.

Construction of local time series of climate anomalies

Local time series of climate anomalies $\Delta\overline{V}_{\mathrm{scen}}(x,m,y)$ for the four climate variables were obtained by multiplying the scaling coefficients $V^*(x,m)$ with the $\Delta T_{\mathrm{glob}}(y)$ trajectories for each scenario (Equation 4.2). Because the obtained time series of anomalies are combined with climate observations in the next step (see section 4.2.3), it is necessary to account for the climate change signal already present in these observations. Anomalies are therefore calculated relative to the last year of observations, 2009. This is achieved by subtracting the T_{glob} increase above pre-industrial level for the year 2009 ($\sim$0.9 K) from the T_{glob} trajectories of the MAGICC6 scenarios before multiplying them with the anomaly patterns. In all cases, anomalies were only calculated if the significance level of the slope of the regression model is $>$0.9; otherwise they were set to zero.

For temperature, the obtained local anomalies can be used without any restriction. In the case of cloudiness and precipitation, however, the obtained anomalies may result in an exceedance of the lower and, in the case of cloudiness, also the upper limit of possible values for these variables. For cloudiness this problem is less critical as it is not used directly in impact models but serves, among other parameters, as a proxy for atmospheric transmissivity and emissivity in the estimation of radiation budgets. We therefore consider a simple capping of anomalies to prevent the exceedance of upper and lower limits, a sufficiently accurate solution. In contrast to cloudiness, precipitation is an essential variable and calculation of anomalies that would result in physically implausible negative precipitation rates should be avoided from the beginning. Anomalies for decreasing precipitation are therefore estimated from the regression models for logarithmic precipitation, which is equivalent to the assumption of exponential precipitation decrease. As there is no indi-

cation that precipitation would increase exponentially with T_{glob}, precipitation increases are estimated from the linear regression models for untransformed precipitation. For small change rates, the linear and the exponential approach yield very similar anomalies, while for large change rates the linear approach avoids unrealistically augmented increases and the exponential approach avoids negative precipitation rates (see also Watterson 2008). For estimating rain month frequency anomalies, changes in the linear predictor term of Equation 4.4, i.e. anomalies of logit probabilities, were calculated. These obtained anomalies can be used without restrictions, as the range of logit probabilities is unconstrained. For the transformation into actual frequency anomalies see section 4.2.3.

4.2.3 Creation of climate scenarios from observed climate and derived climate anomalies

In order to obtain complete scenario time series of climate variables $V_{\text{scen}}(x, m, y)$ that can be used for transient impact model simulations, the local scenario time series of climate anomalies $\Delta\overline{V}_{\text{scen}}(x, m, y)$ are combined with time series—here referred to as "reference time series" $V_{\text{ref}}(x, m, y)$—that provide the long-term climatological mean $\overline{V}(x, m)$ and interannual variability $e(x, m, y)$ (Equation 4.1). Reference time series for temperature and cloudiness are constructed from and are consistent with the CRU TS3.1 global climate dataset (Harris et al. 2014); reference time series for precipitation are based the GPCC full reanalysis dataset version 5 (Rudolf et al. 2010).

Because GPCC and CRU datasets have a slightly different land mask, the GPCC dataset was adjusted to the CRU land mask (67 420 grid cells) by filling up missing cells by interpolation. For this, the five neighbouring cells with the highest weight—calculated from distance and angular separation (New et al. 2000)—within a 450 km radius were used. If <5 values were available, the interpolation was performed on this reduced data basis; if <2, the precipitation from the CRU TS3.1 dataset was used. Grid cells only present in the GPCC land mask but not in the CRU land mask were excluded. Altogether, 767 grid cells were introduced by interpolation, 298 grid cells were directly taken from CRU TS3.1, and 1013 grid cells were omitted from the GPCC dataset.

106-yr reference time series covering the scenario period (2010–2115) were composed as a random sequence of years from historical observations of the period 1961–2009. To preserve interannual autocorrelation, spatial coherence, and correlation among climate variables, all months and grid cells for all climate variables were taken from the same year. Prior to resampling, the trend in temperature was removed in a way that the detrended time series of temperature are representative for the climatologic mean of year 2009 obtained from the trend analysis. In the process of data preparation, observations of precipitation and cloudiness were found to exhibit strong interannual/interdecadal variability, which negatively affects the robustness of estimated trends. In order to avoid spurious effects from

removing these trends, the original data were used directly for generating the reference time series for cloudiness and precipitation. The time series of resampled observations obtained are assumed to represent variability and climatology for the reference year 2009, to be consistent with the reference year for the derived anomalies. This consistency between the constructed reference time series, derived anomaly time series, and observations allows for seamless combination of historic observations with future climate projections and thus for transient impact model runs.

The combination of the anomalies with the reference time series is a crucial step and related to the general problem of whether to apply climate anomalies as an absolute change:

$$V_{\text{scen}}(x, m, y) = V_{\text{ref}}(x, m, y) + \Delta\overline{V}_{\text{scen}}(x, m, y) \tag{4.5}$$

or a relative change:

$$V_{\text{scen}}(x, m, y) = V_{\text{ref}}(x, m, y) \cdot \frac{\overline{V}_{\text{base}}(x, m) + \Delta\overline{V}_{\text{scen}}(x, m, y)}{\overline{V}_{\text{base}}(x, m)} \tag{4.6}$$

where $\overline{V}_{\text{base}}(x, m)$ is the basis for the anomalies in the AOGCM, i.e. the long-term climatological mean of the AOGCM's representation of present-day climate. Where biases in the AOGCM's representation of present-day climate are small, the application of anomalies as relative change imposes a similar mean change to the scenario time series than the application as absolute change. That is, the difference between the mean of the scenario time series and the reference time series is similar to the original anomaly. As biases increase, climate anomalies are progressively altered with the relative approach. This alteration is an expression of the adjustment of the absolute anomaly derived from a biased base level in the AOGCM to the observed level, which is the actual motivation for using the relative approach. The relevance of this adjustment is particularly apparent where decreases from overestimated levels in the AOGCM are applied to lower observed levels. Without the attenuation of the anomaly by the relative approach the application of a negative change might well lead to negative values. However, for the reverse case—increases from underestimated levels—this approach is less favourable as it may lead to an unrealistic augmentation of the absolute anomaly.

Another difference between the two approaches is that with the absolute application of anomalies interannual variability remains unchanged, while with the relative application interannual variability is altered in a way that the coefficient of variation remains constant. The relevance of this variability adjustment is most apparent for cases where negative anomalies bring the mean of the scenario time series close to zero. In these cases a corresponding decrease of variability is required to prevent the occurrence of negative values.

The procedures used to apply the anomaly time series to the reference time series for different climate variables are described in the remaining part of this section. In order to improve readability, the parameters x and m are omitted; only the parameter y is used to differentiate terms that vary over time from time-invariant terms. Thus, Equations 4.7–4.14 can be seen to describe the processes for a particular location x and month m but apply to all locations and months.

Temperature

Since temperature biases in AOGCMs are very small compared to absolute temperature levels, the application as absolute or relative change would give very similar results. However, temperature anomalies are commonly treated as absolute changes in the literature and are thus applied as absolute change here:

$$T_{\mathrm{scen}}(y) = T_{\mathrm{ref}}(y) + \Delta\overline{T}_{\mathrm{scen}}(y) \tag{4.7}$$

where $T_{\mathrm{scen}}(y)$, $T_{\mathrm{ref}}(y)$, and $\Delta\overline{T}_{\mathrm{scen}}(y)$ are the temperature time series of the scenario, the reference time series, and the time series of anomalies, respectively.

Cloudiness

For cloudiness, anomalies were applied as relative changes. Due to the problem of augmentation of anomalies when applied as relative change to higher observed levels, there is a risk of exceeding the upper 100 % limit in these cases. Increases in cloudiness are therefore applied as relative decreases of cloudlessness, i.e. 100 % – cloudiness:

$$\mathrm{Cld}_{\mathrm{scen}}(y) = \begin{cases} \mathrm{Cld}_{\mathrm{ref}}(y) \cdot \frac{\overline{\mathrm{Cld}}_{\mathrm{base}} + \Delta\overline{\mathrm{Cld}}_{\mathrm{scen}}(y)}{\overline{\mathrm{Cld}}_{\mathrm{base}}} & \text{for } \Delta\overline{\mathrm{Cld}}_{\mathrm{scen}}(y) < 0 \\ 100 - (100 - \mathrm{Cld}_{\mathrm{ref}}(y)) \cdot \frac{100 - \left(\overline{\mathrm{Cld}}_{\mathrm{base}} + \Delta\overline{\mathrm{Cld}}_{\mathrm{scen}}(y)\right)}{100 - \overline{\mathrm{Cld}}_{\mathrm{base}}} & \text{for } \Delta\overline{\mathrm{Cld}}_{\mathrm{scen}}(y) > 0 \end{cases} \tag{4.8}$$

with $\mathrm{Cld}_{\mathrm{scen}}(y)$, $\mathrm{Cld}_{\mathrm{ref}}(y)$, $\Delta\overline{\mathrm{Cld}}_{\mathrm{scen}}(y)$, and $\overline{\mathrm{Cld}}_{\mathrm{base}}$ denoting the cloudiness time series of the scenario, the reference time series, the time series of anomalies, and the present-day climatological mean cloudiness in the AOGCM, respectively. For consistency with the anomalies and the reference time series, $\overline{\mathrm{Cld}}_{\mathrm{base}}$ needs to represent the simulated climatological mean for the year 2009. It is estimated by adding the cloudiness anomaly for a 0.9 K warming to the climatological mean of the control run (see section 4.2.2).

Precipitation

The application of precipitation anomalies is particularly challenging because of the importance of precipitation as key variable in impact assessments and the partially very large biases in simulated present-day precipitation. In cases where simulated precipitation in the control run is very low, small absolute increases correspond to very large relative changes. When applied to significantly higher observed precipitation rates, the absolute changes can become unrealistically large. Other studies have therefore proposed to use absolute changes or limit the relative changes in such cases (Carter et al. 1994, Hulme et al. 1995). Füssel (2003) notes that the problem depends on the degree of underestimation of present-day precipitation rates by AOGCMs and proposes a seamless transition from a relative towards an absolute application of anomalies, depending on the degree of underestimation. Here we adopt the approach by Füssel (2003) with some modifications required for the application to time series (see also Gerten et al. 2011, where a similar approach was used). Anomalies are applied as relative change, but as the underestimation of present-day precipitation in the AOGCM increases, the applied relative change is reduced so that the resulting mean change in the scenario time series becomes increasingly similar to the absolute change:

$$P_{\mathrm{scen}}(y) = P_{\mathrm{ref}}(y) \cdot \left[1 + \left(\frac{\Delta\overline{P}_{\mathrm{scen}}(y)}{\overline{P}_{\mathrm{ref}}}\right)\left(\frac{\overline{P}_{\mathrm{ref}}}{\overline{P}_{\mathrm{base}}}\right)^{\lambda}\right] \tag{4.9}$$

with

$$\lambda = \begin{cases} \sqrt{\frac{\overline{P}_{\mathrm{base}}}{\overline{P}_{\mathrm{ref}}}} & \text{for } \overline{P}_{\mathrm{base}} < \overline{P}_{\mathrm{ref}} \\ 1 & \text{for } \overline{P}_{\mathrm{base}} \geq \overline{P}_{\mathrm{ref}} \end{cases} \tag{4.10}$$

with $P_{\mathrm{scen}}(y)$, $P_{\mathrm{ref}}(y)$, and $\Delta\overline{P}_{\mathrm{scen}}(y)$ denoting the precipitation time series of the scenario, the reference time series, and the time series of anomalies, respectively; and $\overline{P}_{\mathrm{ref}}$ and $\overline{P}_{\mathrm{base}}$ denoting the climatological means of the reference time series and the year 2009 in the AOGCM, respectively. Estimation of $\overline{P}_{\mathrm{base}}$ is analogous to estimation of $\overline{\mathrm{Cld}}_{\mathrm{base}}$ (see section 4.2.3). The exponent λ determines the degree to which an anomaly is applied as absolute or relative change. If $\lambda = 1$, Equation 4.9 is equivalent to the relative interpretation of precipitation anomalies. If present precipitation is underestimated by the AOGCM, lower values of λ diminish the applied relative anomaly. If λ approaches zero, the factor applied to the values of the reference time series results in a shift of its mean equal to the absolute anomaly $\Delta\overline{P}_{\mathrm{scen}}(y)$. Because all anomalies are applied as a factor, the coefficient of variation is preserved in the scenario time series, which implies changes in interannual variability.

Rain month frequency

Based on the logistic regression model estimated from the AOGCM simulations, the probability of rain month occurrence was estimated for each month of the scaled scenario time series as follows:

$$p_{\text{scen}}(y) = \frac{e^z}{1+e^z} \quad \text{with} \quad z = \text{logit}\,(p_{\text{ref}}) + \beta^* \cdot \Delta T_{\text{glob}}(y) \tag{4.11}$$

where $p_{\text{scen}}(y)$ is the probability of year y in the scenario to be a rain month and p_{ref} the probability of rain month occurrence in the reference time series—i.e. the fraction of rain months in that series. In cases where p_{ref} is either 0 or 1, $\text{logit}\,(p_{\text{ref}})$ cannot be calculated and was set to a value of -7 and 7, respectively. This is equivalent to values for p_{ref} of about $1/1100$ and $1 - 1/1100$, respectively. The term $\beta^* \cdot \Delta T_{\text{glob}}(y)$ denotes the anomaly of the logit rain month probability estimated from the logistic regression model and T_{glob} anomalies (see section 4.2.2). Because the intercept and the slope of the logistic regression model are both estimated by fitting the model to the scenario data, extreme values are sometimes obtained for β^* where rain month probability is 0 or 1 and some singular dry or rain months occur towards the higher end of the temperature range. When used with the estimated intercept β_0, these slopes correspond to very small changes in rain month probability but produce unrealistically augmented probability changes when applied to p_{ref} in Equation 4.11. In order to avoid this effect, only slopes with a corresponding estimate for the intercept between -7 and 7 were applied; otherwise no change was applied. This rule applied to about 5.5 % of all significant estimates for β^*.

The application of p_{scen} to the reference time series entails the removal of excess and the introduction of additional rain months by means of a stochastic process. For this procedure, a random sequence $w(y)$ of uniformly distributed numbers between 0 and 1 is generated, which serves as a decision criterion on whether a rain month is introduced or removed in year y. If $p_{\text{scen}}(y)$ is smaller than p_{ref} a rain month is removed if

$$w(y) \geq \frac{p_{\text{scen}}(y)}{p_{\text{ref}}} \tag{4.12}$$

Conversely, if $p_{\text{scen}}(y)$ is larger than p_{ref}, a rain month is introduced if

$$1 - w(y) \geq \frac{1 - p_{\text{scen}}(y)}{1 - p_{\text{ref}}} \tag{4.13}$$

The precipitation event to be introduced is randomly chosen from the precipitation distribution of the respective reference time series. In cases where the reference time series has no rain month at all, a synthetic rainfall distribution is generated by interpolation from up to five neighbour cells with at least one precipitation event in their distribution. The

selection criterion for these cells was taken to be the highest interpolation weight from all cells within a radius of 450 km. Interpolation weights were calculated as in New et al. (2000) with account for distance and angular separation.

In order to preserve the spatial and temporal coherence of the precipitation field, the same random number sequence $w(y)$ was used for all grid cells and months of the year. The rationale behind this procedure is that for neighbouring cells with similar $p_{\mathrm{scen}}(y)$ and p_{ref}, rain months get removed or inserted in the same year. In order to avoid an overlap with the removal of rain months, however, the reflected sequence $1 - w(y)$ was used as decision criterion for the introduction of rain months. The procedure was applied prior to the scaling of precipitation amounts described in the preceding sections. Average reference precipitation used in Equations 4.9 and 4.10 was calculated from this modified reference time series.

Wet-day frequency

An additional information required by many impact models is the number of wet days per month. Due to the sparse availability of daily rainfall data from AOGCMs and strong biases in frequency distribution of rainfall intensities in many AOGCMs, this information is hard to extract from these models. The number of wet days per month is therefore estimated based on New et al. (2000) using the relationship between monthly precipitation sum and number of wet days:

$$\mathrm{WD}(y) = \overline{\mathrm{WD}}_{\mathrm{obs}} \left(\frac{P(y)}{\overline{P}_{\mathrm{obs}}} \right)^{\gamma} \tag{4.14}$$

where $P(y)$ and $\mathrm{WD}(y)$ represent the time series for precipitation sum and the estimated number of wet days of a month and grid cell, respectively. The exponent γ is assumed to be 0.45, which was found by New et al. (2000) to yield best results. The values $\overline{\mathrm{WD}}_{\mathrm{obs}}$ and $\overline{P}_{\mathrm{obs}}$ represent the observed 1961–1990 mean monthly wet-day frequency and precipitation sum, respectively. The former was derived from CRU TS3.1 (Harris et al. 2014) and the latter from GPCC version 5 (Rudolf et al. 2010). The means were calculated over the entire 30-yr period, including totally dry months. Because the datasets for wet days and precipitation are based on different station networks they are not fully consistent, i.e. there are cases where rain months have zero wet days (and vice versa). The absolute minimum for $\overline{\mathrm{WD}}_{\mathrm{obs}}$ is the fraction of rain months in the 30-yr period, which means that at least one wet day has to exist for each rain month. If the estimate of $\overline{\mathrm{WD}}_{\mathrm{obs}}$ is smaller than that, it was set to that minimum. This estimation procedure delivers conservative estimates of wet-day frequency for the scenario period, since the relationship between wet-day frequency and monthly precipitation sum is assumed to be constant over time.

4.3 Results and discussion

4.3.1 Properties of scaling patterns extracted from AOGCM simulations

The scaling patterns extracted from AOGCM simulations are the core component of the scenario-building described in this paper. They provide information on spatial and temporal heterogeneity of climate change signals for primary climate variables as projected by different AOGCMs. In this section, an overview is given of the spatial coverage of fits that are significant and of basic properties of the derived patterns (mean and standard deviation). The focus is primarily on a comparison of the different climate variables with some indication of the inter-model spread. A comprehensive overview with values for individual AOGCMs is presented in Table 4.1.

An apparent difference between the climate variables is the spatial and temporal coverage of significant slope parameters of the regression models obtained from the AOGCM simulation. As described in section 4.2.2, only slope estimates with a statistical significance >0.9 were accepted and used for the scaling. Each slope estimate is representative for a specific area (size of grid cell) and a specific time period of the year (length of month). In order to assess the spatial and temporal coverage of significant slope estimates, the product of area and duration for each significant slope is calculated and summed up. The sum is related to the product of total land area and length of the year to arrive at a percentage of spatial and temporal coverage.

Averaged over all AOGCMs, spatial and temporal coverage of significant slopes is 99.9 %, 82.0 %, and 78.2 % for temperature, cloudiness and precipitation, respectively (value for precipitation composed of 46.9 % significant increases in the linear case and 31.3 % significant decreases in the logarithmic case; Table 4.1). The average coverage of significant slopes for the logistic regression models for rain month probability is 10.9 % and 10.3 % if regression models with extreme intercepts are excluded (see section 4.2.3). Although there is considerable variation in spatial coverage of significant fits among individual AOGCMs (see Table 4.1), the relative magnitude of coverage for the different variables is consistent over all models. Near full coverage is found for temperature, followed by moderate to high coverage for cloudiness and precipitation (including both increases and decreases). Coverage of significant precipitation increases is in all cases higher than for decreases although values are similar in some cases. In all cases, coverage of significant changes of rain month frequency is smallest.

Although the coverage of significant changes for cloudiness, precipitation, and rain month frequency is significantly lower than for temperature, this must not be interpreted as an indication of limited applicability of the pattern-scaling approach for these variables. A major difference between temperature and the other variables is that for the former only positive trends occur, while the other variables display a mixture of positive and negative

Table 4.1: Overview over coverage of significant changes, pattern mean, and pattern standard deviation for temperature, cloudiness, precipitation, and rain month frequency for individual AOGCMs. Note that for precipitation coverage decreases refer to decreases of logarithmic precipitation. For calculation of pattern mean and standard deviation, decreases of logarithmic precipitation are converted to precipitation.

	Temperature			Cloudiness			Precipitation				Rain month frequency		
	coverage signif. change	Pattern mean (K)	Pattern stdDev (K)	coverage signif. change	Pattern mean (%)	Pattern stdDev (%)	coverage signif. increase	coverage signif. decrease	Pattern mean ($\mathrm{mm\,d^{-1}}$)	Pattern stdDev ($\mathrm{mm\,d^{-1}}$)	coverage signif. change	Pattern mean (K)	Pattern stdDev (K)
CCCMA-CGCM3.1	100.0 %	1.35	0.51	90.7 %	0.21	1.75	62.4 %	29.2 %	0.06	0.16	10.1 %	−0.0006	0.0194
CNRM-CM3	99.9 %	1.29	0.49	81.7 %	−0.75	1.67	48.0 %	29.8 %	0.03	0.20	7.5 %	−0.0017	0.0149
CSIRO-MK3.0	100.0 %	1.30	0.49	81.1 %	−0.91	1.72	37.0 %	29.3 %	0.00	0.19	7.8 %	−0.0038	0.0339
GFDL-CM2.0	100.0 %	1.40	0.50	78.7 %	−1.16	1.57	36.6 %	32.8 %	−0.01	0.27	13.8 %	−0.0063	0.0244
GFDL-CM2.1	99.7 %	1.43	0.58	77.7 %	−1.05	1.70	35.4 %	34.8 %	−0.02	0.27	13.5 %	−0.0074	0.0275
GISS-EH	99.3 %	1.33	0.50	81.9 %	0.37	2.09	45.3 %	30.9 %	0.04	0.32	5.0 %	−0.0017	0.0286
GISS-ER	99.9 %	1.37	0.44	75.6 %	−0.53	1.45	46.5 %	31.4 %	0.05	0.26	6.9 %	−0.0030	0.0215
IAP-FGOALS-g1.0	100.0 %	1.25	0.45	73.0 %	−0.37	0.97	39.0 %	32.5 %	0.03	0.15	4.0 %	0.0034	0.0287
INM-CM3.0	100.0 %	1.29	0.45	72.1 %	−0.40	1.39	46.3 %	31.2 %	0.03	0.18	5.8 %	−0.0016	0.0149
IPSL-CM4	100.0 %	1.37	0.40	87.5 %	−1.19	1.66	36.6 %	36.1 %	0.02	0.24	12.3 %	−0.0027	0.0209
MIROC3.2(hires)	100.0 %	1.23	0.42	85.3 %	−0.40	1.78	46.4 %	34.2 %	0.00	0.22	7.1 %	−0.0016	0.0154
MIROC3.2(medres)	100.0 %	1.36	0.55	91.6 %	−0.43	2.02	51.3 %	38.0 %	0.03	0.20	11.7 %	−0.0018	0.0161
MIUB-ECHO-G	100.0 %	1.40	0.59	87.3 %	−0.41	1.26	57.0 %	29.0 %	0.07	0.20	14.8 %	−0.0052	0.0253
MPI-ECHAM5	100.0 %	1.36	0.44	82.9 %	−0.62	1.33	46.3 %	28.0 %	0.02	0.19	20.4 %	−0.0072	0.0230
MRI-CGCM2.3.2a	100.0 %	1.18	0.42	82.2 %	−0.08	1.27	51.8 %	31.4 %	0.03	0.17	14.2 %	−0.0029	0.0213
NCAR-CCSM3	100.0 %	1.27	0.58	87.2 %	0.02	1.39	61.0 %	24.9 %	0.07	0.17	10.4 %	0.0018	0.0259
NCAR-PCM1	100.0 %	1.19	0.63	80.3 %	−0.13	1.22	55.1 %	25.5 %	0.06	0.17	10.5 %	−0.0003	0.0272
UKMO-HadCM3	100.0 %	1.39	0.47	79.7 %	−0.89	1.70	45.5 %	32.4 %	−0.01	0.29	8.5 %	−0.0034	0.0276
UKMO-HadGEM1	99.8 %	1.34	0.58	81.9 %	−0.50	1.44	43.6 %	32.2 %	−0.01	0.30	11.2 %	−0.0013	0.0197
min	99.3 %	1.18	0.40	72.1 %	−1.19	0.97	35.4 %	24.9 %	−0.02	0.15	4.0 %	−0.0074	0.0149
max	100.0 %	1.43	0.63	91.6 %	0.37	2.09	62.4 %	38.0 %	0.07	0.32	20.4 %	0.0034	0.0339
median	100.0 %	1.34	0.49	81.9 %	−0.43	1.57	46.3 %	31.4 %	0.03	0.20	10.4 %	−0.0018	0.0230
mean	99.9 %	1.32	0.50	82.0 %	−0.49	1.55	46.9 %	31.3 %	0.03	0.22	10.3 %	−0.0025	0.0230

trends (see Figures 4.3–4.6). This implies the existence of transition zones between areas with positive and negative trends in the monthly fields where trends are de facto zero and therefore no significant slopes can be found. In addition, cloudiness and precipitation both exhibit strong interannual variability that tends to mask weak trends that primarily occur around such transition zones. Similarly, the estimation of parameters of the logistic regression model for change of rain month frequency is hampered by the stochastic nature of this variable. Moreover, vast areas with a rain month frequency of 100 % (e.g. in the high latitudes and the wet tropics) remain unaffected by the occurrence of dry months under climate change (Figure 4.6).

For each derived anomaly pattern two statistics—mean and standard deviation—are calculated in order to characterise the patterns. We took into account the spatial and temporal coverage of the individual slopes—i.e. by weighting them with the respective cell area and length of month. Because the aim is to illustrate the properties of the entire pattern as it is applied, grid cells and months without a significant slope are included as zero values.

Averaged over all AOGCMs the mean anomaly of temperature increase over land is estimated to be 1.32 K per 1 K increase of T_{glob} (from 14.0 °C in the reference time series). Because T_{glob} anomalies and local temperature anomalies used in the regression are estimated from the same data, the value demonstrates that the land surface heats up much more than the whole of the global surface. This phenomenon is well known and is caused by the higher heat storage capacity of the oceans, which cause them to heat up less (Lambert and Chiang 2007). Although temperature trends are found to be always positive over land (Figure 4.3), there is considerable heterogeneity in the degree of warming in different regions and times of the year. This heterogeneity is captured by the pattern's standard deviation, which on average over all AOGCMs is 0.5 K. The mean and standard deviation for individual models are in the range of 1.18–1.43 and 0.40–0.63, respectively (Table 4.1).

The prevalence of a clear mean signal in the pattern is unique to temperature among the variables considered here. For cloudiness the average pattern mean is −0.49 %—less than 1 % of the mean cloudiness over land in the reference time series (55.3 %). The relatively small mean change is contrasted by a higher standard deviation of 1.55 %, which reveals the distinct spatial and temporal pattern of changes in cloudiness. This is consistent over all individual AOGCMs, which are characterised by mean changes between −1.19 and 0.37 %, and pattern standard deviations between 0.97 and 2.09 %, respectively.

For the calculation of pattern mean and standard deviation for precipitation, the decreases of logarithmic precipitation that make up the decreasing part of the pattern need to be converted to absolute changes in precipitation. Although the nonlinearity of exponential decrease may lead to an augmentation of precipitation decreases, the effect remains small due to the small magnitude of slopes of logarithmic precipitation decrease (−0.10,

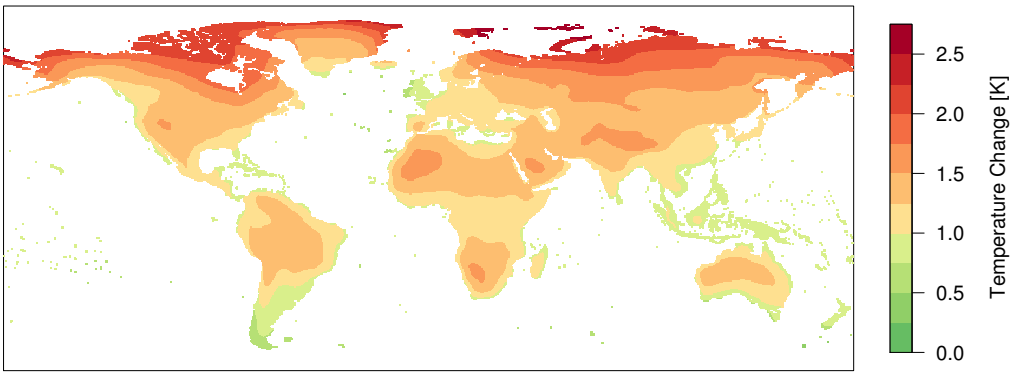

Figure 4.3: Multi-model mean of the actual applied annual mean change in near surface air temperature in K per 1 K of ΔT_{glob} (Equation 4.16).

average over all AOGCMs). Averaged over all AOGCMs a mean precipitation change of $0.026\,\mathrm{mm\,d^{-1}}$ (millimetre per day) is found, which is equivalent to $\sim$1 % of the mean precipitation rate over land in the reference time series ($2.27\,\mathrm{mm\,d^{-1}}$). Similar than for cloudiness, this small mean change is contrasted by a much larger standard deviation of $0.22\,\mathrm{mm\,d^{-1}}$ (averaged over all AOGCMs). Corresponding values for individual AOGCMs range between -0.016 and $0.069\,\mathrm{mm\,d^{-1}}$, and between 0.15 and $0.32\,\mathrm{mm\,d^{-1}}$ for mean and standard deviation, respectively (Table 4.1).

The slopes of the logistic regression for changes in rain month frequency are difficult to interpret in their original form and were therefore converted to changes in the fraction of rain months for the calculation of statistics. Averaged over all AOGCMs the mean change is -0.0025 rain months per month, which corresponds to an average loss of one rain month in about 33 yr on the entire land surface (including areas with no change). Average standard deviation of rain month changes is 0.028 rain months per month. For individual AOGCMs mean rain month frequency changes are between -0.0074 and 0.0034 rain months per month with standard deviations between 0.015 and 0.034.

4.4 Significance of scaling patterns extracted from AOGCM simulations

The assumption of a linear relationship between change in T_{glob} and mean local change of a climate variable V considered is central to pattern scaling. Although it is generally accepted that this assumption holds well for temperature (Mitchell 2003), it may not be fully valid for other climate variables. The focus of this section is therefore on a comparison between the different variables rather than between the different AOGCMs. However, values for individual AOGCMs are presented in Table 4.2.

For ordinary linear square models, such as those fitted to the AOGCM data for pattern extraction, the total sum of squares (TSS) equals the sum of explained sum of squares (ESS) and residual sum of squares (RSS). For the pattern extraction, this is described in Equation 4.15.

$$\sum_{y=1}^{N}[\Delta V(x,m,y)]^2 = \sum_{y=1}^{N}[V^*(x,m)\cdot\Delta T_{\mathrm{glob}}(y)]^2 + \sum_{y=1}^{N}[\Delta V(x,m,y) - V^*(x,m)\cdot\Delta T_{\mathrm{glob}}(y)]^2 \tag{4.15}$$

Based on this relationship, it is possible to evaluate the significance of the extracted patterns by comparing the explained sum of squares $\sum_{y=1}^{N}[V^*(x,m)\cdot\Delta T_{\mathrm{glob}}(y)]^2$ to the total sum of squares $\sum_{y=1}^{N}[\Delta V(x,m,y)]^2$ to provide a measure of explained variance. However, this measure is incomplete without an analysis of how much of the residual sum of squares $\sum_{y=1}^{N}[\Delta V(x,m,y) - V^*(x,m)\cdot\Delta T_{\mathrm{glob}}(y)]^2$ can be attributed to interannual variability inherent to the climate system. This variability cannot be captured by the linear regression, and the separation of the climate signal from the background variability is in fact the basic principle of the pattern-scaling approach. For the analysis of the residual sum of squares the variance of the control run $\mathrm{Var}_{\mathrm{cntrl}}(x,m)$ was multiplied with the number of values N in the residual sum of squares to obtain an estimate of the total sum of squared interannual variability to be expected in the scenario data.

Because Equation 4.15 is valid for every single regression model, the evaluation metrics derived from its terms can be calculated for every model, grid cell, and month. In order to facilitate a comparison of the performance for different variables, area-weighted means over all land cells for the different square sums are calculated for each model and month and then again averaged.

For the ratio of explained sum of squares to total sum of squares (ESS/TSS), ensemble means of 0.78, 0.20, 0.16, and 0.15 are found for temperature, cloudiness, precipitation (increases only), and logarithmic precipitation (decreases only), respectively. Corresponding ensemble means for ratios of residual mean of squares to control run variance ($\mathrm{RSS}/(N\cdot\mathrm{Var}_{\mathrm{cntrl}})$) are 0.93, 1.01, 1.29, and 1.13, respectively. Although ratios of explained variation for cloudiness, precipitation, and logarithmic precipitation appear to be very small, the comparison of residual variance to the control run variance reveals that most of the unexplained variation can be attributed to the high interannual variability of these variables. This is a clear indication that the derived patterns have a strong significance and can be used in a scenario-building framework such as the one applied here.

Table 4.2: Overview of individual AOGCMs' ratios of explained sum of squares (ESS) to total sum of squares (TSS) and ratios of residual sum of squares (RSS) to scaled control run variance ($N \cdot \mathrm{Var}_{\mathrm{cntrl}}$) for temperature, cloudiness, increasing precipitation, and decreasing logarithmic precipitation. In all cases, only significant linear regression models are included. The scaling of control run variance is necessary to make it comparable to RSS, which is calculated for N values.

	Temperature		Cloudiness		Increasing Precipitation		Decreasing Log. Precipitation	
	ESS/TSS	RSS/($N \cdot \mathrm{Var}_{\mathrm{cntrl}}$)	ESS/TSS	RSS/($N \cdot \mathrm{Var}_{\mathrm{cntrl}}$)	ESS/TSS	RSS/($N \cdot \mathrm{Var}_{\mathrm{cntrl}}$)	ESS/TSS	RSS/($N \cdot \mathrm{Var}_{\mathrm{cntrl}}$)
CCCMA-CGCM3.1	0.86	0.88	0.28	0.92	0.19	1.31	0.18	1.09
CNRM-CM3	0.81	0.87	0.21	0.96	0.15	1.28	0.16	1.14
CSIRO-MK3.0	0.72	0.98	0.20	1.34	0.10	1.23	0.12	1.12
GFDL-CM2.0	0.69	0.99	0.18	1.04	0.12	1.37	0.13	1.18
GFDL-CM2.1	0.70	0.98	0.18	1.01	0.10	1.30	0.16	1.15
GISS-EH	0.66	0.89	0.18	1.01	0.24	1.20	0.21	1.03
GISS-ER	0.74	0.96	0.16	0.97	0.25	1.26	0.16	1.03
IAP-FGOALS-g1.0	0.70	0.82	0.11	0.93	0.15	1.09	0.09	0.96
INM-CM3.0	0.72	0.89	0.15	0.96	0.15	1.20	0.13	1.09
IPSL-CM4	0.83	0.95	0.32	1.00	0.27	1.53	0.18	1.20
MIROC3.2(hires)	0.86	0.98	0.28	1.00	0.14	1.40	0.13	1.17
MIROC3.2(medres)	0.86	0.97	0.28	1.01	0.17	1.37	0.13	1.15
MIUB-ECHO-G	0.87	0.89	0.21	0.97	0.24	1.38	0.16	1.22
MPI-ECHAM5	0.79	1.00	0.14	1.05	0.11	1.34	0.11	1.21
MRI-CGCM2.3.2a	0.82	1.01	0.23	1.01	0.14	1.25	0.13	1.15
NCAR-CCSM3	0.82	0.88	0.19	1.00	0.20	1.21	0.12	1.13
NCAR-PCM1	0.77	0.82	0.11	1.01	0.14	1.15	0.08	1.10
UKMO-HadCM3	0.79	0.98	0.25	1.01	0.15	1.33	0.22	1.22
UKMO-HadGEM1	0.81	0.95	0.19	1.00	0.13	1.34	0.19	1.19
all	0.81	0.92	0.21	1.00	0.17	1.30	0.14	1.14
min	0.66	0.82	0.11	0.92	0.10	1.09	0.08	0.96
max	0.87	1.01	0.32	1.34	0.27	1.53	0.22	1.22
median	0.79	0.95	0.19	1.00	0.15	1.30	0.13	1.15
mean	0.78	0.93	0.20	1.01	0.16	1.29	0.15	1.13

Even the relatively high value of $(\mathrm{RSS}/(N \cdot \mathrm{Var}_{\mathrm{cntrl}}))$ for increasing precipitation (1.29) is not critical if one considers that increases of mean precipitation are usually accompanied by increases in variability. Because a transformation to logarithmic values diminishes this effect, the ratio of residual variance to control run variance is very close to unity (0.98) if it is calculated for increasing logarithmic precipitation. It should be mentioned, however, that precipitation change in the AOGCM simulations is also influenced by factors such as atmospheric aerosol loading, as these effects are not captured by the extracted patterns and therefore contribute to higher $(\mathrm{RSS}/(N \cdot \mathrm{Var}_{\mathrm{cntrl}}))$ ratios. The ratio of residual variance to control run variance smaller than unity for temperature means that the residual variation is generally slightly smaller than expected from the interannual variability estimated from the control run. This is an indicator for the strong relationship between local temperature anomalies and T_{glob} anomalies captured by the derived patterns. When using these patterns to predict local temperature anomalies in conjunction with actual $\Delta T_{\mathrm{glob}}(y)$, the part of interannual variability that can be explained by interannual variability of $\Delta T_{\mathrm{glob}}(y)$ is included which reduces the residual error. In contrast, the estimation of control run variance is based on a constant mean climatology and therefore includes the part of variability that is correlated to the variability in $\Delta T_{\mathrm{glob}}(y)$.

4.5 Applied local anomalies for 1 degree of global warming

The dataset for systematic climate impact assessment presented here is a combination of extracted patterns and the reference time series of temperature, precipitation, and cloudiness. While properties of the scaling patterns were discussed in the preceding section, this section explores the actual anomalies by which the scenario time series are shifted. For each variable the scaling patterns that represent the anomalies for a 1-degree increase in T_{glob} are applied to the reference time series according to the methodology described in section 4.2.3. Thereby, the absolute change $V^*(x,m)\cdot 1\,\mathrm{K}$ is altered, depending on the application method and the degree of disagreement between observed and simulated present-day climate. From the obtained time series multi-model means of the actual applied annual mean change are calculated:

$$\overline{\Delta\overline{V}}_{\mathrm{appl,1\,K}}(x) = \frac{1}{19 \cdot 12} \sum_{i=1}^{19} \sum_{m=1}^{12} \left[\overline{V}_{\mathrm{scen,1\,K}}(x,m,i) - \overline{V}_{\mathrm{ref}}(x,m)\right] \tag{4.16}$$

where $\overline{V}_{\mathrm{scen,1\,K}}(x,m,i)$ is the long-term climatological mean of the scenario time series for a T_{glob} increase by 1 K in location x, month m, and AOGCM i.

The alteration of anomalies by the application procedure is an important aspect of the methodology described in this paper. It is, however, a very general problem how to interpret and apply AOGCM-derived changes in climatological means when these means are biased.

If the observed climatology is underestimated the simulated change may underestimate the actual change and vice versa, providing that changes derived from a biased representation of reality are a meaningful source of actual change at all. All assessments that are based on anomalies obtained from AOGCM simulations are confronted with this problem and have to deal with the question whether to use the unchanged absolute anomalies or adjust them according to the biases in the AOGCM's presentation of actual conditions. In cases where anomalies are combined with observations, an adjustment is often inevitable, as a direct use of anomalies can cause an exceedance of valid ranges for some variables (e.g. most variables have a positivity constraint). In these cases a relative application of anomalies provides a convenient and plausible way of accounting for the different base levels in simulations and observations. There are, however, no objective criteria on whether and how to perform this adjustment. Hence, any solution represents a choice that cannot be validated in a meaningful way. Our methodology is no exception from that. It is grounded on common practice found in the impact literature, aiming to fulfil the particular requirements of the pattern-scaling approach, while minimising alterations of the original signal. In place of a validation, we here complement the presentation of applied anomalies in the end product by a presentation of the alteration of the original anomalies. Multi-model means of the alteration of the original anomalies $V^*(x,m) \cdot 1\,\mathrm{K}$ in $\overline{V}_{\mathrm{scen},1\,\mathrm{K}}(x,m,i)$ are calculated as

$$\overline{\Delta\overline{V}}_{\mathrm{alt},1\,\mathrm{K}}(x) = \frac{1}{19 \cdot 12} \sum_{i=1}^{19} \sum_{m=1}^{12} \left[\left| \overline{V}_{\mathrm{scen},1\,\mathrm{K}}(x,m,i) - \overline{V}_{\mathrm{ref}}(x,m) \right| - \left| V^*(x,m,i) \cdot 1\,\mathrm{K} \right| \right] \tag{4.17}$$

The omission of the sign of change by the modulo function in Equation 4.17 ensures that augmentations always have a positive sign and attenuations always have an negative sign, regardless of the sign of change.

For temperature, the actual applied anomalies for a 1-degree increase in T_{glob} (Figure 4.3) are identical to the scaling pattern, as temperature anomalies are applied as absolute changes (Equation 4.7). The spatial distribution of mean annual temperature changes across all AOGCMs exhibits the same overall behaviour as presented and discussed for the CMIP3 ensemble in IPCC (2007a). For the considered land area there are no incidents of decreasing local temperature with increasing T_{glob}. Below average warming (green colours) is only found in the vicinity of oceans, which is the result of the thermal inertia of the oceans. Overall, warming on the land surface is above average with a distinct pattern of polar amplification (stronger warming towards higher latitudes). Behind the multi-model annual mean change there is substantial variation in regional temperature change both among different AOGCMs and during the course of the year (see Appendix C). Disparity among AOGCMs is lower than the projected mean change—i.e. there is some

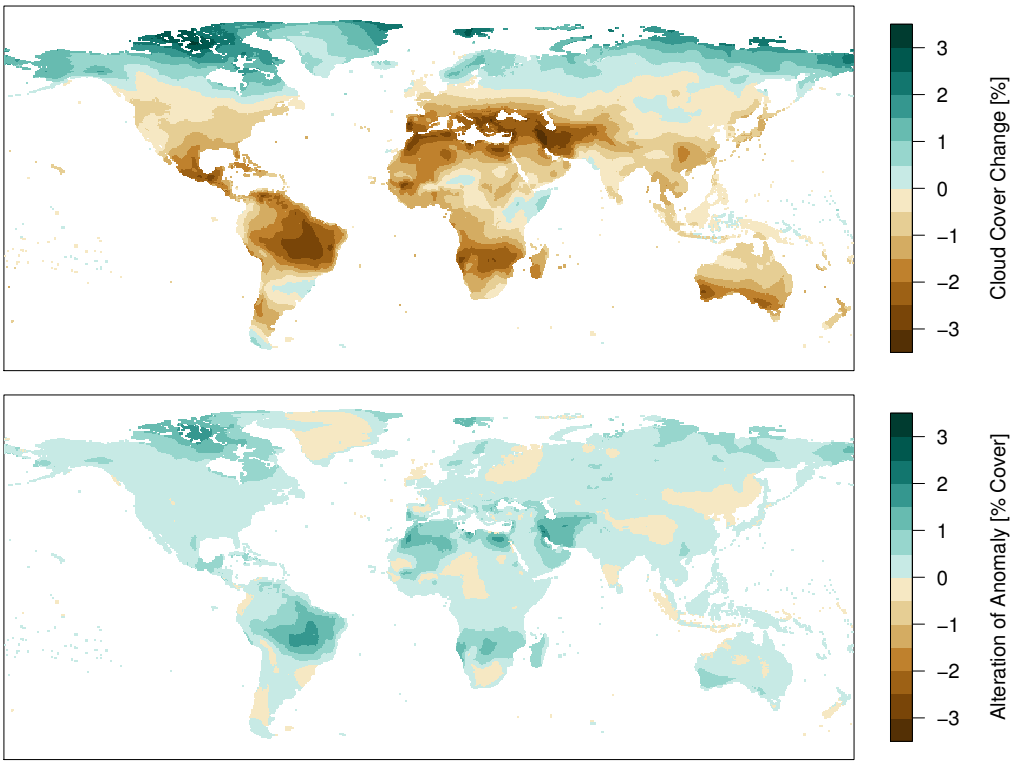

Figure 4.4: Upper panel: multi-model mean of the actual applied annual mean change in cloudiness in % cloud cover per 1 K of ΔT_{glob} (Equation 4.16). Lower panel: multi-model mean of the alteration of the original anomaly in % cloud cover for 1 K of ΔT_{glob} (Equation 4.17); positive values indicate an augmentation and negative values indicate an attenuation, regardless of the direction of change.

disagreement in the magnitude but not in the direction of change. Seasonality of change is particularly strong in the high northern latitudes and broadly follows the pattern of polar amplification. Hence, the strong average increase projected for these areas does not occur uniformly over the year.

Actual applied anomalies for cloudiness are a mix of cloud cover increases and decreases (Figure 4.4). Strong decreases are found in the Mediterranean, the Middle East, southern Africa, southern Australia, Central America, and the Amazon region. Increases are constrained to the higher northern latitudes and the Horn of Africa. In some areas, such as the northernmost latitudes, the Amazon, and some parts of Africa, variation of projected annual cloud cover change among AOGCMs is high with inter-model standard deviation exceeding the mean change (see Appendix C). Significant seasonality in the multi-model mean is limited to a few regions such as the Amazon, Central Asia and northeastern Canada only (see Appendix C). Regions with pronounced seasonality do not always coincide with regions of strong mean change, which indicates a mix of increases and decreases throughout

the year that cancel out each other in the annual mean.

Alteration of the absolute signal, averaged over all months and AOGCMs, by the application method described in section 4.2.3 is depicted in the lower panel of Figure 4.4. In most cases the application method augments the original signal, which means that decreases of cloudiness tend to be associated by underestimation and increases by overestimation of present-day cloud cover. However, in most cases the average alteration of the original signal is less than $\pm 0.5\,\%$. Significant alteration of the signal only occurs in northern Canada, the Amazon, the Middle East, and some parts of Africa—all of these regions being characterised by strong mean changes (Figure 4.4, upper panel).

The multi-model mean of annual precipitation change is shown in Figure 4.5 (upper panel). As for temperature and cloudiness, precipitation changes are consistent with results presented in IPCC (2007a). Significant decreases prevail in the Mediterranean, the Middle East, South Africa, southern Australia, Central America and Patagonia; increases are projected for the Boreal zone, South and Southeast Asia, East Africa, and parts of South America. For some regions such as the Amazon, Sub-Saharan Africa, and Southeast Asia inter-model standard deviation is high (see Appendix C), indicating considerable disagreement in the magnitude and in some cases even sign of mean annual precipitation change for the different AOGCMs. Seasonality of change is less pronounced but seems to occur in regions where the inter-model spread is high—i.e. the wet tropics but also in temperate North America and Europe (see Appendix C).

Although large biases in the AOGCMs impair the applicability of derived anomalies the alteration of the scaled anomalies by the application method is well controlled and rarely exceeds $\pm 0.05\,\mathrm{mm\,d^{-1}}$. Significant alterations primarily occur in mountainous regions (Andes, Rocky Mountains, Himalayas) where the AOGCMs' coarse spatial resolution impedes the correct representation of sub-grid orographic effects. In average, our application method attenuates rather than augments the original anomaly, which indicates that AOGCMs tend to overestimate observed precipitation rates. It is not the progressive reduction of the relative anomaly by the λ exponent with increasing underestimation in the AOGCM (Equation 4.9) that causes the overall attenuation. The reduction of the relative anomaly applies to both increases and decreases and merely compensates for the asymmetry in the relative application of anomalies derived from differently biased AOGCM baselines. While the attenuation in case of overestimation can never exceed the original anomaly when applied as relative change, the augmentation in case of underestimation in the AOGCM can become many times bigger than the original anomaly. With our approach, in contrast, the original anomaly is also augmented with increasing underestimation in the AOGCM, but reaches a maximum augmentation by a factor of about two for a five-fold underestimation and then declines towards unity for a completely rain-free AOGCM baseline.

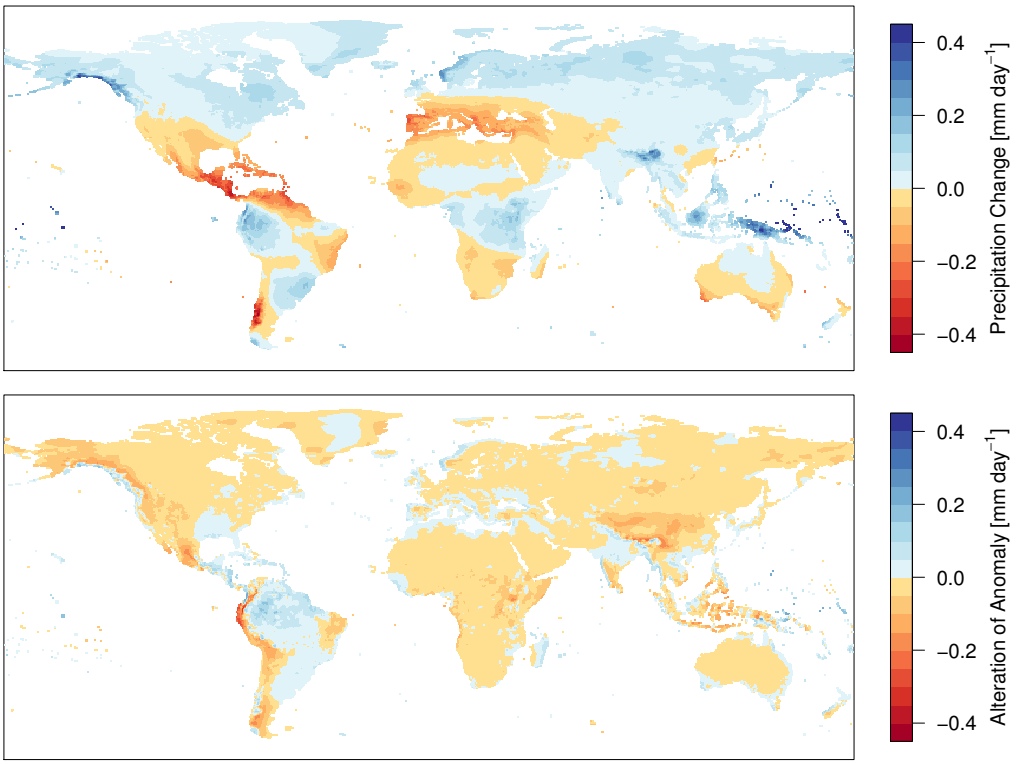

Figure 4.5: Upper panel: multi-model mean of the actual applied annual mean change in precipitation rate in mm d^{-1} per 1 K of ΔT_{glob} (Equation 4.16). Lower panel: multi-model mean of the alteration of the original anomaly in mm d^{-1} for 1 K of ΔT_{glob} (Equation 4.17); positive values indicate an augmentation and negative values indicate an attenuation, regardless of the direction of change.

Changes in rain month frequency are rarely analysed and here their explicit consideration in a pattern-scaling framework is unique. The rain month frequency changes, averaged over all AOGCMs and months, shown in the upper panel of Figure 4.6, exhibit both increases and decreases although decreases prevail. As already discussed in section 4.3.1, changes occur predominately in areas that are already today characterised by intermittent rainfall occurrence while regions such as North America, northern Europe, and Siberia remain unaffected. Regions of strong rain month frequency decrease broadly agree with key regions of decreases in average rainfall, but some noteworthy differences exist. Almost entire South America and Australia are, on average, affected by rain month frequency decrease while the picture for change in rainfall amount is much more mixed. In the Mediterranean, southern Europe is much less affected by rainfall amounts, while the opposite can be stated for North Africa. In southern Africa decreases in rain month frequency stretch much further up north along the east coast.

Variation of rain month frequency change among AOGCMs is pronounced but generally

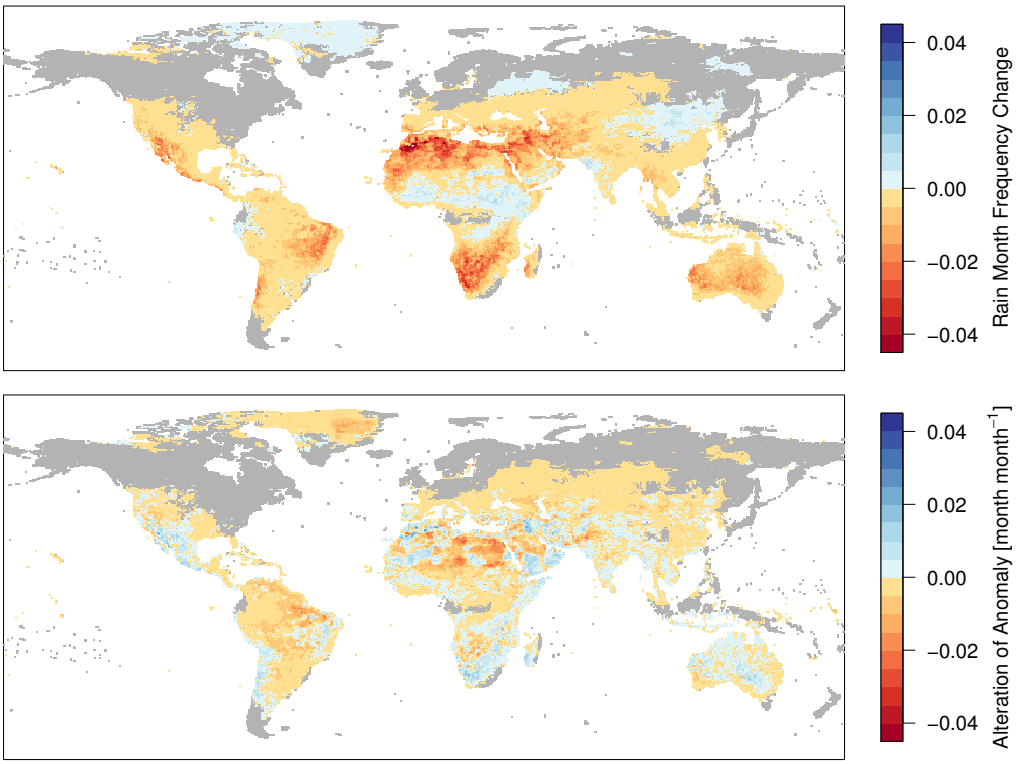

Figure 4.6: Upper panel: multi-model mean of the actual applied annual mean change in rain month frequency in month/month for a ΔT_{glob} of 1 K (Equation 4.16). Lower panel: multi-model mean of the alteration of the original anomaly in month/month for 1 K of ΔT_{glob} (Equation 4.17); positive values indicate an augmentation and negative values indicate an attenuation, regardless of the direction of change.

follows the pattern of strong decreases (see Appendix C). Thus, different models disagree primarily in the magnitude rather than in the direction of change. Seasonality of change is in the same magnitude as the inter-model variation and also exhibits a similar pattern (see Appendix C). Hence, decreases in rain month frequency in some months can be very high, while little change occurs in others.

Anomalies of rain month frequency are significantly altered by the application method (see Figure 4.6, lower panel). Although logit-transformed frequency anomalies are applied as absolute changes (see section 4.2.3), the different reference levels in the AOGCM and the observations result in very different actual frequency anomalies when transformed back. Equation 4.11 implies a sigmoid shape for the relationship between rain month frequency and ΔT_{glob}, which means that a given $\beta^* \cdot \Delta T_{\text{glob}}(y)$ produces the strongest change in rain month frequency when applied to a rain month frequency of 0.5; with reference values closer to 0 and 1 the effect progressively decreases. Consequently, augmentations of the signal occur when frequencies in the AOGCM are close to 0 or 1 and projected changes are

applied to observed rain month frequencies closer to 0.5. Attenuations occur in cases where changes are estimated from intermediate rain month frequency levels in the AOGCM and applied to reference frequencies closer to 0 or 1.

In summary, the multi-model mean of applied annual change for the different variables presented here are—where applicable—consistent with the results presented in IPCC (2007a). Although the application method can significantly alter the absolute anomaly for some variables, these alterations are not arbitrary but a consequence of the biases in AOGCMs. We believe that the application methods chosen for the different climate variables are well justified and fulfil the aim of providing the necessary adjustment while minimizing unnecessary alterations.

4.6 Conclusions

Here we present a newly composed dataset of climate change scenarios for systematic assessments of climate change impacts as a function of T_{glob} increase. The dataset combines observations, information extracted from AOGCM simulations, and results from a reduced complexity climate model into physically plausible climate change scenarios for a wide range of global mean temperature increases. The scenarios are designed to reach global mean temperature increases above pre-industrial levels between 1.5 and 5 degrees (in 0.5 degree steps) around the year 2100. The scaling patterns extracted for 19 AOGCMs from the CMIP3 data base for temperature, cloudiness, and precipitation represent the key component for linking local climate change to changes in T_{glob}. We discuss the properties of these patterns and demonstrate that they preserve the original AOGCM climate change properties with sufficient accuracy. The methodology for combining the local climate anomalies (derived from the scaling patterns and ΔT_{glob} trajectories) with observations is extensively discussed as it has the potential to alter the derived raw anomalies. We show that alterations of climate anomalies by the application method are a necessary adjustment of anomalies obtained from biased AOGCM baselines. The additional material used for creating the dataset—global datasets on observed historical climate and the reduced complexity climate model MAGICC6—are not further discussed in this paper. They are well documented in other literature.

Supplementary material related to this chapter is available in Appendix C.

Acknowledgments

This work was supported by ILRI and the CGIAR research program on Climate Change, Agriculture and Food Security (CCAFS). Further support was given by GLUES (Global As-

sessment of Land Use Dynamics, Greenhouse Gas Emissions and Ecosystem Services), a scientific coordination and synthesis project of the German Federal Ministry of Education and Research's (BMBF's) "Sustainable Land Management" programme (Code 01LL0901A), and the WATCH (FP6, grant no. 036946), CLIMAFRICA (FP7, grant no. 244240) and ERMITAGE (FP7, grant no. 265170) projects funded by the European Commission.

We acknowledge the modelling groups, the Programme for Climate Model Diagnosis and Intercomparison (PCMDI) and the WCRP's Working Group on Coupled Modelling (WGCM) for their roles in making available the WCRP CMIP3 multi-model dataset. Support of this dataset is provided by the Office of Science, US Department of Energy.

Chapter 5

Freshwater resources under success and failure of the Paris climate agreement

An edited version of this chapter has been published as: J. Heinke, C. Müller, M. Lannerstad, D. Gerten, and W. Lucht. Freshwater resources under success and failure of the Paris climate agreement. *Earth System Dynamics*, 10(2):205–217, 2019a. doi: 10.5194/esd-10-205-2019

Abstract

Population growth will in many regions increase the pressure on water resources and likely increase the number of people affected by water scarcity. In parallel, global warming causes hydrological changes which will affect freshwater supply for human use in many regions. This study estimates the exposure of future population to severe hydrological changes relevant from a freshwater resource perspective at different levels of global mean temperature rise above pre-industrial level (ΔT_{glob}). The analysis is complemented by an assessment of water scarcity that would occur without additional climate change due to population change alone; this is done to identify the population groups that are faced with particularly high adaptation challenges. The results are analysed in the context of success and failure of implementing the Paris Agreement to evaluate how climate mitigation can reduce the future number of people exposed to severe hydrological change. The results show that without climate mitigation efforts, in the year 2100 about 4.9 billion people in the SSP2 population scenario would *more likely than not* be exposed to severe hydrological change, and about 2.1 billion of them would be faced with particularly high adaptation challenges due to already prevailing water scarcity. Limiting warming to 2 °C by a successful implementation of the Paris Agreement would strongly reduce these numbers to 615 million and 290 million, respectively. At the regional scale, substantial water-related risks remain at 2 °C, with more than 12 % of the population exposed to severe hydrological change and high adaptation challenges in Latin America and the Middle East and north Africa region. Constraining ΔT_{glob} to 1.5 °C would limit this share to about 5 % in these regions.

5.1 Introduction

Within the 2030 Agenda for Sustainable Development of the United Nations (United Nations 2015), "access to clean water and sanitation" is one of the 17 sustainable development goals (SDGs). For other SDGs, such as "zero hunger" and "affordable and clean energy", access to sufficient water resources is a precondition (ICSU 2017). Already today, more than 2 billion people live in countries where total freshwater withdrawals exceed 25 % of the total renewable freshwater resource (United Nations 2017). Population increase and economic development are expected to further increase pressure on water resources leading to enormous challenges for water resource management to maintain or increase water supply. Climate change potentially aggravates this challenge in some regions by altering precipitation patterns in time and space, increasing atmospheric demand, or accelerating glacial melt, to name just a few. Such changes can lead to a reduction in total physical water availability, but also a change in the flow regime, which may lead to more frequent or more severe drought events or an increased risk of flooding (Döll and Schmied 2012). All these changes affect water supply management and will make meeting the demand and achieving SDGs more costly or impossible.

As of April 2017, 194 countries responsible for >99 % of global greenhouse gas emissions have signed the Paris climate agreement that aims at "holding the increase in the global average temperature to well below 2 °C above pre-industrial levels and pursuing efforts to limit the temperature increase to 1.5 °C above pre-industrial levels" (UNFCCC 2015). However, the Intended Nationally Determined Contributions submitted by countries so far are insufficient to achieve this goal, probably leading to a median warming of 2.2 °C to 3.5 °C by 2100 if no further efforts are taken (Rogelj et al. 2016). With the announced withdrawal of the US from the agreement and all major industrialized countries currently failing to meet their pledges (Victor et al. 2017), even a more extreme warming cannot be ruled out. It is therefore timely to assess the climate change impacts associated with a success (limit warming to 1.5 or 2 °C) and a failure of the Paris Agreement (exceeding 2 °C). The purpose of this study is to provide such an assessment for the water sector by systematically quantifying hydrological changes relevant from a freshwater resource perspective at different levels of global warming between 1.5 and 5 °C above pre-industrial levels in steps of 0.5 °C. The most extreme level of 5 °C thereby marks an upper boundary consistent with the median warming for a scenario without climate policy (3.1 °C to 4.8 °C; Rogelj et al. (2016)).

Unlike most global assessments of climate change impacts on water resources, which have employed a measure of water stress like the water crowding index (WCI; Falkenmark (1989)) or the withdrawal-to-availability ratio (WTA; Raskin et al. (1996)), here we analyse hydrological changes relevant from a water resource perspective directly. This allows us to

focus on climate-induced hydrological change alone (unobscured by the effects of population change) and to include aspects of hydrological change important from a water resource perspective other than mean annual discharge (MAD), on which both WCI and WTA are based. In order to gain a detailed and comprehensive understanding of changes in the water sector, this study analyses climate impacts with respect to a decrease in mean water availability, growing prevalence of hydrological droughts, and an increase of flooding hazards. To estimate these hydrological changes, three key metrics are used to assess flow regime changes: (i) MAD, (ii) the average number of drought months per year (ND), and (iii) the 10-year flood peak (Q10). Severe hydrological change is defined as crossing a critical threshold (defined below) for at least one of these key metrics. By combining these changes with spatially explicit population projections consistent with shared socio-economic pathways (SSPs; Jones and O'Neill (2016)), the number of people exposed to severe hydrologic changes is estimated for each level of ΔT_{glob}.

However, looking at the total number of people affected by severe hydrological change provides only limited insights into the consequences of severe hydrological change and the challenges for adaptation. These are greatly determined by the underlying population-driven water-scarcity level; that is, when options for supply-side management are exhausted or become too costly under water-scarcity conditions, the focus of water management has to shift towards demand management (Falkenmark 1989, Ohlsson and Turton 1999). Thus, adaptation to severe hydrological change under already water-scarce conditions will also have to involve demandside management strategies to prevent negative social and economic consequences. Because demand-side options are complex and their implementation is faced with behavioural, economic, political, and institutional obstacles (Kampragou et al. 2011, Russell and Fielding 2010), adaptation to severe hydrological change is more challenging under already water-scarce conditions. To account for this aspect, we apply the WCI to estimate the future population pressure on water resources under the assumption of no climate change and jointly analyse climate-induced severe hydrological change and population-driven water scarcity.

5.2 Methods

5.2.1 Population scenarios

For the estimation of future population affected by severe hydrological change and to calculate WCI, we use spatially explicit population projections from Jones and O'Neill (2016, 2017). These are based on the SSP national population projections (KC and Lutz 2017) and have been downscaled making additional assumptions on urbanization consistent with the respective SSP storyline. The five SSP storylines are designed to cover a broad range of future socio-economic development pathways with plausible future changes in

demographics, human development, economy, institutions, technology, and environment (O'Neill et al. 2017). However, they do not account for the impact of climate change on development pathways. For this study we only use the population projections of the SSPs. The analysis focuses on the middle-of-the-road scenario SSP2 (with a total population of 9.0 billion in 2100), but we use the other scenarios (with a total population between 6.9 and 12.6 billion in 2100) to test the sensitivity of our findings to different population scenarios.

5.2.2 Climate scenarios

In order to systematically assess climate change impacts on freshwater resources, we use the PanClim climate scenarios described in Heinke et al. (2013a). The dataset consists of 8 different scenarios of ΔT_{glob} obtained with the MAGICC6 model (Meinshausen et al. 2011a) based on greenhouse gas emissions that result in a range of warming levels above pre-industrial (∼1850) conditions from 1.5 °C to 5.0 °C in steps of 0.5 °C in 2100 (2086–2115 average). For each ΔT_{glob} pathway, the local response in climate variables is emulated for 19 different general circulation models (GCMs) from the Coupled Model Intercomparison Project Phase 3 (CMIP3) ensemble using a pattern-scaling approach. In so doing, normalized climate anomalies (changes per 1.0 °C of ΔT_{glob} increase) of temperature, precipitation, and cloud cover for each month of the year in each 0.5° × 0.5° grid cell are obtained by linear regression between time series of climate variables and the corresponding time series of ΔT_{glob}. The unexplained variance of these linear models is in the same order of magnitude (temperature and cloud cover) or only slightly larger (precipitation) than inter-annual variability in the pre-industrial control run without anthropogenic forcing, indicating that most of the climate change information is captured by the obtained patterns. The normalized climate anomalies are used to calculate local climate anomalies for any given ΔT_{glob} relative to the year 2009 (when ΔT_{glob} was 0.9 °C above the pre-industrial level). These local climate anomalies were then applied to monthly reference time series of local climate that represent average conditions and variability in 2009.

A total of 152 climate scenarios (8 ΔT_{glob} pathways × 19 GCM patterns) for the period 1901–2115 are obtained. Up to the year 2009, time series are based on mean air temperature and cloud cover from CRU TS3.1 (Harris et al. 2014) and precipitation from the Global Precipitation Climatology Centre's (GPCC) full reanalysis dataset version 5 (Schneider et al. 2014). The reference time series for the period 2010–2115, to which climate anomalies are applied, is created from the historic datasets by random resampling with replacement. Further details on the climate scenarios have been described by Heinke et al. (2013a).

5.2.3 Impact model

For assessing the impacts of climate change on the hydrological cycle, we employ the LPJmL Dynamic Global Vegetation Model version 4 (LPJmL4) that simulates the growth of natural vegetation and managed land coupled with the global carbon and hydrological cycles (Schaphoff et al. 2018b,c). The model has been extensively evaluated showing good performance in representing the global hydrological cycle (Rost et al. 2008, Schaphoff et al. 2018a). LPJmL has been widely applied in water resource assessments (Gerten et al. 2011, Jägermeyr et al. 2016, Rockström et al. 2014, Steffen et al. 2015b).

For the simulations conducted here, the model is first run without land use for a spin-up period of ∼5000 years using pre-industrial atmospheric CO_2 concentrations and climate data from 1901 to 1930. This is followed by a second spin-up of 390 years up to 2009, during which atmospheric CO_2 concentrations and climate vary according to historical observations, and constant land use of the year 2000 is prescribed (Fader et al. 2010). All 152 scenario simulations are initialized from this state, assuming constant land use over the whole simulation period and atmospheric CO_2 concentrations consistent with the respective ΔT_{glob} scenario (Heinke et al. 2013a). All simulations are performed without direct anthropogenic intervention on freshwater resources (water withdrawals and dam operation) as their effects are assumed to be captured by the WCI.

In addition to the 152 ΔT_{glob} scenarios one additional simulation for the period 2010–2115 is carried out using the reference climate data without any anomalies applied and with constant atmospheric CO_2 concentrations of the year 2009. This simulation represents a no climate change setting for which transient time series with inter-annual variability (but without a general trend) are produced. This scenario is used as the reference simulation for the comparison with the other climate scenarios. Because the sequence of dry and wet years is identical in all scenarios and the reference case, any differences between the scenarios and the no-climate-change reference simulation can be attributed to global warming. Within this paper we analyse the 30-year time period from 2086 to 2115 in which the average temperature increase equals ΔT_{glob}.

5.2.4 Hydrological change metrics

The focus of this study is on hydrological changes due to climate change that are relevant from a water resource perspective. "Water resources" refers to "blue" water—the water that can be withdrawn from rivers, lakes, and aquifers, and which can be directly managed by humans—as opposed to "green" water, i.e. the soil moisture in the root zone from local precipitation that can only be used by locally growing plants (Rockström et al. 2014).

Here we use river discharge as an approximation of the blue water resource. River discharge is simulated in LPJmL by means of a linear storage cascade (Schaphoff et al.

2018b) along a river network defined by the Simulated Topological Network (STN-30p) flow direction map (Vörösmarty et al. 2000, 2011). The simulated discharge of a grid cell includes all the water that enters the cell from upstream areas and all surface and subsurface runoff generated within the cell. Although water is often withdrawn from lakes and aquifers, no more than the possible recharge to these storages can be withdrawn over a prolonged period. Therefore, river discharge as computed with LPJmL represents a good approximation of the total renewable blue water resource (excluding non-renewable fossil groundwater from aquifers with very long recharge times).

Three metrics relevant from a water resource perspective, i.e. mean annual discharge (MAD), the number of drought months per year (ND), and the 10-year flood peak (Q10), are calculated for each grid cell for the 8 levels of ΔT_{glob} and 19 GCM patterns. Severe hydrological change is defined as crossing a critical threshold for at least one of these three metrics: a greater than 20 % decrease in MAD, an increase of 50 % in ND, and an increase in Q10 by 30 % (further described below). Based on these results we determine the lowest level of ΔT_{glob} in each grid cell at which the thresholds for each of the metrics are transgressed in more than 50 % of GCM runs (at least 10 out of 19). This transgression in more than 50 % of GCMs corresponds to the *more likely than not* likelihood category used in IPCC AR5 (Mastrandrea et al. 2011).

Mean water availability

Changes in MAD are used as a measure for changes in mean water availability, assuming that a substantial decline in MAD will make it difficult to satisfy existing and future societal water demands with the existing water supply infrastructure. We define a decrease in MAD by 20 % or more as a severe hydrological change that requires some form of management intervention (either on the supply or the demand side). The same threshold was also used by Schewe et al. (2014) to define severe decrease in annual discharge.

Hydrological drought

The occurrence of prolonged periods of below-average discharge, mostly initiated by inter-annual climate variability, is referred to as hydrological drought. To provide stable water supply to society, water supply systems are adjusted to seasonal variability and drought regimes. A substantial increase in drought periods thus impairs the capability of existing water management infrastructure.

We apply a drought identification method proposed by van Huijgevoort et al. (2012) to determine which months of a monthly time series of river discharge are in drought condition. The method is based on a combination of the threshold level method (TLM) and the consecutive dry month method (CDM). The TLM method classifies a month as drought-

stricken if discharge falls below a given threshold (here the month-specific discharge that is exceeded 80 % of the time). However, in ephemeral rivers a method that accounts for the duration of dry periods is more appropriate since the TLM would classify all months with zero flow as drought. We adopt this combination of TLM and CDM from van Huijgevoort et al. (2012) but make some modifications to obtain a more robust and plausible algorithm. First, a month-specific discharge threshold is applied to identify drought months according to the TLM method. Then, if the TLM threshold is zero and the number of drought months in a given calendar month (e.g. January) exceeds 20 %, the CDM is used to determine which of the months with zero discharge can be classified as drought months. To this end, the number of preceding consecutive TLM droughts is determined for each month with zero discharge in the given calendar month. Finally, a threshold is selected that retains only the months with the longest preceding dry period so that the total number of drought months in that calendar month is 20 %. The TLM and CDM thresholds are determined from the reference simulation representing present-day climate conditions. These thresholds are then used to estimate the number of drought months for all climate scenarios. Note that the thresholds are derived from and applied to the continuous 30-year time series, which allows for the detection of multi-year droughts.

We define an increase in the average number of drought months per year (ND) by 50 % (i.e. from 20 % to 30 %) as a severe hydrological change that will require an upgrade of existing water management systems to maintain a reliable water supply.

Flood hazard

All water supply infrastructure should be designed to withstand typical flooding events. A flood with a return time of 50–100 years (Q100) is typically used as a reference case (Coles 2001). However, spillways of critical infrastructure such as dams and reservoirs are designed for even more severe flood events, with a return time of 1000 years or more (Dyck and Peschke 1995). An increase in the magnitude of floods poses a serious threat to water management systems with potentially disastrous consequences.

The magnitude of extreme events with long return periods is usually derived from much shorter observed time series of annual maximum floods by fitting a suitable extreme value distribution (e.g. a Gumbel or generalized extreme value, GEV, distribution; Coles (2001)). The obtained extreme value distribution is then used to extrapolate the magnitude of flood events with long return periods. This procedure can also be used to detect changes in the magnitude or the return time of such events from two fitted extreme value distributions (Dankers et al. 2014). However, fitting a GEV distribution to 5-day average peak flow estimates form LPJmL using L moments (Hosking and Wallis 1995) gave good fits (p value of Kolmogorov-Smirnov test >0.9) in only about half of all cases. In order to estimate the change in flood hazard for all grid cells, we analyse changes in the magnitude of floods with

a 10-year return time (Q10), which are directly derived by determining the 5-day average peak flow that is exceeded in 3 out of 30 years (technically a return time of 10.33 years).

We use the cases where a good fit of the GEV to data was achieved to assess how well the estimated changes in directly derived Q10 can be used as a proxy for changes in events with a higher return time (Q100 or Q1000) derived from GEVs. Because the overall goal is to detect a severe increase in Q100 or Q1000, we estimate how many false positives and false negatives occur when a threshold of 20 % or 30 % increase, respectively, in Q10 is used. False positives are defined as increases in Q10 by more than 20 % or 30 %, which does not coincide with an increase in Q100 or Q1000 by at least 10 %; false negatives are defined as an increase in Q100 or Q1000 by more than 50 %, which do not coincide with an increase in Q10 by at least 20 % or 30 %. For Q100, we find that a threshold of 20 % for Q10 produces 6.3 % and 4.7 % of false positives and negatives, respectively; a threshold of 30 % produces 2.6 % and 11.0 % of false positives and negatives, respectively. For Q1000 the figures are much higher with 15.9 % (10.7 %) of false positives and 33.8 % (47.0 %) of false negatives for a threshold of 20 % (30 %) for Q10. This demonstrates that Q10 can be used as proxy to detect severe changes in Q100 with reasonable accuracy but not to detect severe changes in Q1000.

We give the avoidance of false positives a higher priority to obtain conservative estimates of flood hazard increase. Therefore, we choose an increase in Q10 by 30 % as a threshold to detect a severe increase in flooding hazard that needs to be addressed by investment in enhancing flood resistance of water supply infrastructure or by changing reservoir operation schemes to increase the safety buffer for flood protection (at the cost of storage capacity for water supply). However, it needs to be kept in mind that this indicator only detects about half of the increases in Q1000 by more than 50 %, which can be particularly harmful to water management infrastructure.

5.2.5 Grid-based water crowding indicator

In order to determine where transgressions of severe hydrological change thresholds in the three metrics matter most, we estimate which part of the global population is experiencing water stress in the absence of additional climate change. We use the WCI originally proposed by Falkenmark (1989) to assess different levels of population pressure on water resources. Originally, the water crowding index was applied at the country scale, which may hide important within-country variations (Arnell 2004). With improved spatial resolution of population data and a desire to use natural hydrological units, instead of administrative boundaries, it has become more common to calculate WCI at the basin scale (Arnell and Lloyd-Hughes 2014, Falkenmark and Lannerstad 2004, Gerten et al. 2013, Gosling and Arnell 2016). In this paper, we develop a new calculation procedure to obtain a measure of water crowding that can be calculated and interpreted at the grid-cell scale. This can

then be combined with the simulated hydrological changes at the grid-cell scale to estimate hydrological change for different levels of water crowding.

To calculate the effective population pressure on the total available water within each grid cell, we treat local (within grid cell) runoff and the inflow from each upstream cell i separately. The upstream cells of any given grid cell can be derived from the STN-30p flow direction map (Vörösmarty et al. 2000), which is also used to simulate discharge in LPJmL. While local runoff w_0 is assumed to be fully available to the local population p_0, the inflow from each upstream cell w_i is equally shared between local population p_0 and effective upstream population p'_i corresponding to that inflow (Equation 5.1).

$$w' = w_0 + \sum_{i=1}^{N} w_i \cdot \frac{p_0}{p'_i + p_0} \tag{5.1}$$

The obtained effective water quantity w' is the effective available water in that grid cell. Relating local population p_0 to w' yields the effective water crowding index WCI$'$ (Equation 5.2) for the respective cell.

$$\mathrm{WCI}' = \frac{p_0}{w'} \tag{5.2}$$

Multiplying WCI$'$ with the total water w (sum of local runoff and all inflows) gives the effective population p' (Equation 5.3) that is required for the calculation of WCI$'$ in the downstream cell.

$$p' = \mathrm{WCI}' \cdot w = p_0 \frac{w}{w'} \tag{5.3}$$

Because p' of all upstream cells must be known to determine WCI$'$, the calculation for a whole basin starts at the fringes (in cells with no inflow, i.e. where $w_i = p'_i = 0$) and continues consecutively to the basin outlet.

Five different WCI levels can be distinguished, each characterized by a different degree of water scarcity (Falkenmark 1989). WCI below 100 people per flow unit (p/fu; 1 fu = $10^6\,\mathrm{m}^3\,\mathrm{year}^{-1}$) are considered uncritical, *quality and dry-season problems* occur between 100 and 600 p/fu, and water stress occurs between 600 and 1000 p/fu. Beyond 1000 p/fu a population experiences *absolute water scarcity*, and the level of 2000 p/fu is interpreted as the *water barrier* beyond which all available water resources are utilized. With increasing degrees of water scarcity it becomes progressively harder to fulfil societal water demand by supply-side management and coping with *absolute water scarcity* has to involve demand-side management options (Falkenmark 1989). It is reasonable to assume that adaptation to severe hydrological change under *absolute water scarcity* will not be possible by adjusting water supply infrastructure alone but will also require demand management strategies. Because of the big behavioural, economic, political, and institutional challenges associated

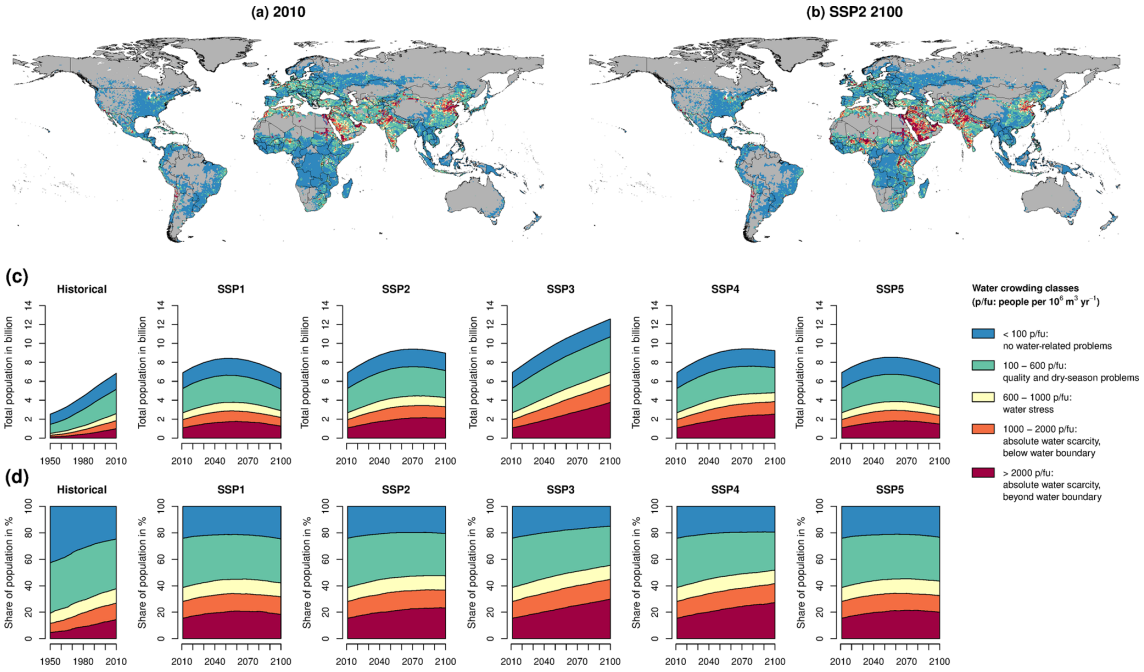

Figure 5.1: Spatial pattern of water crowding in 2010 **(a)** and in 2100 for SSP2 population **(b)**. Absolute **(c)** and percentage share of total population **(d)** in different water crowding classes from 1950 to 2010 and from 2011 to 2100 in five different SSP population scenarios under current water availability, i.e. assuming no climate change.

with demand management (Kampragou et al. 2011, Russell and Fielding 2010), we assess exposure to severe hydrological change within the population group experiencing *absolute water scarcity* and within the population group that does not.

5.3 Results

5.3.1 Change in water crowding driven by population change

Between 1950 and 2010 the number of people that live with *absolute water scarcity* (WCI $>$ 1000 p/fu) has increased more than 6 fold from 295 million (11.7 % of global population) to 1.83 billion (26.8 % of global population) due to population growth alone. In the same time period, the number of people beyond the *water barrier* (WCI $>$ 500 p/fu) within that group has increased more than 8 fold from 118 million (4.7 % of global population) to 988 million people (14.5 % of global population), so that its share within the group of people living under *absolute water scarcity* has increased from 40.2 % to 53.9 % (Figure 5.1c and d).

This trend is projected to continue in the future under all five SSP population scenarios (Figure 5.1c and d). The total number of people living under *absolute water scarcity* in

2100 due to population change alone (without any additional climate change) is projected to be higher than today (2010) in all scenarios reaching 2.16–5.65 billion (31.5 %–44.9 % of global population), with higher global population being associated with higher absolute and relative numbers of affected people. The number of people who live beyond the *water barrier* is projected to increase to 1.26–3.77 billion (18.4 %–29.9 % of global population, 58.4 %–66.7 % of population under *absolute water scarcity*).

5.3.2 Severe changes in hydrologic conditions under different levels of ΔT_{glob}

Under the majority of climate change patterns within the range of ΔT_{glob} considered in this study, severe decreases in mean water availability, severe increases in droughts, and severe increases in flood hazard occur in many abundantly populated regions. We estimate that 4.93 billion people (54.9 % of global population) would *more likely than not* be exposed to severe hydrological change in the SSP2 population scenario if ΔT_{glob} reaches 5 °C by 2100 (Figure 5.2a; for other SSP scenarios see Supplement Figure D.2). Out of these, 1.09 billion, 1.26 billion, and 1.31 billion would *more likely than not* be exposed to a severe decrease in mean water availability, a severe increase in droughts, and a severe increase in flood hazard, respectively (Figure 5.2b–d). Note that severe decreases in mean water availability and severe increases in droughts often coincide, which leads to relatively large number of people (889 million) being *more likely than not* exposed to both of these aspects of severe hydrological change. For 2.15 billion people a transgression of the critical threshold for a mix of the three different aspects of severe hydrological change is projected in more than half of the GCMs. The pace at which these levels are reached with increasing ΔT_{glob} is not linear and differs for the three aspects of severe hydrological change. The additional number of people that become exposed to a severe decrease in mean water availability at each step of ΔT_{glob} first increases and then declines again, with the by far largest increment occurring between 2 and 2.5 °C. A similar pattern is found for exposure to severe increase in droughts with the difference that the largest increase occurs between 1.5 and 2 °C. The increment of people becoming exposed to severe increase in flood hazard is very small until 2 °C warming and then steadily increases with ΔT_{glob}. This overall pattern of varying increase in exposure to severe hydrological change with increasing ΔT_{glob} is very similar across all five SSP population scenarios considered here (Figure D.2).

If global warming was limited to 2 °C by a successful implementation of the Paris Agreement, the number of people *more likely than not* exposed to severe hydrological change under SSP2 could be limited to only 615 million people (6.9 % of global population; Figure 5.2a), protecting almost 9 out of 10 people (87.5 %) from exposure to severe hydrological change compared to a warming by 5 °C. Because exposure to increased flooding hazard remains very low until 2 °C warming, the majority of the remaining population would be

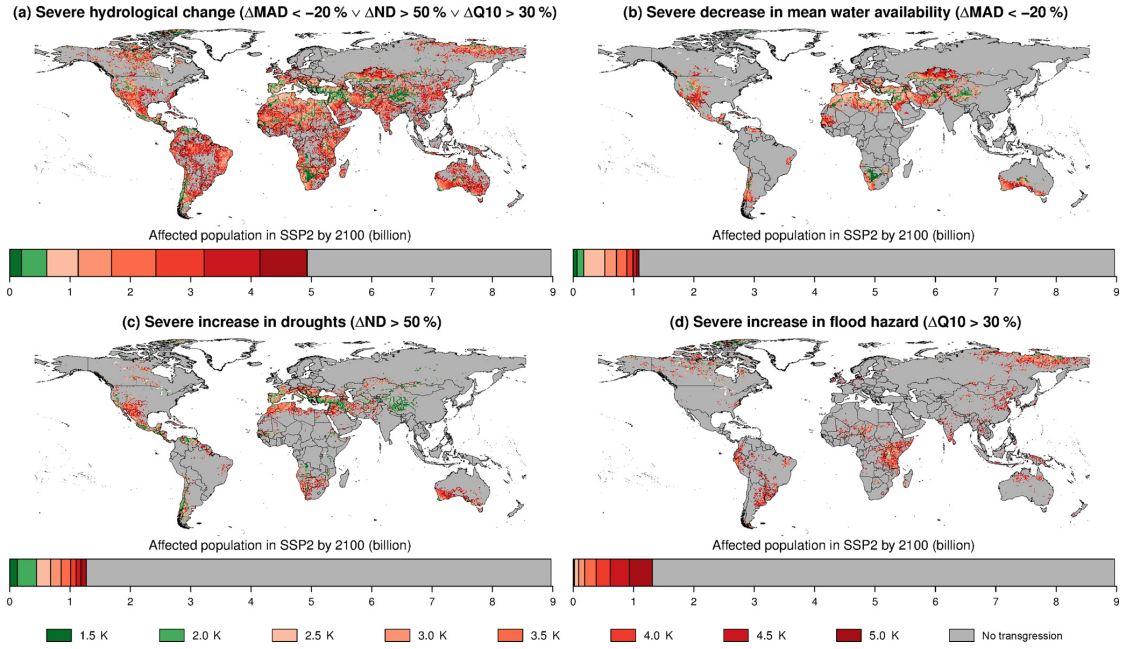

Figure 5.2: ΔT_{glob} at which severe hydrological changes occur in more than half of the GCMs (10 out of 19). Bars underneath the maps indicate population exposed to the respective severe changes for the SSP2 population scenario.

exposed to severe decreases in mean water availability and severe increases in droughts (Figure 5.2b–d). If warming could be limited to 1.5 °C the number of people *more likely than not* exposed to severe hydrological change could be reduced even more to 195 million people (Figure 5.2a), a further reduction by more than two-thirds (68.4 %) compared to 2 °C warming. However, even a partial failure of the Paris Agreement with an exceedance of the 2 °C target by only 0.5 °C would lead to an increase in the number of people exposed to severe hydrological change to 1.14 billion (Figure 5.2a)—almost a doubling (84.6 % increase) compared to a warming by 2 °C. The main contribution to this strong increase comes from increased exposure to severe decreases in mean water availability and severe increases in droughts, with exposure to severe increases in flood hazard only playing a minor role at these temperature levels (Figure 5.2b–d). Although the total number differs across different population scenarios, the percentage of global population that can be protected from exposure to severe hydrological change by ambitious climate mitigation efforts is very similar across all population scenarios (Figure D.2).

5.3.3 Severe hydrological changes and water scarcity

To get an indication of the adaptation challenges associated with the exposure to severe hydrological change, we use the assessment of future water scarcity due to population change to distinguish two principal adaptation domains. Coping with water scarcity conditions

(WCI $>$ 1000 p/fu) even without further aggravation by climate change requires a combination of supply-side and demand-side management measures (Falkenmark 1989, Ohlsson and Turton 1999). Therefore, water demand management interventions will also have to play a role in the adaptation to severe hydrological change under already water-scarce conditions. In contrast, adaptation to severe hydrological change under comparatively abundant water availability conditions (WCI $\leq$ 1000 p/fu) may be achieved by adjusting water supply infrastructure alone. Although water demand management is generally desirable and may have economic co-benefits (Brooks 2006), it faces many political, legal, and behavioural obstacles for its implementation and may not be practical in all contexts (Kampragou et al. 2011, Russell and Fielding 2010).

Under the assumption of no climate change, as much as 3.30 billion people (36.8 % of global population) are estimated to live under *absolute water scarcity* by 2100 in the SSP2 scenario. For all aspects of severe hydrological change and across the whole range of ΔT_{glob}, the proportion of people *more likely than not* exposed to severe hydrological change is much larger in this category than in the rest of the population (Figure 5.1). This asymmetric distribution of impacts is most pronounced for severe decreases in mean water availability, severe increases in flood hazard, and for severe hydrological change in general (Figure 5.1a, c, and d). This finding is largely independent of the population scenario (Figure D.3 in Appendix D).

Because of the challenges associated with the implementation of demand-side management interventions, the population already experiencing water scarcity in the absence of climate change is of primary concern when analysing exposure to severe hydrological change. We estimate that 2.14 billion people (23.9 % of global population) in the SSP2 population scenario would be affected by water scarcity due to population change and *more likely than not* exposed to climate-related severe hydrological change if ΔT_{glob} would rise to 5 °C by 2100 (Figure 5.1a). Out of these, 538 million (6.0 % of global population), 500 million (5.7 % of global population), and 640 million (7.1 % of global population) would more *more likely than not* be exposed to a severe decrease in mean water availability, a severe increase in droughts, and a severe increase in flood hazard, respectively (Figure 5.1b–d). For 875 million people, a transgression of thresholds for a mix of different aspects of severe hydrological change is found in more than half of the GCMs. A successful implemention of the Paris Agreement that would limit warming to 2 °C would dramatically reduce the number of people under *absolute water scarcity* and *more likely than not* exposed to severe hydrological change to 290 million (3.2 % of global population). With even more ambitious mitigation efforts sufficient to limit warming to 1.5 °C warming could further reduce this number to as little as 116 million people (1.3 % of global population). For a failure of the Paris Agreement with temperature rising to 2.5 °C (3 °C) this number would rise to 543 (824) million people.

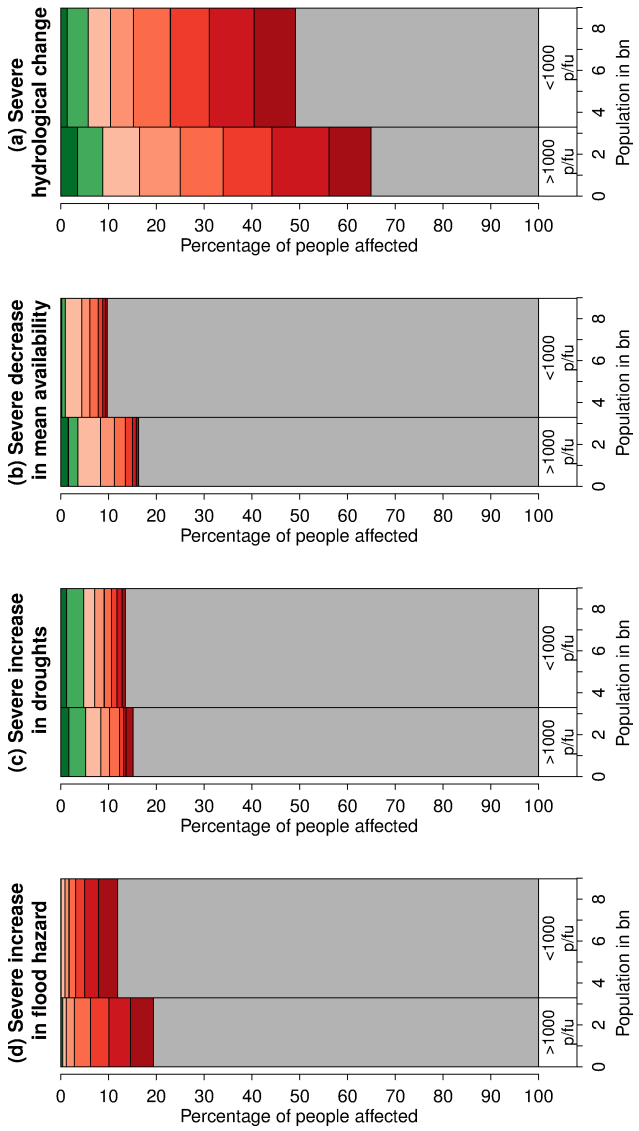

Figure 5.3: Fraction of SSP2 population in 2100 exposed to severe hydrological change at different levels of ΔT_{glob} (as shown in Figure 5.2) divided over two water scarcity categories: population already experiencing *absolute water scarcity* (>1000 p/fu) in the absence of climate change and rest of population (≤1000 p/fu). The total number of people in each class is given on the y axis, and the fraction of people exposed to severe hydrological change in each class is given on the x axis. Colour scale for ΔT_{glob} same as in Figure 5.2.

Table 5.1: Number of people in 2100 for the SSP2 population scenario that would experience *absolute water scarcity* (>1000 p/fu) under present-day climate conditions and be *more likely than not* exposed to severe hydrological change at different levels of ΔT_{glob} in different world regions (population in million, percentage of population in region in brackets). Regions are MEA (Middle East and north Africa), ANZ (Australia and New Zealand), SAS (South Asia), SSA (sub-Saharan Africa), LAM (Latin America), NAM (USA and Canada), EUR (Europe, excluding Russia), EAS (East Asia), RCA (Russia and Central Asia), and SEA (Southeast Asia).

	Total population	Population >1000 p/fu	Population with >1000 p/fu and exposed to severe hydrologic change					
			1.5 °C	2.0 °C	2.5 °C	3.0 °C	4.0 °C	5.0 °C
MEA	740	416 (56.2 %)	48.0 (6.5 %)	101.9 (13.8 %)	193.2 (26.1 %)	222.4 (30.0 %)	270.9 (36.6 %)	320.4 (43.3 %)
ANZ	51	27 (52.2 %)	0.0 (0.0 %)	0.6 (1.2 %)	1.5 (2.9 %)	3.7 (7.3 %)	9.6 (18.8 %)	17.8 (35.0 %)
SAS	2282	1005 (44.1 %)	17.1 (0.7 %)	38.7 (1.7 %)	80.7 (3.5 %)	200.8 (8.8 %)	461.8 (20.2 %)	651.2 (28.5 %)
SSA	2395	890 (37.2 %)	16.8 (0.7 %)	42.8 (1.8 %)	113.2 (4.7 %)	191.0 (8.0 %)	371.5 (15.5 %)	575.9 (24.0 %)
LAM	662	230 (34.7 %)	27.7 (4.2 %)	79.8 (12.0 %)	87.5 (13.2 %)	101.0 (15.3 %)	131.3 (19.8 %)	175.2 (26.5 %)
NAM	510	166 (32.6 %)	4.2 (0.8 %)	6.4 (1.2 %)	26.9 (5.3 %)	39.3 (7.7 %)	58.7 (11.5 %)	86.8 (17.0 %)
EUR	579	161 (27.9 %)	0.4 (0.1 %)	14.6 (2.5 %)	31.0 (5.4 %)	42.8 (7.4 %)	70.0 (12.1 %)	90.6 (15.7 %)
EAS	913	253 (27.7 %)	0.1 (0.0 %)	2.4 (0.3 %)	4.4 (0.5 %)	16.5 (1.8 %)	61.7 (6.8 %)	163.3 (17.9 %)
RCA	198	44 (22.1 %)	1.9 (1.0 %)	3.1 (1.6 %)	5.0 (2.5 %)	6.9 (3.5 %)	9.7 (4.9 %)	11.1 (5.6 %)
SEA	642	106 (16.5 %)	0.0 (0.0 %)	0.0 (0.0 %)	0.0 (0.0 %)	0.0 (0.0 %)	12.2 (1.9 %)	48.7 (7.6 %)
World	8971	3298 (36.8 %)	116 (1.3 %)	290 (3.2 %)	543 (6.1 %)	824 (9.2 %)	1457 (16.2 %)	2141 (23.9 %)

The remaining number of people exposed to severe hydrological change at 2 °C warming, as well as the implications of more ambitious mitigation efforts or a failure of the Paris Agreement, differs greatly among world regions (Table 5.1, for countries assigned to each region see Figure D.4). About 63 % of the 290 million people who live under *absolute water scarcity* and are *more likely than not* exposed to severe hydrologic change at 2 °C warming live in Latin America (LAM) and the Middle East and north Africa region (MEA), where they make up more than 12 % of the population in those regions. Another 28 % of the 290 million live in South Asia (SAS) and sub-Saharan Africa (SSA), but due to high population numbers in these regions their share remains below 2 %. The high share of population affected by *absolute water scarcity* and severe hydrological change in LAM and MEA is particularly worrying since a failure to overcome the obstacles associated with the implementation of appropriate demand management can have negative societal and economic consequences not only for these people but for the whole region. More ambitious mitigation efforts that keep warming below 1.5 °C would reduce the number of affected

people by more than half, to 6.5 % in MEA and 4.2 % in LAM. In all other regions, the share of affected population would drop below 1 %.

Failure of the Paris Agreement would substantially increase exposure to severe hydrological change in many regions. In 5 out of 10 regions, the number of people affected by *absolute water scarcity* and severe hydrological change at least doubles if the 2 °C target is exceeded by only 0.5 °C and reaches a share of (almost) 5 % of affected population in the region in SSA, North America (NAM), and Europe (EUR). The strongest absolute increase (though not a doubling) in the number of affected people occurs in the MEA region, where more than one-quarter of the population in that region would be affected at 2.5 °C warming. Between 2.5 and 3 °C warming, the increases in number of affected people is strongest in South Asia (SAS), SSA, NAM, and EUR. At 4 °C warming, the share of affected population exceeds 10 % in 7 out of 10 regions, with MEA, Australia and New Zealand (ANZ), SAS, SSA, and LAM being most strongly impacted. At 5 °C warming, the share of affected population reaches 43.3 % in MEA and 35.0 % in ANZ; exceeds 20 % in SAS, SSA, and LAM; and exceeds 15 % in NAM, EUR, and East Asia (EAS). In Russia and Central Asia (RCA) and Southeast Asia (SEA) the share of affected people remains below 5 %, partly due to a low share of population under high water crowding and less severe hydrologic change.

Although numbers differ among population scenarios, the overall pattern of where and how much change occurs in the different regions is consistent across all SSP population scenarios. A comprehensive overview of population under high water crowding and affected by severe hydrologic change in different world regions for all population scenarios is given in Figure D.5.

5.4 Discussion

Our estimate that 26.8 % of global population today live under *absolute water scarcity* (>1000 p/fu) is within the range of 21.0 %–27.5 % (average 24.7 %) reported by previous studies applying the WCI on river basin level (Gerten et al. 2013, Arnell and Lloyd-Hughes 2014, Kummu et al. 2016). Estimates of future SSP populations living in river basins with >1000 p/fu under present-day climate conditions are given by Arnell and Lloyd-Hughes (2014) who estimate a range of 39.5 %–54.2 % for the affected global population across different SSP scenarios. This is considerably higher than the range of our estimates of 31.5 %–44.9 %; but due to the lack of other comparable studies, it is not clear whether these discrepancies are caused by the choice of the hydrological model or by the difference in scale (basin or grid cell) at which the WCI is calculated. However, using the same hydrological model as in our study, Gerten et al. (2013) estimate that 38.5 % of global population in the revised A2r scenario (Grübler et al. 2007) from the Special Report on Emissions Scenarios

would live in river basins with >1000 p/fu under current climate conditions, which is close to our estimate of 41.0 % for the SSP3 scenario, to which the A2r scenario is comparable in terms of total population (12.3 billion compared to 12.6 billion in 2100). In contrast, the corresponding estimate by Arnell and Lloyd-Hughes (2014) is as high as 54.2 % for the SSP3 scenario, which indicates that using LPJmL to assess water scarcity generally tends to result in lower estimates of future population affected by water scarcity.

A direct comparison of hydrological changes estimated here to previous studies is not straightforward due to the unique design of this study. Only few global studies have assessed climate change impacts on water resources as a function of ΔT_{glob} (Gerten et al. 2013, Schewe et al. 2014, Gosling and Arnell 2016), but they typically focus on changes in MAD and report changes in the number of people affected by water scarcity. A relevant study for comparison is Schewe et al. (2014), which analyses changes in MAD obtained from an ensemble of 10 global hydrological models (GHMs) forced by climate scenarios from five different GCMs. The overall pattern of changes in MAD simulated by LPJmL across 19 GCMs agrees well with results from Schewe et al. (2014), but exhibits a generally lower magnitude of changes (see Figure D.6 and Figure 1 in Schewe et al. (2014)). Thus, MAD changes simulated by LPJmL (both increases and decreases) tend to be smaller than simulated by most other GHMs. This becomes even more apparent when comparing the percentage of people affected by a q20 % decrease in MAD. For a ΔT_{glob} of 2.5 °C (equivalent to an additional warming of 1.9 °C relative to the control simulation) we estimate a median share of 8.6 % of affected global population across all GCMs. This is substantially lower than the median value of 13 % of affected population estimated for 2 °C additional warming by Schewe et al. (2014) and approximately represents their lower end of the interquartile range. This can be attributed to the response of dynamic vegetation in LPJmL that is not included in most other GHMs (Schewe et al. 2014).

In summary, the global and regional estimates of population living under *absolute water scarcity* and being exposed to severe hydrological change obtained from LPJmL are lower than from most other GHMs. Thus, the estimates of population affected by water scarcity and severe hydrological change presented in this paper should be regarded as conservative estimates.

Apart from these uncertainties in model projections, the results of a global study like ours are necessarily determined by simplifications and generalization in the data analysis. The most important generalization in this study are the choice of aspects of severe hydrological change and the corresponding critical thresholds. While not all selected aspects may be relevant in all cases (e.g. where supply is primarily fulfilled from groundwater), we believe that in the vast majority of cases they reflect important hydrological properties that are relevant from a freshwater resource perspective. The respective thresholds may also differ depending on hydrological and other local conditions, and using unique global

values will always produce a number of false positives and false negatives. However, the selected thresholds are rather conservative, and thus are expected to produce more false negatives than false positives. Another aspect is the choice of the WCI to differentiate population groups in terms of adaptation challenges. This indicator is widely applied because it only requires data on mean water availability and population numbers, but it can neither account for hydrological aspects that limit the utilization of water resources nor for actual per capita water requirements. Despite these shortcomings of the WCI, it gives a rough impression of the overall population pressure on water resources, which is linked to the challenges to adapt to severe hydrological change. Last but not least, it is important to note that this study only addresses quantity aspects of freshwater resources and does not consider water quality.

5.5 Conclusions

Future freshwater supply will be affected by population growth and climate change, which are both subject to uncertainty and heterogeneous distribution patterns. Under all five SSP population projections considered here, a strong increase in the number of people living under *absolute water scarcity* in 2100 to 2.16–5.65 billion (31.5 %–44.9 % of global population) is projected, with higher global population resulting in higher absolute numbers but also larger proportions of global population being affected. Because of the importance of water demand management for coping with *absolute water scarcity*, which is more difficult to implement than supply management, these parts of the global population will face higher challenges for adaption to severe hydrological change that affects water supply.

If global warming would continue unabated to reach 5 °C above pre-industrial levels in 2100, 4.93 billion people (54.9 % of global population) in the SSP2 population scenario would *more likely than not* be exposed to severe hydrological change. Out of those, 2.14 billion people (23.9 % of global population) would already experience *absolute water scarcity* due to high population pressure on water resources, making adaptation to such changes more challenging. With a successful implementation of the Paris Agreement limiting global warming to 2 °C, the number of people affected by severe hydrological change could be reduced to 615 million people (6.9 % of global population), of which 290 million (3.2 % of global population) would already experience *absolute water scarcity*. If temperature increase could be limited to 1.5 °C, the number of people exposed to severe hydrological change could be further reduced to 195 million (2.2 %) and 116 million (1.3 %), respectively. However, only a partial failure of the Paris Agreement with temperature rising to 2.5 °C would almost double the number of people *more likely than not* exposed to severe hydrological change, in total and among those already experiencing *absolute water scarcity*, compared to a 2 °C warming.

Due to the heterogeneous spatial distribution of *absolute water scarcity* and severe hydrological change, the proportion of population exposed to severe hydrological change with increased adaption challenges reaches 12.0 % in Latin America and 13.8 % in the Middle East and north Africa region even if global warming could be limited 2 °C by a successful implementation of the Paris Agreement. A failure to overcome the obstacles associated with the implementation of appropriate demand management can have negative societal and economic consequences not only for these people but for the whole region. Thus, 2 °C mean global warming cannot be considered a safe limit of warming in these regions. More ambitious mitigation efforts that would keep warming at, or below, 1.5 °C could substantially reduce that risk by reducing the share of population exposed to severe hydrological change and with increased adaption challenges by more than half in these two regions and globally.

Code and data availability

The CRU TS3.1 historical climate data are available from `http://catalogue.ceda.ac.uk/uuid/ac3e6be017970639a9278e64d3fd5508` (University of East Anglia Climatic Research Unit et al. 2013). The temperature-stratified climate scenarios of the PanClim dataset along with the matched GPCC historical precipitation data are available from `http://www.panclim.org` (Heinke et al. 2013b). Historic gridded population estimates up to the year 2010 are based on the Gridded Population of the World, Version 3 (GPWv3) Data Collection (CIESIN and CIAT 2005), which have been edited and provided by the Inter-Sectoral Impact Model Intercomparison Project (ISIMIP 2012, Warszawski et al. 2014). The gridded historical population data are available from `https://www.isimip.org/gettingstarted/details/13/` (CIESIN and CIAT 2005) and the future scenario population data are available from `https://doi.org/10.7927/H4RF5S0P` (Jones and O'Neill 2017). The STN-30p flow direction map can be downloaded from `https://doi.org/10.3334/ORNLDAAC/1005` (Vörösmarty et al. 2011). The model code of LPJmL4 is publicly available from `https://doi.org/10.5880/pik.2018.002` (Schaphoff et al. 2018c) or via the GitHub project page `https://github.com/PIK-LPJmL/LPJmL` (last access: 5 February 2019). The core output of the analysis in this paper—consisting of historic and future scenario water crowding estimates as well as hydrological indicators for 19 GCMs an 8 levels of global mean temperature increase at 0.5° resolution—has been made available under a Creative Commons Attribution 4.0 License and is available for download from `https://doi.org/10.5281/zenodo.2562056` (Heinke et al. 2019b). All results presented in this paper are based on this core output. All primary data, model code, model outputs and scripts that have been used to produce the core output and the results presented in this paper are archived at the Potsdam Institute for Climate Impact Research and are

available upon request.

Supplementary material related to this chapter is available in Appendix D.

Acknowledgements

This work was in part supported by German Federal Ministry of Education and Research (BMBF) through the project SUSTAg (031B0170A). The authors would like to thank the two anonymous referees for helpful comments on the manuscript.

Chapter 6

Water use in global livestock production—opportunities and constraints for increasing water productivity

An edited version of this chapter has been submitted for publication as: J. Heinke, M. Lannerstad, D. Gerten, P. Havlík, M. Herrero, A. Notenbaert, H. Hoff, and C. Müller. Water use in global livestock production—opportunities and constraints for increasing water productivity. *Water Resources Research*, submitted

Abstract

Increasing population, change in consumption habits, and climate change will likely increase the competition for freshwater resources in the future. Exploring ways to improve water productivity especially in food and livestock systems is important for tackling the future water challenge. Here we combine detailed data on feed use and livestock production with FAO statistics and process-based crop-water model simulations to comprehensively assess water use and water productivity in the global livestock sector. We estimate that annually 4666 km^3 of blue and green water is used for the production of livestock feed, equaling about 44 % of total agricultural water use. Livestock water productivity (LWP; protein produced per m^3 of water) differs by several orders of magnitude between livestock types, regions, and production systems, indicating a large potential for improvements. For pigs and broilers, we identify large opportunities to increase LWP by increasing both feed water productivity (FWP; feed produced per m^3 of water) and feed use efficiency (FUE; protein produced per kg of feed) through better crop and livestock management. Even larger opportunities to increase FUE exist for ruminants, while the overall potential to increase their FWP is low. Substantial improvements of FUE can be achieved for ruminants by supplementation with feed crops, but corresponding improvements in LWP are offset by lower FWP caused by higher water requirements of feed crops. Therefore, LWP of ruminants, unlike for pigs and poultry, does not always benefit from a trend towards intensification, as this is often accompanied by increasing crop supplementation.

6.1 Introduction

Driven by increasing global population and rising per capita food demand, global production of animal source foods (ASF) has more than tripled over the last 50 years, accompanied by a threefold increase of crops used for animal feed (FAO 2018). One third of all cropland is now being used to produce feed crops (Steinfeld et al. 2006) and one quarter of the ice-free land area of the world is occupied by pastures (FAO 2018). Continued population growth and an unbroken trend towards more meat-based diets will put enormous pressure on the food system in the coming decades (Alexandratos and Bruinsma 2012, Bodirsky et al. 2015). In total, global agricultural output will have to increase by 70 % to 110 % by 2050. The major part of both the production and consumption of animal products is expected to take place in developing countries (Alexandratos and Bruinsma 2012, Godfray et al. 2010).

Already today, more than 2 billion people live in countries where total freshwater withdrawals exceed 25 % of the total renewable freshwater resource (United Nations 2017). Population growth and climate change are both projected to substantially increase water scarcity for large portions of humanity (Heinke et al. 2019a). Water is one of the most basic resources needed in agricultural production and agriculture is the single largest water user accounting for 69 % of global freshwater withdrawals (FAO 2016) and an even higher share of consumptive freshwater use. In addition to this 'blue water', agriculture consumes many times more 'green water', i.e. soil moisture from naturally infiltrated rainfall on both irrigated and rainfed agriculture land (Rost et al. 2008). In view of rising food demand, it is imperative to limit further increase in agricultural water demand by seeking ways to produce more per unit of water.

Previous studies have estimated consumptive water use (CWU) by the livestock sector as a whole (de Fraiture et al. 2007, Mekonnen and Hoekstra 2012, Weindl et al. 2017) and for different ASF in different countries (Mekonnen and Hoekstra 2012). The vast majority of the CWU by the livestock sector is related to the production of feed, whereas only about 2 % of it is water for drinking and servicing (Mekonnen and Hoekstra 2012). Thus, the estimation of the feed amounts from different sources required to produce ASF and the water use associated with the production of this feed are central to the estimation of CWU for livestock production. We here use a comprehensive dataset from Herrero et al. (2013), which provides estimates of production of ASF and corresponding use of feed from different sources for four types of ruminants in eight different production systems and four different monogastric animal types in two different production systems in 29 world regions. In total, 919 different combinations ('livestock production units') are distinguished. The dataset is based on a mechanistic digestion and metabolism model (Herrero et al. 2008) to provide biologically plausible estimates and is harmonized to FAOSTAT to match reported use of

crops for feed (concentrate feed) and production of ASF around the year 2000. The state-of-the-art dynamic global vegetation, hydrology and crop model LPJmL4 (Schaphoff et al. 2018b) is used to estimate the water required to produce feed crops, cultivated forages, and grazed grass. Unlike previous studies that have only accounted for the direct water use—i.e., the evapotranspiration occurring during the growing period—we also include the evapotranspiration that occurs from fallow cropland outside the growing period as an indirect water use in our estimates of CWU of feed and ASF. Accounting for the indirect fallow water use is particularly important when comparing annual and perennial crops, in which the former would be unjustifiably favored when only growing period evapotranspiration (ET) were used.

The goal of this study is twofold. First, we aim to provide revised estimates of CWU in global agriculture, i.e. how much of it is attributable to the livestock sector and to the different ASF in different regions and production systems. Second, we analyze how variations in livestock water productivity (LWP; defined as g protein produced per m^3 of CWU) are caused by variations in feed water productivity (FWP; defined as kg feed produced per m^3 of CWU) and variations feed use efficiency (FUE; defined as g protein produced per kg of feed) and assess the possible implications for the potential to improve LWP.

6.2 Materials and Methods

Estimation of livestock water use and water productivity requires information about feed use by livestock, the amount of protein produced from the feed, and the water used for producing the feed. Feed use and production in the global livestock sector are based on data from Herrero et al. (2013), which provides detailed information for 919 different combinations of livestock production type, production system, and world regions, hereafter referred to as livestock production units. Livestock production types differ by animal species, use of feed types, and produced ASF types (Table 6.1). For each of the two ruminant types 'bovines' and 'sheep & goats', a 'meat' and a 'diary' sub-type is distinguished, which produce only meat or both milk and meat, respectively. Each of the four can occur in up to eight ruminant production systems (Robinson et al. 2011) in each of 28 world regions. All ruminants rely on roughage (grazed biomass, crop residues, and cultivated forages) as primary feed source with up to 50 % supplementation of feed crops. The effect of feed composition and nutritional quality on FUE is explicitly accounted for by applying a mechanistic digestion and metabolism model. For poultry, meat producing broilers and egg producing layer hens are distinguished for industrial production, whereas smallholder production is assumed to produce both eggs and meat simultaneously (dual-purpose poultry). All poultry are fed with feed crops but depending on the region, a significant part

of the feed in smallholder production may come from alternative but unaccounted feed sources, such as scavenging and uneaten food (Herrero et al. 2013). Pigs in both industrial and smallholder production only produce meat and are fed with feed crops. However, like smallholder poultry, pigs in smallholder production also partially rely on unaccounted feed sources, which is why we treat them as a separate livestock production type here.

Table 6.1: Overview over livestock types, the products they produce, in which livestock production system they can occur, the feed types they receive, and on which water resources they rely.

Livestock types	Products	Livestock production systems	Feed types	Water resources
meat bovines	meat	LGA, LGH, LGT, MXA, MXH, MXT, Urban, Other	grazed biomass, crop residues, forages, grains	blue, green suitable, green marginal
dairy bovines	milk, meat	LGA, LGH, LGT, MXA, MXH, MXT, Urban, Other	grazed biomass, crop residues, forages, grains	blue, green suitable, green marginal
meat sheep & goats	meat	LGA, LGH, LGT, MXA, MXH, MXT, Urban, Other	grazed biomass, crop residues, forages, grains	blue, green suitable, green marginal
dairy sheep & goats	milk, meat	LGA, LGH, LGT, MXA, MXH, MXT, Urban, Other	grazed biomass, crop residues, forages, grains	blue, green suitable, green marginal
industrial pigs	meat	industrial	grains	blue, green suitable
smallholder pigs	meat	smallholder	grains, unaccounted sources	blue, green suitable
broilers	meat	industrial	grains	blue, green suitable
layer hens	meat	industrial	grains	blue, green suitable
dual-purpose poultry	eggs, meat	smallholder	grains, unaccounted sources	blue, green suitable

Livestock production systems: LGA - livestock grazing arid; LGH - livestock grazing humid; LGT - livestock grazing temperate; MXA - mixed arid; MXH - mixed humid; MXT - mixed temperate; Urban - urban systems; Other - other systems

Green and blue water use for the production of the different feed components (feed crops, cultivated forages, grazed biomass, and crop residues) fed to animals in the 919 livestock production units is estimated from simulations with the dynamic global vegetation and hydrology model LPJmL4, which includes process-based representations of crop and grazing land dynamics (Schaphoff et al. 2018b, see section E.1 for details). Global production and related water use for 62 crops and crop groups are estimated using maps of harvested area and total cultivated area from MIRCA2000 (Portmann et al. 2010) and national yield statistics from FAOSTAT (FAO 2018). Total production for all crops was estimated by multiplying harvested area with national yield from FAOSTAT. ET during the growing seasons of 18 major crops was estimated from LPJmL4 simulations by determining

the management intensity for which simulated yield best matches yield from FAOSTAT at country level. For all other crops, ET of a generic annual and a generic perennial crop type was used. ET from off-season and full-year fallow land was estimated assuming bare soil (black fallow) and assigned to crops based on harvested area and cropping intensity (see section E.2 for details).

From the thus obtained estimates of CWU for harvested crops we determine CWU related to crops and crop products utilized for food, feed, and other uses at national level by using the information about trade and utilization given in the FAOSTAT Food Balance Sheets and Commodity Balances Sheets (FAO 2018). Only net imports and exports are accounted for and a global trade pool is assumed for each commodity. Water for commodity quantities reported as waste is proportionally distributed to food, feed, and other uses, resulting in a decrease in water productivity for actually utilized commodities (for further details see section E.3).

Production of cultivated forage and related CWU was estimated using maps of harvested area from MIRCA2000, gridded yield estimates from (Monfreda et al. 2008), and simulated ET from LPJmL4 (section E.2). The utilization of cultivated forage in each livestock production unit was estimated by adjusting the amounts of occasional feed use from (Herrero et al. 2013) until they matched the estimated forage production in the corresponding ruminant productions systems (see section E.4 for details). The difference between occasional feed demand and estimated use of fodder grasses was added to the demand for grazed biomass.

For the estimation of CWU for grazed biomass we performed a series of LPJmL4 simulations with a wide range of grazing intensities to determine the maximum biomass yield and corresponding ET (section E.1). To estimate potentially available biomass for grazing, yields were multiplied with the sum of grassland and woodland and barren and sparsely vegetated land from the GAEZ land cover dataset (IIASA/FAO 2012). For India, 10 % of built-up land were added to account for roadside grazing and grazing on small pasture patches within human settlements (Spate and Learmonth 2017). Total grass demand on production unit level was downscaled to grid cell level using the spatial distribution of ruminants and ruminant production systems given by the Gridded Livestock of the World version 2 dataset (Robinson et al. 2014). Inconsistencies in the downscaling of grass demand were resolved by redistributing excess demand within the respective ruminant production system and, if insufficient, within the respective region (see section E.5 for details). The CWU for the estimated grazing demand in each grid cell was estimated by multiplying with annual ET per kg of grazed grass determined for the maximum yield scenario. Finally, the area potentially available for grazing according to the GAEZ land cover dataset and the definition above is reduced to match "land under permanent meadows and pastures" reported by FAOSTAT (FAO 2018) in each country (see section E.5 for details).

No water use was allocated to crop residues (straws and stovers), thus assuming that their use for feed has no environmental or economic consequences. We acknowledge that this assumption is debatable, especially for agricultural productions systems where biomass is scarce. But assessing the implications of residue use (and the water use allocated to it) would require comprehensive knowledge of many economic, environmental, and management aspects of agricultural production that are not available globally.

6.3 Results and Discussions

6.3.1 Livestock water use from global agricultural lands

In total, an annual water quantity of 20 236 km^3 is evaporated from global agricultural lands, with 7677 km^3 green water and 1324 km^3 blue water from cropland and 11 235 km^3 green water from pastures, averaged over the period 1998–2002 (Figure 6.1). In contrast to pastures, which are more or less permanently covered by grasses, a wide range of seasonal crops with short and long growing seasons are predominantly cultivated on cropland. Thus, most cropland is only temporarily covered by crops, so that only 4572 km^3 of the total green ET from cropland occurs during growing periods and 3104 km^3 during seasonal and annual fallow periods. Because fallow is part of the rotational use of cultivated lands, its ET is included in our analysis as an integral part of the CWU of crops. Annual blue water ET from fields during the growing period is 910 km^3 and no blue ET is assumed to occur from fallow assuming there is no irrigation in these periods. As the conveyance efficiency of irrigation infrastructure is low in many parts of the world (Rost et al. 2008), an additional 414 km^3 of blue water evaporates from open canals and temporary storages for the provision of irrigation water to the field.

In Figure 6.1 the annual ET from global agricultural lands is divided into CWU for six principal biomass utilization categories. About 5048 km^3/yr of total cropland ET (56 %) are attributed to the production of 'food crops', 2980 km^3/yr (33 %) to the production of 'feed crops' and 'forages', and 888 km^3/yr (10 %) to the production of biomass for 'other uses', mainly fibers and biofuels. A small amount of 85 km^3/yr cropland ET (<1 %) could not be allocated to any use due to inconsistencies in trade statistics. From pastures, 1686 km^3/yr of annual ET (15 %) are allocated to the production of 'grazed biomass'. The remaining ET from pastures is associated with biomass which supports other functions of pastoral ecosystems, such as wildlife and carbon sequestration (Schyns et al. 2019). Overall, 10 602 km^3/yr of green and blue ET from global agricultural lands are allocated to the production of biomass for human use as food, animal feed, fiber and biofuels.

In total, the global livestock sector annually appropriates 4666 km^3/yr of green and blue water for the production of feed crops, forages, and grazed biomass (Figure 6.1), equaling about 23 % of the total ET from global agricultural land and 44 % of total CWU

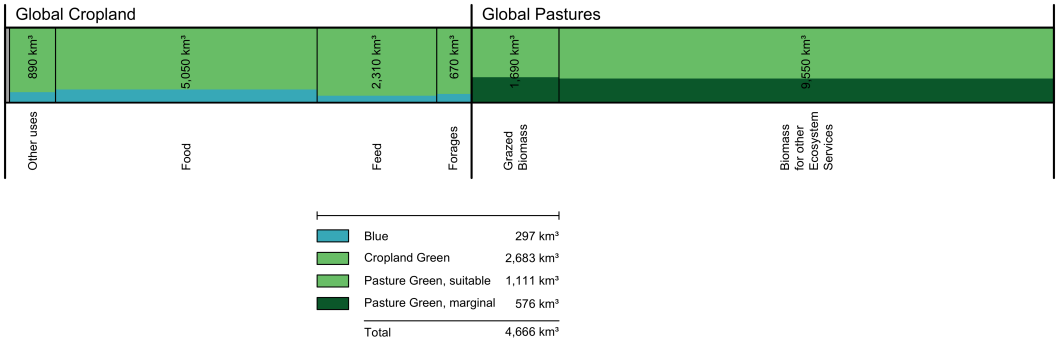

Figure 6.1: Total ET from global agricultural lands, year 2000, divided over cultivated lands and pastures, and differentiated into blue ET, green ET from cultivated lands, and green ET from pastures, differentiated as suitable for crop cultivation or marginal, i.e. not suitable. The bar is divided over six utilization categories. Total CWU for global livestock production include CWU from feed crops, forages, and grazed biomass. The grey section denotes cropland ET that could not be allocated to any utilization.

for agricultural biomass for human use. Out of the annual total CWU in global livestock production, 4369 km^3/yr (94 %) are from green water, which is slightly more than the 4159 km^3/yr of green water used for food crops. However, more than one third of the green water used in livestock production is from pastures, which are often located on marginal lands where livestock rearing is the only viable agricultural land use. Hence, the green water from large parts of pastures is not directly comparable to the green water from cropland as it could not be used alternatively for crop production. Applying a 'crop suitability index' (IIASA/FAO 2012) reveals how much pasture land could be fruitfully converted to cropland, and in turn, how much of the green water on these convertible pastures could support growth of crops. We find that 576 km^3/yr (34 %) out of the annual green CWU related to grazed biomass are from marginal pastures (crop suitability index <0.1) and 1111 km^3/yr from pastures suitable for crop production. The proportion of ET from marginal pastures in total pasture ET it is very similar (33 %).

Even though the contribution of green water is substantial and may be the primary source of water in some production systems, the global amount of 3794 km^3/yr crop-suitable green CWU used for feed production is only 9 % smaller than the green CWU for food crops. In contrast, only 297 km^3/yr of blue water is used for feed production, which is still about one third of the 889 km^3/yr blue water used for food crops. In addition to the blue CWU in feed production, the livestock sector also requires blue water for drinking and servicing. Globally, the evaporation from these blue water withdrawals amounts to 27 km^3/yr (Alcamo et al. 2003). This equals 9.1 % of the blue CWU and 0.6 % of total CWU for feed production.

6.3.2 Water use for livestock types and livestock products

In total, the global livestock sector generates an annual human edible protein supply of 53.7 MtP (year 2000; Figure 6.2), with a global average LWP of 11.5 gP/m^3. About half of annual production (29.2 MtP) but almost two thirds of total annual livestock CWU (2975 km^3) can be attributed to ruminants, and the remaining production (24.5 MtP) and CWU (1691 km^3) are associated with monogastric animals. Thus, monogastric animals produce almost 50 % more protein per unit of total CWU than ruminants (14.5 gP/m^3 compared to 9.8 gP/m^3). The composition of CWU of ruminants and monogastric animals differs due to the fundamentally different composition of feed. Because the digestion system of ruminants is well-suited to digest cellulose feeds, the largest part of their global average feed mix (92 %) consists of roughage, with grass from pastures making up the largest part (74 % of roughage). As a result, most of the CWU of ruminants (57 %) is green water from pastures, of which about one third is from marginal land. Monogastric animals, on the other hand, are only fed with concentrate feed (feed crops and animal by-products) so that CWU for this group only consists of green and blue water from cropland (Table 6.1). Although the share of blue water in CWU from cropland is larger for ruminants (11.3 %) than for monogastric animals (9.0 %), the share of blue in total CWU of ruminants is only 4.9 % due to the large contribution of green water from pastures.

The division into nine livestock production types allows for a more in-depth analysis of water use and production. When assessing the relative importance for supplying human edible proteins, the single largest contributor is the bovine dairy production providing 37.3 %, followed by almost equally large protein supply from industrial pigs, 13.7 %, industrial broiler, 13.4 %, and meat bovines, 13.0 %. The smallest protein contributions come from the sheep & goat production, with 1.9 % from the dairy category and 2.2 % from the meat type. The appropriation of CWU by livestock production types is different from their contribution to production, with meat bovines being the single largest water user with 30.9 % of total livestock CWU, followed by dairy bovines, 18.3 %, and industrial pigs, 14.9 %; smallest quantities are appropriated by layer hens, 4.4 %, smallholder dual purpose poultry, 3.9 %, and smallholder pigs, 2.3 %. Composition of CWU for the different production types largely follows the overall patterns found for ruminant and monogastric animals. However, among monogastric animals, comparatively high shares of 12 % blue water are found for both smallholder types (smallholder pigs and dual-purpose poultry), which is a result of the geographical distribution of production, i.e., a large part of production happens in regions with a high share of irrigation on cropland. Among ruminants, a comparatively high share of blue water is found for dairy bovines, which is mainly caused by the high share of cultivated feed crops and forages in the feed mix (21.5 % compared to 14.6 % average for remaining ruminants). The share of green CWU from marginal pastures

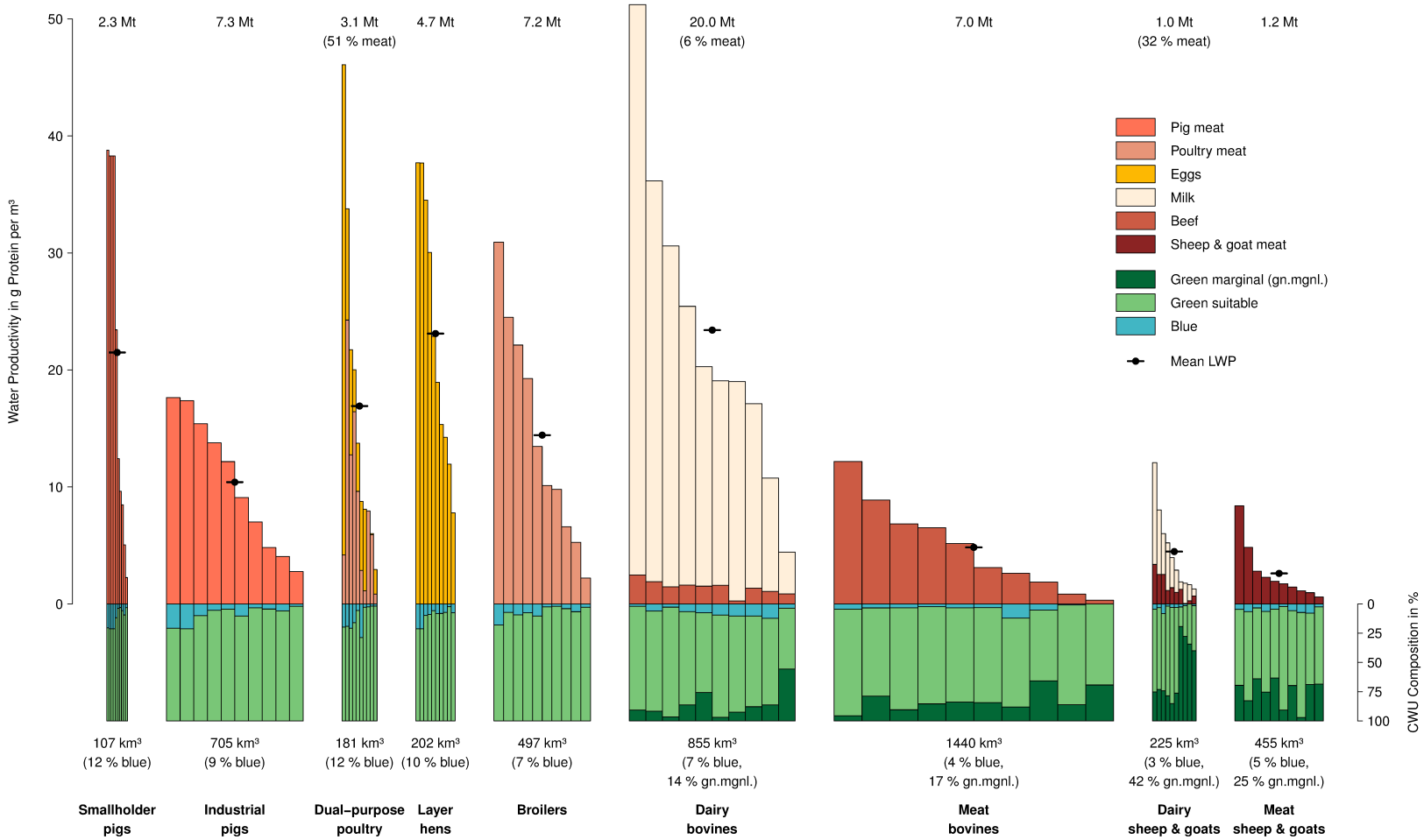

Figure 6.2: CWU (km^3/yr), production of protein (MtP), and LWP (gP/m^3) for the global livestock sector, differentiated for nine livestock production types, three water sources and three protein sources. For each livestock type the water productivity, CWU, and protein production is presented for ten equal parts of total CWU to enable a direct comparison. Surfaces shown for protein and CWU, respectively, are comparable in scale. Total production and CWU per livestock production type are given on top and below, respectively. The dashed dot indicates average LWP for each livestock production type.

differs by a factor three among ruminant production types, which is mainly the result of differences in the share of green marginal water in grazing CWU (27.5 % for meat bovines to 58.4 % for dairy sheep & goats) but also of the contribution of grazing to the overall feed mix (60.4 % for dairy bovines to 76.0 % for dairy sheep & goats).

The different patterns of CWU attribution and contribution to production by the nine livestock production types translate into different livestock water productivities. Highest average LWP are found for dairy bovines with 23.4 gP/m^3, followed by layer hens, 23.1 gP/m^3, and smallholder pigs, 21.5 gP/m^3. Lowest LWP is 2.6 gP/m^3 for meat sheep & goats—almost ten times lower than for dairy bovines—, followed by 4.5 gP/m^3 for dairy sheep & goats and 4.8 gP/m^3 meat bovines. However, even larger LWP differences are found within livestock production types. In Figure 6.2, the total CWU appropriated by each of the nine production types is sorted from high to low LWP and divided into ten equal CWU portions; for each tenth, the composition of CWU and the amount and composition of protein produced from it are shown. Average LWP of the most and least efficiently used CWU tenth varies at least fivefold for layer hens and up to nearly 40-fold for meat bovines. As a result, the LWP ranges of the different livestock production types overlap, with low LWP found in each of the nine types. Thus, the average value is only an indicative value for each production type, as large parts of the production can be produced both with a much lower and a much higher water use per unit product. Also, due to the differences in the geographical distribution of production it is difficult to draw conclusions about general differences between livestock production types.

6.3.3 Drivers for variations in livestock water productivity

The huge differences in LWP (Figure 6.2) are the result of the wide range of conditions under which livestock rearing and feed production takes place. Many of these conditions are subject to crop and livestock management (fertilizer, pesticides, crop and livestock species, breeds, animal health) and can be improved to increase LWP. Other conditions, mainly environmental factors such as climate and soils, cannot be changed but may be addressed by management (e.g., by providing housing or shelter for animals). Due to incomplete knowledge about all different management factors that determine LWP in our analysis, it is not possible to fully quantify the 'management gap'—i.e., the difference between current and best management—and the corresponding productivity gap. In the following we will instead analyze the contribution from variations in feed water productivity (FWP; an aggregated measure of how efficiently water is used to produce the feed mix) and feed use efficiency (FUE; a measure of how efficiently the feed is used to produce meat, milk, and eggs) to variations in LWP and provide a qualitative assessment of the opportunities to improve LWP and the possible constraints and trade-offs.

In contrast to the previous section, where LWP was analyzed for the total volume of

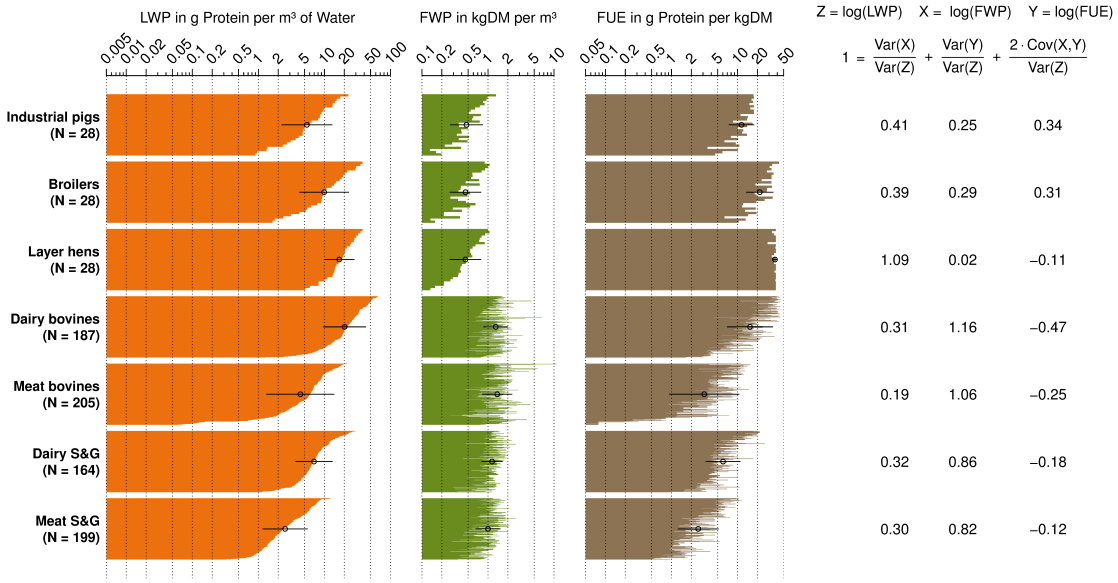

Figure 6.3: LWP and its components FWP and FUE, all sorted by LWP. Mean and the range of ±1 standard deviation calculated from the log-transformed variables are indicated (black open dot with whiskers for standard deviation). The table shows a partitioning of variance in log(LWP) into variance in log(FWP), variance in log(FUE), and double covariance of llog(FWP) with log(FUE) (see section E.6 for details).

CWU, this section focusses on the differences in production conditions across regions and production systems. To facilitate an undistorted comparison of LWP, FWP, and FUE estimates, each production unit (one region for monogastric animals or one production system in a region for ruminants) is weighted equally, regardless of its contribution to total CWU and production. Smallholder pigs and poultry are omitted, because FWP and FUE cannot be calculated for these due to the contribution of feed from unaccounted sources. Also, all values for the Pacific Islands region have been excluded as most estimates in this region appear extreme or even implausible, probably due to unreliable FAO statistics of feed use, animal numbers, and production.

Contribution of variations in FWP and FUE to variations in LWP

In Figure 6.3, the LWP in different regions and production systems is shown sorted from high to low, along with the corresponding distribution of FWP and FUE (all values in the same order as LWP) for each livestock production type. The logarithmic representation is required to overcome the difference in scale and magnitude, so that it is possible to visually and statistically analyse the variations in LWP, FWP and FUE.

By comparing the patterns of log(FWP) (green), log(FUE) (brown), and log(LWP) (orange) in Figure 6.3, it is possible to draw conclusions about how differences in FWP and

FUE determine the variations of LWP. For industrial pigs and broilers, the histograms of log(FUE) and log(FWP) (ordered from high to low LWP) both exhibit a similar gradient from high to low, indicating that they contribute about equally to variations in LWP but also that they are to some degree correlated. For layer hens, FUE is more or less constant across regions and the gradient of log(FWP) closely resembles the gradient of log(LWP), indicating that variations in LWP are almost entirely caused by differences in FWP. For ruminants, variations in log(FUE) are generally larger than variations in log(FWP) (indicated by the range of ± 1 standard deviation in Figure 6.3), and the histogram of log(FUE) therefore shows a similar gradient from high to low than log(LWP), whereas the distribution of log(FWP) appears to be more or less random in relation to LWP.

Decomposition of total variance of log(LWP) into variance of log(FWP), variance of log(FUE), and double covariance between covariance of log(FWP) with log(FUE) (Table in Figure 6.3, see section E.6 for details), confirms the visual interpretation of Figure 6.3 and reveals further details that support the assessment of potentials to improve LWP. The covariance component therein can be interpreted as the contribution of correlation between FWP and FUE to total variance. For industrial pigs and broilers, the contribution from variance in log(FWP) (column 1) is larger than the contribution from variance in log(FUE) (column 2), which means that reducing variations in FWP would have a greater effect on reducing variations in LWP than reducing variations in FUE. However, for improving LWP it is also important how much of the variation in FWP and LWP can be addressed through management. Because animal housing allows for complete control of environmental conditions, FUE in industrial pig and broiler production can in principal be increased to the observed maximum in any part of the world with optimal management, whereas differences in environmental conditions will always result in variations of FWP even under optimal management. Mueller et al. (2012) have estimated that for most major crops the differences in management explain 60 % to 80 % of yield variability and that global crop production of these crops could be increased by 47 % to 70 % by improving nutrient and water management. Given that the response of FWP to increasing yield is not linear (Rockström et al. 2007) and that improvements in FWP can also be achieved through agricultural water management (Jägermeyr et al. 2016), these numbers should be directly interpreted as the potential to improve FWP, but they clearly highlight the importance of crop management for increasing LWP through improvements of FWP. For industrial layer hens, the contribution of log(FUE) to log(LWP) is very small, which means that variations in LWP are almost entirely determined by variations in FWP, so that LWP can only be improved by increasing FWP.

The dominant influence of variations in FUE for causing the variations in LWP of ruminants is the result of both a lower variance of FWP and a higher variance of FUE for ruminant types compared to industrial pigs and poultry. The lower variance in FWP for

ruminants is caused by the low variance of water productivity of grazed biomass (44 % lower than for feed crops), which in average make up about 68 % of ruminant feed. This also means that the potential to increase FWP of ruminant feed is much smaller than for industrial pigs and poultry. Not only because variance in FWP is lower but because water productivity of grazed biomass as defined here (section E.5) is entirely the result of environmental conditions and not subject to management. The high variance in FUE of ruminants is primarily the result of the diversity in ruminant management across regions and production systems, from smallholder ruminant rearing in developing countries to commercial production in high-income countries (Herrero et al. 2013). Variance of log(FUE) is especially large for meat and also dairy bovines. This implies a large potential to increase LWP for ruminants and particularly for meat and dairy bovines by increasing FUE. Although ruminants often spend at least part of their lifetime grazing on pastures where they are exposed to environmental conditions, it is in principal possible to minimize the exposure to detrimental climatic conditions by providing suitable shelter or rear ruminants entirely indoors. Thus, FUE can in principal be increased to its theoretical maximum in any part of the world but doing so may not always be practical.

Causes and implications of correlation between FWP and FUE

If FWP and FUE were unrelated, the variance of log(LWP) would be the sum of only variances of log(FWP) and log(FUE). However, for all livestock production types in our analysis we find correlations between FUE and LWP of varying sign and strength, which amplify or diminish the variance of log(LWP) by the double covariance between log(FWP) and log(FUE) (Figure 6.3, column 3). For industrial pig and broilers, about one third of total variance of log(LWP) can be attributed to a positive correlation between FWP and FUE. For all other livestock production types, a negative correlation between FWP and FUE results in a reduction of variance of log(LWP).

Understanding the underlying reasons for these correlations is crucial for assessing their implications for LWP improvements. Given the design of the study and the data and models used, three major drivers can be expected to cause a correlation between FWP and FUE in the results presented here: environmental conditions, socio-economic context, and feed composition. All livestock species are sensitive to climatic stress, in particular heat stress under high temperature and humidity (Nardone et al. 2006), leading to decreased overall productivity. Temperature extremes also affect plant growth and development (Hatfield and Prueger 2015), but many other abiotic factors such as soil type, insolation, and precipitation are only relevant for crops and grasses and have no direct impact on livestock. Thus, variations in temperature can cause FUE and FWP to become positively correlated but the effect is possibly small. A much stronger influence on the correlation between FUE and FWP can be expected from the socio-economic context in which feed cultivation and

livestock rearing take place. Although crop-based feed is also traded internationally, the vast majority of feed is grown domestically (FAO 2018). Thus, access to capital, knowledge, and technology within a country determine how well both feed crops and livestock are managed, causing FUE and FWP to become positively correlated. Finally, variations in the composition of feed can cause FUE and FWP to be negatively correlated, when feed components with a high nutritional value (e.g., maize and soya) lead to a higher FUE and lower FWP, because they provide more energy to livestock but require more water to be grown.

Correlation between FWP and FUE for industrial pigs and poultry. The effect of climatic conditions on the correlation between FUE and FWP found for industrial pigs and poultry is most likely negligible because these livestock types are usually reared indoors (Herrero et al. 2013). Also, FUE for monogastric animals was estimated from literature and does not account for differences in composition or quality of feed (Herrero et al. 2013). Thus, the positive relationship between FWP and FUE for industrial pigs and broilers is most likely attributable to the influence of the socio-economic context on crop and livestock management. This is supported by a strong correlation of FWP and FUE with regional per-capita gross domestic product (GDP), which can be taken as proxy for the socio-economic development level (Spearman's rho all between 0.59 and 0.61; see Table E.3). There is no obvious explanation for the inverse relationship between FWP and FUE found for industrial layer hens. They receive the same feed mix as industrial broilers, so their FWP shows the same strong correlation with GDP, but correlation of FUE with GDP is negative (Spearman's rho -0.35).

Because the positive relationship between FWP and FUE of industrial pigs and broilers in Figure 6.3 is the result of a common socio-economic context, an improvement of FWP and FUE by appropriate management interventions will not lead to a parallel improvement in FUE and FWP, respectively, and the management gaps causing variations in FWP, FUE, and eventually LWP have to be addressed individually. However, both FWP and FUE would benefit from improved conditions socio-economic that support a development towards intensification in the agricultural sector. Even if a causal relationship for the negative correlation between FWP and FUE cannot be ruled out, the contribution of covariance between log(FWP) and log(FUE) to total variance of log(LWP) is very small, making it unlikely that to improvements in FWP through targeted management interventions or a trend towards intensification would be substantially offset by a corresponding decreases in FUE.

Correlation between FWP and FUE for ruminants. The influence of socio-economic context on the correlation between FUE and FWP can be expected to also apply for rumi-

nants, but because most of ruminant feed is grazed biomass, whose water productivity is not influenced by management in our analysis, the overall effect is probably weaker. Environmental conditions, on the other hand, are likely to also play a role as most ruminants spend at least part of their lifetime grazing on pasture, where they can become exposed to climatic stress. However, both are drivers that lead to positive correlation between FUE and FWP, while the correlation found in Figure 6.3 for ruminants is negative. Because ruminants are fed a wide variety of feed mixes—composed of components with very different nutritional quality and water requirements—and because influence of feed quality on FUE is explicitly accounted for in the data from Herrero et al. (2013), inverse effects of feed composition on FWP and FUE are a possible explanation for a negative correlation between FWP and FUE.

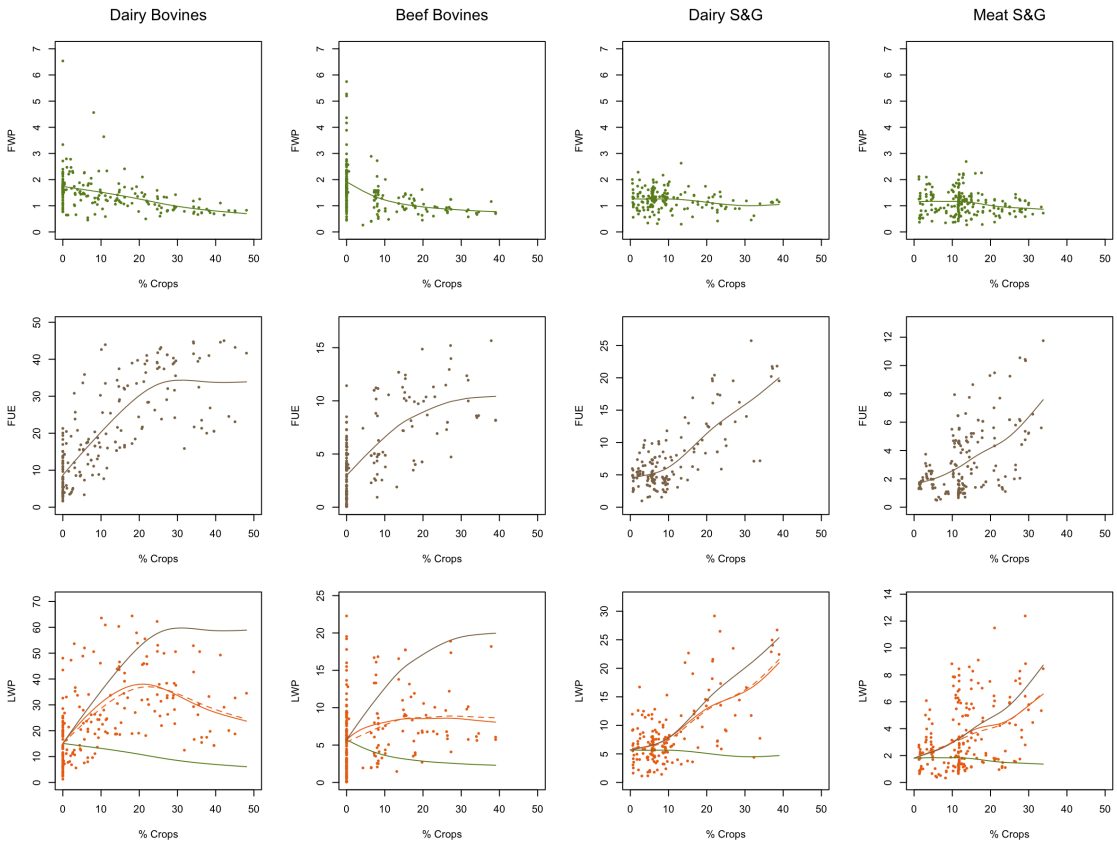

Figure 6.4: Relationship between the percentage of crop-based feed (grain, concentrates) in the feed mix of ruminants and FUE and FWP, and the resulting effect on LWP. Solid lines in FUE and FWP are smoothing splines fitted to the data. Solid lines in LWP are the product of the splines fitted to FWP and FUE (orange), the product of the spline fitted to FWP and constant FUE for 0 % grain use (brown), and the product of the spline fitted to FUE and constant FWP for 0 % grain use (green). The dashed orange line in LWP is the smoothing spline directly fitted to LWP values.

In Figure 6.4, the effect of supplementation with feed crops on FWP, FUE, and resulting LWP is shown for all ruminant types. Adding crop-based feed with a high energy and protein content to the primarily grass-based diet of ruminants improves the nutritional value of the whole feed mix and leads to an increase in FUE (brown, middle row). But because the WP of crops is much lower than the WP of grass (0.56 kgDM/m^3 in average for crops compared to 1.45 kgDM/m^3 for grazed biomass) this comes at the cost of a lower overall FWP (green, top row). Since the increase in FUE is stronger than the decrease in FWP, supplementation with feed crops always result in a higher LWP compared to an entirely roughage-based diet (orange, bottom row). However, at least for bovines, FUE gains from supplementation with feed crops appear to diminish at high crop shares, so that LWP reaches a maximum at about 20 % feed crops in the feed mix and declines thereafter.

Akin to supplementation with feed crops, the incorporation of crop residues (straws and stovers) in ruminant feed also has an effect on FWP and FUE with opposite sign. Due to no water cost and low nutritional value, feeding crop residue to ruminants has a positive effect on FWP and a negative effect on FUE (Figure 6.5). Although the strength of both effects is similar over the considered range of residue shares, it appears that moderate inclusion of crop residues (up to about 30 %) into feed of bovines tends to have a negative effect on LWP, whereas higher shares lead to an increase in LWP. The latter is caused by a strong increase in FWP for high shares of crop residues, which is the consequence of the assumption of no water cost for residues (for a diet consisting entirely of crop residues, FWP would approach infinity). For sheep & goats, the smaller range of residue shares in the dataset and the limited number of data points hamper the identification of a pattern in LWP to feeding crop residues to, but it is likely that it follows a similar general pattern than for bovines.

Although the responses of FUE and FWP to crop supplementation and incorporation of crop residues in Figures 6.4 and 6.5 can be fully explained by the consequences of varying feed composition, they are also influenced by other aspects of crop and livestock management. We find that the share of feed crops is positively and the share of crop residues in the feed mix is negatively correlated with GDP for all ruminant types (Spearman's rho 0.38 to 0.64 for fraction of feed crops and 0.28 to 0.43 for fraction of crop residues; see Table E.3), so that high rates of supplementation with feed crops tend to be associated with a high overall level of intensification in both crop and livestock production, whereas high rates of residue use tend to be associated with a low level of agricultural intensification. These correlations are likely to contribute to the observed responses to crop supplementation by diminishing the decline of FWP and enhancing the increase of FUE. Likewise, the observed decline of FUE in response to incorporation of crop residues in feed is to some degree attributable to poorer overall livestock management.

Because of the unknown contribution of general crop and livestock management to the

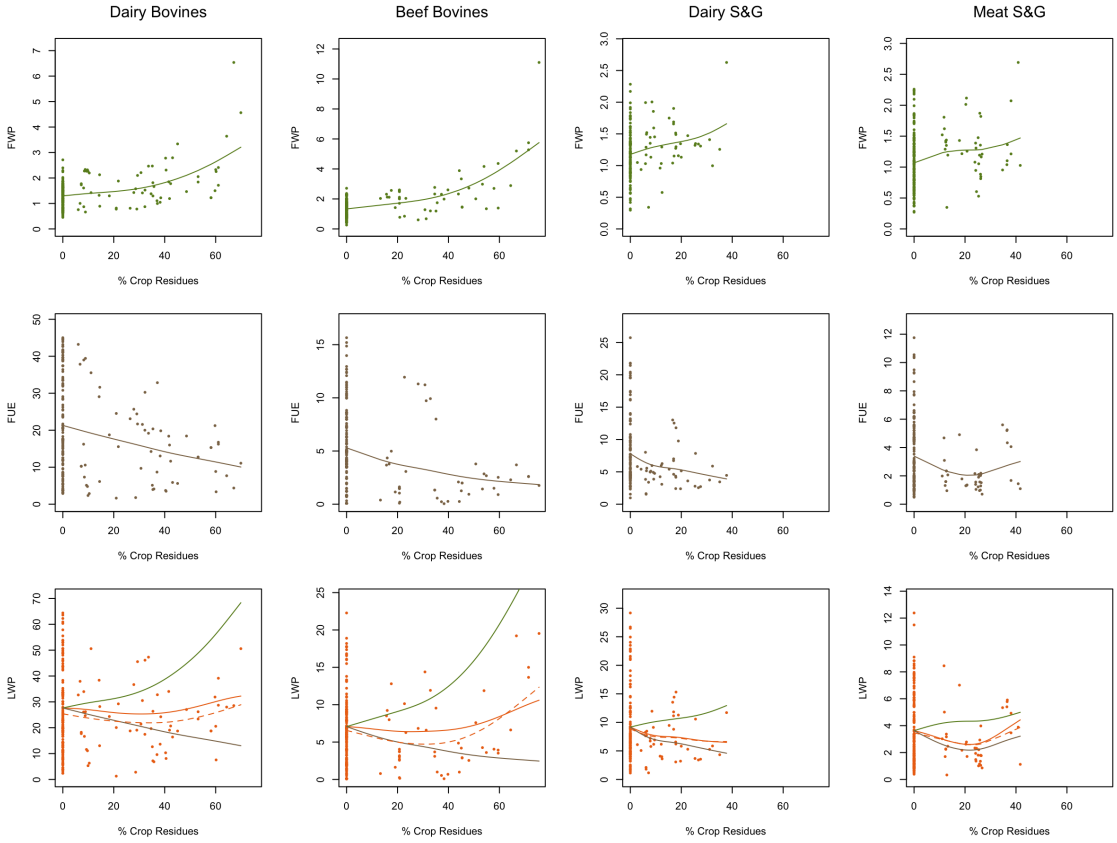

Figure 6.5: Relationship between the percentage of crop residues used in the feed mix and FUE and FWP, and the resulting effect on LWP. Solid lines in FUE and FWP are smoothing splines fitted to the data. Solid lines in LWP are the product of the splines fitted to FWP and FUE (orange), the product of the spline fitted to FWP and constant FUE for 0 % stover use (brown), and the product of the spline fitted to FUE and constant FWP for 0 % stover use (green). The dashed orange line in LWP is the smoothing spline directly fitted to LWP values.

responses of FUE and FWP, specific features of the pattern in Figures 6.4 and 6.5 such as the apparent maximum of LWP at 20 % crop supplementation fractions and the apparent minimum of LWP at 30 % residue incorporation for bovines must not be interpreted as having general validity. However, direct effects of feed composition on FUE and FWP are fundamental mechanisms that lead to a trade-off between improving or FUE or FWP through feed composition at the cost of lower FWP or FUE, respectively. Optimizing the feed mix of ruminants in a specific setting bears a great potential for improving LWP but requires details knowledge about the response of FUE to changes in feed composition and about water requirements for producing the different feed components. For reaping maximum benefits, the interactions between interactions between feed mix and other crop and livestock management aspects need to be considered, as these can drastically change

the responses of FWP and FUE (e.g., better crop management can compensate a drop in FWP and better livestock management can enhance the FUE increases thorough feeding interventions). And technological innovations, such as pre-treatment of residues to improve their nutritional quality (Blümmel et al. 2018), can potentially weaken or resolve the trade-off between FWP and FUE. In specific applications, it is also critical to reassess the validity of the water allocation rules applied in our global study. For example, assigning no water to residues could lead to misleading conclusions when using crop residues for feed causes nutrient mining from agricultural soils (Lutz et al. 2019).

Last but not least, our results suggest that LWP of ruminants, unlike for industrial pigs and poultry, does not always benefit from a trend towards intensification in the whole agricultural sector. Because better overall livestock management tends to be associated with high rates of supplementation with feed crops, the corresponding decline in FWP can lead to a lower in LWP in intensively managed systems.

6.3.4 Comparison with ET and CWU estimates from literature

Our estimate of total cropland ET (8587 km^3/yr) is lower than the estimates reported by Hanasaki et al. (2010) and Siebert and Döll (2010) but larger than the estimate by Liu and Yang (2010) (Table 6.2). Since all these estimates are based on the same cropland dataset (Ramankutty et al. 2008), the difference should be attributable to other input data and model formulations used here. However, the estimate of fallow ET from Liu and Yang (2010) appears very low and probably only includes ET from cropland outside the growing period, whereas our and the other estimate also include ET from land not cultivated every year. The share of fallow ET in total cropland ET in our analysis is 36 %, which agrees well with the corresponding estimates of 36 % and 32 % from Hanasaki et al. (2010) and Siebert and Döll (2010), respectively.

Our estimate of 5482 km^3/yr for ET during the growing period is somewhat below the range of estimates reported by all other studies (5938 km^3/yr to 7130 km^3/yr). This is consistent with the general underestimation of ET by LPJmL4 (Schaphoff et al. 2018a), although at least two of the studies (de Fraiture et al. 2007, Weindl et al. 2017) also make different assumptions about cropland extent and area harvested. The share of 17 % crop ET from blue water sources in our analysis is close to the estimates from four other studies and equivalent to the average across all studies (17 %). Our estimate of 414 km^3/yr consumptive blue water losses from irrigation water supply infrastructure, which is not included in the figures shown in Table 6.2, is close to the corresponding estimate of 440 km^3/yr from de Fraiture et al. (2007).

When looking at total growing period CWU for barley, maize, wheat, and soybeans, we find that the sum of ET estimated for these four important feed crops in our analysis is about 20 % lower than the sum of the corresponding estimates from Mekonnen and Hoek-

Table 6.2: Estimates of ET components from cropland and pastures and CWU components allocated to livestock. To facilitate comparison of estimates from different studies, the values reported in this table do not account for the consumptive losses of irrigation. All ET and CWU totals are in km^3/yr.

	de Fraiture et al. (2007)	Mekonnen and Hoekstra (2011, 2012)	Hanasaki et al. (2010)	Liu and Yang (2010)	Siebert and Döll (2010)	Weindl et al. (2017)	Our study
Year	2000	1996–2005	2000	1998–2002	1998–2002	2000	1998–2002
ET cropland			11070	7323	9823		8587
ET fallow			3990	1385	3137		3105
ET growing period	6690	6670	7080	5938	6685	6100	5482
Crop ET from blue sources	16.9 %	13.5 %	21.6 %	15.6 %	17.7 %	16.6 %	16.6 %
Total CWU barley		200			161		139
Total CWU maize		648			693		691
Total CWU wheat		964			858		665
Total CWU soybeans	427	363			399		229
Total CWU crops for livestock	1312	1304				2170	1846
ET Pastures			12960			16520	11235
Green CWU grazing	840	913				2590	1686

stra (2011) and Siebert and Döll (2010). For barley, wheat, and soybeans, the difference between our estimates and the two other studies is quite large but there are also large differences between Mekonnen and Hoekstra (2011) and Siebert and Döll (2010). Our estimate for total growing period CWU for maize is nearly identical to the estimate from Siebert and Döll (2010) and slightly larger than the estimate from Mekonnen and Hoekstra (2011). The differences between estimates from different studies can in part be attributed to different assumptions about the harvested area of crops as well as differences in terms of start and length of growing periods. However, one fundamental difference between the two other studies and ours is that LPJmL4 can account for changes in ET due differences in crop leaf area index under different crop management intensities, which is an important determinant of crop water productivity (Rockström et al. 2007).

The share of crop ET allocated to CWU of livestock production in our analysis is 33 %, which is much larger than the corresponding estimates of 18 % and 20 % from de Fraiture et al. (2007) and Mekonnen and Hoekstra (2012), respectively, and slightly lower than the 36 % estimated by Weindl et al. (2017). Neither de Fraiture et al. (2007) nor Mekonnen and Hoekstra (2012) provide sufficient information that could help to explain their low shares of crop ET allocated to livestock production. However, according to FAOSTAT, 70 % of barley, 67 % of maize, and 18 % of global wheat production are used for feed and account together for 44 % of total concentrate feed used for livestock production. Applying

these shares to CWU estimates for these crops from Mekonnen and Hoekstra (2011) would allocate about 750 km^3/yr of ET to livestock production. Together with their 600 km^3/yr of ET for 'fodder crops' (Mekonnen and Hoekstra 2011), this amounts to more than the total crop ET allocated to livestock production by Mekonnen and Hoekstra (2012). Only a small part of this discrepancy can be explained by their higher than average feed used in countries with a lower than average CWU per kg feed, which results in less ET attributed to feed when country-specific values are used (about 20 % in our analysis). More important is the assumed use of concentrate feed in livestock production (1 GtDM/yr in total) in Mekonnen and Hoekstra (2012), which is very low compared to the about 1.3 GtDM/yr of concentrate feed used in livestock production according to FAOSTAT and in our analysis. Thus, our higher share of crop ET attributed to livestock production appears more realistic in light of FAO statistics.

Estimates of ET from pastures varies greatly among studies, which can be primarily attributed to differences in the assumed distribution and extent of pasture lands, which is highly uncertain (Fetzel et al. 2017). However, the assumed extent of pasture extent has little importance for the estimation of livestock CWU as only the ET related to biomass actually grazed by ruminants is accounted for. Estimates of CWU for grazed biomass are basically determined by the estimated grazing requirement and the water productivity of pastures. The grazing demand from Herrero et al. (2013) used in our analysis is 2.4 GtDM/yr and the average grass water productivity is 1.45 $kgDM/m^3$. The estimate from de Fraiture et al. (2007) assumes a global constant grass water productivity of 1.3 $kgDM/m^3$ so that grazing demand must be about 1.1 GtDM/yr—less than half than in our study. Mekonnen and Hoekstra (2012) provide no direct information of their assumed grazing demand or how grass water productivity was estimated at all. Based on the information that they use data from Bouwman et al. (2005) to disaggregate their estimated amount of required roughage into demand for grass and other components, it appears that their grazing demand is similar to ours, about 2.4 GtDM/yr. This would imply a global average grass water productivity of 2.6 $kgDM/m^3$, a value exceeded for only 2.5 % of global grazing CWU in our analysis. Weindl et al. (2017) estimate a grazing CWU of 2930 km^3/yr in 2010 for a grazing demand of 4.0 GtDM/yr, which corresponds to an average grass water productivity of 1.35 $kgDM/m^3$. While average grass water productivity agrees well with our estimate, grazing demand is much higher than in any other study.

6.4 Conclusions

We combine estimates of animal feed consumption and production from Herrero et al. (2013), estimates of CWU for the various feed types simulated with LPJmL4 (Schaphoff et al. 2018b), and FAO statistics (FAO 2018), to obtain compute livestock CWU and LWP

for 919 different production units representing the global livestock sector. An important novelty is that our estimates of CWU for crops and livestock include the ET that occurs outside the growing season of crops from fallow land. This allows for a straightforward comparison between CWU estimates for seasonal and perennial crops and across production systems with different cropping intensity.

Our results show that annually 4666 km^3 of water are required to produce the feed consumed by the global livestock sector, equaling about 23 % of the total ET from global agricultural lands and 44 % of total CWU for biomass for human use. About 76 % of this water is ET during the growing season of crops and grass and the remainder is ET from fallow land and transportation losses of irrigation water. With blue water contributing only about 7 % to total livestock CWU, the livestock sector is primarily green water dependent. About half of the green water is ET from pastures, of which one third occurs from pastures on marginal land with no alternative use in crop production.

Our analysis reveals huge differences in LWP both among and within different livestock types. By analyzing the interaction of variations in FWP and FUE to produce the variations in LWP we find that variations in LWP of industrial pigs and broilers are to a similar extent caused by variations in both FWP and FUE, that variations in LWP of industrial layer hens are almost exclusively determined by variations in FWP, and that variations in LWP of ruminants are dominated by variations in FUE though with substantial contributions from variations in FWP. About one third of variability in LWP of industrial pigs and broilers is caused by a correlation between FWP and FUE, and variations in LWP of bovines and, to a lesser degree, sheep & goats are dampened by a negative correlation between FWP and FUE.

The variability in FUE of industrial pigs and broilers in our analysis can be entirely attributed to different management and efficiency gaps could be addressed by appropriate livestock management interventions. Variability in FWP is the result of differences in both management and environmental conditions, which means that variations in FWP can only partially be reduced by improved crop and land management. Because the positive relationship between FUE and FWP is the result of the influence of the overall level of intensification in the agricultural sector on crop and livestock management, improvements in either factor will not lead to an improvement in the other factor. Variability of LWP for industrial layer hens is much smaller than for other monogastric livestock types and are almost entirely the result of variations in FWP. Since only the part of the variations in FWP that are not related to different environmental conditions can be reduced through management, the overall potential to increase LWP for layer hens is comparatively small.

Variability of LWP for ruminants is dominated by variations in FUE, which are mainly caused by differences in livestock management and may thus be greatly reduced by closing efficiency gaps through appropriate management improvements in the livestock sector.

Variability in FWP is much smaller than for pigs and poultry and more strongly determined by environmental conditions, which implies a comparatively small potential to improve LWP of ruminants through interventions aiming at improving FWP. However, because we did not account for the effect of pasture management on WP of grazed biomass, the potential to improve FWP of ruminants through improved pasture management could not be assessed. The negative correlation between FUE and FWP found for all ruminant types can be mainly attributed to opposite effects of feed composition on FUE and FWP: Improvements in FUE through supplementation with feed crops are accompanied by a reduction in FWP due to the lower WP of feed crops compared to grass. And improvements in FWP through incorporation of crop residues are offset by lower FUE caused by their lower nutritional value. How these trade-offs play out in a specific production system essentially depends on the nutritional value of the different feed components, the water requirements to produce them, and how animals respond to changes in the feed mix. Detailed knowledge about these factors is needed to determine the feed composition that results in the best LWP under the given production conditions, but to unlock the full LWP potential, also the interaction of these factors with other management interventions aiming at increasing FWP and FUE has to be taken into account.

Supplementary material related to this chapter is available in Appendix E.

Acknowledgments, Samples, and Data

This work was supported by ILRI and the CGIAR research program on Water, Land and Ecosystems (WLE). Further support was provided the German Ministry for Education and Research (BMBF) through the MACMIT project (grant no. 01LN1317A) and the SUSTAg project (grant no. 031B0170A).

The core output of the analysis in this paper—consisting of estimates of consumptive water use from tree different sources in 919 global units—will be made publicly available under a Creative Commons Attribution 4.0 License. All primary data, model code, model outputs and scripts that have been used to produce the core output will be archived at the Potsdam Institute for Climate Impact Research and be available upon request.

Chapter 7

Synthesis and outlook

7.1 Summary and key findings

The overarching goal of this thesis is to improve the understanding of climate change impacts on water resources, how this will affect water availability for future populations, and what scope for adaptation exists. Within this very broad topic, this thesis focusses specifically on climate change impacts on blue water resources and the scope for reducing water demand by improving water productivity in livestock production. In section 1.2, three main research question have been formulated to which the studies presented in chapters 2 to 6 provide answers. In the following sections, the key findings of the individual studies are summarised, organised by their contributions to the main research questions.

7.1.1 What is the impact of different levels of global warming on river discharge?

The studies presented in chapter 2 (Schewe et al. 2014), chapter 3 (Haddeland et al. 2014) and chapter 5 (Heinke et al. 2019a) all analyse climate change impacts on river discharge as a measure of renewable blue water resources. A common feature of all three studies is that climate change impacts are presented as a function of global mean temperature increase rather than by comparing different emission scenarios. In fact, the studies in chapters 2 and 3 are among the first examples that systematically assess the impact of different levels of global warming on river discharge. However, both studies are based on GCM simulations forced with RCP emission scenarios (Meinshausen et al. 2011b) and report impacts for selected time periods in these scenarios where given changes in global mean temperature are reached (Tang and Lettenmaier 2012). The main disadvantage of this approach is that different temperature levels are reached in different years in the same emission scenario and GCM (and the same temperature level in different years in different scenarios or GCM) and that differences in the magnitude of temperature increase among

GCMs limits the range of temperature levels that can be analysed. To overcome these problems, the 'PanClim' dataset of climate scenarios was developed, which covers a broad range of global mean temperature increases (1.5 K to 5 K increase above pre-industrial level in steps of 0.5 K) that are reached around the year 2100 in all scenarios (Figure 4.2). The development and validation of the dataset is described in chapter 4. The dataset is based on a pattern-scaling approach using monthly climate change patterns obtained for 19 different GCMs and trajectories of GMT increase obtained with the MAGICC6 model (Meinshausen et al. 2011a). The study presented in chapter 5 is based on this dataset, which allows to cover a broader range of global mean temperature increase from 1.5 K to 5 K all reached in 2100.

A unique feature of the analyses in chapters 2 and 3 is that they not only use multiple GCMs to account for the uncertainties in spatial patterns of climate change for given levels of global mean temperature change but also multiple global hydrological models (GHMs) to account for the uncertainties how changes in climate conditions are translated into changes of river discharge. Chapter 2 is based on results of the Inter-Sectoral Impact Model Intercomparison Project (ISIMIP; Warszawski et al. 2014) and focusses on changes in 'naturalised' discharge (without anthropogenic impacts other than climate change). Chapter 3 synthesises results from ISIMIP and from the Water Model Intercomparison Project (WaterMIP; Haddeland et al. 2011, Harding et al. 2011) and focusses on both climate impacts and direct human impacts (dams and water withdrawals) on river discharge. The analysis in chapter 5 is based on a single hydrological model but considers a larger ensemble of GCMs. It also goes beyond analysing changes in mean annual discharge but also considers other aspects of changes in streamflow important from a water resources perspective—that is, increased number of drought months and increased magnitude of floods.

All three studies (chapters 2, 3 and 5) show similar spatial patterns of changes in mean annual discharge due to climate change that are also broadly consistent across different levels of global mean temperature increase. Common large-scale features in the multi-model means are increases in the high northern latitudes and eastern Africa, and decreases in the Mediterranean, the Middle East, and parts of North and South America (Figures 2.1, 3.1 and 5.2). In these regions, most members in the multi-model ensembles of the respective studies agree on the sign of change, which together with the agreement among studies indicates a high level of confidence at least in the direction of projected annual discharge changes. For other regions such as central Europe, western Africa, China, and eastern part of the US, the multi-model means of the tree studies show only weak change, which is a result of disagreement on the direction of change among ensemble members rather than an agreement on weak change. Thus, projections of mean annual discharge are highly uncertain in these regions and large increases and decreases cannot be excluded. The attribution of the ensemble variance in projected mean annual discharge change to

GCM and GHM variance in chapter 2 shows that projection uncertainty is dominated by GCM uncertainty for example in East Africa, Southeast Asia, and central America, and dominated by GHM uncertainty for example in parts of North and South Africa, central Europe, and central Asia (Figure 2.1). However, only 5 different GCMs are used in this study and the fact that many regions that have a rather low contribution of GCM uncertainty show diverging trends in Figure D.6—which is based on 19 GCMs and a single GHM—indicates that the importance of GCM uncertainty may be underestimated. On the other hand, the high level of agreement on declining annual discharge found in chapter 5 for some regions (e.g., western US and northern Africa) are not apparent in the results in chapters 2 and 3, which highlights the potential underestimation of projection uncertainty when only using a single GHM.

In chapter 3, climate change impacts on mean annual discharge are compared to decreases in annual discharge due to anthropogenic water consumption. Many river basins in the Middle East, Central Asia, and China—prominent examples include Euphrates-Tigris, Amu Darya, and Huang He—are severely affected by human interventions causing annual discharge reductions of more than 15 % (multi-model median of seven GHMs; Figure 3.1). In several other basins around the world, including Colorado, Nile, Orange, and Murray-Darling, the multi-model median of mean annual discharge decrease is between 5 % and 15 %. The most severely impacted among world's large river basins is the Indus basin in which, according to the multi-model median, as much as 47 % of the available blue water is consumed. However, the estimates among individual ensemble members vary between 18 % and 79 %, with an interquartile range from 29 % to 62 %. Such large differences among ensemble members prevail in all basins for which a strong human impact is estimated and are the result of differences in modelled reference (naturalised) discharge and water consumption; different reservoir operation schemes and withdrawal routines further add to the large uncertainties.

Discharge changes due to global mean temperature increase will interact with the reductions of annual discharge from human water consumption, leading to a further decrease, diminish the human impact signal, or completely override it—turning a decrease into an increase. Even for a moderate increase of global mean temperature to 2 K above pre-industrial levels, the magnitude of change in annual discharge from climate change alone are stronger and more widespread than the changes from human water consumption, so that the global pattern of the combined effect of the two will be dominated by the impact of climate change (Figure 3.1). However, in basins most severely impacted by direct human interventions, such as Colorado, Euphrates-Tigris, Indus, and Huang He, changes will remain dominated by reductions due to human water withdrawals, even for increases in global mean temperature to 3 K above pre-industrial levels (Figure 3.3).

Climate change will not only lead to changes in mean annual discharge but also alter

characteristics of streamflow related to variability—i.e., the temporal distribution of stream flow. Such changes are assessed in chapter 5 by analysing changes in the number of hydrological drought months and in the magnitude of floods under different levels of global mean temperature increase. Drought months are defined as abnormal deviation from the long-term average monthly flow; in ephemeral rivers the duration of low-flow periods is used as an additional criterion (section 5.2.4). Changes in the magnitude of floods are defined as changes in the annual 5-day average peak flood with a 10-year return period, which is shown do be a reasonable proxy for changes in foods with a return period up to 100 years (section 5.2.4). For moderate increases of global mean temperature up to 2 K, severe increases in drought months by 50 % are projected by the majority of ensemble members for parts of the Mediterranean region, the Middle East, and Central America (Figure 5.2). Between 2 K and 3.5 K of global mean temperature increase almost the entire Mediterranean region and Central America but also parts of sub-Saharan Africa and Australia become affected. Beyond 3.5 K warming, the expansion of areas where a severe increase in drought months is projected by the majority of ensemble members slows down, with most of the change happening in Australia, North America, and southern Africa. Severe increases in the magnitude of floods by more than 30 % are almost non-existent in the majority of ensemble members for global mean temperature increases of less than 2 K, except for few scattered locations in the subarctic region. With global mean temperature increases beyond 2 K, severe increases of floods become increasingly prevalent in many parts of the world with particularly widespread occurrences in eastern Africa, northwestern and southeastern South America, and the subarctic region. The expansion of areas affected by severe increases in flooding continues and even accelerates up to 5 K warming, the highest level of global mean temperature increase assessed in chapter 5.

Overall, the spatial distribution of increases in number of drought months and increases in floods coincide with decreases and increases, respectively, in mean annual discharge. However, whether and at which increase in global mean temperature crosses the thresholds marking severe increases in droughts or floods often does not coincide with crossing corresponding thresholds for severe changes in mean annual discharge. In some parts in Central Asia and North America, for example, severe decreases in mean annual discharge are not accompanied by severe increases in drought events, and in some parts of Europe and Central America, severe increases in drought events are not accompanied by severe decreases in mean annual discharge.

7.1.2 How do climate related changes in river discharge affect human water resources?

The climate related changes in river discharge analysed in chapters 2, 3 and 5 provide the basis for assessments of climate change impacts on human water resources. Different indi-

cators are used to relate the different aspects of change in streamflow analysed in the three studies to impacts on water resource. Chapter 2, which analyses mean annual discharge, estimates the number of people exposed to severe decreases in annual discharge as well as the number of people living under water scarcity. Chapter 3 evaluates changes in the cumulative abstraction-to-demand ratio of irrigation water use, which are calculated from model estimates of irrigation water requirements and actual withdrawals, and do not only account for changes in annual discharge but also for changes in its temporal distribution. Chapter 5, like chapter 3, analyses the number of people exposed to severe decreases in mean annual discharge but complements this information with an assessment of exposure to severe increases in drought months and severe increases in the magnitude of floods. Water scarcity of future population is calculated assuming present-day climate conditions to identify those parts of global population that will likely be faced with particularly high challenges for adoption to severe hydrological changes.

In chapter 2, a decrease of mean annual discharge by more than 20 % or more than one standard deviation of 1980–2010 annual discharge is used as an indicator for a severe reduction of renewable water resources for which serious adaptation challenges are likely to arise. For a warming of 1 K above present-day conditions (1.7 K above pre-industrial levels), the multi-model median of people exposed to such a severe reduction in renewable freshwater resources is estimated to be 8 % of global population the SSP2 scenario (Figure 2.2). For a warming of 2 K and 3 K the number rises to 14 % and 17 % of global population, respectively. However, the spread across the multi-model ensemble is large with an overall range from 3 % to 36 % and interquartile range from 9 % to 22 % of global population affected at 2 K warming. Most of this uncertainty is due to differences among hydrological models, which are responsible for about three quarters of the ensemble variance; only one quarter is due to differences among GCMs. The two models in the ensemble that simulated vegetation dynamics—one of them being the model used in the analysis in chapter 5—yield generally smaller reductions in water resources than the other models in the GHM ensemble. The effect of elevated atmospheric CO_2 concentrations on discharge changes, however, is found to be small.

While the analysis of changes in freshwater resource availability provides insights on adaptation challenges, it does not allow to draw conclusions about the impact of climate induced hydrological change on water resource scarcity in an absolute sense. To assess this aspect, a simple measure of water scarcity is used in chapter 2, which relates total water resources to total population at the country scale. The indicator provides a measure of average per-capita blue water availability without taking into account actual per-capita water requirements. For present-day hydrological conditions and population numbers, the median estimate across the multi-model ensemble for people living in countries with an annual blue water availability of less than 500 m^3 per capita (characterised as absolute

water scarcity) and 1000 m^3 per capita (chronic water scarcity) is 1.5 % and 3 % of global population, respectively, with estimates among individual ensemble members ranging from 0 % to 4 % for the <500 m^3 class and 1 % to 8 % for the <1000 m^3 class (Figure 2.3). With increasing levels of global mean temperature and increasing population numbers according to the SSP2 scenario, the multi-model median of global population living in countries below 500 m^3 per capita (1000 m^3 per capita) increases to 6 % (13 %) at 1 K, 8 % (21 %) at 2 K, and 12 % (24 %) at 3 K warming above present-day level. The spread of estimates from individual models increases with increasing temperature levels, reaching an overall range from 4 % to 29 % (12 % to 45 %) and an interquartile range from 9 % to 14 % (18 % to 29 %) for a warming by 3 K. As for severe reductions in annual discharge, the contribution of differences among GHMs to total ensemble variance is much larger than from differences among GCMs, with a ratio of about 3:1.

Increases in the estimates of population living in water-scarce countries reported in chapter 2 are to a large extent driven by population increase, which leads to a decrease in per-capita water availability even with no change in total water resources. To determine the contribution of climate change to the overall increase, the number of people living in water scarce countries caused by population change alone is estimated by relating future population to present-day (1980–2010) water availability. The results show that the number of people experiencing absolute water scarcity (<500 m^3 per capita) is increased by nearly 40 % (multi-model median) for a warming by 1 K and 2 K compared to the number of people experiencing absolute water scarcity due to population change alone; for a warming by 3 K, the amplification is somewhat lower at 25 % (Figure 2.3). Likewise, the multi-model median of amplification in the <1000 m^3 class is highest at 1 K warming with nearly 30 %, drops to about 20 % at 2 K, and is close to zero at 3 K. This apparent decline of the climate effect with increasing strength of climate change can be attributed to the fact that the underlying changes in water availability are obtained from GCM simulations in which higher warming levels occur later in the 21^{st} century, and that the population numbers at the respective points in time are used to estimate water scarcity. Thus, higher levels of global warming are associated with higher population numbers, resulting in higher estimates of water-scarce population due to population change alone against which the pure climate effect is compared. This means that the estimated amplification of water-scarce population depends on the relative timing of climate and population change in the underlying climate simulations and population scenario and cannot be generalised to evaluate, for example, the consequences of different levels of global mean temperature increase in 2100. It is also important to recognise that reported changes of global population in water-scarce countries represent net changes which may obscure strong but diverging changes in water scarcity in different parts of the world.

Although per-capita water availability is a suitable measure to quantify supply-side

effects of water scarcity, the problems that countries and people are faced with to satisfy their water needs also depend on the amount of water needed to fulfil all societal needs (see section Human dependence on water resources). Per-capita water demand for domestic and industrial purposes strongly depend on the economic conditions and water saving technologies in place, while irrigation water demand is essentially determined by the need to compensate insufficient or unstable moisture supply of crops from rainfall (i.e., a lack of green water). With irrigation being responsible for more than 90 % of global consumptive water use, differences in societal water requirements are largely determined by the conditions under which food is grown and most water use does not occur where people live but where irrigation takes place. The analysis of climate change impacts on irrigation water scarcity in chapter 4 provides insights on this important aspect of water resource use, taking into account climate-related changes in both irrigation water demand and water availability. Irrigation water scarcity is quantified by means of the cumulative abstraction-to-demand (CAD) ratio, the ratio of actual irrigation water consumption to potential irrigation water requirements (i.e., irrigation water consumption when water supply is not limited). Global average estimates of CAD under present-day conditions (1971–2000) ranges from 0.38 to 0.71 across the multi-model ensemble with a median of 0.58 and an interquartile range of 0.42 to 0.65 (Figure 3.5). The large uncertainties are largely caused by differences in irrigation water requirements and river discharge estimated by the models, but also reflect differences in the way models account (or do not account) for groundwater withdrawals and reservoir operation. However, for most agricultural land under irrigation today a CAD ratio of >0.8 is estimated by the majority of ensemble members and only for some heavily irrigated areas in southern North America, North Africa, South Asia and northern China the multi-model median of CAD is below 0.5 (Figure 3.4). Keeping all non-climate-related drivers such as irrigated cropland extent, crop distribution, irrigation efficiencies, and reservoir operation constant throughout the simulation period, the multi-model median of CAD decreases with increasing global mean temperature in most areas with irrigation today, indicating an increase in irrigation water scarcity. Globally, the multi-model median of CAD decreases to 0.55 and 0.52 for an increase in global mean temperature to 2 K and 3 K above pre-industrial levels (increase by 1.6 K and 2.6 K from 1971–2000), respectively. Particularly strong decreases in CAD occur in Mexico, the southern USA, Brazil, southern Europe, the Mediterranean, and northern China where decreases in CAD in some places exceed 0.1 in the majority of ensemble members already for an increase in global mean temperature of 2 K above pre-industrial levels. For most of these areas, a decrease in annual discharge is found in chapters 2 and 3, indicating that decreases in CAD can to a large extent be attributed to a decrease in water availability. However, potential irrigation water demand is projected to rise in almost all regions by the majority of ensemble members, but actual irrigation water consumption rarely increases by

the same amount to completely match this, resulting in a decline in CAD even when discharge is not projected to decreases (Figure 3.5). A more detailed attribution of increases in irrigation water scarcity to increases in irrigation water demand and decreases in water availability was not possible based on available model simulations and would require specifically designed experiments.

The analysis of climate change impacts on water resources in chapter 5 focusses on severe hydrological change that is likely to exceed the conditions for which existing water supply infrastructure has been designed, so that investments in adaptation will be needed. This is similar to the analysis of severe decreases in annual discharge in chapter 2 but improves on it in two major aspects. First, using the climate scenarios described in chapter 4, the analysed levels of global mean temperature increase are all reached at the same time (around year 2100) and can therefore be combined with population estimates for that year, allowing a straightforward attribution of population exposure to severe hydrological change to climate change. In addition, the use of these climate scenarios also provides estimates for a much wider range of global mean temperature increase. Second, by not only analysing changes in mean annual discharge but also taking into account severe increases in the number of drought months and severe increases in the magnitude of extreme flooding events, chapter 5 provides a much more comprehensive assessment of climate-related risks to water resources and supply infrastructure.

For an increase in global mean temperature increase in line with the 2-degree target (1.1 K additional warming over year 2009) and an assumed population as in the SSP2 population scenarios, about 615 million people (7 % of global population) are projected to become exposed to severe hydrological change by the majority of ensemble members (Figure 5.2). With increasing levels of global mean temperature increase, the number of people projected to become exposed to severe hydrological change grows at an increasingly faster rate: While about 500 million more people become exposed to severe hydrological change between 2 K and 2.5 K, it is almost 1 billion more people between 4 K and 4.5 K. For a warming to 5 K above pre-industrial levels (the highest temperature level analysed in chapter 5), nearly 5 billion people (55 % of global population) are projected to become exposed to severe hydrological change by the majority of ensemble members. Other population scenarios with different global population numbers in 2100 give different estimates of number of people exposed to severe hydrological change, but the percentage of total population exposed is similar across population scenarios (Figure D.2).

At lower levels of global warming (to about 2.5 K), severe hydrological change mainly consists of severe decreases in annual discharge and severe increases in droughts. At higher levels of global warming, severe increases in flooding are projected to occur more often and become an important driver for the increase in population exposed to severe hydrological change. In fact, for most people for which exposure to severe hydrological change is pro-

jected by the majority of ensemble members at higher temperatures, a mixture of all three different aspects of severe hydrological change occurs. Based on such a large disparities in the type of hydrological change among ensemble members, solid recommendations for planned adaptation to hydrological change are almost impossible.

The analysis of severe hydrological change alone only allows to draw conclusions about the need for adaptation of water supply infrastructure. In situations of water-scarcity, however, supply-side management may be insufficient or too costly and needs to be complemented by appropriate demand-side management measures to prevent negative social and economic impacts. Implementation of demand-side management measures, on the other hand, is often complicated by behavioural, economic, political, and institutional obstacles, making adaptation under water-scarce condition more challenging. To account for this, the future population pressure on blue water resources in the absence of additional climate change is estimated in chapter 5 to determine where severe hydrological change will act on top of already prevailing water scarcity. For the SSP2 population scenario, about 3.3 billion people (37 % of global population) are found to experience water scarcity, defined to occur when >1000 people share 1 million m^3 of annual discharge (equivalent to an annual blue water availability of 1000 m^3 per person), under present-day hydrological conditions (Figure 5.1). Up to a warming of 5 K above pre-industrial levels, almost two thirds of water-scarce population (2.1 billion people) are projected to become affected by severe hydrological change by the majority of ensemble members, while for only about half of the remaining population (2.8 billion people) such changes are projected (Figure 5.3). This asymmetry of exposure to severe hydrological change between population shares with high versus those with low pressure on water resources is apparent at all levels of warming and in all population scenarios analysed in chapter 5 (Figure D.3).

By constraining global mean temperature increase to 2 K above pre-industrial levels by appropriate mitigation efforts, the number of people projected to become exposed to severe hydrological change (mainly a decrease in mean availability and/or an increase in drought months) under already prevailing water scarcity could be dramatically reduced to 290 million in the SSP2 population scenario. While this represents a mere 3.2 % of global population, almost two thirds of these people (182 million) are located in Latin America and the Middle East and north Africa, where they constitute about 12 % and 14 %, respectively, of the total population in these regions (Table 5.1). Such a high share of population affected by severe hydrological change and high pressure in water resources can have negative societal and economic consequences not only for these people but for the whole region if the obstacles associated with the implementation of appropriate demand management cannot be overcome.

7.1.3 How much water is used by the global livestock sector, and what are the opportunities and constraints for improving water productivity?

By using a newly developed dataset of feed use and productivity in the global livestock sector and combining it with ET estimates from a crop model, FAO statistics, and additional spatial datasets, chapter 6 provides estimates of CWU for feed production and LWP for 919 different livestock production units around the world. Because feed crops are cultivated on cropland, traded around the world, and partly derived from co-products of food production, an assessment of livestock water use must be built on a comprehensive account of agricultural water use. Thus, chapter 6 also provides estimates of ET from global agricultural land and how much of it contributes to the production of food, feed, and biomass for other uses. All estimates are averages for around the year 2000 (1998–2002), because more recent data on feed use and livestock productivity are not available.

Annual ET from global agricultural land amounts to 20 236 km^3/yr, of which 11 235 km^3/yr are from pastures and 9001 km^3/yr are from cropland (Figure 6.1). About 15 % of the ET from cropland (1324 km^3/yr) is blue water supplied through irrigation (including evaporative losses). About one third of the total ET from cropland (2980 km^3/yr) can be attributed to feed production (feed crops and cultivated forages). The remainder is related to food production (56 % of cropland ET) and production of biomass for fibres and biofuels (10 %). There is a notable difference in the composition of CWU for these three categories, with blue water making up about 18 % and 16 % of total CWU for feed crops and other uses, respectively, but only 10 % for CWU related to feed production. In consequence, only about 22 % of total blue water consumption for irrigation (297 km^3/yr) is related to feed production. Of the annual total ET from pastures, only 15 % (1686 km^3/yr) are CWU for grazed biomass, while the remainder is associated with biomass that supports other functions of grassland ecosystems like wildlife and carbon sequestration. CWU for grazed biomass is entirely green water and about one third (576 km^3/yr) is from pastures on marginal lands, where livestock rearing is often the only agricultural use of this water. Overall, the annual water use for feed production amounts to 4666 km^3/yr, which is about 44 % of total CWU for agricultural biomass for human use.

Total annual supply of human edible protein by the global livestock sector is 53.7 MtP/yr, which gives a global average LWP of 11.5 gP/m^3. Ruminants (bovines, sheep, and goats) contribute about half of annual production (29.2 MtP/yr) but are responsible for almost two thirds of CWU (2975 km^3/yr). The remaining production (24.5 MtP/yr) and CWU (1691 km^3/yr) are associated with monogastric animals (pigs and poultry). Thus, monogastric animals produce about 50 % more protein per m^3 of total CWU than ruminants. However, because about two thirds of ruminant feed is grazed biomass, blue water con-

tributes only 5 % (146 km^3/yr) to total CWU of ruminants, while CWU of pigs and poultry contains 9 % (151 km^3/yr) of blue water. Thus, protein from ruminants requires on average less blue water for production than protein from pigs and poultry.

Large differences also exists between livestock types within these ruminants and monogastric animals categories. For example, meat bovines are responsible for about half of ruminants' CWU (1440 km^3/yr) but supply only 7 MtP/yr of protein, while dairy bovines produce 20 MtP/yr of protein from 855 km^3/yr of CWU. Although the CWU of dairy bovines contains a higher share of blue water than the CWU of meat bovines (7.1 % compared to 3.8 %), the much higher LWP of dairy bovines makes them more blue water efficient. In fact, average LWP of dairy bovines is the highest of all livestock types (23.4 gP/m^3), and protein from dairy bovines also has the lowest blue water requirement among all livestock types (3 l/gP).

Livestock production takes place under a wide range of conditions, which results in huge variations in LWP even within the same livestock type. The average LWP of the most and least efficiently used 10 % of CWU differs between a factor five for layer hens and more than 40 for meat bovines (Figure 6.2). Differences in LWP of industrial pigs and broilers in different regions of the world are to a similar extent caused by variations in feed water productivity (FWP in kg dry matter per m^3) and feed uses efficiency of livestock (FUE in g protein per kg dry matter). LWP is further amplified by positive correlations between FWP and FUE, which contributes about one third of total variance in LWP of industrial pigs and poultry (Figure 6.3). Differences in LWP of industrial layer hens are almost entirely caused by variations in FWP—i.e., FUE is approximately constant across different world regions. Differences in LWP of ruminants across world regions and production systems are generally much larger than for industrial pigs and poultry and are dominated by variations in FUE. A negative correlation across production units between FWP and FUE dampens the variance of LWP for ruminant types.

These variations in FWP and FUE and the extent by which they can be attributed to inefficient management determine the opportunities to improve LWP by improvements in FWP and FUE through appropriate management interventions. Industrial pigs and poultry are usually reared indoors under controlled environmental conditions, which means that variations in FUE can be entirely attributed to differences in livestock management and maximum FUE can be achieved by optimal livestock management. Variability of FWP for industrial pigs and poultry is determined by environmental conditions and crop management, which constrains the potential for improvements in FWP through better crop and land management. The positive correlations between FWP and FUE for industrial pigs and broilers can be explained by the influence of the overall level of agricultural intensification on both crop and livestock management. This means that management interventions aiming to improve either FWP or FUE do not automatically lead to corresponding increases

in the respective other factor, but that LWP of industrial pigs and poultry will benefit from improvements in both FWP and FUE driven by an overall trend towards agricultural intensification.

The huge differences in FUE of ruminants indicate a large potential to increase LWP through better livestock management. However, most ruminants spend at least part of their lifetime grazing on pastures, where they are exposed to environmental conditions. The extent to which variations in FUE of ruminants are caused by different environmental condition is difficult to quantify but it is most likely not the dominating factor. In addition, adverse effects of environmental conditions (e.g., heat stress) can be mitigated by providing shelter or by rearing ruminants entirely indoors. Ruminants consume large amounts of grazed biomass, for which management effects on water productivity were not accounted for in chapter 6. As a result, variations of FWP for ruminants are not only much smaller compared to variations in FWP for industrial pigs and poultry but are also to a much larger degree determined by environmental conditions, which implies an overall much smaller potential to increase LWP by increasing FWP of ruminants. In reality, however, variations in WP of grazed biomass may in fact be sensible to management so that the variability of FWP is probably more important than implied by the results in chapter 6.

The negative correlation between FWP and FUE for ruminants can be explained by the effect of supplementation with feed crops, which increases overall FUE at the cost of lower FWP because WP for crops is much lower than for grass (Figure 6.4). Likewise, incorporating crops residues into ruminant feed increases FWP but will lead to lower FUE (Figure 6.5). Thus, increases of FUE that are either a direct result of or accompanied by improved nutritional composition of the feed mix (more feed crops, less crop residues) are generally accompanied by lower FWP, which offsets the improvement in LWP. This fundamental relationship means that LWP of ruminants, unlike for pigs and poultry, does not always increase with increasing levels of agricultural intensification.

7.2 Conclusions

7.2.1 Outcome

The overarching goal of this thesis was to improve the understanding of climate change impacts on water resources, how this will affect water availability for future population, and what scope for adaptation exists. Within this very broad topic this thesis has focused specifically on climate change impacts on river discharge and blue water resources, and the scope for reducing water demand by improving water productivity in livestock production.

The results presented in chapters 2, 3 and 5 corroborate the findings of earlier studies that have quantified climate change impacts on river discharge but extend existing literature in several important aspects. Chapters 2 and 3 are among the first studies that employ

an ensemble of hydrological models to account for the uncertainty in translating changes in climatic conditions into changes in river discharge and water resource availability. The results demonstrate that hydrological models are a major source of uncertainty, exceeding the uncertainty originating from GCM in many regions and in aggregate global metrics of climate change impacts on human blue water resources.

Chapters 3 and 5 go beyond analysing changes in mean annual discharge and assess changes in simulated irrigation water withdrawals and changes in discharge variability (floods and droughts), respectively. In particular, the results in chapter 5 show that climate-related risk for human water resources are severely underestimated when only changes in mean annual discharge are considered.

A common feature of all three studies that set them apart from previous studies is that climate change impacts are analysed as a function of global mean temperature increase rather than by comparing the outcomes for different scenarios of atmospheric greenhouse-gas concentrations. Such a design is tailored to inform climate change mitigation negotiations and the current political debate about climate change that are centred around temperature goals. While the temperature stratification in chapters 2 and 3 is derived from simulations following RCP scenarios, chapter 5 is based on a novel dataset of climate scenarios described in chapter 4 that was specifically designed for such analyses and overcomes many of the disadvantages of simpler approaches. The overarching conclusion that can be drawn from the three studies is that severe climate-related impacts on river discharge and human water resources can be largely mitigated by constraining global mean temperature increase to 2 K above pre-industrial levels. But due to the pronounced spatial heterogeneity of hydrological changes, some regions such as the Mediterranean will be severely affected at 2 K or even 1.5 K warming above pre-industrial levels. Because of the large uncertainties in the results, however, more widespread impacts at these temperature levels a cannot be excluded.

Chapter 6 presents a new comprehensive assessment of consumptive water use in global livestock production and estimates of livestock water productivity for more than 900 different livestock production units. Livestock water use has been estimated by previous studies but the use of a novel dataset of feed use and productivity in the livestock sector provides a level of detail and consistency that allows for an in-depth analysis of the origin of the large variations in LWP across regions and production systems. The results show that large improvements in LWP can be achieved for pigs and poultry by improving management in feed production and livestock management alike. For ruminants, the largest potential lies in improving livestock management but improvements in feed use efficiency achieved or accompanied by increased supplementation with feed crops come at the cost of higher water requirements to produce the feed, which reduces the overall improvement in LWP. This inverse effect of feed composition on feed water productivity and feed use efficiency

is an important constraint for the achievable LWP in ruminant production.

7.2.2 Limitations and perspectives for further research

All estimates of contemporary as well as projections of future hydrological conditions, water use, and water productivity are subject to large uncertainties because of the unknown development of socio-economic drivers of global change, imperfections in the applied models, and errors in the underlying data.

Uncertainty in future socio-economic development has two dimensions that are relevant for the assessment of future water resources: the unknown development of anthropogenic greenhouse-gas emissions that drive climate change, and the unknown development in important societal aspects such as demographics, human development, economic growth, and technology that determine how societies are affected by and respond to climate change impacts. These two dimensions are typically covered by the different RCP and SSP scenarios, respectively, and are considered conceptually independent (van Vuuren et al. 2014), although not all RCP/SSP combinations are plausible (Riahi et al. 2017). The problem that future greenhouse-gas emissions are unknown is not resolved by analysing climate impacts as a function of global mean temperature increase, but doing so emphasises that the level of climate change is not just another source of uncertainty but a policy goal. In contrast, the overall socio-economic development described by the SSP narratives is not considered an explicit part of climate policy. However, the socio-economic setting in which climate impacts occur has enormous influence on how these changes affect future population. For example, the difference between the socio-economic consequences of a 2 K warming in a SSP1 and a SSP3 world is most likely much larger than the differences between a 2 K and a 3 K warming in an SSP1 world. In chapter 5, this uncertainty was addressed by testing the robustness of key conclusions under different SSP population scenarios. But other important aspects such as the technological and institutional capacity to adapt to water scarcity were not considered because they are so far only qualitatively and globally characterised by the SSP narratives. To improve assessments of the consequences of hydrological change for human water resources and the scope for adaptation, a thorough quantification of these aspects will be essential. A recent study by Graham et al. (2018) has assessed the potential to reduce future water demand by the adoption of water-saving technologies across all SSPs but the results are only provided for world regions and do not account for the impact of climate change on water resources. However, the study demonstrates how SSP narratives can be translated into quantitative scenarios of the water sector.

The quantification of climate change on future hydrological conditions relies on at least two types of models: GCMs that translate scenarios of changes in atmospheric concentrations of greenhouse gases into spatially explicit projections of future climate conditions,

and hydrological models that translate changes in climate conditions into changes in hydrological conditions. A third source of uncertainty is how GCM outputs are translated into inputs for hydrological models. Usually, only certain aspects of climate change (e.g., mean changes) are used or some form of bias correction is applied, which has a strong impact on the hydrological changes simulated by hydrological models (Hagemann et al. 2011). Chapters 2 and 3 employ an ensemble approach to account for the uncertainty in projections of future hydrological conditions that originate from model errors in both model types. Chapter 5 is based on a single hydrological model but accounts for uncertainty in climate projections by using a large ensemble of GCMs. Although the use of model ensembles is an established approach to assess uncertainties in model results, it is limited by how well the ensemble represent the diversity of possible models. However, thorough analysis of individual model behaviour can provide an understanding of wrongly implemented or missing processes that then can inform model improvements or at least provide a basis for ranking model performance. For the climate modelling community, CMIP provides a framework to coordinate more than 20 different model intercomparison projects and to jointly evaluate the outcomes (Eyring et al. 2016a). A similar framework for impact models, including global and regional hydrological models, is provided by ISIMIP (Warszawski et al. 2014).

The lack of biophysical and socio-economic data that characterise the current state of the world or errors in existing data are a major obstacle for assessment of present-day human water resources. For example, the analysis presented in chapter 6 crucially depends on a newly developed dataset on feed use and productivity in the global livestock sector. But because the dataset is essentially a breakdown of FAO statistics based on a mechanistic livestock model and additional data sources, it is subject to uncertainties originating from the model, the supplementary data, and the FAO statistics themselves. This is also true for the subsequent estimation of CWU and LWP, which further involves a crop model, a number of different spatial datasets, as well as several harmonisation procedures to overcome the inconsistencies among the different datasets. Thus, although the conclusion about LWP improvements and constraints are likely to be robust because they are in line with established knowledge about livestock, the individual estimates of CWU and LWP are subject to potentially large uncertainties. However, since for most of the used datasets neither explicit accounts for uncertainties nor alternative sources exist, it is almost impossible to quantify these uncertainties. A greater diversity in such datasets would be a first step to at least get an understanding of the magnitude of uncertainty and provide the basis for improvements. A notable example in this regard is the study by Fritz et al. (2015), which compares different global and regional land cover datasets, quantifies the uncertainties, and produces an improved hybrid global cropland map. However, for many crucial data sources such as FAO statistics, alternative data sources are unlikely to become available. A second important track is the development of new datasets that

cover previously unquantified aspects of our world. Such datasets can originate from new satellite missions such as the planned L-band radar system Tandem-L but also from new methods that make better use of existing remote sensing information. A particular promising example for the latter is the use of deep learning approaches to exploit the wealth of information in hyperspectral satellite imagery (Paoletti et al. 2019).

Both, improvement of existing and development of new datasets do not only support more complex analyses of present-day water use and water resource but also the improvement of hydrological models by providing information required to improve existing parameterisations, introduce new processes, and evaluate model performance.

Appendix A

Supporting information for "Multimodel assessment of water scarcity under climate change"

An edited version of this appendix has been published as Supplement to: J. Schewe, J. Heinke, D. Gerten, I. Haddeland, N. W. Arnell, D. B. Clark, R. Dankers, S. Eisner, B. M. Fekete, F. J. Colón-González, S. N. Gosling, H. Kim, X. Liu, Y. Masaki, F. T. Portmann, Y. Satoh, T. Stacke, Q. Tang, Y. Wada, D. Wisser, T. Albrecht, K. Frieler, F. Piontek, L. Warszawski, and P. Kabat. Multimodel assessment of water scarcity under climate change. *Proceedings of the National Academy of Sciences of the United States of America*, 111(9):3245–50, 2014. doi: 10.1073/pnas.1222460110

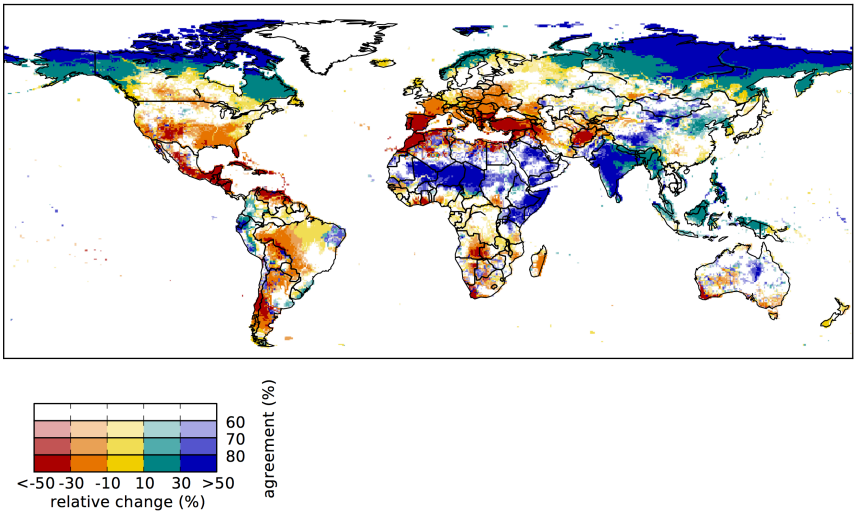

Figure A.1: As Figure 2.1 (upper panel) in the main text, but for a warming of 3 °C.

Table A.1: Middle years of 31–year periods corresponding to the different levels of global warming (compared to present–day, i.e. the 1980—2010 average) in the individual GCMs under RCP8.5. Population projections for these same years were used, except at the 0 °C level which was assumed to correspond to year–2000 population.

warming level	HadGEM2-ES	IPSL-CM5A-LR	MIROC-ESM-CHEM	GFDL-ESM2M	NorESM1-M
0 °C	1995	1995	1995	1995	1995
1 °C	2021	2027	2023	2040	2035
2 °C	2044	2047	2043	2071	2062
3 °C	2062	2065	2061	-	2086*

* A 27–year period from 2073-–2099 was used.

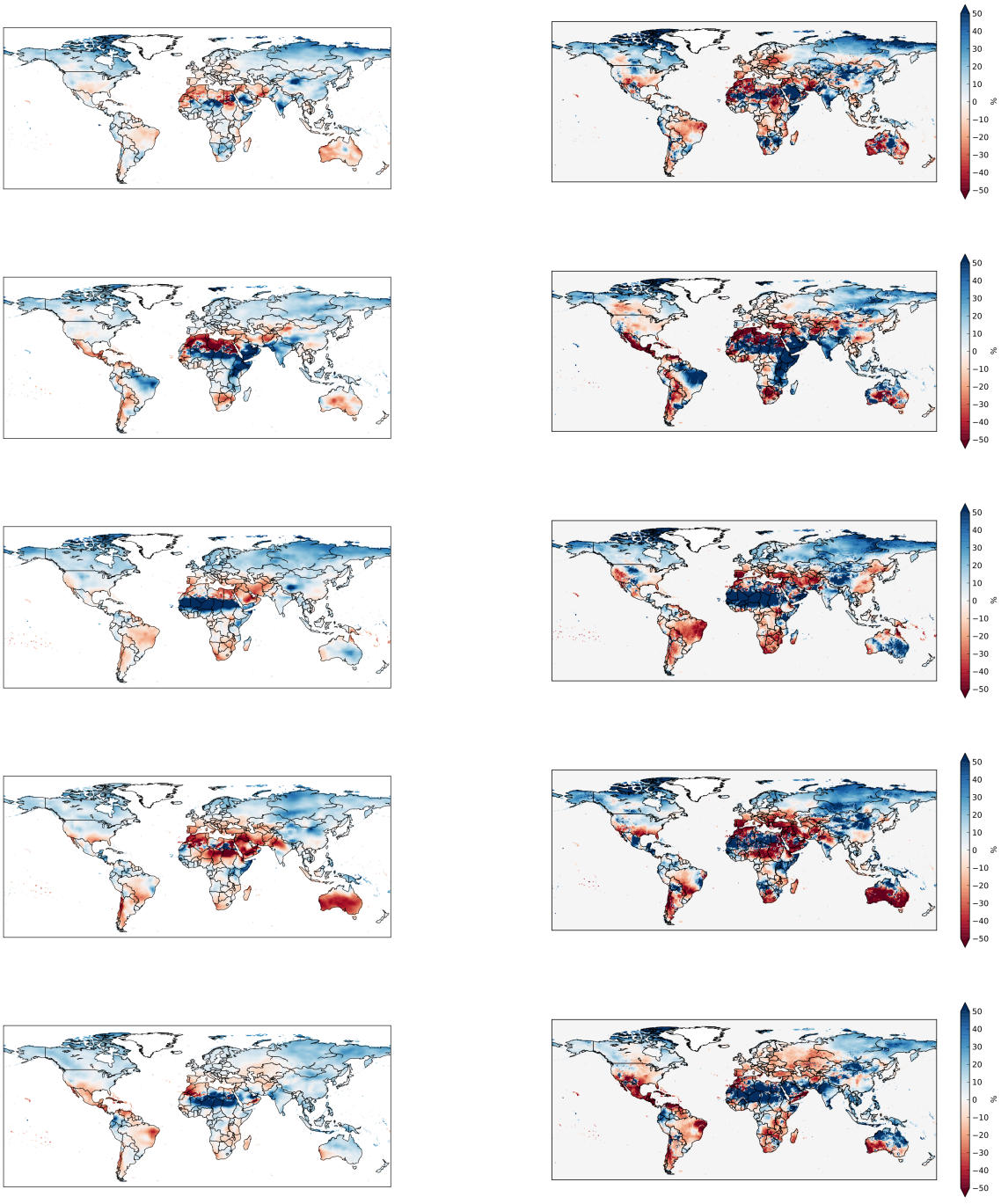

Figure A.2: Relative change in precipitation (left) and discharge (right; average over all GHMs) at 2 °C compared to present–day, under RCP8.5, for (top to bottom) HadGEM2-ES, IPSL-CM5A-LR, MIROC-ESM-CHEM, GFDL-ESM2M, and NorESM1-M.

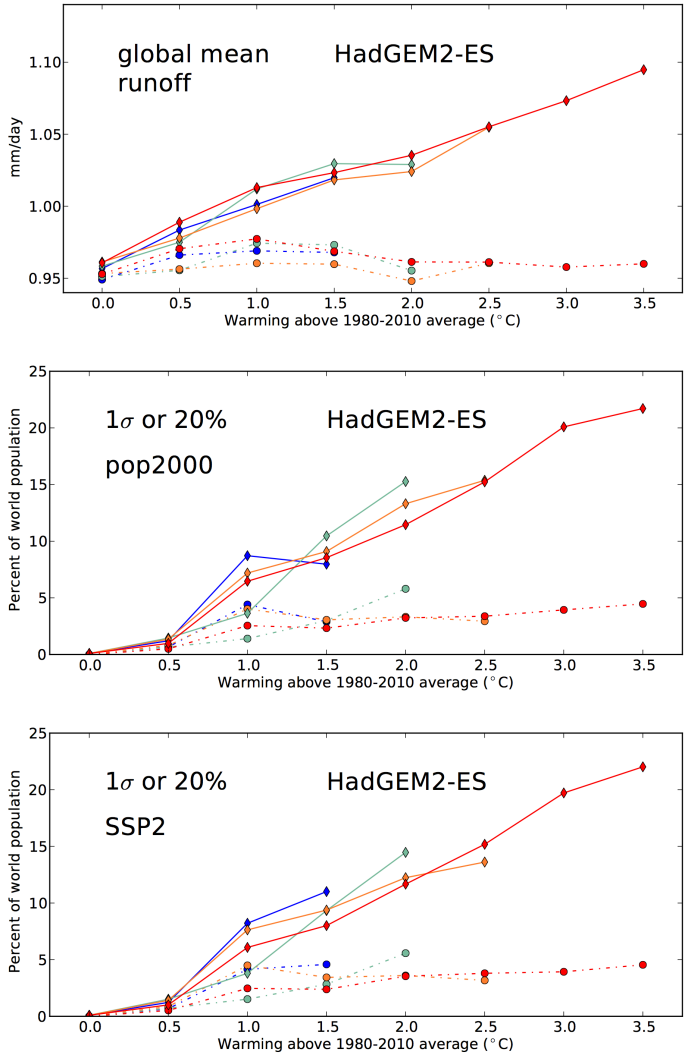

Figure A.3: Effect of different rates of global warming on global impact metrics. Shown are results for one GCM (HadGEM2-ES), two GHMs (solid and dotted lines) and all four RCPs (RCP2.6, dark blue; RCP4.5, turquoise; RCP6.0, orange; RCP8.5, red) at different levels of global warming. Upper panel: Globally averaged runoff. Middle and lower panel: Same metric as shown in Figure 2.2 (upper panel) in the main paper. Middle panel: Assuming constant present–day (2010) population. Lower panel: Assuming population change according to SSP2.

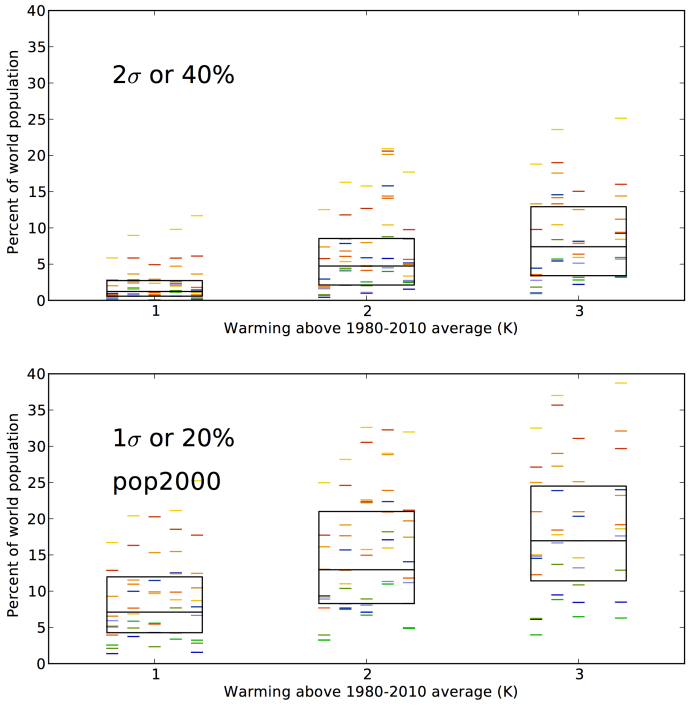

Figure A.4: As upper panel of Figure 2.2 in the main paper, but (upper panel) for a reduction by more than 2σ or by more than 40 %; and (lower panel) assuming constant year–2000 population.

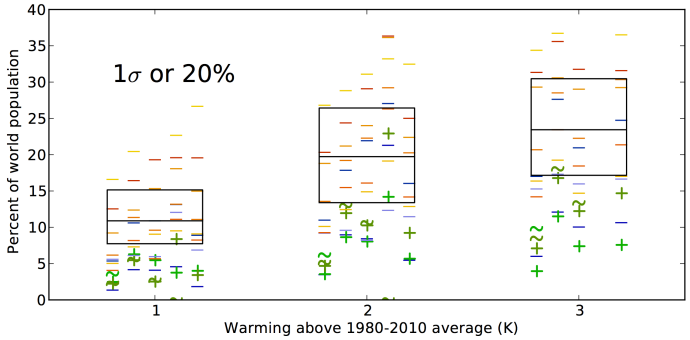

Figure A.5: As upper panel of Figure 2.2 in the main paper, but with the quartiles and median (shown by the black boxes) computed without the models that include vegetation dynamics (JULES and LPJmL). The individual results of those models are highlighted in green colors, where + denotes runs with varying atmospheric CO_2 concentration, and $\sim$ denotes runs where CO_2 concentration has been varied according to historical values up until the year 2000, and held constant at the year–2000 level thereafter.

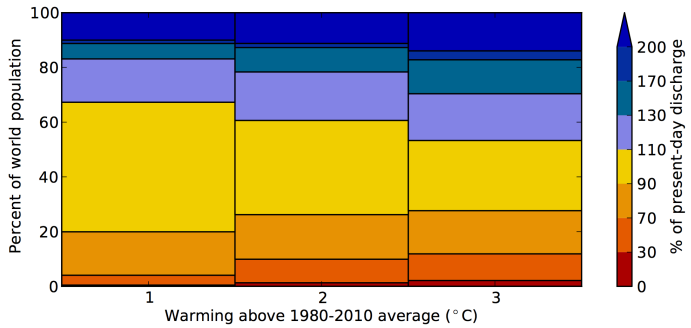

Figure A.6: Population affected by different levels of discharge increase or decrease. Shown is the multi–model mean of the percentage of the world population living in grid cells where 31–year average discharge is a certain percentage of present–day (1980—2010) discharge, at 1 °C, 2 °C, and 3 °C of global warming, under RCP8.5 and SSP2.

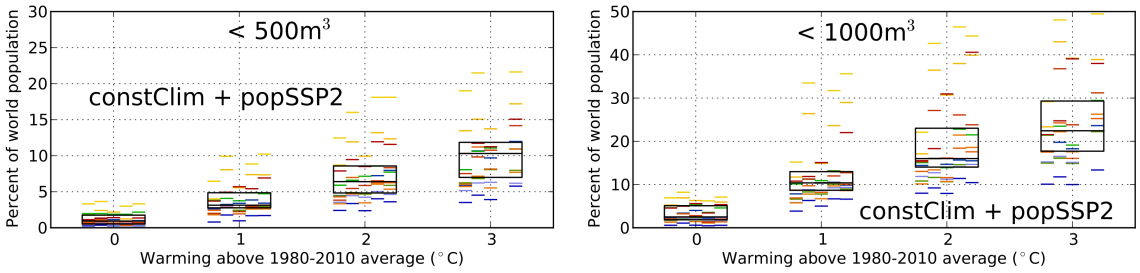

Figure A.7: As Figure 2.3 *A* and *B* in the main paper, but using a "Constant climate" scenario (1980—2010 average discharge). SSP2 population data from the same years as in Figure 2.3 *A* and *B* are used, relating the population time series to the temperature axis via the RCP8.5.

Table A.2: Main characteristics of the GHMs as used in this study, based on Haddeland et al. (2011).

Model name	Time step length	Meteorological forcing[a]	Energy balance	Evaporation scheme[b]	Runoff scheme[c]	Snow scheme	Vegetation dynamics	CO_2 effect[d]	References
DBH	1h	P, T, W, Q, LW, SW, SP	Yes	Energy balance	Infiltration excess	Energy balance	No	Constant	Tang et al. (2007, 2008)
H08	Daily	R, S, T, W, Q, LW, SW, SP	Yes	Bulk formula	Saturation excess, non-linear	Energy balance	No	No	Hanasaki et al. (2008a,b)
JULES	30 mins	R, S, T, W, Q, LW, SW, SP	Yes	Penman-Monteith	Infiltration excess, saturation excess, groundwater	Energy balance	Yes	Varying	Best et al. (2011), Clark et al. (2011)
LPJmL	Daily	P, T, LW_n, SW	No	Priestley-Taylor	Saturation excess	Degree-day	Yes	Varying	Bondeau et al. (2007), Rost et al. (2008)
Mac-PDM.09	Daily	P, T, W, Q, LW_n, SW	No	Penman-Monteith	Saturation excess, non-linear	Degree-day	No	No	Arnell (1999), Gosling and Arnell (2011)
MATSIRO	1 hr	R, S, T, W, Q, LW, SW, SP	Yes	Bulk formula	Infiltration excess, saturation excess, groundwater	Energy balance	No	Constant	Takata et al. (2003), Pokhrel et al. (2012)
MPI-HM	Daily	P, T, W, Q, LW_n, SW, SP	No	Penman-Monteith	Saturation excess, non-linear	Degree-day	No	No	Hagemann and Gates (2003), Stacke and Hagemann (2012a)
PCR-GLOBWB	Daily	P, T	No	Hamon	Saturation Excess Beta Function	Degree Day	No	No	Wada et al. (2010, 2011), van Beek et al. (2011)
VIC	Daily, 3hr snow	P, T, W, Q, LW, SW, SP	Only for snow	Penman-Monteith	Saturation excess, non-linear	Energy balance	No	No	Liang et al. (1994), Lohmann et al. (1998)
WaterGAP	Daily	P, T, LW_n, SW	No	Priestley-Taylor	Beta function	Degree day	No	No	Döll et al. (2003, 2012), Flörke et al. (2013)
WBM	Daily	P, T	No	Hamon	Saturation Excess	Empirical temp and precip based formula	No	No	Vörösmarty et al. (1998), Wisser et al. (2010)

[a] R: rainfall rate, S: snowfall rate, P: precipitation rate (rain and snow calculated in the model), T: air temperature, W: wind speed, Q: air specific humidity, LW: downwelling longwave radiation; LW_n: net longwave radiation; SW: downwelling shortwave radiation, SP: surface pressure.
[b] Bulk formula: Bulk transfer coefficients are used when calculating turbulent heat fluxes.
[c] Non-linear: Subsurface runoff is a non-linear function of soil moisture.
[d] CO_2 concentration in calculation of stomatal conductance.

Appendix B

Supporting information for "Global water resources affected by human interventions and climate change"

An edited version of this appendix has been published as Supplement to: I. Haddeland, J. Heinke, H. Biemans, S. Eisner, M. Flörke, N. Hanasaki, M. Konzmann, F. Ludwig, Y. Masaki, J. Schewe, T. Stacke, Z. D. Tessler, Y. Wada, and D. Wisser. Global water resources affected by human interventions and climate change. *Proceedings of the National Academy of Sciences of the United States of America*, 111(9):3251–6, 2014. doi: 10.1073/pnas.1222475110

B.1 SI Models and Data

The global hydrological models (GHMs) included in this study are H08 (Hanasaki et al. 2006, 2008a), the Lund-Potsdam-Jena managed land dynamic global vegetation and water balance model (LPJmL) (Biemans et al. 2011, Bondeau et al. 2007, Rost et al. 2008), the Max Planck Institute – hydrology model (MPI-HM) (Hagemann and Gates 2003, Stacke and Hagemann 2012b), the PCRaster global water balance model (PCR-GLOBWB) (Wada et al. 2011, van Beek et al. 2011), the variable infiltration capacity macroscale hydrologic model (VIC) (Liang et al. 1994, Lohmann et al. 1998, Haddeland et al. 2006), water – a global assessment and prognosis model (WaterGAP) (Döll et al. 2003, Döll and Siebert 2002, Flörke et al. 2013), and the water balance/transport model (WBMplus) (Wisser et al. 2008). Six of the seven models have implemented general reservoir operating rules based on the purpose(s) of the dam, the hydrological conditions of the basin, and model-simulated water demands downstream of the dam. In H08, PCR-GLOBWB, VIC, WaterGAP, and WBMplus, the dams built in the year 2000 or before are included throughout the simulation period. In LPJmL, the dams are included in the simulations corresponding to the year they were built. The total storage capacity included in the modeling schemes varies from $4038\,\mathrm{km}^3$ to $6197\,\mathrm{km}^3$ (Table B.1). This volume is between 3.5 % and 5 % of mean annual precipitation (here, $\sim 128\,000\,\mathrm{km}^3 \cdot \mathrm{y}^{-1}$ in the period 1971–2000) and equals ∼10 % of mean annual runoff.

Information on irrigated areas are taken from various sources (Table B.1). In LPJmL, fraction irrigated areas increases in the period 1971–2000 and is constant thereafter. In the other models, irrigated areas stay constant during the entire simulation period. H08 includes a crop growth module that estimates the cropping period necessary to obtain mature total plant biomass and crop yield and estimates crop growth using heat unit theory. When the accumulated heat units reach the potential heat units required for the maturity of the crop, the crop is harvested (Hanasaki et al. 2008a). LPJmL calculates a growing season for each crop. Sowing dates are determined as a function of climate- and crop-specific thresholds regarding temperature and/or precipitation. Phenological development toward maturity is modeled using heat unit theory, and harvest occurs as soon as maturity is reached. Rice is assumed to grow twice a year in tropical Asia. For more information on the LPJmL crop model, see Bondeau et al. (2007). MPI-HM, PCR-GLOBWB, VIC, and WaterGAP do not include any crop growth module, and hence vegetation parameters are prescribed. MPI-HM defines the irrigated fraction of grid cell based on from the MIRCA2000 dataset (Portmann et al. 2010), and plants in this fraction are allowed to transpire freely. PCR-GLOBWB uses crop-specific calendar and growing season length obtained from the MIRCA2000 dataset (Portmann et al. 2010), which accounts various growing seasons of 26 crop types and regional cropping practices, and distinguishes up to

Table B.1: Data sources

Model name	Dams	Irrigated areas, ref(s).
H08	507 dams with a storage capacity of 4411 km^3. *World Register of Dams* (ICOLD 2007).	Siebert et al. (2005), Siebert et al. (2007)
LPJmL	7000 dams, storage capacity of 6148 km^3. GranD database (Lehner et al. 2011).	Fader et al. (2010)
MPI-HM	Dams not included.	Portmann et al. (2010)
PCR-GLOBWB	6862 dams, total storage capacity of 6197 km^3. GranD database (Lehner et al. 2011).	Portmann et al. (2010)
VIC	514 dams, total storage capacity of 4542 km^3. *World Register of Dams* (ICOLD 2007, Vörösmarty et al. 1997).	Siebert et al. (2005)
WaterGAP	487 dams with a storage capacity of 4038 km^3. *World Register of Dams* (ICOLD 2007)	Portmann et al. (2010)
WBMplus	668 large dams, total storage capacity of 4726 km^3 (Vörösmarty et al. 1997), in addition to thousands of small dams.	Thenkabail et al. (2009)

nine subcrops that represent multicropping systems per grid cell. In PCR-GLOBWB, the crop types were aggregated to paddy and nonpaddy crop type considering distinct flooding irrigation for most of paddy fields. VIC makes use of country-specific cropping calendars obtained from AQUASTAT (FAO 2013), US Geological Survey, and various sources of information for Europe directly for each region in question (Haddeland et al. 2006). In WaterGAP, each 150-d period within a year for a specific grid cell is ranked according to specific temperature and precipitation criteria for rice and nonrice (Döll and Siebert 2002). The optimal 150-y period is thereafter chosen as the growing season for each particular cell. WBMplus includes dual planting seasons in regions where this is appropriate, and cropping calendar is based on Climatic Research Unit/Food and Agriculture Organization datasets (Wisser et al. 2008). In this paper, potential irrigation water consumption represents irrigation water consumed given water is freely available. All models included in the study simulate this quantity. Four of the models, H08, LPJmL, PCR-GLOBWB, and VIC, also simulate actual irrigation water consumption, which is defined as irrigation water consumed when water availability is taken into account.

H08, LPJmL, PCR-GLOBWB, and WaterGAP take into account water withdrawals and consumptive water use for domestic and industrial purposes. MPI-HM, VIC, and WBMplus do not take into account water use in other sectors than agriculture. H08 has obtained national information on water withdrawals from the AQUASTAT database (FAO 2013). H08 thereafter converts this information to gridded data by weighting the population distribution and national boundary information provided by the Center for

International Earth Science Information Network of Columbia University and Centro Internacional de Agricultura Tropical (CIESIN and CIAT 2005). The values are converted to the consumptive amount using the factors 0.10 for domestic water and 0.15 for industrial water (Shiklomanov 2000). WaterGAP calculates current and future numbers on water withdrawals and use in the domestic and industrial sectors based on population data, per capita income, thermal electricity production, and future projections on industrial and technological changes (Wisser et al. 2008). LPJmL makes direct use of the WaterGAP numbers on water requirements in sectors other than agriculture. Similar to WaterGAP, PCR-GLOBWB uses socioeconomic (e.g., population numbers, gross domestic product or GDP) and technological (e.g., electricity production, energy consumption) data to estimate and project water withdrawals in the domestic and industrial sectors (Wada et al. 2011). In PCR-GLOBWB, water recycling or recycling ratio (0.4–0.8) was calculated per country on the basis of GDP and was used to estimate return flow and subsequently consumptive water use for the domestic and industrial sectors.

B.2 River Basin Information and Results

Table B.2 includes information on basin area, area equipped for irrigation, reservoir storage, and simulated discharge for river basins mentioned in the main article.

B.3 Glossary

Potential Water Withdrawals. Water withdrawn given unlimited water supply, i.e., water is assumed available.

Potential Water Consumption. Potential water use (water consumed) given unlimited water supply, in addition to water from precipitation.

Actual Water Withdrawals. Actual water withdrawn from lakes/reservoirs/rivers/groundwater, taking water availability into account.

Actual Water Consumption. Actual water use (water consumed) when taking water availability into account. Water consumed given actual water withdrawals, in addition to water from precipitation.

Cumulative Abstraction to Demand. The cumulative abstraction-to-demand (CAD) index (Hanasaki et al. 2008b) was designed for global hydrological models that can explicitly simulate the daily river discharge and water withdrawals and consumption. The index directly indicates whether water is available when it is needed. CAD is a dimensionless

Table B.2: Measures of human impacts in some key river basins.

River basin	Area, km^2	Irrigated area, km^2	Reservoir storage, km^3	Naturalized discharge, $km^3 \cdot y^{-1}$	Human impact discharge, $km^3 \cdot y^{-1}$	Irrigated area cf. total area, %	Reservoir storage cf. naturalized discharge, %	Human impact discharge cf. naturalized discharge, %
Mississippi	3 231 192	126 843	177	899	883	3.9	20	98
Nile	2 900 394	35 330	164	492	463	1.2	33	94
Chang Jiang	1 924 169	180 845	73	888	844	9.4	267	95
Ganges-Brahmaputra	1 574 419	287 880	9	1338	1271	18.3	0.7	95
Murray-Darling	1 058 486	14 513	15	57	55	1.4	26	96
Amu Darya	1 036 704	67 199	50	111	91	6.5	45	82
Oranje	956 592	4057	15	22	20	0.4	71	94
Euphrat-Tigris	871 562	61 204	122	111	80	7.0	109	71
Indus	838 899	145 923	43	172	91	17.4	25	53
Mekong	795 076	28 474	13	533	514	3.6	2.4	96
Huang He	758 554	58 720	72	83	62	7.7	288	74
Columbia	666 482	31 944	79	176	171	4.8	45	97
Colorado	636 691	13 720	86	35	31	2.2	250	89

Area is calculated based on the DDM30 river network (Döll and Lehner 2002). Irrigated area is area equipped for irrigation according to Siebert et al. (2005). Reservoir storage numbers are calculated based on the largest reservoirs in the river basins (ICOLD 2007, Vörösmarty et al. 1997). Discharge numbers are the ensemble median simulated values in the control period (1971—2000).

fraction, and the equation can be written as follows:

$$CAD = \frac{\sum_{Year=y1}^{Year=y2} \sum_{DOY=1}^{DOY=365} AIrrCon_{Year,DOY}}{\sum_{Year=y1}^{Year=y2} \sum_{DOY=1}^{DOY=365} PIrrCon_{Year,DOY}}, \tag{B.1}$$

where $AIrrCon$ represents "actual irrigation water consumed" and $PIrrCon$ represents "potential irrigation water consumed" (see above).

Appendix C

Supporting information for "A new climate dataset for systematic assessments of climate change impacts as a function of global warming"

An edited version of this appendix has been published as Supplement to: J. Heinke, S. Ostberg, S. Schaphoff, K. Frieler, C. Müller, D. Gerten, M. Meinshausen, and W. Lucht. A new climate dataset for systematic assessments of climate change impacts as a function of global warming. *Geoscientific Model Development*, 6(5):1689–1703, 2013a. doi: 10.5194/gmd-6-1689-2013

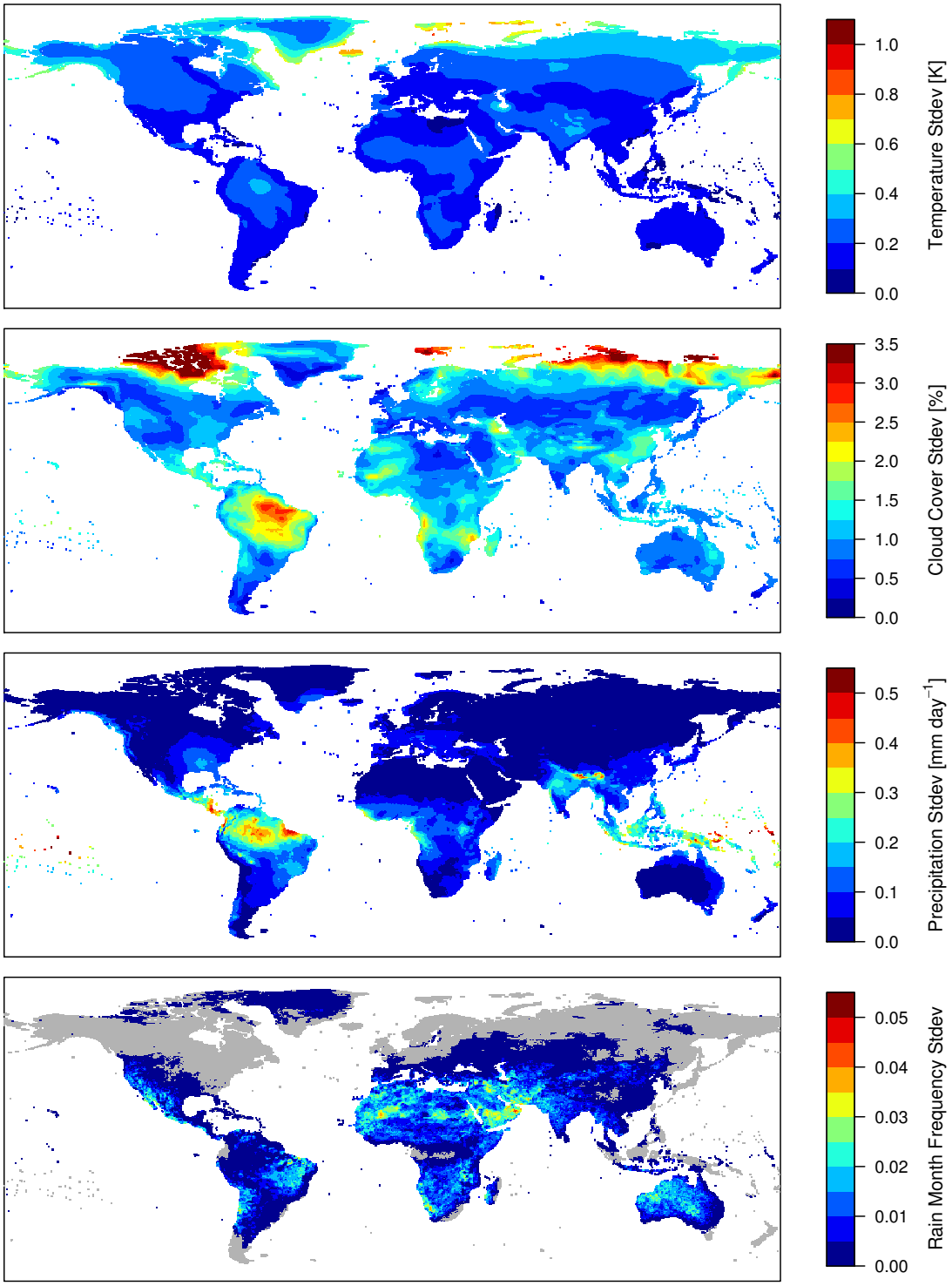

Figure C.1: Inter-model standard deviation of mean annual change for a 1-degree increase in global mean temperature over all AOGCMs.

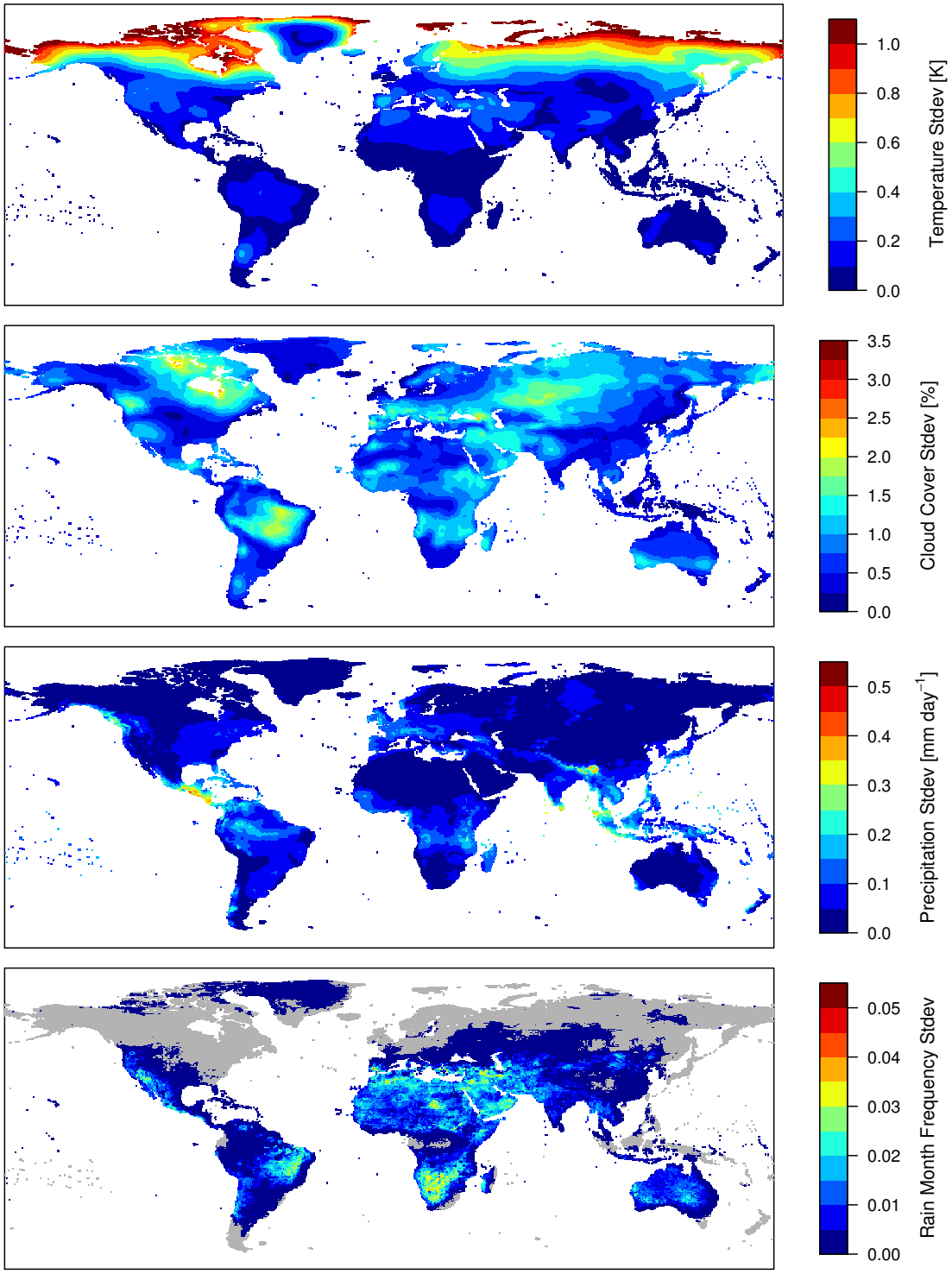

Figure C.2: Seasonality of change for a 1-degree increase in global mean temperature expressed by the standard deviation of monthly mean anomalies (averaged over all AOGCMs).

Appendix D

Supporting information for "Freshwater resources under success and failure of the Paris climate agreement"

An edited version of this appendix has been published as Supplement to: J. Heinke, C. Müller, M. Lannerstad, D. Gerten, and W. Lucht. Freshwater resources under success and failure of the Paris climate agreement. *Earth System Dynamics*, 10(2):205–217, 2019a. doi: 10.5194/esd-10-205-2019

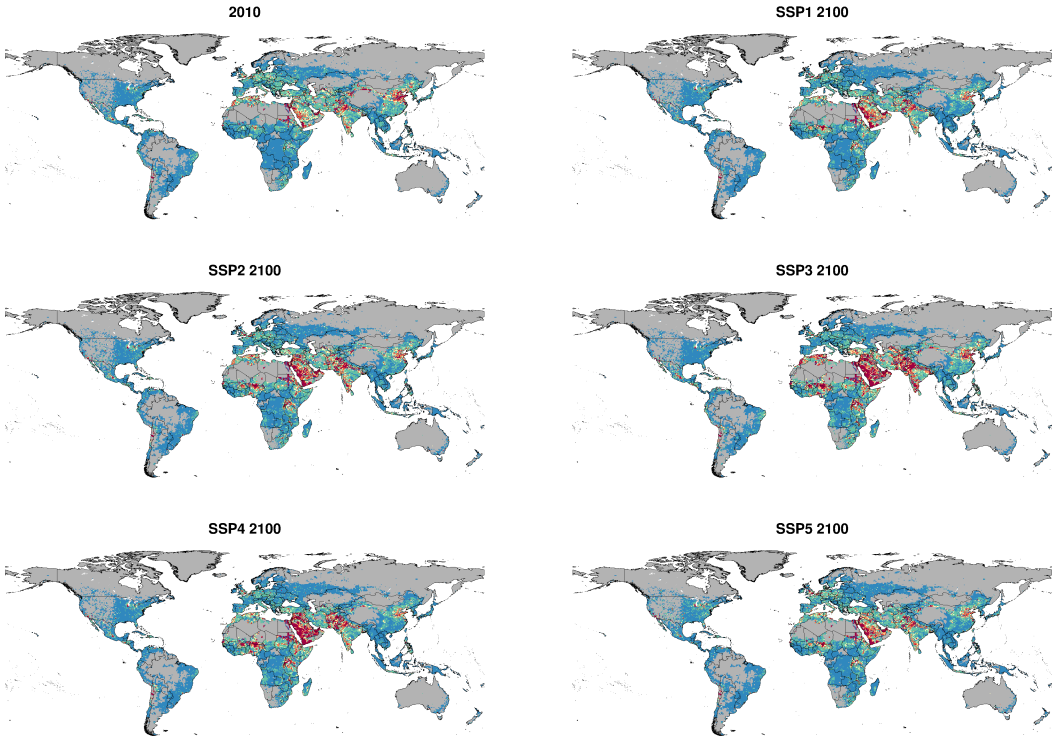

Figure D.1: Spatial patterns of water crowding in 2010 and for five different population scenarios in 2100 under current water availability, i.e. assuming no climate change.

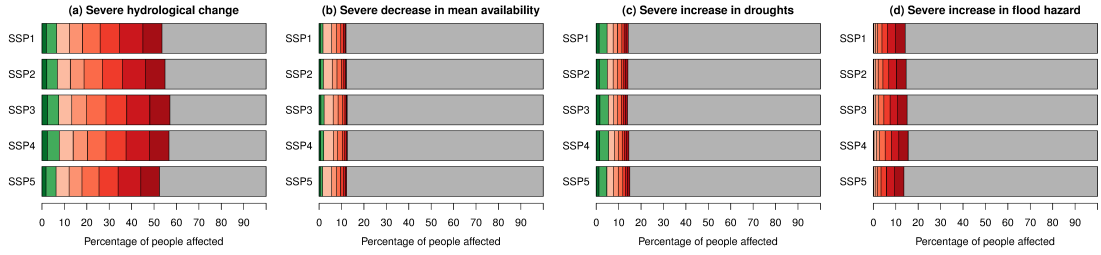

Figure D.2: Proportion of total population more likely than not exposed to severe hydrological change at different levels of ΔT_{glob}.

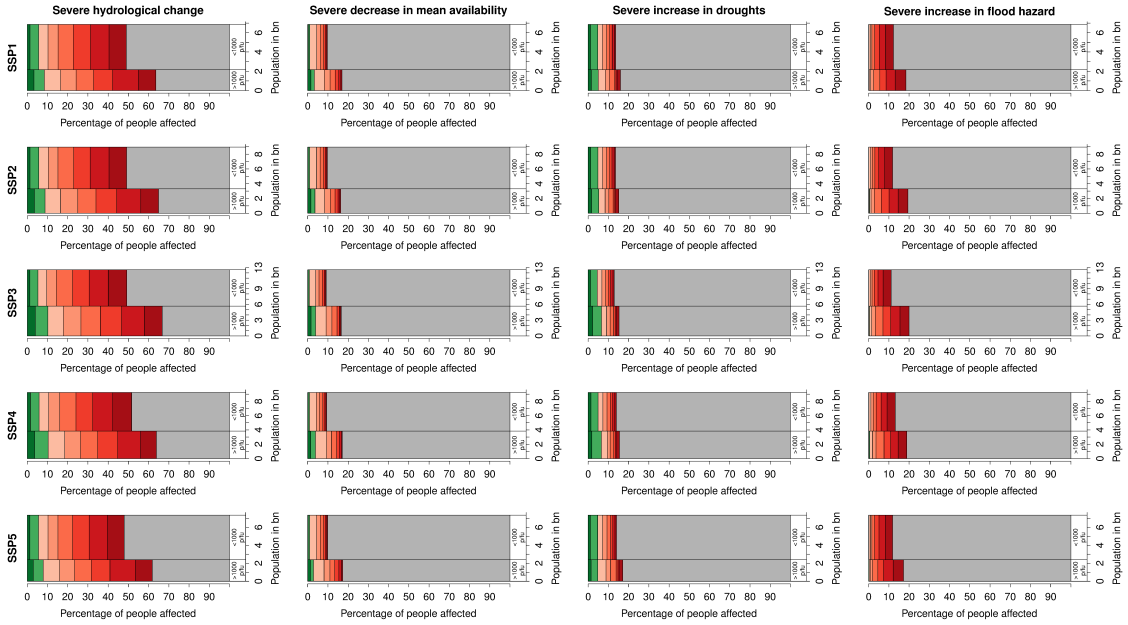

Figure D.3: Fraction of population in 2100 exposed to severe hydrological change at different levels of ΔT_{glob} divided over two water scarcity categories: population already experiencing absolute water scarcity (>1000 p/fu) in the absence of climate change and rest of population (≤1000 p/fu). The total number of people in each class is given on the y-axis, and the fraction of people exposed to severe hydrological change in each class is given on the x-axis.

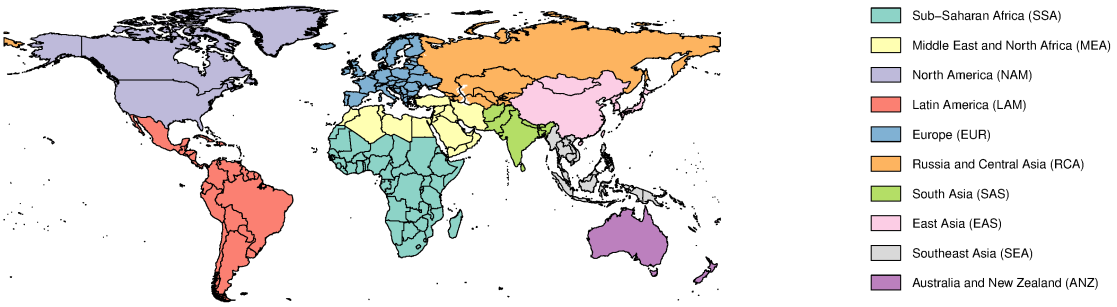

Figure D.4: Map of world regions.

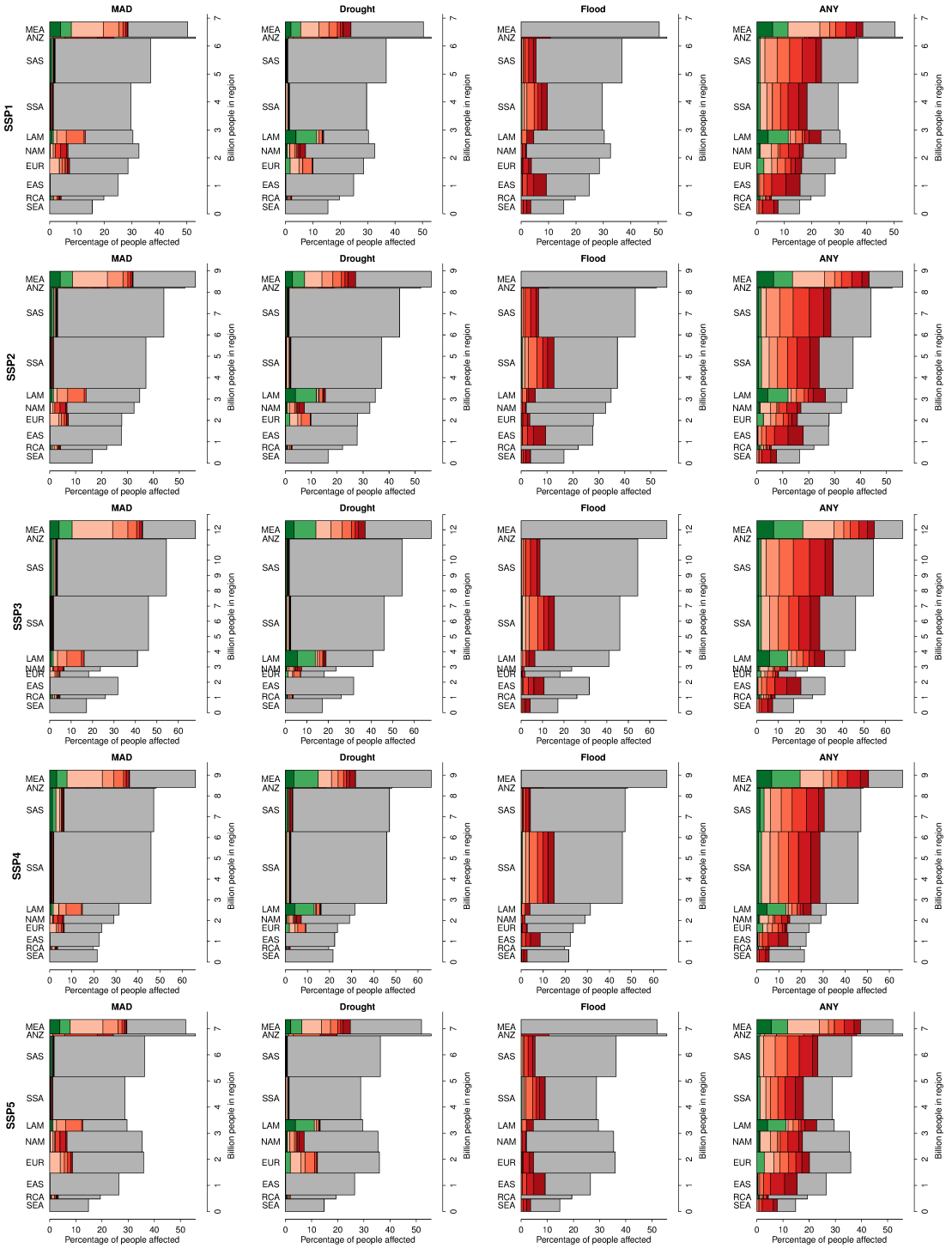

Figure D.5: Proportion of population in 2100 in different world regions that would experience absolute water scarcity (>1000 p/fu) under present-day climate conditions (total length of bar) and be more likely than not exposed to severe hydrological change at different levels of ΔT_{glob}.

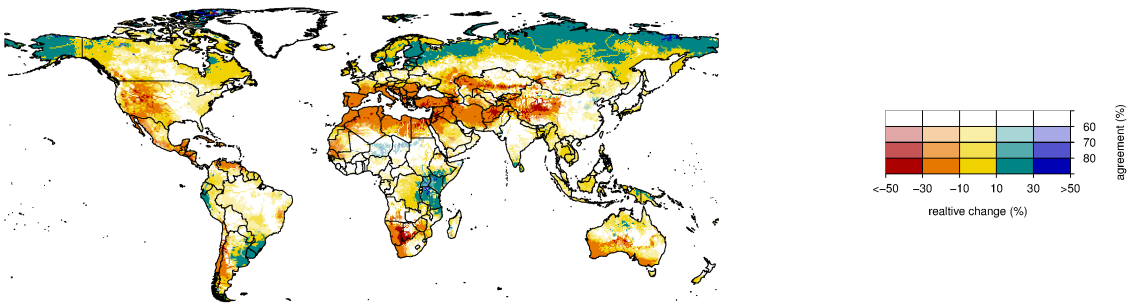

Figure D.6: Relative change in MAD compared to control simulation for a ΔT_{glob} (above pre-industrial level) of 2.5 °C. Color hues show the multimodel mean change, and saturation shows the agreement on the sign of change across all GCMs (percentage of GCMs agreeing on the sign). Because ΔT_{glob} for the control simulation is 0.6 °C, the changes are representative for 1.9 °C additional warming relative to the control simulation and can thus be compared to the changes for 2 °C additional warming shown in Fig. 1 in Schewe et al. (2014).

Appendix E

Supporting information for "Water use in global livestock production—opportunities and constraints for increasing water productivity"

An edited version of this appendix has been submitted for publication as a Supplement to: J. Heinke, M. Lannerstad, D. Gerten, P. Havlík, M. Herrero, A. Notenbaert, H. Hoff, and C. Müller. Water use in global livestock production—opportunities and constraints for increasing water productivity. *Water Resources Research*, submitted

E.1 LPJmL simulations

For the estimation of CWU associated with the production of different feed types, we employ the LPJmL Dynamic Global Vegetation Model version 4 (LPJmL4) that simulates the growth of natural vegetation and managed land in coupling with the global carbon and hydrological cycle (Schaphoff et al. 2018b). Two types of managed land are considered in LPJmL4: (i) managed grasslands with a mix of three different herbaceous plant functional types, which are managed by grazing or mowing (Rolinski et al. 2018); and (ii) agricultural land with crops represented by 12 irrigated or rainfed crop functional types (CFTs) for which the maximum achievable leaf area index (LAI_{max}) can be prescribed to account for agricultural management intensity (Bondeau et al. 2007, Fader et al. 2010). The model is able to distinguish ET from rainfall water (green) and water added through irrigation (blue) and has been used to estimate green and blue CWU over the growing period in previous studies (Gerten et al. 2011, Rockström et al. 2009, Rost et al. 2008). The model has been extensively evaluated showing good performance in representing the global hydrological cycle (Rost et al. 2008, Schaphoff et al. 2018a) and grassland dynamics (Rolinski et al. 2018).

For the estimation of crop CWU in our study the model was first run for the period 1901–1980 to bring soil moisture to equilibrium and obtain a robust estimation of sowing dates. After that, a series of model simulations for seven different levels of agricultural management intensity (LAI_{max}) was performed. No land use information was used in these simulations but each of the 12 CFTs was cultivated on a small fraction of each grid cell as rainfed and irrigated crop; the remainder of the grid cell was simulated as bare soil. From each of the seven simulations we obtain crop yield and ET during the growing season (separate for green and blue) for each CFT in each grid cell under rainfed and irrigated conditions. In addition, we also obtain estimates of consumptive irrigation water losses related to conveyance for each CFT in each grid cell, total annual bare soil ET in each grid cell, and off-season bare soil ET for each rainfed and irrigated CFT in each grid cell (calculated as the difference between total annual bare soil ET and ET that occurred from the bare soil part of the grid cell during the growing season of the respective CFT). For crops not represented by one of the CFTs (Table E.1), ET was estimated based on a generic perennial and annual crop type. The generic perennial crop is represented by a perennial managed grassland (Rolinski et al. 2018, Schaphoff et al. 2018b), whereas the generic annual crop is represented by the CFT that gives the median of total growing period ET of all CFTs with non-zero ET per grid cell.

For the estimation of CWU related to grazing a series of simulations with grazing intensities between 0.2 and 4 (in steps of 0.2) $gC/(m^2\,d)$ is performed from which the highest total grass yield in the period 1998–2001 and the corresponding annual ET is determined.

This is necessary because LPJmL4 calculates daily gross primary productivity (GPP) on managed grasslands based on abiotic factors and actual leaf area (Rolinski et al. 2018). A larger leaf area generally results in higher GPP but the increase in GPP diminishes with higher leaf area and is limited by the available photosynthetically active radiation. Maintenance respiration of standing biomass reduces the amount of GPP available for plant growth (net primary productivity), which limits the amount of standing biomass under given environmental conditions. Removal of grass biomass through grazing influences both GPP and respiration and results in a non-linear and site dependent response of carbon dynamics to grazing (Rolinski et al. 2018).

All simulations were performed using temperature from CRU TS2.23, precipitation from GPCC version 7, monthly number of rain days estimated following the procedure described by Heinke et al. (2013a), short and longwave radiation from ERA-Interim, soil information from Harmonized World Soil Database, and historic atmospheric CO_2 concentrations. The model was run a spatial resolution of 0.5 x 0.5 arc-degrees.

E.2 Estimation of ET from global cropland and CWU of global crop production

To estimate total ET from the global cultivated land and allocate it to CWU of global crop production the following datasets are used:

- Landcover data from Global Agro-ecological Zones (GAEZ) database (IIASA/FAO 2012), 5 arc-minutes spatial resolution, reference year 2000
- Cropland extent from Global Agricultural Lands (Ramankutty et al. 2008), 5 arc-minutes spatial resolution, reference year 2000
- Harvested area of 26x2 (rainfed and irrigated) crop (groups) and the sum of the cultivated area from MIRCA2000 (Portmann et al. 2010), 5 arc-minutes spatial resolution, reference year 2000
- FAOSTAT yield statistics for 163 food and non-food crops aggregated to 62 primary crops and crop groups distinguished in Commodity Balances (CB; FAO 2018), national data, reference year 2000 (1998–2002 average)
- Yield of cultivated forages from (Monfreda et al. 2008), 5 arc-minutes spatial resolution, reference year 2000
- LPJmL estimates of yield, green ET, and blue ET during the growing period for 7 management intensity levels for 12 annual crops, representing important crop groups and one generic annual and one generic perennial crop type to represent all other

crops, each rainfed and irrigated, 0.5 arc-degree spatial resolution, reference year 2000 (1998–2002 average)

- LPJmL estimates of off-season fallow ET for each CFT and full year fallow ET, 0.5 arc-degree spatial resolution, reference year 2000 (1998–2002 average)

One important novelty of this study is the inclusion of ET from fallow land in estimates of CWU related to crop production. This requires information about the area of fallow land–i.e., the difference between physical cropland extent and cultivated area within a year–in each grid cell. Although MIRCA2000 is based on cropland extent from Global Agricultural Lands, the latter was modified by Portmann et al. (2010) by introducing cropland in grid cells with harvested area but zero cropland extent. To estimate the cropland extent in those cells, the cell-specific sum of harvested area was divided by the average cropping intensity (ratio of harvested area to cropland extent) in the MIRCA2000 mapping unit (country or state) in which the cell is located. Because the modified cropland extent is not provided with the MIRCA2000 dataset, we modify cropland extent from Global Agricultural Lands following the procedure described by Portmann et al. (2010). In addition, we also reduce cropland extent in all grid cells where it is larger than five times the annual cultivated area to comply with the FAO definition of cropland as land that is cultivated at least once in five years (FAO 2018). Finally, both cropland extent and harvested area are reduced (maintaining cropping intensity) in grid cells where cropland extent exceeds the total land area given by GAEZ. Overall, global cropland extent is increased by about 3.2 % by these adjustments, while the global sum of harvested area is reduced by 0.9 %.

Evapotranspiration (ET) during the growing season of crops varies with management, with better management leading to higher ET due to larger leaf area (Rockström et al. 2007). To account for this aspect and its impact on CWU, we determine simulated national yield estimates for each management level for each FAO crop represented by a CFT by multiplying the rainfed and irrigated crop yield of the corresponding CFT in each grid cell with the rainfed and irrigated harvested area of the corresponding crop in MIRCA2000 (see Table E.1 for the CFT and MIRCA crop type assumed to represent each FAO crop). Yield estimates from LPJmL4 were converted from carbon to fresh matter (as reported by FAO) using crop specific carbon content given in Table E.1. The management level for which the simulated national average yield best matches the yield reported in FAO is then assumed to be representative for the whole country and estimates of growing season ET for the specific crop are obtained from the corresponding LPJmL simulation. For 18 major crops, representing about three quarters (72.2 %) of global harvested area, ET was determined following this procedure. For all remaining crops, the management level could not be determined due to a lack of appropriate representation in the model, and growing

season ET was estimated from the generic perennial and annual crop types. All estimates of growing season ET are obtained separate for green (from rainfall water) and blue water (water added through irrigation. In addition, evaporation related to the transport of irrigation water to the field (conveyance losses) was estimated based on country specific irrigation efficiencies (Jägermeyr et al. 2016). Losses from reservoirs were not accounted for.

As a novelty, our estimates of CWU include bare soil ET from cultivated land outside the growing period (seasonal fallow) and from cropland not cultivated (fallow land). ET from fallow land in each grid cell is estimated by multiplying the difference between cropland extent and annual cultivated area with the full year ET from bare soil, assuming no vegetation cover on fallows. The result is then allocated to individual crops proportional to their harvested area in each grid cell. The ET of seasonal fallow is estimated for each crop by multiplying off season bare soil ET of the corresponding CFT with the harvested area of the crop in each grid cell. However, in cases of multi-cropping (harvested area larger than cultivated land) this would lead to an overestimation of ET from seasonal fallow as the estimation of off-season bare soil ET for CFTs assumes a single growing season per year (see section E.1). In such cases, we calculate the difference between full year bare soil ET from the cultivated area and the sum of bare soil ET that would occur during the growing season of all harvested crops in each grid cell and divide by the sum of ET from seasonal fallow for all individual crops. The obtained ratio is be smaller than 1 if multi-cropping occurs in a grid cell. In such cases, multiplying ET from seasonal fallow for all individual crops with this factor properly mitigates an overestimation of total ET from seasonal fallow.

As the result we obtain for each gird cell an estimate of total ET from cropland and CWU for each crop with its ET components growing period green, growing period blue, seasonal fallow green, and fallow land green. From this, national sums of CWU for each crop are determined for each crop. Corresponding estimates of national production for each crop are calculated from the yield reported by FAO and the harvested area given by MIRCA2000. For MIRCA crop types representing more than one FAO crop, the harvested area in each grid cell was attributed to the FAO crops according to their relative proportions in national harvested area reported by FAO. For the crop type "fodder grasses" in MIRCA2000, yield estimates were not available from FAO and gridded yield estimates from (Monfreda et al. 2008) were used instead. To account for the amount of seed required to grow crops, the ratio of seed to total production was estimated for each crop in each country from FAO production statistics and then applied to our production estimates. The result can be interpreted as net production and implicitly assumes that seeds are derived from last year's production.

E.3 CWU of utilization of crops and crop products for food, feed, and other uses

To estimate CWU related to utilization of crops the following datasets are used:

- FAOSTAT Food Balance Sheets (FAO 2018), national data, reference year 2000 (1998–2002 average)
- FAOSTAT Commodity Balances (FAO 2018), national data, reference year 2000 (1998–2002 average)

Food Balance Sheets (FBS) and Commodity Balances (CB) report domestic production quantity, import quantity, export quantity, stock changes and domestic supply for each commodity in each country. Further, partition of total domestic supply over the following utilization categories is reported: food, feed, other uses, processing, waste, and seed. FBS and CB overlap to a large extent, but FBS contain additional information about nutritional value of food supply, while CB provide information about the utilization of non-edible crops and commodities such oilseed meals, a by-product of vegetal oil production and an important livestock feed. We combine both datasets to obtain a complete picture of the food system.

As the quantity used as seed has already been accounted for on the production side (section E.2), domestic supply is recalculated as the sum of the amounts in the remaining utilization categories food, feed, other uses, processing and waste. The difference between domestic supply and net production was taken as net import or export, respectively, neglecting stock changes and reexport.

The combined and harmonized dataset provides a comprehensive accounting of biomass flows in the food system and provides the basis to allocate the CWU associated with the production of primary crops to the utilization of these crops and derived products. In the first step, the CWU associated with exports is calculated by multiplying export quantities with the specific CWU (CWU per kgDM, referred to as *cwu* in the following) of the respective production. Because FBS and CB do not provide information on bilateral trade, export quantities and corresponding CWU contribute to a global trade pool for each commodity with a combined *cwu*. The CWU associated with imports is obtained by multiplying the import quantities with the *cwu* of the trade pool, and the result is added to the total CWU of domestic production. Thus, the *cwu* of domestic supply for a given commodity in net exporting countries equals the *cwu* of production, while the *cwu* of domestic supply in net importing countries is the weighted average of *cwu* of domestic production and *cwu* in the trade pool. The estimated *cwu* of domestic supply is then multiplied with the amounts in the different utilisation categories to allocate CWU to each utilisation category. Because we do not consider waste explicitly in this study but as an

inefficiency in the food system, we distribute the amount of CWU allocated to waste among the other utilization categories proportional to their relative size.

About 81 % of global CWU associated with domestic supply of primary food crops is allocated to either food, feed, or other uses by the procedure described in the previous paragraph. The remainder is allocated to the utilization category 'processed', from which the production of secondary commodities is derived. The relationship between primary and secondary products is documented in the form of commodity trees (FAO 2000) and in the definitions and standard of FBS and CB (FAO 2018). About 64 % of the CWU allocated to the 'processed' category of primary crops is related to oil crops such as soybeans, rapeseed, and groundnuts. The processed amount of oil crops is unambiguously related to the production of oil and oil cakes (extraction residues), which are reported for each oil crop. Another 20 % are related to sugar crops (sugar cane and sugar beets), from which sugar and molasses are derived as secondary products. The remainder and all processing quantities of secondary oil crop products, sugars, and molasses (less than 5 % of CWU of primary crop supply) are assumed to contribute to the production of reported beverages.

For the allocation of CWU associated with the processed amounts of commodities to the derived commodities, a value weight (often referred to as functional unit in life cycle assessments) must be defined for each co-product. Previous studies have defined value weights based on market prices (Hanasaki et al. 2010, Mekonnen and Hoekstra 2011), but monetary value is not an intrinsic property of a commodity and can vary considerably in space and time. For example, the average price ratio of soybean oil to soybean cake is about 2.3 over the period 1998–2002 but on a monthly basis price ratios varied between 1.4 and 4.2 in this period (World Bank 2019). A simple alternative is dry weight, but this would treat different components such as sugars, dietary fibre, protein, and fat equally despite their different calorie contents. Combined calorie content, however, ignores the role of proteins as essential nutrients in the human diet and treats them equal to sugars (they have the calorie content). To overcome this problem, we define a simple value index vi for each commodity, which weighs nutritious carbohydrates (sugars and starch) lower than fat to reflect their lower calorie content (4 kcal/g compared to 9 kcal/g) but weighs proteins equal to fats despite their lower calorie content (4 kcal/g) to account for their importance in human nutrition Equation E.1):

$$vi = f_{fat} + \frac{4}{9} f_{carb} + f_{protein} \tag{E.1}$$

where f_{fat}, f_{carb}, and $f_{protein}$ are the fractions of fat, nutritious carbohydrates, and protein in the considered commodity. We note that the selection of the relative value of proteins compared to primarily energy bearing components is completely arbitrary and that

Equation E.1 could be extended to account for various other nutritional aspects. However, the purpose if *vi* is to provide value weights for co-products that are based on the intrinsic properties of these products while mitigating the shortcomings of using calorie content. The composition of secondary commodities derived from processing of primary crops, as well as the values of *vi* estimated from it are given in Table E.2. The CWU associated with the processed amounts of commodities is allocated to the derived commodities proportional their total value (product of *vi* and quantity of derived products). The trade of derived commodities is calculated in the same way as for primary crops, i.e., assuming a global trade pool and accounting for net exports and imports only.

Cultivated forages are not accounted for in the records of FAOSTAT. The domestic production calculated from MIRCA2000 harvested area for fodder grasses and average yield for forages from (Monfreda et al. 2008), is therefore assumed to equal domestic supply and all domestic supply is assumed to be used as livestock feed.

As the result we obtain estimates of CWU required to produce the amounts used for food, feed, or other uses of each commodity. The total sum of these CWU components should be equal to the total ET from global cropland but is in fact slightly smaller because for most commodities the trade balance is not fully closed.

E.4 CWU of feed crops and cultivated forages

FAOSTAT only provides information about the total amount of each commodity used as livestock feed but not on how they are combined with each other and additional components to supply the feed for the different types of livestock production (animal types, production systems). Herrero et al. (2013) developed a global dataset of livestock production and biomass use for 8 animal types (meat bovines, dairy bovines, meat sheep & goats, dairy sheep & goats, pigs, broilers, layer hens, and dual-purpose poultry) in 28 world regions (see Havlík et al. 2014) for grouping of countries to regions). For ruminants (bovines and sheep & goats), 8 different production systems are distinguished: livestock grazing arid (LGA), livestock grazing humid (LGH), livestock grazing temperate (LGT), mixed arid (MXA), mixed humid (MXH), mixed temperate (MXT), other systems (Other), and urban systems (Urban). For monogastric animals (pigs and poultry), production in industrial and smallholder systems is distinguished. In total, the dataset provides detailed information about the amount and composition of feed and the amount of produced livestock products around the year 2000 in 919 production units (combinations of animal type, production system, and world regions). Four different principal feed types are distinguished: *grains* (crop-based feed), *grass* from direct grazing and as silage, *occasional feeds* (cut-and-carry forages and roadside grazing), and *stovers* (fibrous crop residues). *Grains* comprise all feed reported in FBS and CB and are grouped into ten different grain feed types (see Table E.1

for grouping of FAO commodities into grain feed types). Animals in different production units receive different amounts of each grain feed component depending on physiological needs and management decisions. The total use of each grain feed type in a region is harmonized to FAOSTAT. For further details see Herrero et al. (2013).

For the allocation of CWU associated with the amount of each FBS and CB commodity used for feed, the detailed CWU estimates for each commodity and country are aggregated to regional sums of CWU for each of the ten grain feed types. Then, the share of feed use in each production unit is determined for each grain feed type and CWU is distributed according to these shares.

In contrast to grain feeds, *forages* cannot be matched to a single feed type reported by Herrero et al. (2013). *Occasional feeds* appear to be the closest match, but this feed type also includes other feed components such as roadside grazing. On the other hand, the feed type *grass* is not restricted to grazed biomass but also includes grass silage. Therefore, it is no surprise that our estimate of regionally available *forages* does not match the estimated use of *occasional feeds* by Herrero et al. (2013). To overcome these discrepancies, we merge the *grass* and *occasional feeds* categories to obtain a total demand for grass-like biomass that has to be fulfilled by available *forages* and grazing on grasslands. To estimate the amount of *forages* used by each animal type in each production system, we intersect the map of forage production with the map of ruminant production systems (Robinson et al. 2014) and determine the amount of *forages* in each production system. We then determine for each production system the ratio of available *forages* to total grass demand and the ratio of *occasional feeds* to total grass demand. The two ratios are averaged to obtain a reference point for the utilization of *forages* across production systems, which reflects the amount of available *forages* as well as the estimated use of *occasional feeds* in Herrero et al. (2013). The thus obtained fractions of *forages* use in the production systems of a region are then scaled to match the total amount of available *forages* in the region. To prevent an exceedance of the 0 to 1 interval, the scaling is performed by increasing or decreasing all logit-transformed fractions of *forages* uses within a region by the same increment. The logit-transformation of each fraction x is defined as

$$\text{logit}(x) = \log\left(\frac{x}{1-x}\right) \tag{E.2}$$

and has the effect that the same increment in logit-transformed fractions corresponds to a smaller change in actual fractions the closer these fractions are to 0 or 1. Between 0.25 and 0.75, the relationship is approximately linear. After scaling the logit fractions these are transformed back to actual fractions following Equation E.3:

$$\text{logit}^{-1}(y) = \frac{1}{1 + \exp(-y)} \tag{E.3}$$

After the total use of *forages* was determined for each production system, the use of *forages* by the different animal types within each production system needs to be inferred. For this, the fraction of *occasional feeds* in total grass demand in the data from Herrero et al. (2013) is taken as a starting point. The fractions of different animal types in each production system are then scaled by increasing or decreasing the logit-transformed fractions by the same increment until the sum of *forages* use matches the total use in the production system.

The total grass demand that is not fulfilled by *forages* is assumed to be *grazed biomass* from pastures.

E.5 CWU of grazed biomass

The estimation of CWU related to grazed biomass is based on the following datasets:

- Landcover data from Global Agro-ecological Zones (GAEZ) database (IIASA/FAO 2012), 5 arc-minutes spatial resolution, reference year 2000
- FAOSTAT statistics of pasture area (FAO 2018), national data, reference year 2000 (1998–2002 average)
- Spatial distribution of ruminants and map of ruminant production systems from Gridded Livestock of the World database version 2 (GLW2; Robinson et al. 2014), 30 arc-seconds spatial resolution, reference year 2006
- Grazing demand for bovines and sheep & goats (Herrero et al. 2013), adjusted for actual availability of forages (see section E.4), regional data by production system, reference year 2000
- LPJmL estimates of maximum yield and corresponding green ET from managed grasslands (see section E.1), 0.5 arc-degree spatial resolution, reference year 2000 (1998–2002 average)

Annual grass yields are converted to dry matter using a carbon content 0.4763 gC/kgDM for leaves (Kattge et al. 2011). Grid cells with an annual grass yield of less than 1 gDM/(m^2 yr) are categorized as unproductive and will not be considered as grazing areas in the subsequent analysis. In productive cells, the corresponding evapotranspiration is used to determine *cwu*.

For the determination of pasture areas, we start with a broad definition of areas potentially suitable for grazing, which consist of the categories "grassland and woodland" and "barren and sparsely vegetated land" in the GAEZ land cover dataset (IIASA/FAO 2012). For India, we also added 10 % of "built-up land" to account for roadside grazing and grazing on small pasture patches within human settlements (Spate and Learmonth 2017). Multiplying the thus determined potential grazing area with the potential grass yield described in the previous paragraph determines the total biomass available for grazing in each grid cell.

The total grazing demand for bovine and sheep & goats by region and production system is downscaled to grid cell level using the spatial distributions of ruminants and the map of ruminant production systems from GLW2 (Robinson et al. 2014). The high-resolution data from GLW2 is first aggregated to determine the number of bovines and sheep & goats in each production system for each 5 arc-minute grid-cell. The grazing demand for bovines and sheet & goats in each production system is then distributed proportional to the spatial distribution of respective animal numbers. The demand in grid cells where annual grazing demand is smaller than 1 gDM/(m^2 yr) of rangeland is set to zero and fulfilled from the other grid cells of that system and region.

A comparison of estimated grazing demand by grid cell to estimated potential grass availability shows that demand exceeds availability in many cases. In total, 22.3 % of global grass demand cannot be fulfilled in the grid cells it has been allocated to. While some of these inconsistences can be attributed to the use of different data and simplifying assumptions (e.g., same feed composition and amount for all animals within a system and regions), most of it can be attributed to the fact that the spatial disaggregation of ruminants in GLW2 is not based on any measure of grassland extent or productivity. To resolve the mismatch between grazing demand and availability we redistribute the excess demand from grid cells where demand cannot be met to grid cells with surplus availability. In most cases, the total amount of biomass available in the production systems within regions is sufficiently large so that the excess demand can be fulfilled from grid cells with the same production system. To minimize the distortion of the original distribution of grazing demand, the redistribution is done by increasing the logit-transformed ratios of grass demand to available grass in all grid cell of the respective production system by the same value until the total grazing demand for that systems has been fulfilled. Only in a few regions such as India and MENA region, the total demand in some production systems exceeds the sum of biomass available for grazing in all grid cells of the respective system. In those cases, the logit-transformed demand-to-availability ratio in all grid cells of the respective region is increased until the remaining demand excess is fulfilled.

After all demand for grazed biomass is distributed to grid cells, the corresponding CWU is calculated by multiplying this demand with the *cwu* in each grid cell. Total CWU for

each animal type in each production system and region is then determined by summing up the CWU for the spatially disaggregated demand. It is important to emphasize that the obtained CWU estimates only comprise a fraction of the ET from grazing lands, which corresponds to the fraction of potentially available biomass for grazing that is actually used. The remaining biomass and associated CWU is assumed to support biodiversity and other ecosystem services such as carbon sequestration in grassland ecosystems. The assumption that the fraction of grassland ET allocated to CWU for grazing is proportional to the fraction of utilized available biomass is equivalent to the assumption that only this fraction of grazing land is fully grazed, while the rest remains untouched. We acknowledge that such a linear scaling of the impact of partial grazing on grassland ecosystems may be a simplification, but it provides a transparent and reproducible approach. A thorough assessment of the impacts of grazing on grassland ecosystems is beyond the scope of this analysis.

Our estimate of grazing lands, comprising all land potentially available for grazing and excluding only unproductive and unused land ($<1\,\mathrm{gDM/(m^2\,yr)}$ available or used, respectively), is in total about 10.0 million $\mathrm{km^2}$ larger than the 34.1 million $\mathrm{km^2}$ of global "land under permanent meadows and pastures" reported by FAOSTAT (FAO 2018). To obtain a realistic estimate of total pasture ET, we reduce the fraction of grasslands not utilized for grazing by a constant factor for each region. In the Australia and New Zealand region, our estimate of grazing lands is about one third smaller than the estimate in FAOSTAT so that also our final estimate of pasture in this region remains lower than the FAOSTAT estimate. In India, Japan, South Korea, and the Rest of South Asia region, the area of grazing land required to fulfil the grazing demand in these regions is larger than the area reported by FAOSTAT so that our final estimate of pasture area in these regions exceeds the FAOSTAT estimate. Overall, our adjusted estimate of global pasture extent is with 33.5 million $\mathrm{km^2}$ very close to the FAOSTAT estimate.

E.6 Decomposition of variance in livestock water productivity

A central part of this paper is to assess the origin of variations in livestock water productivity (LWP; $\mathrm{gP/m^3}$). LWP is the product of two principal factors: feed water productivity (FWP; $\mathrm{kgDM/m^3}$) and feed use efficiency (FUE; gP/kgDM):

$$\mathrm{LWP} = \mathrm{FWP} \cdot \mathrm{FUE} \tag{E.4}$$

In order to facilitate the decomposition of variance in LWP into its components, we

apply a logarithmic transformation and obtain:

$$\log(\text{LWP}) = \log(\text{FWP}) + \log(\text{FUE}) \tag{E.5}$$

The variance of the sum of two variables $X + Y$, is the sum of covariances between the summed variable and its summands:

$$\text{Var}(X + Y) = \text{Cov}(X + Y, X) + \text{Cov}(X + Y, Y) \tag{E.6}$$

Thus, the variance of log(LWP) can be decomposed into the two covariances of log(LWP) with log(FWP) and log(FUE).

It is important to note that the logarithmic transformation of variables removes the scale-dependency of variances, effectively producing estimates of standard deviation that can be interpreted in relative terms. For example, an interval of ± 0.5 around the mean of a log-transformed variable is equivalent to the interval from $-39\,\%$ to $+65\,\%$ around the mean of the untransformed variable. It is only through this transformation that the variances of the two factors FWP and FCU become comparable and that their interaction can be analysed in a meaningful way.

Table E.1: List of FAO commodities and their assignment to feed items. For primary crops, the corresponding crop type in MIRCA2000, the CFT by which it is represented in LPJmL, and the carbon content is given.

FAO Item	Type	MIRCA2000 Crop	LPJmL CFT	Carbon gC/g	Feed Item
Alcohol, Non-Food	Vegetal Food				CrpO
Apples and products	Vegetal Food	Others Perennial	Generic perennial	0.063	CrpO
Bananas	Vegetal Food	Others Perennial	Generic perennial	0.109	CrpO
Barley and products	Vegetal Food	Barley	Temperate cereals	0.388	Barl
Beans	Vegetal Food	Pulses	Pulses	0.399	Puls
Beer	Vegetal Food				CrpO
Beverages, Alcoholic	Vegetal Food				CrpO
Beverages, Fermented	Vegetal Food				CrpO
Brans	Vegetal Food				CerO
Cassava and products	Vegetal Food	Cassava	Tropical roots	0.163	CrpO
Cereals, Other	Vegetal Food	Others Annual	Generic annual	0.389	CerO
Citrus, Other	Vegetal Food	Citrus	Generic perennial	0.068	CrpO
Cloves	Vegetal Food	Others Perennial	Generic perennial	0.420	CrpO
Cocoa Beans and products	Vegetal Food	Cocoa	Generic perennial	0.595	CrpO
Coconut Oil	Vegetal Food				OlsO
Coconuts - Incl Copra	Vegetal Food	Others Perennial	Generic perennial	0.382	OlsO
Coffee and products	Vegetal Food	Coffee	Generic perennial	0.460	CrpO
Cottonseed	Vegetal Food	Cotton	Generic annual	0.466	OlsO
Cottonseed Oil	Vegetal Food				OlsO
Dates	Vegetal Food	Date Palm	Generic perennial	0.341	CrpO
Fruits, Other	Vegetal Food	Others Perennial	Generic perennial	0.070	CrpO
Grapefruit and products	Vegetal Food	Citrus	Generic perennial	0.041	CrpO
Grapes and products (excl wine)	Vegetal Food	Grapes	Generic perennial	0.069	CrpO
Groundnut Oil	Vegetal Food				OlsO
Groundnuts (in Shell Eq)	Vegetal Food	Groundnuts	Groundnuts	0.507	OlsO
Honey	Vegetal Food				CrpO
Infant food	Vegetal Food				CrpO
Lemons, Limes and products	Vegetal Food	Citrus	Generic perennial	0.052	CrpO
Maize and products	Vegetal Food	Maize	Maize	0.392	Corn
Maize Germ Oil	Vegetal Food				OlsO
Millet and products	Vegetal Food	Millet	Tropical cereals	0.408	SgMi
Miscellaneous	Vegetal Food				CrpO
Molasses	Vegetal Food				CrpO
Nuts and products	Vegetal Food	Others Perennial	Generic perennial	0.567	CrpO
Oats	Vegetal Food	Others Annual	Generic annual	0.400	CerO
Oilcrops Oil, Other	Vegetal Food				OlsO
Oilcrops, Other	Vegetal Food	Others Annual	Generic annual	0.518	OlsO
Olive Oil	Vegetal Food				OlsO
Olives (including preserved)	Vegetal Food	Others Perennial	Generic perennial	0.115	OlsO
Onions	Vegetal Food	Others Annual	Generic annual	0.048	CrpO
Oranges, Mandarines	Vegetal Food	Citrus	Generic perennial	0.077	CrpO
Palm kernels	Vegetal Food	Oil Palm	Generic perennial	0.548	OlsO
Palm Oil	Vegetal Food	Oil Palm	Generic perennial	0.770	OlsO
Palmkernel Oil	Vegetal Food				OlsO

Peas	Vegetal Food	Pulses	Pulses	0.389	Puls
Pepper	Vegetal Food	Others Perennial	Generic perennial	0.362	CrpO
Pimento	Vegetal Food	Others Annual	Generic annual	0.037	CrpO
Pineapples and products	Vegetal Food	Others Perennial	Generic perennial	0.062	CrpO
Plantains	Vegetal Food	Others Perennial	Generic perennial	0.168	CrpO
Potatoes and products	Vegetal Food	Potatoes	Temperate roots	0.086	CrpO
Pulses, Other and products	Vegetal Food	Pulses	Pulses	0.404	Puls
Rape and Mustard Oil	Vegetal Food				OlsO
Rape and Mustardseed	Vegetal Food	Rapeseed	Rapeseed	0.546	OlsO
Rice (Paddy Equivalent)	Vegetal Food	Rice	Rice	0.377	Rice
Ricebran Oil	Vegetal Food				OlsO
Roots, Other	Vegetal Food	Others Annual	Generic annual	0.126	CrpO
Rye and products	Vegetal Food	Rye	Temperate cereals	0.385	CerO
Sesame seed	Vegetal Food	Others Annual	Generic annual	0.583	OlsO
Sesameseed Oil	Vegetal Food				OlsO
Sorghum and products	Vegetal Food	Sorghum	Tropical cereals	0.395	SgMi
Soyabean Oil	Vegetal Food				Soya
Soyabeans	Vegetal Food	Soybeans	Soybean	0.462	Soya
Spices, Other	Vegetal Food	Others Perennial	Generic perennial	0.094	CrpO
Sugar (Raw Equivalent)	Vegetal Food				CrpO
Sugar beet	Vegetal Food	Sugar Beet	Temperate roots	0.079	CrpO
Sugar cane	Vegetal Food	Sugar Cane	Sugarcane	0.128	CrpO
Sugar non-centrifugal	Vegetal Food				CrpO
Sunflower seed	Vegetal Food	Sunflower	Sunflower	0.555	OlsO
Sunflowerseed Oil	Vegetal Food				OlsO
Sweet potatoes	Vegetal Food	Others Annual	Generic annual	0.130	CrpO
Sweeteners, Other	Vegetal Food	Others Annual	Generic annual	0.402	CrpO
Tea (including mate)	Vegetal Food	Others Perennial	Generic perennial	0.393	CrpO
Tomatoes and products	Vegetal Food	Others Annual	Generic annual	0.023	CrpO
Vegetables, Other	Vegetal Food	Others Annual	Generic annual	0.033	CrpO
Wheat and products	Vegetal Food	Wheat	Temperate cereals	0.391	Whea
Wine	Vegetal Food				CrpO
Yams	Vegetal Food	Others Annual	Generic annual	0.132	CrpO
Aquatic Animals, Others	Animal Sourced Food				ANIM
Aquatic Plants	Animal Sourced Food				ANIM
Bovine Meat	Animal Sourced Food				ANIM
Butter, Ghee	Animal Sourced Food				ANIM
Cephalopods	Animal Sourced Food				ANIM
Cream	Animal Sourced Food				ANIM
Crustaceans	Animal Sourced Food				ANIM
Demersal Fish	Animal Sourced Food				ANIM
Eggs	Animal Sourced Food				ANIM
Fats, Animals, Raw	Animal Sourced Food				ANIM
Fish, Body Oil	Animal Sourced Food				ANIM
Fish, Liver Oil	Animal Sourced Food				ANIM
Freshwater Fish	Animal Sourced Food				ANIM
Marine Fish, Other	Animal Sourced Food				ANIM
Meat, Aquatic Mammals	Animal Sourced Food				ANIM
Meat, Other	Animal Sourced Food				ANIM

Milk - Excluding Butter	Animal Sourced Food				ANIM
Molluscs, Other	Animal Sourced Food				ANIM
Mutton and Goat Meat	Animal Sourced Food				ANIM
Offals, Edible	Animal Sourced Food				ANIM
Pelagic Fish	Animal Sourced Food				ANIM
Pigmeat	Animal Sourced Food				ANIM
Poultry Meat	Animal Sourced Food				ANIM
Copra Cake	Livestock Feed				OlsO
Cottonseed Cake	Livestock Feed				OlsO
Groundnut Cake	Livestock Feed				OlsO
Oilseed Cakes, Other	Livestock Feed				OlsO
Palmkernel Cake	Livestock Feed				OlsO
Rape and Mustard Cake	Livestock Feed				OlsO
Sesameseed Cake	Livestock Feed				OlsO
Soyabean Cake	Livestock Feed				Soya
Sunflowerseed Cake	Livestock Feed				OlsO
Fish Meal	Livestock Feed				ANIM
Meat Meal	Livestock Feed				ANIM
Abaca	Non-food	Others Annual	Generic annual	0.418	CrpO
Cotton lint	Non-food	Cotton	Generic annual	0.418	CrpO
Hard Fibres, Other	Non-food	Others Perennial	Generic perennial	0.418	CrpO
Hides and skins	Non-food				ANIM
Jute	Non-food	Others Annual	Generic annual	0.418	CrpO
Jute-Like Fibres	Non-food	Others Annual	Generic annual	0.418	CrpO
Rubber	Non-food	Others Perennial	Generic perennial	0.16	CrpO
Silk	Non-food				ANIM
Sisal	Non-food	Others Perennial	Generic perennial	0.418	CrpO
Soft-Fibres, Other	Non-food	Others Annual	Generic annual	0.418	CrpO
Tobacco	Non-food	Others Annual	Generic annual	0.083	CrpO
Wool (Clean Eq.)	Non-food				ANIM

Table E.2: Content of nutritiuos carbohydrates (starch and sugar), and derived value indices *vi* using Equation E.1 for all FAO commodities derived from other commodities in processes generating two or more co-products.

Name	Starch and sugar (%)	Fat (%)	Protein (%)	Value index	Reference
Cotton lint	0	0	0	3.84	Ten times the value of Cottonseed
Cottonseed	1	18	20	0.38	https://www.feedipedia.org/node/742
Kapok fibre	0	0	0	4.7	Ten times the value of Kapokseed
Kapokseed in shell	0	21	26	0.47	https://www.feedipedia.org/node/12221
Coconuts	5	7	1	0.1	https://ndb.nal.usda.gov/ndb/foods/show/12104 and FAO, 2000
Coir	0	0	0	0.97	Ten times the value of Coconut
Oil, palm	0	100	0	1	https://ndb.nal.usda.gov/ndb/foods/show/04055
Palm kernels	0	44	9	0.53	https://www.feedipedia.org/node/15405
Coconut Oil	0	99	0	0.99	https://ndb.nal.usda.gov/ndb/foods/show/04047
Copra Cake	10	9	20	0.33	https://www.feedipedia.org/node/11997
Cottonseed Oil	0	100	0	1	https://ndb.nal.usda.gov/ndb/foods/show/04502
Cottonseed Cake	8	3	43	0.5	https://www.feedipedia.org/node/12021
Groundnut Oil	0	100	0	1	https://ndb.nal.usda.gov/ndb/foods/show/04042
Groundnut Cake	16	9	45	0.61	https://www.feedipedia.org/node/12159
Palmkernel Oil	0	100	0	1	https://ndb.nal.usda.gov/ndb/foods/show/04513
Palmkernel Cake	3	3	17	0.21	https://www.feedipedia.org/node/12421
Rape and Mustard Oil	0	100	0	1	https://ndb.nal.usda.gov/ndb/foods/show/04582
Rape and Mustard Cake	15	8	32	0.47	https://www.feedipedia.org/node/12502
Sesameseed Oil	0	100	0	1	https://ndb.nal.usda.gov/ndb/foods/show/04058
Sesameseed Cake	6	10	42	0.55	https://www.feedipedia.org/node/12577
Soyabean Oil	0	100	0	1	https://ndb.nal.usda.gov/ndb/foods/show/04044
Soyabean Cake	13	2	46	0.54	https://www.feedipedia.org/node/11682
Sunflowerseed Oil	0	100	0	1	https://ndb.nal.usda.gov/ndb/foods/show/04642
Sunflowerseed Cake	6	13	26	0.42	https://www.feedipedia.org/node/12664
Maize germ oil	0	100	0	1	https://ndb.nal.usda.gov/ndb/foods/show/04518
Maize germ cake	21	2	25	0.36	https://www.feedipedia.org/node/20332
Rice bran oil	0	100	0	1	https://ndb.nal.usda.gov/ndb/foods/show/04037
Rice bran cake	31	4	14	0.32	https://www.feedipedia.org/node/11639
Oilcrops Oil, Other	0	100	0	1	https://ndb.nal.usda.gov/ndb/foods/show/45179959
Oilseed Cakes, Other	11	3	32	0.4	https://www.feedipedia.org/node/12263
Sugar, sugar cane	98	0	0	0.44	https://ndb.nal.usda.gov/ndb/foods/show/19334
Molasses, sugar cane	47	1	4	0.26	https://www.feedipedia.org/node/12341
Sugar, sugar beet	98	0	0	0.44	https://ndb.nal.usda.gov/ndb/foods/show/19334
Molasses, sugar beet	48	0	11	0.32	https://www.feedipedia.org/node/12340
Wheat flour	77	1	10	0.45	https://ndb.nal.usda.gov/ndb/foods/show/20481
Wheat bran	26	3	15	0.3	https://www.feedipedia.org/node/12751
Pot barley	75	1	10	0.44	FAO, 2001
Barley bran	10	13	2	0.19	https://de.wikipedia.org/wiki/Kleie
Milled Rice	80	1	7	0.44	https://ndb.nal.usda.gov/ndb/foods/show/20444
Rice bran	28	15	13	0.4	https://www.feedipedia.org/node/11636
Flour of maize	77	4	7	0.45	https://ndb.nal.usda.gov/ndb/foods/show/20016
Maize bran	34	4	11	0.3	https://www.feedipedia.org/node/12280
Maize germ	13	46	12	0.64	https://www.feedipedia.org/node/20336

Oats rolled	67	6	16	0.52	FAO, 2001
Oat bran	45	7	17	0.44	https://www.feedipedia.org/node/12385
Flour of rye	75	2	11	0.46	https://ndb.nal.usda.gov/ndb/foods/show/20064
Bran of rye	14	9	5	0.2	https://de.wikipedia.org/wiki/Kleie
Flour of millet	75	4	11	0.48	https://ndb.nal.usda.gov/ndb/foods/show/20647
Bran of millet	39	8	13	0.38	https://www.feedipedia.org/node/11690
Flour of sorghum	77	3	8	0.45	https://ndb.nal.usda.gov/ndb/foods/show/20648
Bran of sorghum	31	6	11	0.31	https://www.feedipedia.org/node/12611
Flour cereals n.e.s.	77	1	10	0.45	Same as wheat flour
Bran of cereals n.e.s.	26	3	15	0.3	Same as wheat bran

Table E.3: Spearman's rank correlation coefficients for relationships of GDP with LWP, FWP, FCE, fraction of feed crops in feed mix, fraction of crop residues in feed mix, and water productivity of feed crops in the feed mix.

	LWP	FUE	FWP	Feed crops	Crop residues	$WP_{\text{feed crops}}$
Industrial pigs	0.68***	0.59**	0.59**			0.59**
Broilers	0.75***	0.59**	0.61***			0.61***
Layer hens	0.57**	−0.35	0.61***			0.61***
Dairy bovines	0.52***	0.71***	−0.41***	0.59***	−0.43***	0.61***
Meat bovines	0.44***	0.62***	−0.34***	0.39***	−0.40***	0.56***
Dairy S&G	0.31***	0.48***	−0.23**	0.64***	−0.28***	0.53***
Meat S&G	0.15*	0.25***	−0.13	0.38***	−0.41***	0.51***

Significance codes: *** $p < 0.001$, ** $p < 0.01$, * $p < 0.05$

Bibliography

J. Alcamo, P. Döll, T. Henrichs, F. Kaspar, B. Lehner, T. Rösch, and S. Siebert. Development and testing of the WaterGAP 2 global model of water use and availability. *Hydrological Sciences Journal*, 48:317–337, 2003. doi: 10.1623/hysj.48.3.317.45290.

J. Alcamo, M. Flörke, and M. Märker. Future long-term changes in global water resources driven by socio-economic and climatic changes. *Hydrological Sciences Journal*, 52(2): 247–275, 2007. doi: 10.1623/hysj.52.2.247.

N. Alexandratos and J. Bruinsma. *World agriculture towards 2015/2030: The 2012 Revision.* ESA Working Paper No. 12-03. Food and Agriculture Organization of the United Nations, Rome, 2012.

R. Alkama, M. Kageyama, and G. Ramstein. Relative contributions of climate change, stomatal closure, and leaf area index changes to 20th and 21st century runoff change: A modelling approach using the Organizing Carbon and Hydrology in Dynamic Ecosystems (ORCHIDEE) land surface model. *Journal of Geophysical Research*, 115(D17):D17112, 2010. doi: 10.1029/2009JD013408.

R. E. Alter, E.-S. Im, and E. A. B. Eltahir. Rainfall consistently enhanced around the Gezira Scheme in East Africa due to irrigation. *Nature Geoscience*, 8(10):763–767, 2015. doi: 10.1038/ngeo2514.

N. Arnell. A simple water balance model for the simulation of streamflow over a large geographic domain. *Journal of Hydrology*, 217(3-4):314–335, 1999. doi: 10.1016/S0022-1694(99)00023-2.

N. W. Arnell. Effects of IPCC SRES* emissions scenarios on river runoff: a global perspective. *Hydrology and Earth System Sciences*, 7(5):619–641, 2003. ISSN 1607-7938. doi: 10.5194/hess-7-619-2003.

N. W. Arnell. Climate change and global water resources: SRES emissions and socio-economic scenarios. *Global Environmental Change*, 14(1):31–52, 2004. doi: 10.1016/j.gloenvcha.2003.10.006.

N. W. Arnell and B. Lloyd-Hughes. The global-scale impacts of climate change on water resources and flooding under new climate and socio-economic scenarios. *Climatic Change*, 122(1-2):127–140, 2014. doi: 10.1007/s10584-013-0948-4.

N. W. Arnell, D. P. van Vuuren, and M. Isaac. The implications of climate policy for the impacts of climate change on global water resources. *Global Environmental Change*, 21 (2):592–603, 2011. doi: 10.1016/j.gloenvcha.2011.01.015.

P. J. Ashton. Avoiding Conflicts over Africa's Water Resources. *Ambio*, 31(3):236–242, 2002.

C. Batchelor, J. Hoogeveen, J. M. Faurès, and L. Peiser. Water accounting and Auditing: A sourcebook. Technical report, Food and Agriculture Organization of the United Nations, Rome, Italy, 2017.

B. Bates, Z. Kundzewicz, S. Wu, and J. Palutikof, editors. *Climate Change and Water*. Technical Paper of the Intergovernmental Panel on Climate Change. IPCC Secretariat, Geneva, 2008. ISBN 9789291691234.

M. J. Best, M. Pryor, D. B. Clark, G. G. Rooney, R. L. H. Essery, C. B. Ménard, J. M. Edwards, M. A. Hendry, A. Porson, N. Gedney, L. M. Mercado, S. Sitch, E. Blyth, O. Boucher, P. M. Cox, C. S. B. Grimmond, and R. J. Harding. The Joint UK Land Environment Simulator (JULES), model description – Part 1: Energy and water fluxes. *Geoscientific Model Development*, 4(3):677–699, 2011. doi: 10.5194/gmd-4-677-2011.

A. H. W. Beusen, A. L. M. Dekkers, A. F. Bouwman, W. Ludwig, and J. Harrison. Estimation of global river transport of sediments and associated particulate C, N, and P. *Global Biogeochemical Cycles*, 19(4):GB4S05, 2005. doi: 10.1029/2005GB002453.

H. Biemans, I. Haddeland, P. Kabat, F. Ludwig, R. W. A. Hutjes, J. Heinke, W. von Bloh, and D. Gerten. Impact of reservoirs on river discharge and irrigation water supply during the 20th century. *Water Resources Research*, 47(3):1–15, 2011. doi: 10.1029/2009WR008929.

D. L. Bijl, P. W. Bogaart, T. Kram, B. J. de Vries, and D. P. van Vuuren. Long-term water demand for electricity, industry and households. *Environmental Science & Policy*, 55:75–86, 2016. doi: 10.1016/j.envsci.2015.09.005.

M. Blümmel, F. Teymouri, J. Moore, C. Nielson, J. Videto, P. Kodukula, S. Pothu, R. Devulapalli, and P. Varijakshapanicker. Ammonia Fiber Expansion (AFEX) as spin off technology from 2nd generation biofuel for upgrading cereal straws and stovers for livestock feed. *Animal Feed Science and Technology*, 236(December 2017):178–186, 2018. doi: 10.1016/j.anifeedsci.2017.12.016.

B. L. Bodirsky, S. Rolinski, A. Biewald, I. Weindl, A. Popp, and H. Lotze-Campen. Global Food Demand Scenarios for the 21st Century. *PLOS ONE*, 10(11):e0139201, 2015. doi: 10.1371/journal.pone.0139201.

A. Bondeau, P. C. Smith, S. Zaehle, S. Schaphoff, W. Lucht, W. Cramer, D. Gerten, H. Lotze-campen, C. Müller, M. Reichstein, and B. Smith. Modelling the role of agriculture for the 20th century global terrestrial carbon balance. *Global Change Biology*, 13(3):679–706, 2007. doi: 10.1111/j.1365-2486.2006.01305.x.

A. Bouwman, K. Van der Hoek, B. Eickhout, and I. Soenario. Exploring changes in world ruminant production systems. *Agricultural Systems*, 84(2):121–153, 2005. doi: 10.1016/j.agsy.2004.05.006.

L. R. Boysen, W. Lucht, D. Gerten, V. Heck, T. M. Lenton, and H. J. Schellnhuber. The limits to global-warming mitigation by terrestrial carbon removal. *Earth's Future*, 5(5): 463–474, 2017. doi: 10.1002/2016EF000469.

D. B. Brooks. An Operational Definition of Water Demand Management. *International Journal of Water Resources Development*, 22(4):521–528, 2006. doi: 10.1080/07900620600779699.

T. Carter, M. Parry, H. Harasawa, and S. Nishioka. *IPCC Technical Guidelines for Assessing Climate Change Impacts and Adaptations*. Department of Geography, University College London, UK and the Center for Global Environmental Research, National Institute for Environmental Studies, Japan, 1994. ISBN 0904813118.

Center for International Earth Science Information Network, Columbia University (CIESIN) and Centro Internacional de Agricultura Tropical (CIAT). *Gridded Population of the World Version 3 (GPWv3): Population Grids*. NASA Socioeconomic Data and Applications Center (SEDAC), Palisades, NY, USA, 2005. URL `http://sedac.ciesin.columbia.edu/data/collection/gpw-v3/`.

P. Ciais, C. Sabine, G. Bala, L. Bopp, V. Brovkin, J. Canadell, A. Chhabra, R. DeFries, J. Galloway, M. Heimann, C. Jones, C. Le Quéré, R. Myneni, S. Piao, and P. Thornton. Carbon and Other Biogeochemical Cycles. In T. Stocker, D. Qin, G.-K. Plattner, M. Tignor, S. Allen, J. Boschung, A. Nauels, Y. Xia, V. Bex, and P. Midgley, editors, *Climate Change 2013: The Physical Science Basis. Contribution of Working Group I to the Fifth Assessment Report of the Intergovernmental Panel on Climate Change*. Cambridge University Press, Cambridge, United Kingdom and New York, NY, USA, 2013.

D. B. Clark, L. M. Mercado, S. Sitch, C. D. Jones, N. Gedney, M. J. Best, M. Pryor, G. G. Rooney, R. L. H. Essery, E. Blyth, O. Boucher, R. J. Harding, and P. M. Cox. The Joint

UK Land Environment Simulator (JULES), Model description – Part 2: Carbon fluxes and vegetation. *Geoscientific Model Development Discussions*, 4(1):641–688, 2011. doi: 10.5194/gmdd-4-641-2011.

S. Coles. *An Introduction to Statistical Modeling of Extreme Values*. Springer Series in Statistics. Springer, London, 2001. doi: 10.1007/978-1-4471-3675-0.

R. Dankers, N. W. Arnell, D. B. Clark, P. D. Falloon, B. M. Fekete, S. N. Gosling, J. Heinke, H. Kim, Y. Masaki, Y. Satoh, T. Stacke, Y. Wada, and D. Wisser. First look at changes in flood hazard in the Inter-Sectoral Impact Model Intercomparison Project ensemble. *Proceedings of the National Academy of Sciences*, 111(9):3257–3261, 2014. doi: 10.1073/pnas.1302078110.

W. Dansgaard, S. J. Johnsen, H. B. Clausen, D. Dahl-Jensen, N. S. Gundestrup, C. U. Hammer, C. S. Hvidberg, J. P. Steffensen, A. E. Sveinbjörnsdottir, J. Jouzel, and G. Bond. Evidence for general instability of past climate from a 250-kyr ice-core record. *Nature*, 364(6434):218–220, 1993. doi: 10.1038/364218a0.

J. C. S. Davie, P. D. Falloon, R. Kahana, R. Dankers, R. Betts, F. T. Portmann, D. B. Clark, A. Itoh, Y. Masaki, K. Nishina, B. Fekete, Z. Tessler, X. Liu, Q. Tang, S. Hagemann, T. Stacke, R. Pavlick, S. Schaphoff, S. N. Gosling, W. Franssen, and N. Arnell. Comparing projections of future changes in runoff and water resources from hydrological and ecosystem models in ISI-MIP. *Earth System Dynamics Discussions*, 4(1):279–315, 2013. doi: 10.5194/esdd-4-279-2013.

C. de Fraiture, D. Wichelns, J. Rockström, E. Kemp-Benedict, N. Eriyagama, L. J. Gordon, M. a. Hanjra, J. Hoogeveen, A. Huber-Lee, and L. Karlberg. Looking ahead to 2050: Scenarios of alternative investment approaches. In D. Molden, editor, *Water for Food, Water for Life: A Comprehensive Assessment of Water Management in Agriculture.*, chapter 3, pages 91–145. Routledge, London, 2007. ISBN 9781849773799. doi: 10.4324/9781849773799.

G. Destouni, F. Jaramillo, and C. Prieto. Hydroclimatic shifts driven by human water use for food and energy production. *Nature Climate Change*, 3(3):213–217, 2012. doi: 10.1038/nclimate1719.

P. A. Dirmeyer, X. Gao, M. Zhao, Z. Guo, T. Oki, and N. Hanasaki. GSWP-2: Multimodel Analysis and Implications for Our Perception of the Land Surface. *Bulletin of the American Meteorological Society*, 87(10):1381–1398, 2006. doi: 10.1175/BAMS-87-10-1381.

P. Döll and B. Lehner. Validation of a new global 30-min drainage direction map. *Journal of Hydrology*, 258(1-4):214–231, 2002. doi: 10.1016/S0022-1694(01)00565-0.

P. Döll and H. M. Schmied. How is the impact of climate change on river flow regimes related to the impact on mean annual runoff? A global-scale analysis. *Environmental Research Letters*, 7(1):014037, 2012. doi: 10.1088/1748-9326/7/1/014037.

P. Döll and S. Siebert. Global modeling of irrigation water requirements. *Water Resources Research*, 38(4):8–1–8–10, 2002. doi: 10.1029/2001WR000355.

P. Döll, F. Kaspar, and B. Lehner. A global hydrological model for deriving water availability indicators: model tuning and validation. *Journal of Hydrology*, 270(1-2):105–134, 2003. doi: 10.1016/S0022-1694(02)00283-4.

P. Döll, H. Hoffmann-Dobrev, F. Portmann, S. Siebert, A. Eicker, M. Rodell, G. Strassberg, and B. Scanlon. Impact of water withdrawals from groundwater and surface water on continental water storage variations. *Journal of Geodynamics*, 59-60:143–156, 2012. doi: 10.1016/j.jog.2011.05.001.

S. Dyck and G. Peschke. *Grundlagen der Hydrologie*. Verlag für Bauwesen, Berlin, 3rd edition, 1995. ISBN 3-345-00586-7.

U. Ehret, E. Zehe, V. Wulfmeyer, K. Warrach-Sagi, and J. Liebert. HESS Opinions "Should we apply bias correction to global and regional climate model data?". *Hydrology and Earth System Sciences*, 16(9):3391–3404, 2012. doi: 10.5194/hess-16-3391-2012.

J. Elliott, D. Deryng, C. Müller, K. Frieler, M. Konzmann, D. Gerten, M. Glotter, M. Flörke, Y. Wada, N. Best, S. Eisner, B. M. Fekete, C. Folberth, I. Foster, S. N. Gosling, I. Haddeland, N. Khabarov, F. Ludwig, Y. Masaki, S. Olin, C. Rosenzweig, A. C. Ruane, Y. Satoh, E. Schmid, T. Stacke, Q. Tang, and D. Wisser. Constraints and potentials of future irrigation water availability on agricultural production under climate change. *Proceedings of the National Academy of Sciences*, 111(9):3239–3244, 2014. doi: 10.1073/pnas.1222474110.

V. Eyring, S. Bony, G. A. Meehl, C. A. Senior, B. Stevens, R. J. Stouffer, and K. E. Taylor. Overview of the Coupled Model Intercomparison Project Phase 6 (CMIP6) experimental design and organization. *Geoscientific Model Development*, 9(5):1937–1958, 2016a. doi: 10.5194/gmd-9-1937-2016.

V. Eyring, M. Righi, A. Lauer, M. Evaldsson, S. Wenzel, C. Jones, A. Anav, O. Andrews, I. Cionni, E. L. Davin, C. Deser, C. Ehbrecht, P. Friedlingstein, P. Gleckler, K.-D. Gottschaldt, S. Hagemann, M. Juckes, S. Kindermann, J. Krasting, D. Kunert, R. Levine, A. Loew, J. Mäkelä, G. Martin, E. Mason, A. S. Phillips, S. Read, C. Rio, R. Roehrig, D. Senftleben, A. Sterl, L. H. van Ulft, J. Walton, S. Wang, and K. D. Williams. ESMValTool (v1.0) – a community diagnostic and performance metrics tool

for routine evaluation of Earth system models in CMIP. *Geoscientific Model Development*, 9(5):1747–1802, 2016b. doi: 10.5194/gmd-9-1747-2016.

M. Fader, S. Rost, C. Müller, A. Bondeau, and D. Gerten. Virtual water content of temperate cereals and maize: Present and potential future patterns. *Journal of Hydrology*, 384(3-4):218–231, 2010. doi: 10.1016/j.jhydrol.2009.12.011.

M. Falkenmark. The Massive Water Scarcity Now Threatening Africa - Why Isn't It Being Addressed. *Ambio*, 18(2):112–118, 1989.

M. Falkenmark and M. Lannerstad. Consumptive water use to feed humanity – curing a blind spot. *Hydrology and Earth System Sciences Discussions*, 1(1):7–40, 2004. doi: 10.5194/hessd-1-7-2004.

M. Falkenmark and D. Molden. Wake up to realities of river basin closure. *International Journal of Water Resources Development*, 24(2):201–215, 2008. doi: 10.1080/07900620701723570.

M. Falkenmark and J. Rockström. The New Blue and Green Water Paradigm: Breaking New Ground for Water Resources Planning and Management. *Journal of Water Resources Planning and Management*, 132(3):129–132, 2006. doi: 10.1061/(ASCE)0733-9496(2006)132:3(129).

M. Falkenmark, J. Lundqvist, and C. Widstrand. Macro-scale water scarcity requires micro-scale approaches. *Natural Resources Forum*, 13(4):258–267, 1989. doi: 10.1111/j.1477-8947.1989.tb00348.x.

M. Falkenmark, A. Berntell, A. Jägerskog, J. Lundqvist, M. Matz, and H. Tropp. *On the Verge of a New Water Scarcity: A Call for Good Governance and Human Ingenuity.* SIWI Policy Brief. SIWI, Stockholm, Sweden, 2007.

B. M. Fekete, D. Wisser, C. Kroeze, E. Mayorga, L. Bouwman, W. M. Wollheim, and C. Vörösmarty. Millennium Ecosystem Assessment scenario drivers (1970-2050): Climate and hydrological alterations. *Global Biogeochemical Cycles*, 24(4):GB0A12, 2010. doi: 10.1029/2009GB003593.

T. Fetzel, P. Havlik, M. Herrero, J. O. Kaplan, T. Kastner, C. Kroisleitner, S. Rolinski, T. Searchinger, P. M. Van Bodegom, S. Wirsenius, and K.-H. Erb. Quantification of uncertainties in global grazing systems assessment. *Global Biogeochemical Cycles*, 31(7):1089–1102, 2017. doi: 10.1002/2016GB005601.

G. Flato, J. Marotzke, B. Abiodun, P. Braconnot, S. Chou, W. Collins, P. Cox, F. Driouech, S. Emori, V. Eyring, C. Forest, P. Gleckler, E. Guilyardi, C. Jakob, V. Kattsov,

C. Reason, and M. Rummukainen. Evaluation of Climate Models. In Stocker, T.F., D. Qin, G.-K. Plattner, M. Tignor, S. Allen, J. Boschung, A. Nauels, Y. Xia, V. Bex, and P. Midgley, editors, *Climate Change 2013: The Physical Science Basis. Contribution of Working Group I to the Fifth Assess- ment Report of the Intergovernmental Panel on Climate Change*, volume 9781107057, pages 741–866. Cambridge University Press, Cambridge, United Kingdom and New York, NY, USA, 2013. ISBN 9781107415324. doi: 10.1017/CBO9781107415324.020.

M. Flörke, E. Kynast, I. Bärlund, S. Eisner, F. Wimmer, and J. Alcamo. Domestic and industrial water uses of the past 60 years as a mirror of socio-economic development: A global simulation study. *Global Environmental Change*, 23(1):144–156, 2013. doi: 10.1016/j.gloenvcha.2012.10.018.

Food and Agriculture Organization of the United Nations (FAO). *Technical Conversion Factors for Agricultural Commodities*. FAO, Rome, 2000.

Food and Agriculture Organization of the United Nations (FAO). AQUASTAT statistics database, 2013. Available at `http://www.fao.org/nr/water/aquastat/main/index.stm`, accessed 30 January 2013.

Food and Agriculture Organization of the United Nations (FAO). AQUASTAT website, 2016. Available at `http://www.fao.org/nr/water/aquastat/water_use/index.stm`, accessed 30 January 2019.

Food and Agriculture Organization of the United Nations (FAO). FAOSTAT statistics database, 2018. Available at `http://www.fao.org/faostat/en/#data`, accessed 28 February 2018.

K. Frieler, M. Meinshausen, M. Mengel, N. Braun, and W. Hare. A Scaling Approach to Probabilistic Assessment of Regional Climate Change. *Journal of Climate*, 25(9): 3117–3144, 2012. doi: 10.1175/JCLI-D-11-00199.1.

S. Fritz, L. See, I. Mccallum, L. You, A. Bun, E. Moltchanova, M. Duerauer, F. Albrecht, C. Schill, C. Perger, P. Havlik, A. Mosnier, P. Thornton, U. Wood-Sichra, M. Herrero, I. Becker-Reshef, C. Justice, M. Hansen, P. Gong, S. Abdel Aziz, A. Cipriani, R. Cumani, G. Cecchi, G. Conchedda, S. Ferreira, A. Gomez, M. Haffani, F. Kayitakire, J. Malanding, R. Mueller, T. Newby, A. Nonguierma, A. Olusegun, S. Ortner, D. R. Rajak, J. Rocha, D. Schepaschenko, M. Schepaschenko, A. Terekhov, A. Tiangwa, C. Vancutsem, E. Vintrou, W. Wenbin, M. van der Velde, A. Dunwoody, F. Kraxner, and M. Obersteiner. Mapping global cropland and field size. *Global Change Biology*, 21 (5):1980–1992, 2015. doi: 10.1111/gcb.12838.

F. Fung, A. Lopez, and M. New. Water availability in +2 °C and +4 °C worlds. *Philosophical Transactions of the Royal Society A: Mathematical, Physical and Engineering Sciences*, 369(1934):99–116, 2011. doi: 10.1098/rsta.2010.0293.

H.-M. Füssel. *Impacts analysis for inverse integrated assessments of climate change.* Ph.d thesis, Potsdam University, Potsdam, Germany, Potsdam, Germany, 2003.

H.-M. Füssel, J. Heinke, A. Popp, and D. Gerten. Climate Change and Water Supply. In *Climate Change, Justice and Sustainability*, pages 19–32. Springer Netherlands, Dordrecht, 2012. doi: 10.1007/978-94-007-4540-7_3.

S. Gerber, F. Joos, and I. C. Prentice. Sensitivity of a dynamic global vegetation model to climate and atmospheric CO2. *Global Change Biology*, 10(8):1223–1239, 2004. doi: 10.1111/j.1529-8817.2003.00807.x.

D. Gerten, S. Schaphoff, and W. Lucht. Potential future changes in water limitations of the terrestrial biosphere. *Climatic Change*, 80(3-4):277–299, 2007. doi: 10.1007/s10584-006-9104-8.

D. Gerten, S. Rost, W. von Bloh, and W. Lucht. Causes of change in 20th century global river discharge. *Geophysical Research Letters*, 35(20):L20405, 2008. doi: 10.1029/2008GL035258.

D. Gerten, J. Heinke, H. Hoff, H. Biemans, M. Fader, and K. Waha. Global Water Availability and Requirements for Future Food Production. *Journal of Hydrometeorology*, 12 (5):885–899, 2011. doi: 10.1175/2011JHM1328.1.

D. Gerten, W. Lucht, S. Ostberg, J. Heinke, M. Kowarsch, H. Kreft, Z. W. Kundzewicz, J. Rastgooy, R. Warren, and H. J. Schellnhuber. Asynchronous exposure to global warming: freshwater resources and terrestrial ecosystems. *Environmental Research Letters*, 8 (3):034032, 2013. doi: 10.1088/1748-9326/8/3/034032.

P. J. Gleckler, K. E. Taylor, and C. Doutriaux. Performance metrics for climate models. *Journal of Geophysical Research*, 113(D6):D06104, 2008. doi: 10.1029/2007JD008972.

P. H. Gleick. Basic Water Requirements for Human Activities: Meeting Basic Needs. *Water International*, 21(2):83–92, 1996. doi: 10.1080/02508069608686494.

H. C. J. Godfray, J. R. Beddington, I. R. Crute, L. Haddad, D. Lawrence, J. F. Muir, J. Pretty, S. Robinson, S. M. Thomas, and C. Toulmin. Food Security: The Challenge of Feeding 9 Billion People. *Science*, 327(5967):812–818, 2010. doi: 10.1126/science.1185383.

S. N. Gosling and N. W. Arnell. Simulating current global river runoff with a global hydrological model: model revisions, validation, and sensitivity analysis. *Hydrological Processes*, 25(7):1129–1145, 2011. doi: 10.1002/hyp.7727.

S. N. Gosling and N. W. Arnell. A global assessment of the impact of climate change on water scarcity. *Climatic Change*, 134(3):371–385, 2016. doi: 10.1007/s10584-013-0853-x.

S. N. Gosling, D. Bretherton, K. Haines, and N. W. Arnell. Global hydrology modelling and uncertainty: running multiple ensembles with a campus grid. *Philosophical Transactions of the Royal Society A: Mathematical, Physical and Engineering Sciences*, 368(1926): 4005–4021, 2010. doi: 10.1098/rsta.2010.0164.

S. N. Gosling, R. G. Taylor, N. W. Arnell, and M. C. Todd. A comparative analysis of projected impacts of climate change on river runoff from global and catchment-scale hydrological models. *Hydrology and Earth System Sciences*, 15(1):279–294, 2011. doi: 10.5194/hess-15-279-2011.

N. T. Graham, E. G. R. Davies, M. I. Hejazi, K. Calvin, S. H. Kim, L. Helinski, F. R. Miralles-Wilhelm, L. Clarke, P. Kyle, P. Patel, M. A. Wise, and C. R. Vernon. Water Sector Assumptions for the Shared Socioeconomic Pathways in an Integrated Modeling Framework. *Water Resources Research*, 54(9):6423–6440, 2018. doi: 10.1029/2018WR023452.

G. Grill, B. Lehner, M. Thieme, B. Geenen, D. Tickner, F. Antonelli, S. Babu, P. Borrelli, L. Cheng, H. Crochetiere, H. Ehalt Macedo, R. Filgueiras, M. Goichot, J. Higgins, Z. Hogan, B. Lip, M. E. McClain, J. Meng, M. Mulligan, C. Nilsson, J. D. Olden, J. J. Opperman, P. Petry, C. Reidy Liermann, L. Sáenz, S. Salinas-Rodríguez, P. Schelle, R. J. P. Schmitt, J. Snider, F. Tan, K. Tockner, P. H. Valdujo, A. van Soesbergen, and C. Zarfl. Mapping the world's free-flowing rivers. *Nature*, 569(7755):215–221, 2019. doi: 10.1038/s41586-019-1111-9.

A. Grübler, B. O'Neill, K. Riahi, V. Chirkov, A. Goujon, P. Kolp, I. Prommer, S. Scherbov, and E. Slentoe. Regional, national, and spatially explicit scenarios of demographic and economic change based on SRES. *Technological Forecasting and Social Change*, 74(7): 980–1029, 2007. doi: 10.1016/j.techfore.2006.05.023.

I. Haddeland, T. Skaugen, and D. P. Lettenmaier. Anthropogenic impacts on continental surface water fluxes. *Geophysical Research Letters*, 33(8):L08406, 2006. doi: 10.1029/2006GL026047.

I. Haddeland, D. B. Clark, W. Franssen, F. Ludwig, F. Voß, N. W. Arnell, N. Bertrand, M. Best, S. Folwell, D. Gerten, S. Gomes, S. N. Gosling, S. Hagemann, N. Hanasaki,

R. Harding, J. Heinke, P. Kabat, S. Koirala, T. Oki, J. Polcher, T. Stacke, P. Viterbo, G. P. Weedon, and P. Yeh. Multimodel Estimate of the Global Terrestrial Water Balance: Setup and First Results. *Journal of Hydrometeorology*, 12(5):869–884, 2011. doi: 10.1175/2011JHM1324.1.

I. Haddeland, J. Heinke, F. Voß, S. Eisner, C. Chen, S. Hagemann, and F. Ludwig. Effects of climate model radiation, humidity and wind estimates on hydrological simulations. *Hydrology and Earth System Sciences*, 16(2):305–318, 2012. doi: 10.5194/hess-16-305-2012.

I. Haddeland, J. Heinke, H. Biemans, S. Eisner, M. Flörke, N. Hanasaki, M. Konzmann, F. Ludwig, Y. Masaki, J. Schewe, T. Stacke, Z. D. Tessler, Y. Wada, and D. Wisser. Global water resources affected by human interventions and climate change. *Proceedings of the National Academy of Sciences of the United States of America*, 111(9):3251–6, 2014. doi: 10.1073/pnas.1222475110.

S. Hagemann and L. D. Gates. Improving a subgrid runoff parameterization scheme for climate models by the use of high resolution data derived from satellite observations. *Climate Dynamics*, 21(3-4):349–359, 2003. doi: 10.1007/s00382-003-0349-x.

S. Hagemann, C. Chen, J. O. Haerter, J. Heinke, D. Gerten, and C. Piani. Impact of a Statistical Bias Correction on the Projected Hydrological Changes Obtained from Three GCMs and Two Hydrology Models. *Journal of Hydrometeorology*, 12(4):556–578, 2011. doi: 10.1175/2011JHM1336.1.

S. Hagemann, C. Chen, D. B. Clark, S. Folwell, S. N. Gosling, I. Haddeland, N. Hanasaki, J. Heinke, F. Ludwig, F. Voß, and A. J. Wiltshire. Climate change impact on available water resources obtained using multiple global climate and hydrology models. *Earth System Dynamics Discussions*, 3(2):1321–1345, 2012. doi: 10.5194/esdd-3-1321-2012.

S. Hagemann, C. Chen, D. B. Clark, S. Folwell, S. N. Gosling, I. Haddeland, N. Hanasaki, J. Heinke, F. Ludwig, F. Voss, and A. J. Wiltshire. Climate change impact on available water resources obtained using multiple global climate and hydrology models. *Earth System Dynamics*, 4(1):129–144, 2013. doi: 10.5194/esd-4-129-2013.

A. Haileslassie, D. Peden, S. Gebreselassie, T. Amede, and K. Descheemaeker. Livestock water productivity in mixed crop–livestock farming systems of the Blue Nile basin: Assessing variability and prospects for improvement. *Agricultural Systems*, 102(1-3):33–40, 2009. doi: 10.1016/j.agsy.2009.06.006.

S. Hallegatte. Strategies to adapt to an uncertain climate change. *Global Environmental Change*, 19(2):240–247, 2009. doi: 10.1016/j.gloenvcha.2008.12.003.

N. Hanasaki, S. Kanae, and T. Oki. A reservoir operation scheme for global river routing models. *Journal of Hydrology*, 327(1-2):22–41, 2006. doi: 10.1016/j.jhydrol.2005.11.011.

N. Hanasaki, S. Kanae, T. Oki, K. Masuda, K. Motoya, N. Shirakawa, Y. Shen, and K. Tanaka. An integrated model for the assessment of global water resources – Part 1: Model description and input meteorological forcing. *Hydrology and Earth System Sciences*, 12(4):1007–1025, 2008a. doi: 10.5194/hess-12-1007-2008.

N. Hanasaki, S. Kanae, T. Oki, K. Masuda, K. Motoya, N. Shirakawa, Y. Shen, and K. Tanaka. An integrated model for the assessment of global water resources – Part 2: Applications and assessments. *Hydrology and Earth System Sciences*, 12(4):1027–1037, 2008b. doi: 10.5194/hess-12-1027-2008.

N. Hanasaki, T. Inuzuka, S. Kanae, and T. Oki. An estimation of global virtual water flow and sources of water withdrawal for major crops and livestock products using a global hydrological model. *Journal of Hydrology*, 384(3-4):232–244, 2010. doi: 10.1016/j.jhydrol.2009.09.028.

R. Harding, M. Best, E. Blyth, S. Hagemann, P. Kabat, L. M. Tallaksen, T. Warnaars, D. Wiberg, G. P. Weedon, H. van Lanen, F. Ludwig, and I. Haddeland. WATCH: Current Knowledge of the Terrestrial Global Water Cycle. *Journal of Hydrometeorology*, 12(6):1149–1156, 2011. doi: 10.1175/JHM-D-11-024.1.

I. Harris, P. Jones, T. Osborn, and D. Lister. Updated high-resolution grids of monthly climatic observations - the CRU TS3.10 Dataset. *International Journal of Climatology*, 34(3):623–642, 2014. doi: 10.1002/joc.3711.

D. Hartmann, A. Klein Tank, M. Rusticucci, L. Alexander, S. Brönnimann, Y. Charabi, F. Dentener, E. Dlugokencky, D. Easterling, A. Kaplan, B. Soden, P. Thorne, M. Wild, and P. Zhai. Observations: Atmosphere and Surface. In T. Stocker, D. Qin, G.-K. Plattner, M. Tignor, S. Allen, J. Boschung, A. Nauels, Y. Xia, V. Bex, and P. Midgley, editors, *Climate Change 2013: The Physical Science Basis. Contribution of Working Group I to the Fifth Assessment Report of the Intergovernmental Panel on Climate Change*, chapter 2. Cambridge University Press, Cambridge, United Kingdom and New York, NY, USA, 2013.

J. L. Hatfield and J. H. Prueger. Temperature extremes: Effect on plant growth and development. *Weather and Climate Extremes*, 10:4–10, 2015. doi: 10.1016/j.wace.2015.08.001.

P. Havlík, H. Valin, M. Herrero, M. Obersteiner, E. Schmid, M. C. Rufino, A. Mosnier, P. K. Thornton, H. Böttcher, R. T. Conant, S. Frank, S. Fritz, S. Fuss, F. Kraxner,

and A. Notenbaert. Climate change mitigation through livestock system transitions. *Proceedings of the National Academy of Sciences*, 111(10):3709–3714, 2014. doi: 10.1073/pnas.1308044111.

E. Hawkins and R. Sutton. The Potential to Narrow Uncertainty in Regional Climate Predictions. *Bulletin of the American Meteorological Society*, 90(8):1095–1107, 2009. doi: 10.1175/2009BAMS2607.1.

E. Hawkins and R. Sutton. The potential to narrow uncertainty in projections of regional precipitation change. *Climate Dynamics*, 37(1-2):407–418, 2011. doi: 10.1007/s00382-010-0810-6.

V. Heck, D. Gerten, W. Lucht, and A. Popp. Biomass-based negative emissions difficult to reconcile with planetary boundaries. *Nature Climate Change*, 8(2):151–155, 2018. doi: 10.1038/s41558-017-0064-y.

J. Heinke, S. Ostberg, S. Schaphoff, K. Frieler, C. Müller, D. Gerten, M. Meinshausen, and W. Lucht. A new dataset for systematic assessments of climate change impacts as a function of global warming. *Geoscientific Model Development Discussions*, 5(4):3533–3572, 2012. doi: 10.5194/gmdd-5-3533-2012.

J. Heinke, S. Ostberg, S. Schaphoff, K. Frieler, C. Müller, D. Gerten, M. Meinshausen, and W. Lucht. A new climate dataset for systematic assessments of climate change impacts as a function of global warming. *Geoscientific Model Development*, 6(5):1689–1703, 2013a. doi: 10.5194/gmd-6-1689-2013.

J. Heinke, S. Ostberg, S. Schaphoff, K. Frieler, C. Müller, D. Gerten, M. Meinshausen, and W. Lucht. PanClim future climate scenarios: PanClim: A new climate dataset for systematic assessments of climate change impacts as a function of global warming, 2013b. Available at `http://www.panclim.org`, accessed 5 February 2019.

J. Heinke, C. Müller, M. Lannerstad, D. Gerten, and W. Lucht. Freshwater resources under success and failure of the Paris climate agreement. *Earth System Dynamics*, 10(2):205–217, 2019a. doi: 10.5194/esd-10-205-2019.

J. Heinke, C. Müller, M. Lannerstad, D. Gerten, and W. Lucht. *Core output: Freshwater resources under success and failure of the Paris climate agreement [Dataset]*. Zenodo, 2019b. doi: 10.5281/zenodo.2562056.

J. Heinke, M. Lannerstad, D. Gerten, P. Havlík, M. Herrero, A. Notenbaert, H. Hoff, and C. Müller. Water use in global livestock production—opportunities and constraints for increasing water productivity. *Water Resources Research*, submitted.

S. Hempel, K. Frieler, L. Warszawski, J. Schewe, and F. Piontek. A trend-preserving bias correction – the ISI-MIP approach. *Earth System Dynamics*, 4(2):219–236, 2013. doi: 10.5194/esd-4-219-2013.

M. Herrero, P. Thornton, R. Kruska, and R. Reid. Systems dynamics and the spatial distribution of methane emissions from African domestic ruminants to 2030. *Agriculture, Ecosystems & Environment*, 126(1-2):122–137, 2008. doi: 10.1016/j.agee.2008.01.017.

M. Herrero, P. Havlik, H. Valin, A. Notenbaert, M. C. Rufino, P. K. Thornton, M. Blummel, F. Weiss, D. Grace, and M. Obersteiner. Biomass use, production, feed efficiencies, and greenhouse gas emissions from global livestock systems. *Proceedings of the National Academy of Sciences*, 110(52):20888–20893, 2013. doi: 10.1073/pnas.1308149110.

U. Heyder, S. Schaphoff, D. Gerten, and W. Lucht. Risk of severe climate change impact on the terrestrial biosphere. *Environmental Research Letters*, 6(3):034036, 2011. doi: 10.1088/1748-9326/6/3/034036.

M. M. Hirschmann. Water, Melting, and the Deep Earth H2O Cycle. *Annual Review of Earth and Planetary Sciences*, 34(1):629–653, 2006. doi: 10.1146/annurev.earth.34.031405.125211.

A. Y. Hoekstra and M. M. Mekonnen. The water footprint of humanity. *Proceedings of the National Academy of Sciences*, 109(9):3232–3237, 2012. doi: 10.1073/pnas.1109936109.

H. Hoff, M. Falkenmark, D. Gerten, L. Gordon, L. Karlberg, and J. Rockström. Greening the global water system. *Journal of Hydrology*, 384(3-4):177–186, 2010. doi: 10.1016/j.jhydrol.2009.06.026.

J. R. M. Hosking and J. R. Wallis. A Comparison of Unbiased and Plotting-Position Estimators of L Moments. *Water Resources Research*, 31(8):2019–2025, 1995. doi: 10.1029/95WR01230.

M. Hulme, T. Jiang, and T. Wigley. *SCENGEN: A Climate Change SCENario GENerator. Software User Manual, Version 1.0.* Climatic Research Unit, University of East Anglia, Norwich, UK, 1995.

C. Huntingford and P. M. Cox. An analogue model to derive additional climate change scenarios from existing GCM simulations. *Climate Dynamics*, 16(8):575–586, 2000. doi: 10.1007/s003820000067.

IIASA/FAO. *Global Agro-ecological Zones (GAEZ v3.0).* IIASA, Laxenburg, Austria and FAO, Rome, Italy, 2012.

Institute of Medicine. *Dietary Reference Intakes: The Essential Guide to Nutrient Requirements*. The National Academies Press, Washington, D.C., 2006. ISBN 978-0-309-15742-1. doi: 10.17226/11537.

International Commission of Large Dams (ICOLD). *World Register of Dams*. International Commission of Large Dams, Paris, France, 2007.

International Council for Science (ICSU). *A guide to SDG interactions: from science to implementation*. International Council for Science, Paris, 2017. doi: 10.24948/2017.01.

Inter-Sectoral Impact Model Intercomparison Project (ISIMIP). Population & GDP, 2012. Available at `https://www.isimip.org/gettingstarted/details/13/`, accessed 5 February 2019.

IPCC. *Climate Change 2007: The Physical Science Basis. Contribution of Working Group I to the Fourth Assessment Report of the Intergovernmental Panel on Climate Change*. Cambridge University Press, Cambridge, UK and New York, USA, 2007a.

IPCC. *Climate Change 2007: Impacts, Adaptation and Vulnerability. Contribution of Working Group II to the Fourth Assessment Report of the IPCC*. Cambridge University Press, Cambridge, UK, 2007b. ISBN 9780521880107.

IPCC. *Climate Change 2014: Impacts, Adaptation, and Vulnerability. Part A: Global and Sectoral Aspects. Contribution of Working Group II to the Fifth Assessment Report of the Intergovernmental Panel on Climate Change*. Cambridge University Press, Cambridge, United Kingdom and New York, NY, USA, 2014. ISBN 978-1-107-64165-5.

J. Jägermeyr, D. Gerten, S. Schaphoff, J. Heinke, W. Lucht, and J. Rockström. Integrated crop water management might sustainably halve the global food gap. *Environmental Research Letters*, 11(2):025002, 2016. doi: 10.1088/1748-9326/11/2/025002.

R. James, R. Washington, C.-F. Schleussner, J. Rogelj, and D. Conway. Characterizing half-a-degree difference: a review of methods for identifying regional climate responses to global warming targets. *Wiley Interdisciplinary Reviews: Climate Change*, 8(2):e457, 2017. doi: 10.1002/wcc.457.

E. Jéquier and F. Constant. Water as an essential nutrient: the physiological basis of hydration. *European Journal of Clinical Nutrition*, 64(2):115–123, 2010. doi: 10.1038/ejcn.2009.111.

B. Jiménez Cisneros, T. Oki, N. Arnell, G. Benito, J. Cogley, P. Döll, T. Jiang, and S. Mwakalila. Freshwater resources. In C. Field, V. Barros, D. Dokken, K. Mach, M. Mastrandrea, T. Bilir, M. Chatterjee, K. Ebi, Y. Estrada, R. Genova, B. Girma, E. Kissel,

A. Levy, S. MacCracken, P. Mastrandrea, and L. White, editors, *Climate Change 2014: Impacts, Adaptation, and Vulnerability. Part A: Global and Sectoral Aspects. Contribution of Working Group II to the Fifth Assessment Report of the Intergovernmental Panel on Climate Change*, pages 229–269. Cambridge University Press, Cambridge, United Kingdom and New York, NY, USA, 2014.

B. Jones and B. C. O'Neill. Spatially explicit global population scenarios consistent with the Shared Socioeconomic Pathways. *Environmental Research Letters*, 11(8):084003, 2016. doi: 10.1088/1748-9326/11/8/084003.

B. Jones and B. C. O'Neill. *Global Population Projection Grids Based on Shared Socioeconomic Pathways (SSPs), 2010–2100.* NASA Socioeconomic Data and Applications Center (SEDAC), Palisades, NY, USA, 2017. doi: 10.7927/H4RF5S0P.

M. Jung, M. Reichstein, P. Ciais, S. I. Seneviratne, J. Sheffield, M. L. Goulden, G. Bonan, A. Cescatti, J. Chen, R. de Jeu, A. J. Dolman, W. Eugster, D. Gerten, D. Gianelle, N. Gobron, J. Heinke, J. Kimball, B. E. Law, L. Montagnani, Q. Mu, B. Mueller, K. Oleson, D. Papale, A. D. Richardson, O. Roupsard, S. Running, E. Tomelleri, N. Viovy, U. Weber, C. Williams, E. Wood, S. Zaehle, and K. Zhang. Recent decline in the global land evapotranspiration trend due to limited moisture supply. *Nature*, 467(7318): 951–954, 2010. doi: 10.1038/nature09396.

E. Kampragou, D. F. Lekkas, and D. Assimacopoulos. Water demand management: implementation principles and indicative case studies. *Water and Environment Journal*, 25 (4):466–476, 2011. doi: 10.1111/j.1747-6593.2010.00240.x.

J. Kattge, S. Díaz, S. Lavorel, I. C. Prentice, P. Leadley, G. Bönisch, E. Garnier, M. Westoby, P. B. Reich, I. J. Wright, J. H. Cornelissen, C. Violle, S. P. Harrison, P. M. Van Bodegom, M. Reichstein, B. J. Enquist, N. A. Soudzilovskaia, D. D. Ackerly, M. Anand, O. Atkin, M. Bahn, T. R. Baker, D. Baldocchi, R. Bekker, C. C. Blanco, B. Blonder, W. J. Bond, R. Bradstock, D. E. Bunker, F. Casanoves, J. Cavender-Bares, J. Q. Chambers, F. S. Chapin, J. Chave, D. Coomes, W. K. Cornwell, J. M. Craine, B. H. Dobrin, L. Duarte, W. Durka, J. Elser, G. Esser, M. Estiarte, W. F. Fagan, J. Fang, F. Fernández-Méndez, A. Fidelis, B. Finegan, O. Flores, H. Ford, D. Frank, G. T. Freschet, N. M. Fyllas, R. V. Gallagher, W. A. Green, A. G. Gutierrez, T. Hickler, S. I. Higgins, J. G. Hodgson, A. Jalili, S. Jansen, C. A. Joly, A. J. Kerkhoff, D. Kirkup, K. Kitajima, M. Kleyer, S. Klotz, J. M. Knops, K. Kramer, I. Kühn, H. Kurokawa, D. Laughlin, T. D. Lee, M. Leishman, F. Lens, T. Lenz, S. L. Lewis, J. Lloyd, J. Llusià, F. Louault, S. Ma, M. D. Mahecha, P. Manning, T. Massad, B. E. Medlyn, J. Messier, A. T. Moles, S. C. Müller, K. Nadrowski, S. Naeem, Ü. Niinemets, S. Nöllert, A. Nüske, R. Ogaya, J. Oleksyn, V. G. Onipchenko, Y. Onoda, J. Ordoñez, G. Overbeck, W. A. Ozinga,

S. Patiño, S. Paula, J. G. Pausas, J. Peñuelas, O. L. Phillips, V. Pillar, H. Poorter, L. Poorter, P. Poschlod, A. Prinzing, R. Proulx, A. Rammig, S. Reinsch, B. Reu, L. Sack, B. Salgado-Negret, J. Sardans, S. Shiodera, B. Shipley, A. Siefert, E. Sosinski, J. F. Soussana, E. Swaine, N. Swenson, K. Thompson, P. Thornton, M. Waldram, E. Weiher, M. White, S. White, S. J. Wright, B. Yguel, S. Zaehle, A. E. Zanne, and C. Wirth. TRY - a global database of plant traits. *Global Change Biology*, 17(9):2905–2935, 2011. doi: 10.1111/j.1365-2486.2011.02451.x.

N. R. Kaye, A. Hartley, and D. Hemming. Mapping the climate: guidance on appropriate techniques to map climate variables and their uncertainty. *Geoscientific Model Development*, 5(1):245–256, 2012. doi: 10.5194/gmd-5-245-2012.

S. KC and W. Lutz. The human core of the shared socioeconomic pathways: Population scenarios by age, sex and level of education for all countries to 2100. *Global Environmental Change*, 42:181–192, 2017. doi: 10.1016/j.gloenvcha.2014.06.004.

R. Knutti and J. Sedláček. Robustness and uncertainties in the new CMIP5 climate model projections. *Nature Climate Change*, 3(4):369–373, 2013. doi: 10.1038/nclimate1716.

R. Knutti, R. Furrer, C. Tebaldi, J. Cermak, and G. A. Meehl. Challenges in Combining Projections from Multiple Climate Models. *Journal of Climate*, 23(10):2739–2758, 2010. doi: 10.1175/2009JCLI3361.1.

M. Konzmann, D. Gerten, and J. Heinke. Climate impacts on global irrigation requirements under 19 GCMs, simulated with a vegetation and hydrology model. *Hydrological Sciences Journal*, 58(1):88–105, 2013. doi: 10.1080/02626667.2013.746495.

M. Kummu, P. J. Ward, H. de Moel, and O. Varis. Is physical water scarcity a new phenomenon? Global assessment of water shortage over the last two millennia. *Environmental Research Letters*, 5(3):034006, 2010. doi: 10.1088/1748-9326/5/3/034006.

M. Kummu, J. H. A. Guillaume, H. de Moel, S. Eisner, M. Flörke, M. Porkka, S. Siebert, T. I. E. Veldkamp, and P. J. Ward. The world's road to water scarcity: shortage and stress in the 20th century and pathways towards sustainability. *Scientific Reports*, 6(1): 38495, 2016. doi: 10.1038/srep38495.

Z. W. Kundzewicz, L. J. Mata, N. W. Arnell, P. Döll, B. Jimenez, K. Miller, T. Oki, Z. Şen, and I. Shiklomanov. The implications of projected climate change for freshwater resources and their management. *Hydrological Sciences Journal*, 53(1):3–10, 2008. doi: 10.1623/hysj.53.1.3.

F. H. Lambert and J. C. H. Chiang. Control of land-ocean temperature contrast by ocean heat uptake. *Geophysical Research Letters*, 34(13):L13704, 2007. doi: 10.1029/2007GL029755.

T. S. L'Ecuyer, H. K. Beaudoing, M. Rodell, W. Olson, B. Lin, S. Kato, C. A. Clayson, E. Wood, J. Sheffield, R. Adler, G. Huffman, M. Bosilovich, G. Gu, F. Robertson, P. R. Houser, D. Chambers, J. S. Famiglietti, E. Fetzer, W. T. Liu, X. Gao, C. A. Schlosser, E. Clark, D. P. Lettenmaier, and K. Hilburn. The Observed State of the Energy Budget in the Early Twenty-First Century. *Journal of Climate*, 28(21):8319–8346, 2015. doi: 10.1175/JCLI-D-14-00556.1.

B. Lehner, C. R. Liermann, C. Revenga, C. Vörösmarty, B. Fekete, P. Crouzet, P. Döll, M. Endejan, K. Frenken, J. Magome, C. Nilsson, J. C. Robertson, R. Rödel, N. Sindorf, and D. Wisser. High-resolution mapping of the world's reservoirs and dams for sustainable river-flow management. *Frontiers in Ecology and the Environment*, 9(9):494–502, 2011. doi: 10.1890/100125.

S. L. Lewis and M. A. Maslin. Defining the Anthropocene. *Nature*, 519(7542):171–180, 2015. doi: 10.1038/nature14258.

X. Liang, D. P. Lettenmaier, E. F. Wood, and S. J. Burges. A simple hydrologically based model of land surface water and energy fluxes for general circulation models. *Journal of Geophysical Research*, 99(D7):14415, 1994. doi: 10.1029/94JD00483.

J. Liu and H. Yang. Spatially explicit assessment of global consumptive water uses in cropland: Green and blue water. *Journal of Hydrology*, 384(3-4):187–197, 2010. doi: 10.1016/j.jhydrol.2009.11.024.

D. Lohmann, E. Raschke, B. Nijssen, and D. P. Lettenmaier. Regional scale hydrology: I. Formulation of the VIC-2L model coupled to a routing model. *Hydrological Sciences Journal*, 43(1):131–141, 1998. doi: 10.1080/02626669809492107.

F. Lutz, T. Herzfeld, J. Heinke, S. Rolinski, S. Schaphoff, W. von Bloh, J. J. Stoorvogel, and C. Müller. Simulating the effect of tillage practices with the global ecosystem model LPJmL (version 5.0-tillage). *Geoscientific Model Development*, 12(6):2419–2440, 2019. doi: 10.5194/gmd-12-2419-2019.

K. D. Mankoff, W. Colgan, A. Solgaard, N. B. Karlsson, A. P. Ahlstrøm, D. van As, J. E. Box, S. A. Khan, K. K. Kjeldsen, J. Mouginot, and R. S. Fausto. Greenland Ice Sheet solid ice discharge from 1986 through 2017. *Earth System Science Data*, 11(2):769–786, 2019. doi: 10.5194/essd-11-769-2019.

M. E. Mann. Defining dangerous anthropogenic interference. *Proceedings of the National Academy of Sciences*, 106(11):4065–4066, 2009. doi: 10.1073/pnas.0901303106.

M. D. Mastrandrea, K. J. Mach, G.-K. Plattner, O. Edenhofer, T. F. Stocker, C. B. Field, K. L. Ebi, and P. R. Matschoss. The IPCC AR5 guidance note on consistent treatment of uncertainties: a common approach across the working groups. *Climatic Change*, 108 (4):675–691, 2011. doi: 10.1007/s10584-011-0178-6.

G. Meehl, T. Stocker, W. Collins, P. Friedlingstein, A. Gaye, J. Gregory, A. Kitoh, R. Knutti, J. Murphy, A. Noda, S. Raper, I. Watterson, A. Weaver, and Z.-C. Zhao. Global Climate Projections. In S. Solomon, D. Qin, M. Manning, Z. Chen, M. Marquis, K. Averyt, M. Tignor, and H. Miller, editors, *Climate Change 2007: The Physical Science Basis. Contribution of Working Group I to the Fourth Assessment Report of the Intergovernmental Panel on Climate Change*, chapter 10, pages 747–846. Cambridge University Press, Cambridge, UK and New York, NY, USA, 2007a.

G. A. Meehl. Global Coupled General Circulation Models. *Bulletin of the American Meteorological Society*, 76(6):951–957, 1995.

G. A. Meehl, G. J. Boer, C. Covey, M. Latif, and R. J. Stouffer. The Coupled Model Intercomparison Project (CMIP). *Bulletin of the American Meteorological Society*, 81 (2):313–318, 2000. doi: 10.1175/1520-0477(2000)081<0313:TCMIPC>2.3.CO;2.

G. A. Meehl, C. Covey, K. E. Taylor, T. Delworth, R. J. Stouffer, M. Latif, B. McAvaney, and J. F. B. Mitchell. The WCRP CMIP3 Multimodel Dataset: A New Era in Climate Change Research. *Bulletin of the American Meteorological Society*, 88(9):1383–1394, 2007b. doi: 10.1175/BAMS-88-9-1383.

M. Meinshausen, B. Hare, T. M. L. Wigley, D. Van Vuuren, M. G. J. Den Elzen, and R. Swart. Multi-gas Emissions Pathways to Meet Climate Targets. *Climatic Change*, 75 (1-2):151–194, 2006. doi: 10.1007/s10584-005-9013-2.

M. Meinshausen, N. Meinshausen, W. Hare, S. C. B. Raper, K. Frieler, R. Knutti, D. J. Frame, and M. R. Allen. Greenhouse-gas emission targets for limiting global warming to 2 degrees C. *Nature*, 458(7242):1158–62, 2009. doi: 10.1038/nature08017.

M. Meinshausen, S. C. B. Raper, and T. M. L. Wigley. Emulating coupled atmosphere-ocean and carbon cycle models with a simpler model, MAGICC6 – Part 1: Model description and calibration. *Atmospheric Chemistry and Physics*, 11(4):1417–1456, 2011a. doi: 10.5194/acp-11-1417-2011.

M. Meinshausen, S. J. Smith, K. Calvin, J. S. Daniel, M. L. T. Kainuma, J.-F. Lamarque, K. Matsumoto, S. A. Montzka, S. C. B. Raper, K. Riahi, A. Thomson, G. J. M.

Velders, and D. P. P. van Vuuren. The RCP greenhouse gas concentrations and their extensions from 1765 to 2300. *Climatic Change*, 109(1-2):213–241, 2011b. doi: 10.1007/s10584-011-0156-z.

M. M. Mekonnen and A. Y. Hoekstra. The green, blue and grey water footprint of crops and derived crop products. *Hydrology and Earth System Sciences*, 15(5):1577–1600, 2011. doi: 10.5194/hess-15-1577-2011.

M. M. Mekonnen and A. Y. Hoekstra. A Global Assessment of the Water Footprint of Farm Animal Products. *Ecosystems*, 15(3):401–415, 2012. doi: 10.1007/s10021-011-9517-8.

P. C. D. Milly, K. a. Dunne, and a. V. Vecchia. Global pattern of trends in streamflow and water availability in a changing climate. *Nature*, 438(7066):347–50, 2005. doi: 10.1038/nature04312.

P. C. D. Milly, J. Betancourt, M. Falkenmark, R. M. Hirsch, Z. W. Kundzewicz, D. P. Lettenmaier, and R. J. Stouffer. Stationarity Is Dead: Whither Water Management? *Science*, 319(5863):573–574, 2008. doi: 10.1126/science.1151915.

T. D. Mitchell. Pattern scaling: an examination of the accuracy of the technique for describing future climates. *Climatic Change*, 60(3):217–242, 2003. doi: 10.1023/A:1026035305597.

D. Molden, editor. *Water for Food, Water for Life: A Comprehensive Assessment of Water Management in Agriculture*. Earthscan, London, 2007. ISBN 9781844073962.

C. Monfreda, N. Ramankutty, and J. A. Foley. Farming the planet: 2. Geographic distribution of crop areas, yields, physiological types, and net primary production in the year 2000. *Global Biogeochemical Cycles*, 22(1):1–19, 2008. doi: 10.1029/2007GB002947.

R. H. Moss, J. A. Edmonds, K. A. Hibbard, M. R. Manning, S. K. Rose, D. P. van Vuuren, T. R. Carter, S. Emori, M. Kainuma, T. Kram, G. A. Meehl, J. F. B. Mitchell, N. Nakicenovic, K. Riahi, S. J. Smith, R. J. Stouffer, A. M. Thomson, J. P. Weyant, and T. J. Wilbanks. The next generation of scenarios for climate change research and assessment. *Nature*, 463(7282):747–756, 2010. doi: 10.1038/nature08823.

N. D. Mueller, J. S. Gerber, M. Johnston, D. K. Ray, N. Ramankutty, and J. a. Foley. Closing yield gaps through nutrient and water management. *Nature*, 490(7419):254–7, 2012. doi: 10.1038/nature11420.

C. Müller, W. Cramer, W. L. Hare, and H. Lotze-Campen. Climate change risks for African agriculture. *Proceedings of the National Academy of Sciences*, 108(11):4313–4315, 2011. doi: 10.1073/pnas.1015078108.

S. J. Murray, P. N. Foster, and I. C. Prentice. Future global water resources with respect to climate change and water withdrawals as estimated by a dynamic global vegetation model. *Journal of Hydrology*, 448-449:14–29, 2012. doi: 10.1016/j.jhydrol.2012.02.044.

A. Nardone, B. Ronchi, N. Lacetera, and U. Bernabucci. Climatic Effects on Productive Traits in Livestock. *Veterinary Research Communications*, 30(S1):75–81, 2006. doi: 10.1007/s11259-006-0016-x.

M. New, M. Hulme, and P. Jones. Representing Twentieth-Century Space-Time Climate Variability. Part II: Development of 1901–96 Monthly Grids of Terrestrial Surface Climate. *Journal of Climate*, 13(13):2217–2238, 2000. doi: 10.1175/1520-0442(2000)013<2217:RTCSTC>2.0.CO;2.

M. New, D. Liverman, H. Schroder, and K. Anderson. Four degrees and beyond: the potential for a global temperature increase of four degrees and its implications. *Philosophical Transactions of the Royal Society A: Mathematical, Physical and Engineering Sciences*, 369(1934):6–19, 2011. doi: 10.1098/rsta.2010.0303.

B. Nijssen, G. M. O'Donnell, A. F. Hamlet, and D. P. Lettenmaier. Hydrologic Sensitivity of Global Rivers to Climate Change. *Climatic Change*, 50(1-2):143–175, 2001. doi: 10.1023/A:1010616428763.

C. Nilsson and K. Berggren. Alterations of Riparian Ecosystems Caused by River Regulation. *BioScience*, 50(9):783, 2006. doi: 10.1641/0006-3568(2000)050[0783:AORECB]2.0.CO;2.

L. Ohlsson and A. R. Turton. *The turning of a screw: Social resource scarcity as a bottleneck in adaptation to water scarcity.* Number 1991 in Occasional Paper Series. School of Oriental and African Studies, Water Study Group, University of London, London, UK, 1999.

T. Oki, Y. Agata, S. Kanae, T. Saruhashi, D. Yang, and K. Musiake. Global assessment of current water resources using total runoff integrating pathways. *Hydrological Sciences Journal*, 46(6):983–995, 2001. doi: 10.1080/02626660109492890.

B. O'Neill, T. Carter, K. Ebi, J. Edmonds, S. Hallegatte, E. Kemp-Benedict, E. Kriegler, L. Mearns, R. Moss, K. Riahi, B. V. Ruijven, and D. V. Vuuren. Meeting Report of the Workshop on The Nature and Use of New Socioeconomic Pathways for Climate Change Research. CIRED Working Papers hal-00801931, HAL, 2012.

B. C. O'Neill, E. Kriegler, K. L. Ebi, E. Kemp-Benedict, K. Riahi, D. S. Rothman, B. J. van Ruijven, D. P. van Vuuren, J. Birkmann, K. Kok, M. Levy, and W. Solecki. The

roads ahead: Narratives for shared socioeconomic pathways describing world futures in the 21st century. *Global Environmental Change*, 42:169–180, 2017. doi: 10.1016/j.gloenvcha.2015.01.004.

T. J. Osborn, C. J. Wallace, I. C. Harris, and T. M. Melvin. Pattern scaling using ClimGen: monthly-resolution future climate scenarios including changes in the variability of precipitation. *Climatic Change*, 134(3):353–369, 2016. doi: 10.1007/s10584-015-1509-9.

T. J. Osborn, C. J. Wallace, J. A. Lowe, and D. Bernie. Performance of Pattern-Scaled Climate Projections under High-End Warming. Part I: Surface Air Temperature over Land. *Journal of Climate*, 31(14):5667–5680, 2018. doi: 10.1175/JCLI-D-17-0780.1.

T. N. Palmer, F. J. Doblas-Reyes, R. Hagedorn, and A. Weisheimer. Probabilistic prediction of climate using multi-model ensembles: From basics to applications. *Philosophical Transactions of the Royal Society B: Biological Sciences*, 360(1463):1991–1998, 2005. doi: 10.1098/rstb.2005.1750.

M. Paoletti, J. Haut, J. Plaza, and A. Plaza. Deep learning classifiers for hyperspectral imaging: A review. *ISPRS Journal of Photogrammetry and Remote Sensing*, 158 (September):279–317, 2019. doi: 10.1016/j.isprsjprs.2019.09.006.

M. Parry, N. Arnell, T. McMichael, R. Nicholls, P. Martens, S. Kovats, M. Livermore, C. Rosenzweig, A. Iglesias, and G. Fischer. Millions at risk: defining critical climate change threats and targets. *Global Environmental Change*, 11(3):181–183, 2001. doi: 10.1016/S0959-3780(01)00011-5.

S. Piao, P. Friedlingstein, P. Ciais, N. de Noblet-Ducoudre, D. Labat, and S. Zaehle. Changes in climate and land use have a larger direct impact than rising CO2 on global river runoff trends. *Proceedings of the National Academy of Sciences*, 104(39):15242–15247, 2007. doi: 10.1073/pnas.0707213104.

F. Piontek, C. Müller, T. a. M. Pugh, D. B. Clark, D. Deryng, J. Elliott, F. d. J. Colón González, M. Flörke, C. Folberth, W. Franssen, K. Frieler, A. D. Friend, S. N. Gosling, D. Hemming, N. Khabarov, H. Kim, M. R. Lomas, Y. Masaki, M. Mengel, A. Morse, K. Neumann, K. Nishina, S. Ostberg, R. Pavlick, A. C. Ruane, J. Schewe, E. Schmid, T. Stacke, Q. Tang, Z. D. Tessler, A. M. Tompkins, L. Warszawski, D. Wisser, and H. J. Schellnhuber. Multisectoral climate impact hotspots in a warming world. *Proceedings of the National Academy of Sciences*, 111(9):3233–3238, 2014. doi: 10.1073/pnas.1222471110.

A. J. Pitman, A. Arneth, and L. Ganzeveld. Regionalizing global climate models. *International Journal of Climatology*, 32(3):321–337, 2012. doi: 10.1002/joc.2279.

Y. Pokhrel, N. Hanasaki, S. Koirala, J. Cho, P. J.-F. Yeh, H. Kim, S. Kanae, and T. Oki. Incorporating Anthropogenic Water Regulation Modules into a Land Surface Model. *Journal of Hydrometeorology*, 13(1):255–269, 2012. doi: 10.1175/JHM-D-11-013.1.

R. M. Pope and E. S. Fry. Absorption spectrum (380–700 nm) of pure water II Integrating cavity measurements. *Applied Optics*, 36(33):8710, 1997. doi: 10.1364/AO.36.008710.

F. T. Portmann, S. Siebert, and P. Döll. MIRCA2000-Global monthly irrigated and rainfed crop areas around the year 2000: A new high-resolution data set for agricultural and hydrological modeling. *Global Biogeochemical Cycles*, 24(1):GB1011, 2010. doi: 10.1029/2008GB003435.

C. Prudhomme, I. Giuntoli, E. L. Robinson, D. B. Clark, N. W. Arnell, R. Dankers, B. M. Fekete, W. Franssen, D. Gerten, S. N. Gosling, S. Hagemann, D. M. Hannah, H. Kim, Y. Masaki, Y. Satoh, T. Stacke, Y. Wada, and D. Wisser. Hydrological droughts in the 21st century, hotspots and uncertainties from a global multimodel ensemble experiment. *Proceedings of the National Academy of Sciences*, 2013, 2013. doi: 10.1073/pnas.1222473110.

R Development Core Team. *R: A Language and Environment for Statistical Computing*. R Foundation for Statistical Computing, Vienna, Austria, 2011. URL `https://www.R-project.org/`.

V. Ramanathan and Y. Feng. On avoiding dangerous anthropogenic interference with the climate system: Formidable challenges ahead. *Proceedings of the National Academy of Sciences*, 105(38):14245–14250, 2008. doi: 10.1073/pnas.0803838105.

N. Ramankutty, A. T. Evan, C. Monfreda, and J. A. Foley. Farming the planet: 1. Geographic distribution of global agricultural lands in the year 2000. *Global Biogeochemical Cycles*, 22(1):GB1003, 2008. doi: 10.1029/2007GB002952.

P. D. Raskin, E. Hansen, and R. M. Margolis. Water and sustainability. *Natural Resources Forum*, 20(1):1–15, 1996. doi: 10.1111/j.1477-8947.1996.tb00629.x.

K. Riahi, D. P. van Vuuren, E. Kriegler, J. Edmonds, B. C. O'Neill, S. Fujimori, N. Bauer, K. Calvin, R. Dellink, O. Fricko, W. Lutz, A. Popp, J. C. Cuaresma, S. KC, M. Leimbach, L. Jiang, T. Kram, S. Rao, J. Emmerling, K. Ebi, T. Hasegawa, P. Havlik, F. Humpenöder, L. A. Da Silva, S. Smith, E. Stehfest, V. Bosetti, J. Eom, D. Gernaat, T. Masui, J. Rogelj, J. Strefler, L. Drouet, V. Krey, G. Luderer, M. Harmsen, K. Takahashi, L. Baumstark, J. C. Doelman, M. Kainuma, Z. Klimont, G. Marangoni, H. Lotze-Campen, M. Obersteiner, A. Tabeau, and M. Tavoni. The Shared Socioeconomic Pathways and their energy, land use, and greenhouse gas emissions implications: An overview. *Global Environmental Change*, 42:153–168, 2017. doi: 10.1016/j.gloenvcha.2016.05.009.

E. Rignot, J. Mouginot, B. Scheuchl, M. van den Broeke, M. J. van Wessem, and M. Morlighem. Four decades of Antarctic Ice Sheet mass balance from 1979–2017. *Proceedings of the National Academy of Sciences*, 116(4):1095–1103, 2019. doi: 10.1073/pnas.1812883116.

F. R. Rijsberman. Water scarcity: Fact or fiction? *Agricultural Water Management*, 80 (1-3 SPEC. ISS.):5–22, 2006. doi: 10.1016/j.agwat.2005.07.001.

T. P. Robinson, P. K. Thornton, G. Franceschini, R. L. Kruska, F. Chiozza, A. Notenbaert, G. Cecchi, M. Herrero, M. Epprecht, S. Fritz, L. You, G. Conchedda, and L. See. *Global livestock production systems.* Food and Agriculture Organization of the United Nations (FAO) and International Livestock Research Institute (ILRI), Rome, 2011. ISBN 9789251070338.

T. P. Robinson, G. R. W. Wint, G. Conchedda, T. P. Van Boeckel, V. Ercoli, E. Palamara, G. Cinardi, L. D'Aietti, S. I. Hay, and M. Gilbert. Mapping the Global Distribution of Livestock. *PLoS ONE*, 9(5):e96084, 2014. doi: 10.1371/journal.pone.0096084.

J. Rockström, M. Lannerstad, and M. Falkenmark. Assessing the water challenge of a new green revolution in developing countries. *Proceedings of the National Academy of Sciences*, 104(15):6253–6260, 2007. doi: 10.1073/pnas.0605739104.

J. Rockström, M. Falkenmark, L. Karlberg, H. Hoff, S. Rost, and D. Gerten. Future water availability for global food production: The potential of green water for increasing resilience to global change. *Water Resources Research*, 45(7):1–16, 2009. doi: 10.1029/2007WR006767.

J. Rockström, M. Falkenmark, C. Folke, M. Lannerstad, J. Barron, E. Enfors, L. Gordon, J. Heinke, H. Hoff, and C. Pahl-Wostl. *Water Resilience for Human Prosperity.* Cambridge University Press, Cambridge, UK, 2014. ISBN 978-1-107-02419-9.

M. Rodell, H. K. Beaudoing, T. S. L'Ecuyer, W. S. Olson, J. S. Famiglietti, P. R. Houser, R. Adler, M. G. Bosilovich, C. A. Clayson, D. Chambers, E. Clark, E. J. Fetzer, X. Gao, G. Gu, K. Hilburn, G. J. Huffman, D. P. Lettenmaier, W. T. Liu, F. R. Robertson, C. A. Schlosser, J. Sheffield, and E. F. Wood. The observed state of the water cycle in the early twenty-first century. *Journal of Climate*, 28(21):8289–8318, 2015. doi: 10.1175/JCLI-D-14-00555.1.

J. Rogelj, M. den Elzen, N. Höhne, T. Fransen, H. Fekete, H. Winkler, R. Schaeffer, F. Sha, K. Riahi, and M. Meinshausen. Paris Agreement climate proposals need a boost to keep warming well below 2 °C. *Nature*, 534(7609):631–639, 2016. doi: 10.1038/nature18307.

M. Rogger, M. Agnoletti, A. Alaoui, J. C. Bathurst, G. Bodner, M. Borga, V. Chaplot, F. Gallart, G. Glatzel, J. Hall, J. Holden, L. Holko, R. Horn, A. Kiss, S. Kohnová, G. Leitinger, B. Lennartz, J. Parajka, R. Perdigão, S. Peth, L. Plavcová, J. N. Quinton, M. Robinson, J. L. Salinas, A. Santoro, J. Szolgay, S. Tron, J. J. H. van den Akker, A. Viglione, and G. Blöschl. Land use change impacts on floods at the catchment scale: Challenges and opportunities for future research. *Water Resources Research*, 53 (7):5209–5219, 2017. doi: 10.1002/2017WR020723.

S. Rolinski, C. Müller, J. Heinke, I. Weindl, A. Biewald, B. L. Bodirsky, A. Bondeau, E. R. Boons-Prins, A. F. Bouwman, P. A. Leffelaar, J. A. te Roller, S. Schaphoff, and K. Thonicke. Modeling vegetation and carbon dynamics of managed grasslands at the global scale with LPJmL 3.6. *Geoscientific Model Development*, 11(1):429–451, 2018. doi: 10.5194/gmd-11-429-2018.

S. Rost, D. Gerten, A. Bondeau, W. Lucht, J. Rohwer, and S. Schaphoff. Agricultural green and blue water consumption and its influence on the global water system. *Water Resources Research*, 44(9):1–17, 2008. doi: 10.1029/2007WR006331.

W. F. Ruddiman. *Earth's Climate: Past and Future*. W. H. Freeman, New York, second edi edition, 2007. ISBN 9780716784906.

B. Rudolf, A. Becker, U. Schneider, A. Meyer-Christoffer, and M. Ziese. GPCC Status Report December 2010 (On the most recent gridded global data set issued in fall 2010 by the Global Precipitation Climatology Centre (GPCC)). Technical report, Global Precipitation Climatology Centre, 2010.

S. Russell and K. Fielding. Water demand management research: A psychological perspective. *Water Resources Research*, 46(5):1–12, 2010. doi: 10.1029/2009WR008408.

M. N. Sawka, S. N. Cheuvront, and R. Carter. Human Water Needs. *Nutrition Reviews*, 63(June):S30–S39, 2005. doi: 10.1111/j.1753-4887.2005.tb00152.x.

S. Schaphoff, U. Heyder, S. Ostberg, D. Gerten, J. Heinke, and W. Lucht. Contribution of permafrost soils to the global carbon budget. *Environmental Research Letters*, 8(1): 014026, 2013. doi: 10.1088/1748-9326/8/1/014026.

S. Schaphoff, M. Forkel, C. Müller, J. Knauer, W. von Bloh, D. Gerten, J. Jägermeyr, W. Lucht, A. Rammig, K. Thonicke, and K. Waha. LPJmL4 – a dynamic global vegetation model with managed land – Part 2: Model evaluation. *Geoscientific Model Development*, 11(4):1377–1403, 2018a. doi: 10.5194/gmd-11-1377-2018.

S. Schaphoff, W. von Bloh, A. Rammig, K. Thonicke, H. Biemans, M. Forkel, D. Gerten, J. Heinke, J. Jägermeyr, J. Knauer, F. Langerwisch, W. Lucht, C. Müller, S. Rolinski,

and K. Waha. LPJmL4 – a dynamic global vegetation model with managed land – Part 1: Model description. *Geoscientific Model Development*, 11(4):1343–1375, 2018b. doi: 10.5194/gmd-11-1343-2018.

S. E. Schaphoff, W. von Bloh, K. Thonicke, H. Biemans, M. Forkel, D. Gerten, J. Heinke, J. Jägermeyr, C. Müller, S. Rolinski, K. Waha, E. Stehfest, L. de Waal, U. Heyder, M. Gumpenberger, and T. Beringer. *LPJmL4 Model Code, V. 4.0.* GFZ Data Services, 2018c. doi: 10.5880/pik.2018.002.

J. Schewe, J. Heinke, D. Gerten, I. Haddeland, N. W. Arnell, D. B. Clark, R. Dankers, S. Eisner, B. M. Fekete, F. J. Colón-González, S. N. Gosling, H. Kim, X. Liu, Y. Masaki, F. T. Portmann, Y. Satoh, T. Stacke, Q. Tang, Y. Wada, D. Wisser, T. Albrecht, K. Frieler, F. Piontek, L. Warszawski, and P. Kabat. Multimodel assessment of water scarcity under climate change. *Proceedings of the National Academy of Sciences of the United States of America*, 111(9):3245–50, 2014. doi: 10.1073/pnas.1222460110.

G. A. Schmidt, R. A. Ruedy, R. L. Miller, and A. A. Lacis. Attribution of the present-day total greenhouse effect. *Journal of Geophysical Research*, 115(D20):D20106, 2010. doi: 10.1029/2010JD014287.

U. Schneider, A. Becker, P. Finger, A. Meyer-Christoffer, M. Ziese, and B. Rudolf. GPCC's new land surface precipitation climatology based on quality-controlled in situ data and its role in quantifying the global water cycle. *Theoretical and Applied Climatology*, 115 (1-2):15–40, 2014. doi: 10.1007/s00704-013-0860-x.

M. Scholze, W. Knorr, N. W. Arnell, and I. C. Prentice. A climate-change risk analysis for world ecosystems. *Proceedings of the National Academy of Sciences*, 103(35):13116–13120, 2006. doi: 10.1073/pnas.0601816103.

J. F. Schyns, A. Y. Hoekstra, M. J. Booij, R. J. Hogeboom, and M. M. Mekonnen. Limits to the world's green water resources for food, feed, fiber, timber, and bioenergy. *Proceedings of the National Academy of Sciences*, 116(11):4893–4898, 2019. doi: 10.1073/pnas.1817380116.

I. A. Shiklomanov. Appraisal and Assessment of World Water Resources. *Water International*, 25(1):11–32, 2000. doi: 10.1080/02508060008686794.

I. A. Shiklomanov and J. C. Rodda, editors. *World Water Resources at the Beginning of the 21st Century.* Cambridge Univ Press, Cambridge, UK, international hydrology series edition, 2003.

S. Siebert and P. Döll. Quantifying blue and green virtual water contents in global crop production as well as potential production losses without irrigation. *Journal of Hydrology*, 384(3-4):198–217, 2010. doi: 10.1016/j.jhydrol.2009.07.031.

S. Siebert, P. Döll, J. Hoogeveen, J.-M. Faures, K. Frenken, and S. Feick. Development and validation of the global map of irrigation areas. *Hydrology and Earth System Sciences*, 9(5):535–547, 2005. doi: 10.5194/hess-9-535-2005.

S. Siebert, P. Döll, S. Feick, J. Hoogeveen, and K. Frenken. *Global Map of Irrigation Areas, Version 4.0.1.* Johann Wolfgang Goethe University, Frankfurt am Main, Germany and Food and Agriculture Organization of the United Nations, Rome, 2007.

S. Sitch, C. Huntingford, N. Gedney, P. E. Levy, M. R. Lomas, S. L. Piao, R. A. Betts, P. Ciais, P. M. Cox, P. Friedlingstein, C. D. Jones, I. C. Prentice, and F. I. Woodward. Evaluation of the terrestrial carbon cycle, future plant geography and climate-carbon cycle feedbacks using five Dynamic Global Vegetation Models (DGVMs). *Global Change Biology*, 14(9):2015–2039, 2008. doi: 10.1111/j.1365-2486.2008.01626.x.

J. Smith, K. Sones, D. Grace, S. MacMillan, S. Tarawali, and M. Herrero. Beyond milk, meat, and eggs: Role of livestock in food and nutrition security. *Animal Frontiers*, 3(1): 6–13, 2013. doi: 10.2527/af.2013-0002.

J. B. Smith, S. H. Schneider, M. Oppenheimer, G. W. Yohe, W. Hare, M. D. Mastrandrea, A. Patwardhan, I. Burton, J. Corfee-Morlot, C. H. D. Magadza, H.-M. Fussel, A. B. Pittock, A. Rahman, A. Suarez, and J.-P. van Ypersele. Assessing dangerous climate change through an update of the Intergovernmental Panel on Climate Change (IPCC) "reasons for concern". *Proceedings of the National Academy of Sciences*, 106(11):4133–4137, 2009. doi: 10.1073/pnas.0812355106.

S. Solomon, G.-K. Plattner, R. Knutti, and P. Friedlingstein. Irreversible climate change due to carbon dioxide emissions. *Proceedings of the National Academy of Sciences*, 106 (6):1704–1709, 2009. doi: 10.1073/pnas.0812721106.

A. Sood, S. A. Prathapar, and V. Smakhtin. Green and Blue Water. In J. Lautze, editor, *Key Concepts in Water Resource Management - A Review and Critical Evaluation*, chapter 7, pages 91–102. Routledge, London, UK, earthscan edition, 2014.

O. Sorokhtin, G. Chilingar, and N. Sorokhtin. Chapter 11 - hydrosphere: The patterns of its origin and evolution. In O. Sorokhtin, G. Chilingarian, and N. Sorokhtin, editors, *Evolution of Earth and its Climate: Birth, Life and Death of Earth*, volume 10 of *Developments in Earth and Environmental Sciences*, pages 421 – 438. Elsevier, 2011. doi: https://doi.org/10.1016/B978-0-444-53757-7.00011-8.

O. H. K. Spate and A. T. A. Learmonth. *India and Pakistan: A General and Regional Geography*. Routledge, New York, 2017. ISBN 978-1-315-26605-3.

T. Stacke and S. Hagemann. Development and validation of a global dynamical wetlands extent scheme. *Hydrology and Earth System Sciences Discussions*, 9(1):405–440, 2012a. doi: 10.5194/hessd-9-405-2012.

T. Stacke and S. Hagemann. Development and evaluation of a global dynamical wetlands extent scheme. *Hydrology and Earth System Sciences*, 16(8):2915–2933, 2012b. doi: 10.5194/hess-16-2915-2012.

D. Stainforth, M. Allen, E. Tredger, and L. Smith. Confidence, uncertainty and decision-support relevance in climate predictions. *Philosophical Transactions of the Royal Society A: Mathematical, Physical and Engineering Sciences*, 365(1857):2145–2161, 2007. doi: 10.1098/rsta.2007.2074.

W. Steffen, J. Crutzen, and J. R. McNeill. The Anthropocene: are humans now overwhelming the great forces of Nature? *Ambio*, 36(8):614–21, 2007. doi: 10.1579/0044-7447(2007)36[614:TAAHNO]2.0.CO;2.

W. Steffen, W. Broadgate, L. Deutsch, O. Gaffney, and C. Ludwig. The trajectory of the Anthropocene: The Great Acceleration. *The Anthropocene Review*, 2(1):81–98, 2015a. doi: 10.1177/2053019614564785.

W. Steffen, K. Richardson, J. Rockstrom, S. E. Cornell, I. Fetzer, E. M. Bennett, R. Biggs, S. R. Carpenter, W. de Vries, C. A. de Wit, C. Folke, D. Gerten, J. Heinke, G. M. Mace, L. M. Persson, V. Ramanathan, B. Reyers, and S. Sorlin. Planetary boundaries: Guiding human development on a changing planet. *Science*, 347(6223):1259855–1259855, 2015b. doi: 10.1126/science.1259855.

H. Steinfeld, P. J. Gerber, T. Wassenaar, V. Castel, M. Rosales, and C. de Haan. *Livestocks's long shadow*. Food and Agriculture Organization of the United Nations, Rome, 2006. ISBN 92-5-105571-8.

F. Stenzel, D. Gerten, C. Werner, and J. Jägermeyr. Freshwater requirements of large-scale bioenergy plantations for limiting global warming to 1.5 °C. *Environmental Research Letters*, 14(8):084001, 2019. doi: 10.1088/1748-9326/ab2b4b.

G. L. Stephens, J. Li, M. Wild, C. A. Clayson, N. Loeb, S. Kato, T. L'Ecuyer, P. W. Stackhouse, M. Lebsock, and T. Andrews. An update on Earth's energy balance in light of the latest global observations. *Nature Geoscience*, 5(10):691–696, 2012. doi: 10.1038/ngeo1580.

S. M. Sterling, A. Ducharne, and J. Polcher. The impact of global land-cover change on the terrestrial water cycle. *Nature Climate Change*, 3(4):385–390, 2013. doi: 10.1038/nclimate1690.

K. Takata, S. Emori, and T. Watanabe. Development of the minimal advanced treatments of surface interaction and runoff. *Global and Planetary Change*, 38(1-2):209–222, 2003. doi: 10.1016/S0921-8181(03)00030-4.

Q. Tang and D. P. Lettenmaier. 21st century runoff sensitivities of major global river basins. *Geophysical Research Letters*, 39(6):L06403, 2012. doi: 10.1029/2011GL050834.

Q. Tang, T. Oki, S. Kanae, and H. Hu. The Influence of Precipitation Variability and Partial Irrigation within Grid Cells on a Hydrological Simulation. *Journal of Hydrometeorology*, 8(3):499–512, 2007. doi: 10.1175/JHM589.1.

Q. Tang, T. Oki, S. Kanae, and H. Hu. Hydrological Cycles Change in the Yellow River Basin during the Last Half of the Twentieth Century. *Journal of Climate*, 21(8):1790–1806, 2008. doi: 10.1175/2007JCLI1854.1.

K. E. Taylor, R. J. Stouffer, and G. A. Meehl. An Overview of CMIP5 and the Experiment Design. *Bulletin of the American Meteorological Society*, 93(4):485–498, 2012. doi: 10.1175/BAMS-D-11-00094.1.

R. G. Taylor, B. Scanlon, P. Döll, M. Rodell, R. van Beek, Y. Wada, L. Longuevergne, M. Leblanc, J. S. Famiglietti, M. Edmunds, L. Konikow, T. R. Green, J. Chen, M. Taniguchi, M. F. P. Bierkens, A. MacDonald, Y. Fan, R. M. Maxwell, Y. Yechieli, J. J. Gurdak, D. M. Allen, M. Shamsudduha, K. Hiscock, P. J.-F. Yeh, I. Holman, and H. Treidel. Ground water and climate change. *Nature Climate Change*, 3(4):322–329, 2013. doi: 10.1038/nclimate1744.

C. Tebaldi and J. M. Arblaster. Pattern scaling: Its strengths and limitations, and an update on the latest model simulations. *Climatic Change*, 122(3):459–471, 2014. doi: 10.1007/s10584-013-1032-9.

C. Tebaldi and R. Knutti. Evaluating the accuracy of climate change pattern emulation for low warming targets. *Environmental Research Letters*, 13(5):055006, 2018. doi: 10.1088/1748-9326/aabef2.

P. S. Thenkabail, C. M. Biradar, P. Noojipady, V. Dheeravath, Y. Li, M. Velpuri, M. Gumma, O. R. P. Gangalakunta, H. Turral, X. Cai, J. Vithanage, M. A. Schull, and R. Dutta. Global irrigated area map (GIAM), derived from remote sensing, for the end of the last millennium. *International Journal of Remote Sensing*, 30(14):3679–3733, 2009. doi: 10.1080/01431160802698919.

C. P. Timmer. Behavioral dimensions of food security. *Proceedings of the National Academy of Sciences*, 109(31):12315–12320, 2012. doi: 10.1073/pnas.0913213107.

UNFCCC. Paris Agreement: FCCC/CP/2015/L.9/Rev.1, 2015. Available at `http://unfccc.int/resource/docs/2015/cop21/eng/l09r01.pdf`, accessed 5 February 2019.

United Nations. *Transforming our world: The 2030 agenda for sustainable development*. UN General Assembly, New York, 2015. URL `https://sustainabledevelopment.un.org/post2015/transformingourworld`.

United Nations. *The Sustainable Development Goals Report 2017*. United Nations, 2017. doi: 10.18356/4d038e1e-en.

University of East Anglia Climatic Research Unit, P. D. Jones, and I. C. Harris. *CRU TS3.10: Climatic Research Unit (CRU) Time-Series (TS) Version 3.10 of High Resolution Gridded Data of Month-by-month Variation in Climate (Jan 1901–Dec 2009)*. NCAS British Atmospheric Data Centre, 2013. URL `http://catalogue.ceda.ac.uk/uuid/ac3e6be017970639a9278e64d3fd5508`.

L. P. H. van Beek, Y. Wada, and M. F. P. Bierkens. Global monthly water stress: 1. Water balance and water availability. *Water Resources Research*, 47(7), 2011. doi: 10.1029/2010WR009791.

P. van Breugel, M. Herrero, J. van de Steeg, and D. Peden. Livestock Water Use and Productivity in the Nile Basin. *Ecosystems*, 13(2):205–221, 2010. doi: 10.1007/s10021-009-9311-z.

G. E. van Halsema and L. Vincent. Efficiency and productivity terms for water management: A matter of contextual relativism versus general absolutism. *Agricultural Water Management*, 108:9–15, 2012. doi: 10.1016/j.agwat.2011.05.016.

M. H. J. van Huijgevoort, P. Hazenberg, H. A. J. Van Lanen, and R. Uijlenhoet. A generic method for hydrological drought identification across different climate regions. *Hydrology and Earth System Sciences*, 16(8):2437–2451, 2012. doi: 10.5194/hess-16-2437-2012.

D. P. van Vuuren, E. Kriegler, B. C. O'Neill, K. L. Ebi, K. Riahi, T. R. Carter, J. Edmonds, S. Hallegatte, T. Kram, R. Mathur, and H. Winkler. A new scenario framework for Climate Change Research: Scenario matrix architecture. *Climatic Change*, 122(3):373–386, 2014. doi: 10.1007/s10584-013-0906-1.

S. Vermeulen, P. Aggarwal, A. Ainslie, C. Angelone, B. Campbell, A. Challinor, J. Hansen, J. Ingram, A. Jarvis, P. Kristjanson, C. Lau, G. Nelson, P. Thornton, and E. Wollenberg. Options for support to agriculture and food security under climate change. *Environmental Science & Policy*, 15(1):136–144, 2012. doi: 10.1016/j.envsci.2011.09.003.

S. J. Vermeulen, A. J. Challinor, P. K. Thornton, B. M. Campbell, N. Eriyagama, J. M. Vervoort, J. Kinyangi, A. Jarvis, P. Läderach, J. Ramirez-Villegas, K. J. Nicklin, E. Hawkins, and D. R. Smith. Addressing uncertainty in adaptation planning for agriculture. *Proceedings of the National Academy of Sciences of the United States of America*, 110(21):8357–62, 2013. doi: 10.1073/pnas.1219441110.

D. G. Victor, K. Akimoto, Y. Kaya, M. Yamaguchi, D. Cullenward, and C. Hepburn. Prove Paris was more than paper promises. *Nature*, 548(7665):25–27, 2017. doi: 10.1038/548025a.

C. Vörösmarty, C. Federer, and A. Schloss. Potential evaporation functions compared on US watersheds: Possible implications for global-scale water balance and terrestrial ecosystem modeling. *Journal of Hydrology*, 207(3-4):147–169, 1998. doi: 10.1016/S0022-1694(98)00109-7.

C. J. Vörösmarty. Global Water Resources: Vulnerability from Climate Change and Population Growth. *Science*, 289(5477):284–288, 2000. doi: 10.1126/science.289.5477.284.

C. J. Vörösmarty, K. P. Sharma, B. M. Fekete, A. H. Copeland, J. Holden, J. Marble, and J. A. Lough. The storage and aging of continental runoff in large reservoir systems of the world. *Ambio*, 26(4):210–219, 1997.

C. J. Vörösmarty, B. M. Fekete, M. Meybeck, and R. B. Lammers. Global system of rivers: Its role in organizing continental land mass and defining land-to-ocean linkages. *Global Biogeochemical Cycles*, 14(2):599–621, 2000. doi: 10.1029/1999GB900092.

C. J. Vörösmarty, B. M. Fekete, F. G. Hall, G. Collatz, B. Meeson, S. Los, E. Brown De Colstoun, and D. Landis. *ISLSCP II River Routing Data (STN-30p)*. ORNL Distributed Active Archive Center, Oak Ridge, Tennessee, 2011. doi: 10.3334/ornldaac/1005.

Y. Wada, L. P. H. van Beek, C. M. van Kempen, J. W. T. M. Reckman, S. Vasak, and M. F. P. Bierkens. Global depletion of groundwater resources. *Geophysical Research Letters*, 37(20):L20402, 2010. doi: 10.1029/2010GL044571.

Y. Wada, L. P. H. Van Beek, D. Viviroli, H. H. Drr, R. Weingartner, and M. F. P. Bierkens. Global monthly water stress: 2. Water demand and severity of water stress. *Water Resources Research*, 47(7):1–17, 2011. doi: 10.1029/2010WR009792.

Y. Wada, L. P. H. van Beek, and M. F. P. Bierkens. Nonsustainable groundwater sustaining irrigation: A global assessment. *Water Resources Research*, 48(6), 2012. doi: 10.1029/2011WR010562.

Y. Wada, M. Flörke, N. Hanasaki, S. Eisner, G. Fischer, S. Tramberend, Y. Satoh, M. T. H. van Vliet, P. Yillia, C. Ringler, P. Burek, and D. Wiberg. Modeling global water use for the 21st century: the Water Futures and Solutions (WFaS) initiative and its approaches. *Geoscientific Model Development*, 9(1):175–222, 2016. doi: 10.5194/gmd-9-175-2016.

J. Wallace. Increasing agricultural water use efficiency to meet future food production. *Agriculture, Ecosystems & Environment*, 82(1-3):105–119, 2000. doi: 10.1016/S0167-8809(00)00220-6.

L. Warszawski, K. Frieler, V. Huber, F. Piontek, O. Serdeczny, and J. Schewe. The Inter-Sectoral Impact Model Intercomparison Project (ISI-MIP): Project framework. *Proceedings of the National Academy of Sciences*, pages 1–5, 2013. doi: 10.1073/pnas.1312330110.

L. Warszawski, K. Frieler, V. Huber, F. Piontek, O. Serdeczny, and J. Schewe. The Inter-Sectoral Impact Model Intercomparison Project (ISI–MIP): Project framework. *Proceedings of the National Academy of Sciences*, 111(9):3228–3232, 2014. doi: 10.1073/pnas.1312330110.

I. G. Watterson. Calculation of probability density functions for temperature and precipitation change under global warming. *Journal of Geophysical Research*, 113:D12106, 2008. doi: 10.1029/2007JD009254.

G. P. Weedon, S. Gomes, P. Viterbo, W. J. Shuttleworth, E. Blyth, H. Österle, J. C. Adam, N. Bellouin, O. Boucher, and M. Best. Creation of the WATCH Forcing Data and Its Use to Assess Global and Regional Reference Crop Evaporation over Land during the Twentieth Century. *Journal of Hydrometeorology*, 12(5):823–848, 2011. doi: 10.1175/2011JHM1369.1.

A. P. Weigel, M. A. Liniger, and C. Appenzeller. Can multi-model combination really enhance the prediction skill of probabilistic ensemble forecasts? *Quarterly Journal of the Royal Meteorological Society*, 134(630):241–260, 2008. doi: 10.1002/qj.210.

I. Weindl, B. L. Bodirsky, S. Rolinski, A. Biewald, H. Lotze-Campen, C. Müller, J. P. Dietrich, F. Humpenöder, M. Stevanović, S. Schaphoff, and A. Popp. Livestock production and the water challenge of future food supply: Implications of agricultural management and dietary choices. *Global Environmental Change*, 47:121–132, 2017. doi: 10.1016/j.gloenvcha.2017.09.010.

D. Wisser, S. Frolking, E. M. Douglas, B. M. Fekete, C. J. Vörösmarty, and A. H. Schumann. Global irrigation water demand: Variability and uncertainties arising from agricultural and climate data sets. *Geophysical Research Letters*, 35(24):L24408, 2008. doi: 10.1029/2008GL035296.

D. Wisser, B. M. Fekete, C. J. Vörösmarty, and A. H. Schumann. Reconstructing 20th century global hydrography: a contribution to the Global Terrestrial Network-Hydrology (GTN-H). *Hydrology and Earth System Sciences*, 14(1):1–24, 2010. doi: 10.5194/hess-14-1-2010.

World Bank. World Bank Commodity Price Data (The Pink Sheet), 2019. Available at `http://pubdocs.worldbank.org/en/561011486076393416/CMO-Historical-Data-Monthly.xlsx`, accessed 29 March 2019.

D. C. Zemp, C.-F. Schleussner, H. M. J. Barbosa, R. J. van der Ent, J. F. Donges, J. Heinke, G. Sampaio, and A. Rammig. On the importance of cascading moisture recycling in South America. *Atmospheric Chemistry and Physics*, 14(23):13337–13359, 2014. doi: 10.5194/acp-14-13337-2014.

Y. Zhou, A. H. Sawyer, C. H. David, and J. S. Famiglietti. Fresh Submarine Groundwater Discharge to the Near-Global Coast. *Geophysical Research Letters*, 46(11):5855–5863, 2019. doi: 10.1029/2019GL082749.

Selbständigkeitserklärung

Ich erkläre, dass ich die Dissertation selbständig und nur unter Verwendung der von mir gemäß § 7 Abs. 3 der Promotionsordnung der Mathematisch-Naturwissenschaftlichen Fakultät, veröffentlicht im Amtlichen Mitteilungsblatt der Humboldt-Universität zu Berlin Nr. 42/2018 am 11.07.2018 angegebenen Hilfsmittel angefertigt habe.

Berlin, den 26. März 2020

Jens Heinke